PERFORMANCE OF THE ROOF STRUCTURE AT THE WAGNER FREE INSTITUTE OF SCIENCE: A COMPUTATIONAL SIMULATION AND ITS IMPLICATIONS FOR PLASTER CONSERVATION

Katharine Helene Woodman

A THESIS

In

Historic Preservation

Presented to the Faculties of the University of Pennsylvania in Partial Fulfillment of the Requirements of the Degree of

MASTER OF SCIENCE OF HISTORIC PRESERVATION

2010

Advisor
Michael C. Henry, PE, AIA
Adjunct Professor of Architecture

Program Chair
Randall F. Mason, Ph.D.
Department Chair

Table of Contents

List of Figures

List of Tables

Acknowledgements

I would first like to extend many thanks to the staff at the Wagner Free Institute of Science, who graciously allowed me to pursue this undertaking. In particular, I would like to thank Don Azuma whose assistance and encouragement has been invaluable throughout this process.

I would also like to thank Marlene Goeke for providing the stepping stone upon which this thesis was predicated. She has been a font of information and a wonderful resource.

I would like to extend my gratitude to Frank Matero and Randy Mason, who have both encouraged this thesis and allowed me to pursue my academic interests.

My sincerest thanks and appreciation to my advisor Michael Henry for his dedication, enthusiasm and guidance which has truly helped me grow as both an engineer and preservation professional.

Finally, thanks to Kyle for his help with every aspect of this thesis from brainstorming to editing to modeling. Thank you for your unyielding patience and love.

1 Introduction

The structural performance of historic buildings is a critical concern with respect to safety and functionality. While the decorative surface fabric of a building is the most visible manifestation of its architectural value, the integrity of these surfaces may be affected by the performance of the underlying structure. When symptoms of inadequate structural performance are manifested by cracked or displaced finishes, a structural engineer is generally consulted in order to evaluate the structural integrity of a building. The assessment of the structural behavior of existing (and particularly historic) buildings poses considerable challenges. Data pertaining to both construction and materials is often limited or non-existent; moreover, any further disturbance of the fabric is generally discouraged, limiting the ability of the engineer to perform destructive testing or materials sampling.

In order to understand the structural performance of a building, engineers often rely on conventional means of analysis or rules of thumb which are often too simplistic to accurately describe real behavior. With many historic structures, where deflection, rather than strength is the dominant concern, these conventional methods are frequently not adequate in their prediction of these parameters. As a result, engineers may utilize empirical means such as load testing, or representative measurements using instrumentation such as crack gauges in order to evaluate building performance. While these methods have their uses, they pose significant problems, particularly in their application to historic structures. In addition to high costs, load tests can induce large stresses, causing unforeseen problems and/or potential damage to the structure, while representative readings, while considerably less disruptive, only measure localized response and cannot fully explain the loads, load paths or performance of the entire structure.

More recently, engineers have begun to look towards more sophisticated analytical methods in order to help better simulate and understand structural behavior. In particular, Finite Element Analysis (FEA) has become increasingly prolific in the field. A computational tool, FEA allows one to simulate the geometry, physical constraints, material properties and loads of a structure, and creating a virtual model of the structure from which stresses and deflections can be generated, without any disruption of the physical structure. FEA is particularly useful when it comes to modeling complex structures, such as those exhibiting intricate geometry, non-linear or anisotropic material properties, or are subject to complicated static and dynamic loading patterns. FEA is also extremely useful in assessing both large and small scale structural behavior, from localized high stress intensity at connections, to large scale deflections of domes, buttresses or trusses. In addition to its analytical capabilities, FEA exhibits many other merits, including but not limited to its speed, economy, relative ease of use, and graphical output. Moreover, the graphical nature of FEA allows the user to visualize stresses, strain and deflections, making it visually intuitive even to the layperson.

This thesis seeks to critically analyze the capabilities and limitations of FEA in its application to the diagnostics of historic structures. It will attempt to evaluate the strengths and weaknesses of the method and to ascertain what considerations must be taken into account, if any, to improve its applicability to this field. To do so, FEA will be used to analyze the performance of an actual structure, the roof framing of Wagner Free Institute of Science in Philadelphia, as a case study. A mid-19th century structure and National Historic Landmark, the Wagner Institute retains much of its architectural integrity. However, with the detachment of a large area of ceiling plaster in 2003 and the extensive cracking of the remaining ceiling plaster, the structural integrity of the building's ceiling plaster has become a primary concern to the institution. Though the plaster condition has often been attributed to structural deflection of the roofing system, the correlation between cause and effect remains unconfirmed. A number of structural studies have been performed, but the results are as of yet, inconclusive and therefore further analysis is warranted. The use of FEA has the potential to address both the previous assessments, and to inform the conservation of the plaster ceiling.

The Wagner Institute of Science is an excellent candidate for a case study opportunity for a number of reasons: first, the architectural significance and the conservation philosophy administered by the institution limit considerably the amount of destructive testing that can be performed; second, the building does not exhibit overwhelming structural failures but rather more subtle manifestations of deflection concerns; third, the theoretical structural behavior obtained by conventional analysis does not necessarily correlate to observed performance; and lastly, conventional solutions have provided inconclusive results. The combination of all of these factors render FEA well suited to this type of investigation.

The application of FEA to the Wagner Institute roof structure seeks to accomplish two main objectives. The first objective addresses the Wagner specifically; based on current measurements and documentation evidence of past loading conditions and displacements, this thesis will attempt to understand the response of the structure to certain loads, and to determine if this results in deflections that would crack the ceiling. More generally, the second objective is to answer a number of questions associated with the application of FEA to historic structures, including but not limited to: How much data are necessary in order to generate an effective model? What are the ranges of certain variables, such as environmental loads and what does that mean in terms of the accuracy of the model? What can we do to eliminate unknown variables, and how does our model help us to inform to what extent this is necessary and/or feasible? How can we manipulate the capabilities of the program to accommodate our needs (use different analysis methods)? How do we determine or quantify “success”? Can we still obtain meaningful information from the tool if, for instance, the analysis correctly identifies areas of high stress concentration and/or deflection, but the order of magnitude differs from actual behavior?

2 Finite Element Analysis Literature Review

2.1 History of the Theory of Structural Analysis:[1]

The history of structural analysis is both long and complex, and as such, what follows is but a brief synopsis of the events and personages responsible for the development of the field. Structural analysis can be defined as a set of physical and mathematical laws applied towards the study and prediction of the behavior of structures. Combining the fields of statics, dynamics and materials science, the structural engineer seeks to quantify the behavior of a structure when subjected to various loads, and to gauge its performance based on criteria such as strength or deflection.

Historically, the theory of structures developed quite separately from the practical understanding of structural behavior. By the 3rd century BC, the Greeks had theorized extensively on both physical mechanics and geometry;[2] and though the fundamentals of levers, inclined planes, and pulleys often aided in the means and methods of construction, it was the latter of the subjects that governed the design of these structures. By the Middle Ages, practical geometry had become the standard principle of building. Unconcerned with axioms, theorems or proofs, practical geometry allowed for convenient, repeatable and proven construction. Throughout succeeding years, the accumulation of empirical knowledge based on successful (and unsuccessful) structures

---

[1] The detailed history of structural analysis will not be enumerated in detailed in this thesis; see bibliography for a list of sources dedicated to the history of structural theory and analysis.
[2] By the 3rd century BC, the philosopher Archimedes had written two famous discourses; the first, *On the Equilbrium of Planes*, is perhaps one of the first discussions of the field of statics. The second, entitled *The Method of Mechanical Theorems*, proved how breaking up a body into infinitesimal parts can be used to determine its resultant volume.

was often compiled into rule books, passed on from master to apprentice; these precursors to traditional prescriptive building codes intended to standardize construction and ensure the safety and reliability of new structures that followed to their antecedents in form and function.

Interest in quantifying the static behavior of structures reappeared in western culture[3] during the Renaissance, where the principles of static equilibrium can be discerned amongst the sketches and notes of Leonardo DaVinci. Over a century later, Galileo Galilei's hypothesis of the fracture of a wooden cantilever was immortalized in his sketch in the Dialogue of Two New Sciences (1638) (Figure 1) [4]. In contrast to his predecessors, Galileo's dialogue proposed a new science—the study of the strength of materials—which considered how the size and shape of structural members affects their ability to carry and transmit loads. Galileo's publication prompted further study of the behavior of beams, as exhibited in the experiments of Mariotte (1686); contemporaneously, Robert Hooke's discovery of the law of elasticity[5] (1666) and later analyses of Parent (1713), Coulomb (1773), Euler (1774), Navier (1839) and others laid the framework for the field of elastic structural analysis. By the mid-19th century, these theories had solidified into a unique field, culminating in Squire Whipple's *A Work on Bridge Building* (1847), and marking the official introduction of structural analysis to the practice of design.

[3] Structural analysis continued in the Islamic culture with their translations of Greek works throughout the medieval period.
[4] Galilei, Galileo. *Discorsi e dimostrazioni matematiche, intorno a due nuove scienze*, 1638.
[5] Hooke's Law, commonly stated as F=kx, essentially states that the deflection of a material is proportional to the force applied, and is dependent on the stiffness of the material.

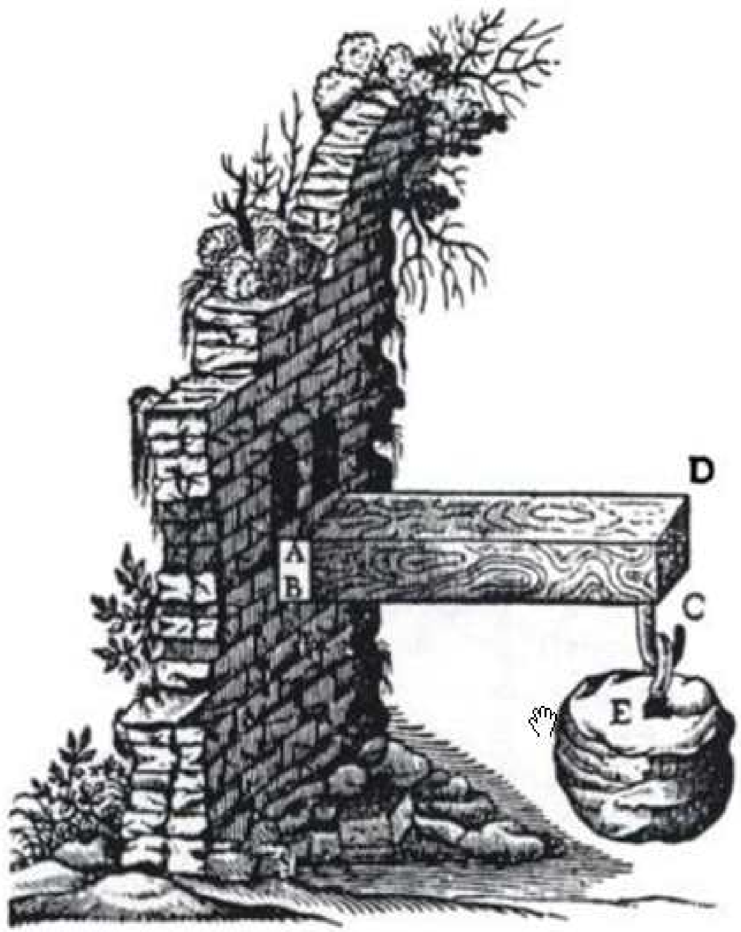

Figure 1: Galileo Galilei's famous sketch of the cantilevered beam, *Discorsi e dimostrazioni matematiche, intorno a due nuove scienze*, 1638

Though the mathematical and theoretical concepts of structural analysis developed substantially from the 1860s to the 1900s, their influence on practical structural design was limited. Despite the advent and mass production of high strength materials during the industrial revolution, materials selection was still based on experimental data obtained from load tests performed by manufacturers, rather than mathematical formulas. As a result, structural design remained limited to "good practice" guidelines (albeit considerably more informed than their rule book predecessors) such as Reynolds and Kent's *Structural Steelwork* (1936) and Dowell's *Competitive Design for Steel Structures* (1937). While these volumes provided more numerical data pertaining to material properties, they did not allow for extrapolation to alternative designs or conditions; in addition, data was confined to statically determinate[6] systems for which graphical methods of frame analysis were highly suited. Despite the advanced capabilities of these new materials, their application to structures was limited by traditional construction techniques and known methods.

The introduction of steel-reinforced concrete and other forms of statically indeterminate systems into the building industry in the late nineteenth century[7], combined with the desire for greater structural spans between supports, led to increased interest in more sophisticated means of analysis. Despite the work of Clapeyron (1857), Maxwell, Castigliano and Mohr in the late nineteenth century, it was not until the 1920s, consequent to the work of Manney in the USA and Ostenfield of Denmark, that the basic

---

[6] A structure is statically determinate if the static equilibrium equations are sufficient for determining the internal forces of the structure. The equilibrium equations for a static body are defined as $\Sigma F=0$ and $\Sigma M=0$, or the sum of all forces (F) and the sum of all moments (M) are equal to zero at all constraints.
[7] Concrete was first invented by the Romans; it was lost for several centuries before it was rediscovered.

approach to truss and framework analysis took form. This method, based on treating displacements as unknown variables, allowed for the solution of statically indeterminate problems, but posed significant issues regarding computation time—an issue that was later addressed by Cross's introduction of the moment distribution method in 1932.[8] These advances sparked a multitude of elegant solution techniques for indeterminate structures, most of which were aimed at circumventing the tedious number of calculations due to large numbers of degrees of freedom. Despite the deployment of large clerical teams solving simultaneous equations, however, the practical application of many of these analysis methods was limited until the advent of high speed computer technology.

2.2 History of Finite Element Analysis

Finite element analysis (FEA) found its roots in the development of linear algebra and matrix theory, just as the work on frame and truss analysis was blossoming. In 1848, the concept of the matrix was first coined by J.J. Sylvester; shortly thereafter followed the work of Arthur Cayley (1855) and Hamilton (1858), and the beginnings of a new branch of mathematics.[9] However, it was not until the 1930s that the concepts of matrix methods would work their way into the structural engineering discipline, most notably in the work of R.A. Frazer, W.J. Duncan and A. R. Collar. Their work in the aerodynamics

[8] Melchers, Robert E. and Richard Hough. *Modeling Complex Engineering Structures.* ASCE Press. Reston, Virginia. 2007. p. 4.
[9] Eugen-Kurrer, Karl. *The History of the Theory of Structures: From Arch Analysis to Computational Mechanics.* Ernst & Sohn Verlag fur Architektur und technische Wissenschaften GmbH & Co. KG. Berlin. 2008. p. 610.

department of the National Physics Laboratory in London resulted in what is considered the first application of matrix algebra to structures when they approximated the vibrational characteristics of airscrew blades by mathematically subdividing the blade into segments and applying unique degrees of freedom to each piece.[10]

The work of Frazer, Duncan and Collar marked a departure from the traditional view of structures as assemblies of two dimensional rods with predictable force-deflection characteristics. In part due to the developments in the aircraft industry, the question of how to analyze a structure such as a plate or a blade of complex geometry, became of extreme interest to engineers. By applying a framework analogy, Hrennikoff (1941) analyzed a plate as a complex system of bars and beams, in which the displacements of the individual beam elements closely approximated those of the original plate. Under this assumption the problem reduces to that of a conventional frame structure which could be analyzed by known methods.[11] Just two years later, Hrennikoff's contemporary Courant pioneered the use of triangular elements in his piecewise polynomial solution of the St. Venant torsional problem.[12] Instead of bars and beams, this time an assembly of small particles triangular elements was used to obtain the overall response of the original system. Courant's work established the first mathematical foundation of the finite element method.

Despite the significance of Courant's work, it was not until the rise of the computer industry in the mid-1950s that the practical implementation of his ideas

---

[10] Ibid. p. 615.
[11] A. Hrenikoff, "Solution of Problems in Elasticity by the Framework Method," *J. Appl. Mech.*, Vol. 8, 1941, pp. 169–175.
[12] Eugen-Kerrer. *The History of the Theory of Structures: From Arch Analysis to Computational Mechanics*. p. 655.

emerged. Beginning in 1954 with the publication of J.H. Argyris' series on the solution of linear structural analysis problems using digital computation, the decade saw an explosion of research and experimentation in the use of computational methods to solve structural problems. In continuation of Courant's work, the 1956 paper of Turner, Clough, Martin and Topp introduced the direct stiffness method to practicing structural engineers by analyzing the wings of an airplane using triangular elements.[13] In 1959 Greenstadt's invention of the discretized continuum allowed for irregularity in element geometry and introduced many of the essential ideas that serve as the mathematical basis for the finite element method as we know it today.

By the end of the decade, the works of countless individuals had culminated into the numerical technique, coined the "finite element method" by Clough in 1960.[14] In the years following its introduction, the finite element method has become increasingly prolific in the field of engineering. Since the publication of the first book on the numerical technique in 1967 (Zienkiewicz and Cheung)[15], its popularity as an engineering tool has grown, driven in part by the growth of computational capabilities of personal computers; between 1964 and 1991, nearly 500 books and 40,000 papers had been written on the subject, and 200 international symposia, conferences and courses have taken place[16]. In addition, commercial software has become an integral part of

---

[13] Brauer, John R. *What Every Engineer Should Know About Finite Element Analysis.* Marcel Dekker Inc. New York, NY. 1993. p. 2.
[14] R. W. Clough, "The Finite Element Method in Plane Stress Analysis," *Proceedings of 2nd ASCE Conference on Electronic Computation*, Pittsburgh, PA, September 8–9, 1960.
[15] O. C. Zienkiewicz and Y. K. Cheung. *The Finite Element Method in Structural and Continuum Mechanics.* McGraw-Hall. London, New York. 1967.
[16] Heubner, Kenneth, et al. *The Finite Element Method for Engineers*. John Wiley & Sons. New York, NY. 2001. p. 11.

contemporary structural and mechanical design. Though the theory of finite element analysis is well established today, its application is extending across disciplines and its implementation is becoming increasingly complex and sophisticated.

2.3 FEA and Historic Preservation

The unique qualities and capabilities of FEA have rendered it a valuable tool in not only the design of new structures, but also in the assessment of existing ones. The first application of FEA to the analysis of historic structures began in the 1970s in the elastic study of gothic cathedrals. This research, pioneered by Robert Mark (1982)[17] and L. Kübler (1974)[18], marked a distinct transition from traditional analysis techniques to computer based methods, and resulted in unprecedented knowledge of the behavior of masonry structures. Just three years later, the use of FEA by Mark allowed for the first comprehensive understanding of the structural behavior of the Pantheon (Figure 2).[19] By the early 1990's, more refined applications of the method had been attempted, including non-linear studies of masonry by Chiostrini, Foraboschi and Sorace[20] (1989) and Barthel (1993)[21]. Within the next few years, the use of FEA in the analysis of a number of

[17] Mark's research spanned the greater part of a decade, culminating in a comprehensive book on the subject in 1982, *Experiments in Gothic Structure*.
[18] Kübler, L., 1974: Computer Analyse der Statik zweier gotischen Kathedralen. *Architectura* 4, pp. 97-111.
[19] Mark, Robert, Paul Hutchinson. "On the Structure of the Roman Pantheon." The Art Bulletin. College Art Association. 1986. pp. 24-34.
[20] Chiostrini, S., Foraboschi, P. and Sorace, S., "Problems connected with the arrangement of a nonlinear finite element method to the analysis of masonry structures." *Structural Repair and Maintenance of Historical Buildings*, Computational Mechanics Publications, 1989. pp. 525-534
[21] Barthel, R.: *Tragverhalten gemauerter Kreuzgewölbe*. Karlsruhe: Universität Karlsruhe. 1993.

historic structures—including the Hagia Sophia (1995)[22] (Fiigure 3**)**, Brussels City Hall (1995)[23], and The National Cathedral in Washington D.C. [24]—had expanded.

By 1991, the method and its application to the historic built environment had made its way into academia in an experimental course taught in the architecture department at UC Berkeley. This cross-disciplinary course, co-taught by engineer Gary Black, historian Stephen Tobriner and then graduate student Stephen Duff[25], used FEA coupled with historic research to study the structural and spatial attributes of buildings, including the cathedrals at Amiens and Chartres, Trinity College Hall, the Minase Shrine in Osaki, as well as several bridges. Most notable was the work on Westminster Hall in London, which represented the first application of FEA to timber structures (Figure 4**)**. The presentation of this course's findings to the Society of Architectural Historians in 1993 brought wide scale recognition of the potential of this technology to the field.[26]

Over the past few decades, FEA has proven to be a valuable tool in the assessment of numerous historic structures. In addition to providing insights into the static and dynamic behavior of these structures (many of which were construction prior to knowledge of structural theory), FEA has also provided a graphic means by which this information can be easily illustrated for non-engineers. These graphical illustrations can

---

[22] Ozkul, Tulay Aksu, Eiichi Kuribayashi. "Structural Characteristics of Hagia Sophia: I—a finite element formulation for static analysis." Building and Environment 42. 2007. Elsevier Science Publishers. Pp. 1212-1218.
[23] Dumortier, S. & W.P. De Wilde. "Finite element study of the Tower of Brussels City Hall". Structural Studies, Repairs and Maintenance of Historic Buildings IV. Volume I. Architectural Studies, Materials and Analysis. 1995. pp. 365-372.
[24] Boothby, T., Atamturktur, S., (2007), "A Guide for the Finite Element Analysis of Historic Load Bearing Masonry Structures," submitted to 10th North American Masonry Conference, St. Louis, Missouri, USA.
[25] Morris, Toby E., R. Gary Black, and Stephen O. Tobriner. "Report on the Application of Finite Analysis to Historic Structures: Westminster Hall, London." Vol. 54, No. 3. Sept. 1995. pp. 336-347.
[26] Ibid. pp. 347.

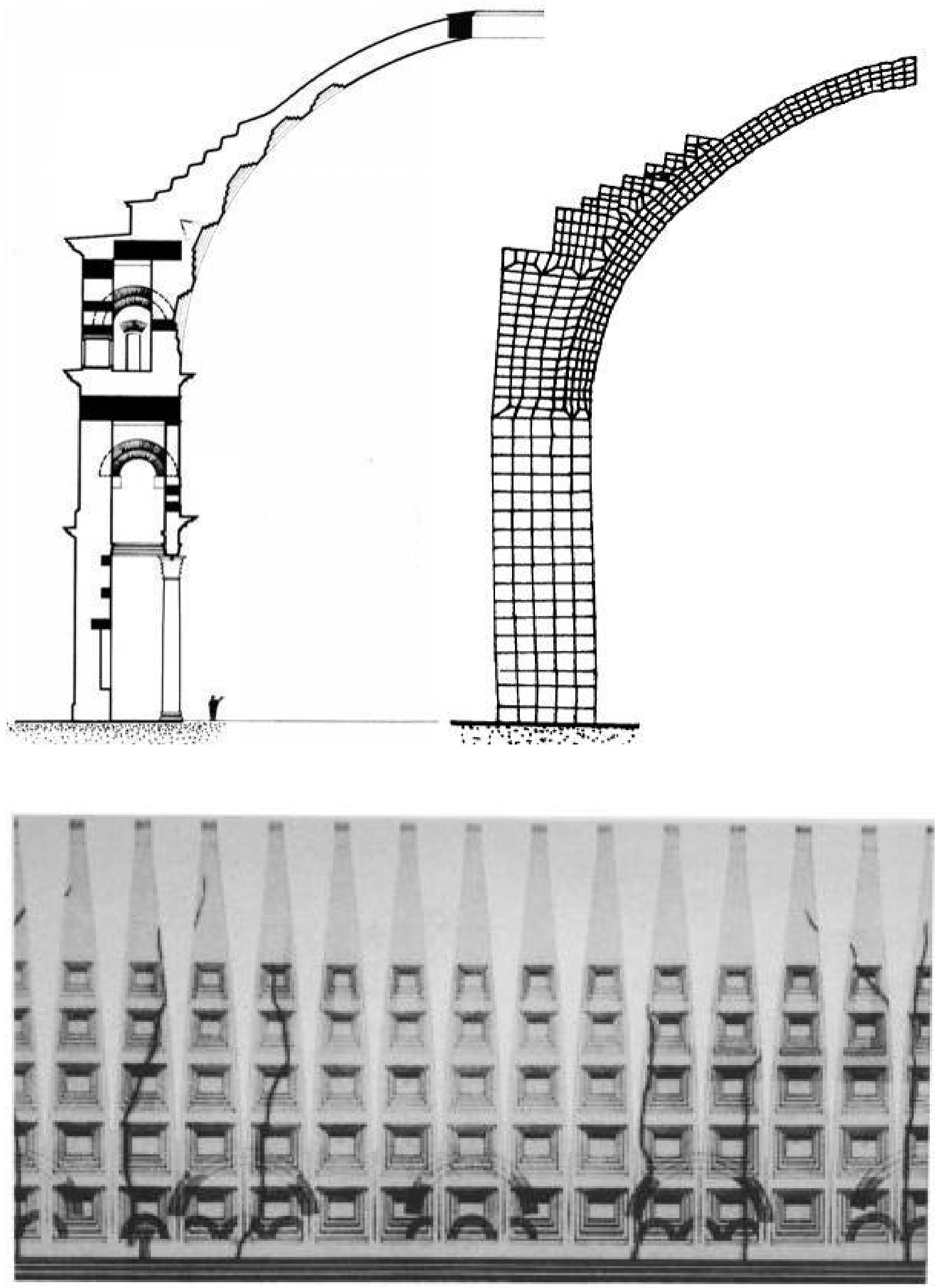

Figure 2: Meridonal section through the Pantheon (top left); exaggerated deformed shape of the finite element section (top right); crack patterns observed about the interior of the dome (Mark, 1982)

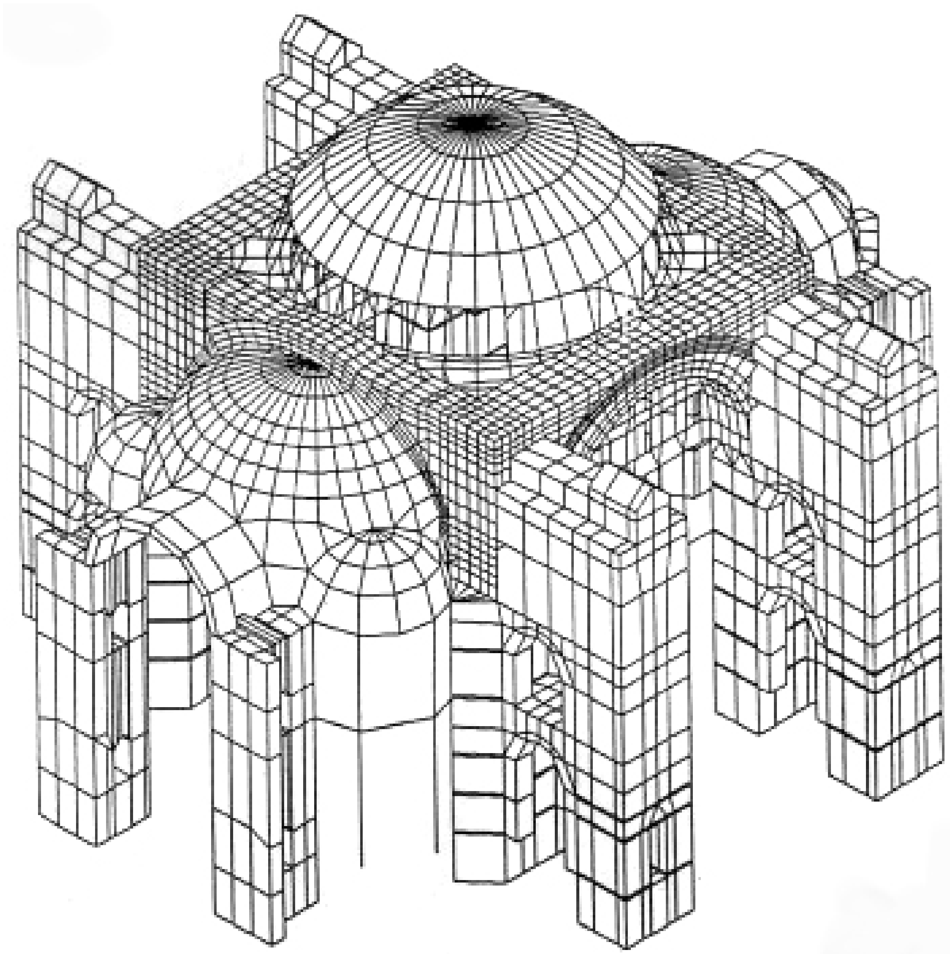

Figure 3: Finite Element Model of Hagia Sophia (Ozkul, Tulay Aksu, Eiichi Kuribayashi., 2007)

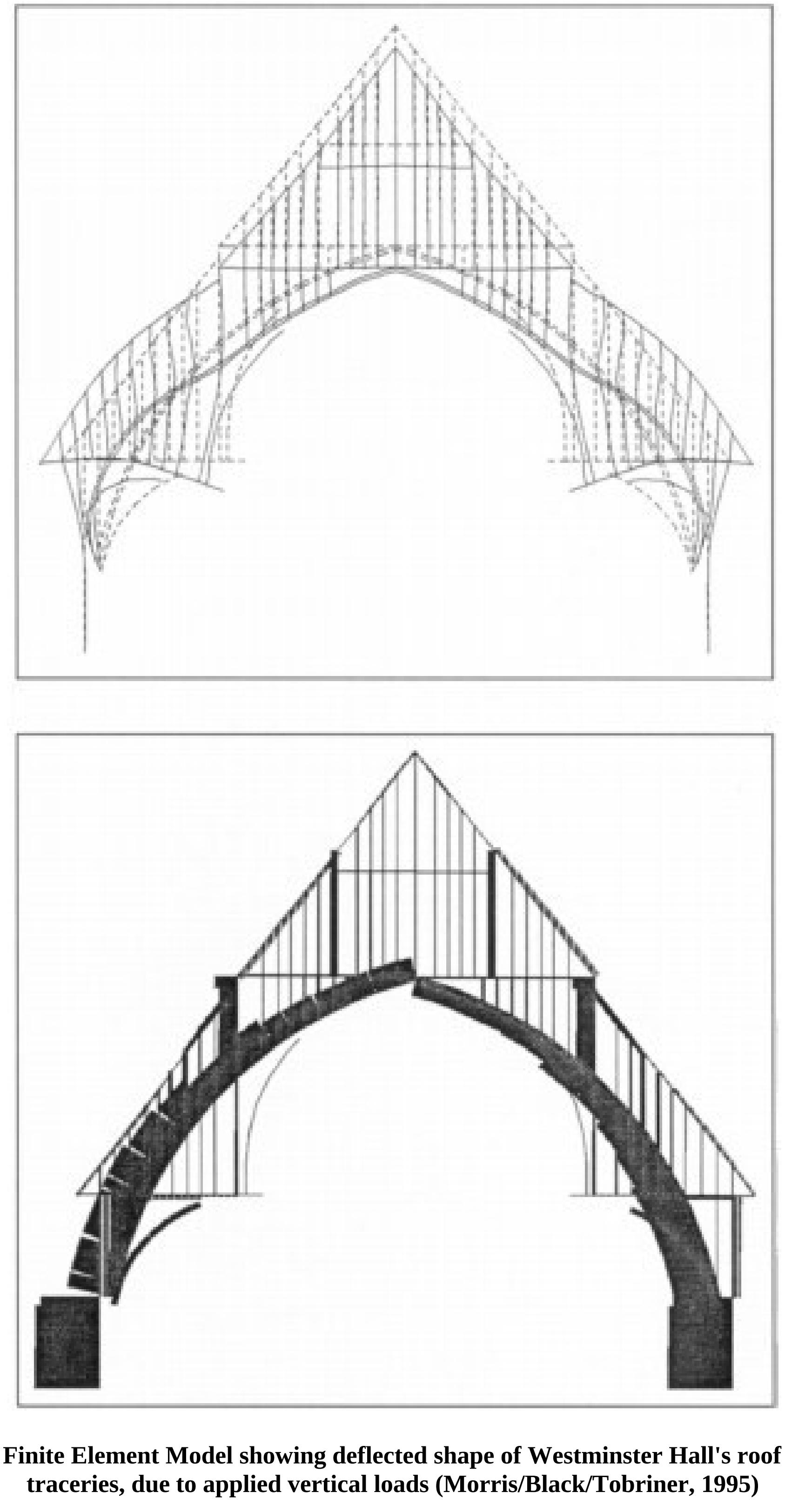

Figure 4: Finite Element Model showing deflected shape of Westminster Hall's roof truss and traceries, due to applied vertical loads (Morris/Black/Tobriner, 1995)

take the form of deflection diagrams, superimposed force diagrams on two or three dimensional representations of structures, or color gradients that simulate load intensity. These visual tools are not only helpful in determining the main load paths through a structure, but may also serve to quickly differentiate between critical structural members and more formal elements. Today, finite element analysis has come to be regarded by many historians and engineers as the best tool to investigate the behavior of historical constructions.[27]

2.4 What is the Finite Element Method

Much of the mathematics of structural analysis takes the form of partial differential equations (PDEs), which may be solved analytically or numerically. Often times, the complexity of these problems render analytical solutions impractical or even impossible, such as in the case of non-linear equations. The finite element method (FEM) is a numerical technique that is intended to solve complex systems of PDEs by converting a continuous domain into a discrete one by projecting the equations from the infinite dimensional space to a finite dimensional space. In so doing, the PDEs are converted from complex equations to a set of simplified algebraic equations, which can be simultaneously solved by computers with relative ease.

In more simplistic terms, the finite element method is analogous to a mosaic, in which very small segments are assembled into a discrete representation of a picture. Each element, like a tessera in a mosaic may be a different shape; for instance, straight lines

[27] Mainstone, Roland J. "Structural Analysis, Structural Insights and Historical Interpretation." The Journal of the Society of Architectural Historians. Vol. 56, No. 3. Sept. 1997. pp. 316-340.

are often used in one-dimensional problems, triangles or quadrilaterals in two-dimensional problems, and tetrahedra in three dimensional problems. These elements are interconnected at a certain number of discrete points along their boundaries, known as nodes. In addition to these boundary nodes, an element may contain additional nodes either along its edge or interior; these nodes contain properties (such as material strength properties) that are specific only to that particular element.

In the finite element method, the value of various unknown variable(s) (displacement, stress, temperature, etc.) are computed at every node location; as such, an increase in nodes results in a more refined solution which will more closely approximate the actual behavior (just as smaller mosaic pieces will tend to better approximate the actual image than large pieces). However, it is also important to evaluate the unknown variable at intermittent points; to do this, one must interpolate between the values at adjacent nodes by defining what are known as interpolation or shape functions. Interpolation functions assume certain local dependence of the unknown (dependent variable) on the domain (independent variable). This relationship may be represented by a linear (the values between the nodes form a straight line), quadratic, or higher order polynomial function.[28] The degree of the polynomial depends on a number of factors such as the number of nodes assigned to the element, the degrees of freedom associated with each node, and continuity requirements imposed at the nodes (Figure 5).[29] While higher order functions generally allow for a more accurate representation of the element

[28] Polynomials are often selected as interpolation functions for the field variable because they are easy to integrate and differentiate.
[29] Often functions are chosen so that the field variable or its derivatives are continuous across adjoining element boundaries.

behavior (and therefore require fewer elements), they are also considerably more expensive with regard to computation time.

After the nodes have been established and the interpolation functions defined, they are then substituted into the original differential equation, or a trial solution in the form of an equivalent integral representation[30]. The equation is then integrated over each individual element and later assembled into a matrix; this matrix, referred to as the local stiffness matrix, is essentially a summary of the properties associated with that element. Because the values of adjacent elements are shared at common nodes, these local stiffness matrices can then be combined into a global matrix that defines the behavior of the entire system. Once the global stiffness matrix is assembled, it can be modified to account for boundary conditions by imposing known loads and displacement conditions at the nodes. When completed, the set of simultaneous algebraic equations can be solved by a computer and the results manipulated in order to compute additional parameters of interest (such as stress, strain, etc.).

Though there are a number of approaches to determining the properties and unknown values associated with the elements, the solution of a continuum problem by the finite element always follows the systematic process described above. To summarize, the following steps are performed:

[30] There are three different ways in which one can formulate the properties of individual elements—the direct approach, the variational approach, and the weighted residuals approach. These will not be elaborated upon in this report; further explanation can be found in Rajasekaran, S., G. Sankarasubramanian. *Computational Structural Mechanics.* Prentice Hall of India. New Dehli. 2001.

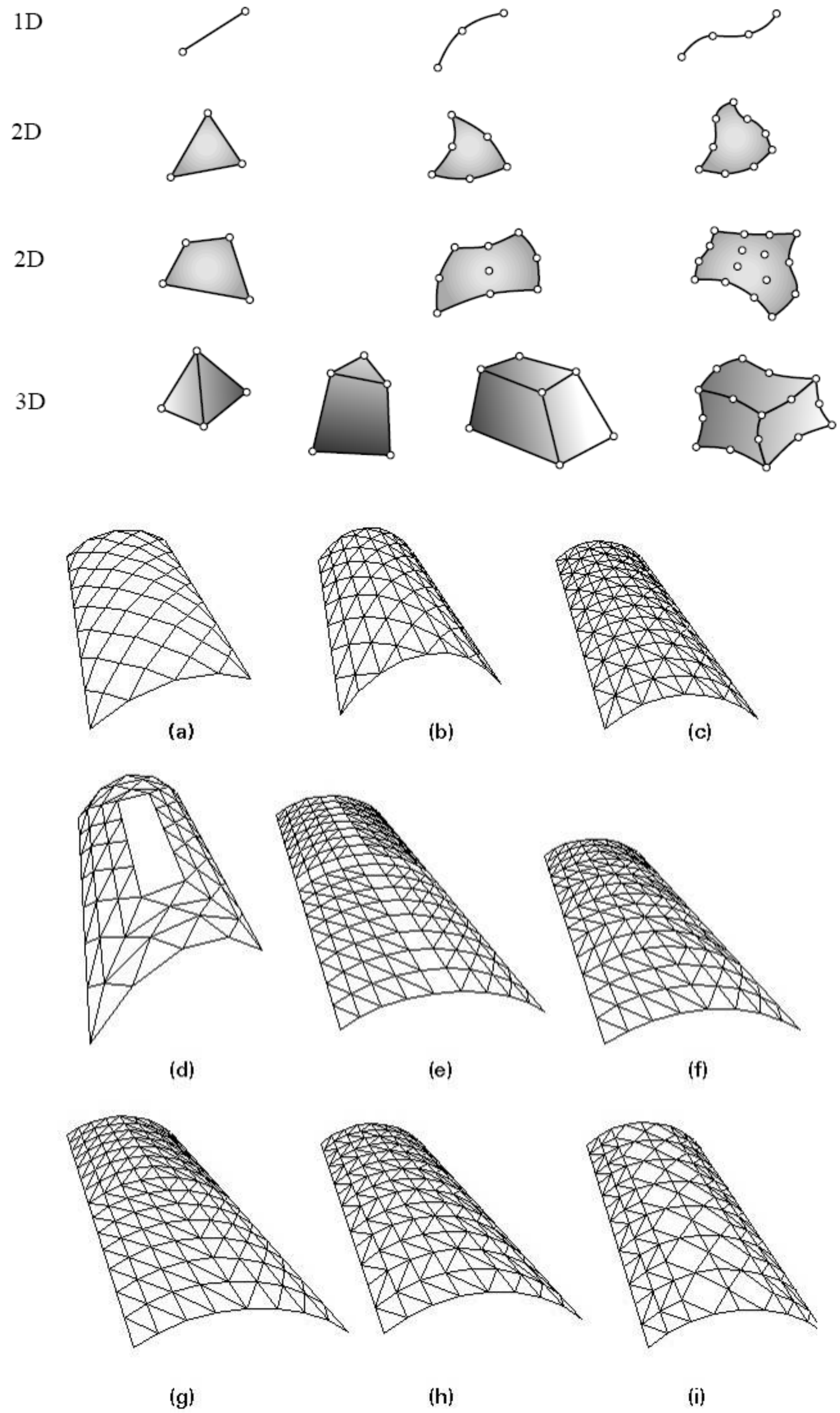

Figure 5: Above: One, two and three dimensional element types (Bau, 2006); Below: Different meshing options for cylindrical vaults (University of Ljubljana, 2000)

1) Discretize the continuum into individual elements;

2) Select appropriate shape or interpolation functions;

3) Determine the element properties and assemble the local stiffness matrices;

4) Assemble the global stiffness matrix;

5) Impose applicable boundary conditions;

6) Solve the set of simultaneous algebraic equations;

7) Extrapolate data from the results.

2.5 FEA Modeling

Current advances in FEA technology have provided us with an unprecedented ability to accurately simulate the behavior of an existing structural assembly. Although the high speed computer has decreased processing time considerably compared to manual calculations, this modern technology has its limitations. FEA allows for very fine discretization, in practice, this is not always a viable option; as such, it is crucial that the user choose a level of modeling complexity that is consistent with the overall accuracy and reliability required of the analysis. The engineer must make informed decisions regarding appropriate geometry, material properties, boundary conditions, loads, and analysis type in order to ensure accurate and useful results.

The necessary accuracy of an FEA model is often a function of the end application of the analysis. There are a number of circumstances that might merit an analysis, including but not limited to: structural failure; performance evaluation; plans for additions or alterations; or even for academic study. Some of these situations may require only simplified approximations of the structure in question. These simplified models are characterized by low order elements or a coarse element discretization (or 'mesh'). Conversely, more refined models are sometimes preferred, consisting of higher order elements and/or a finer mesh.

Often, it is advantageous to use some combination of simplified and refined modeling techniques. This can be accomplished in two ways: through multi-modeling, or through a more recent technique known as substructuring (Figure 6). The former technique merely consists of generating independent models at varying levels of complexity and analytically combining their results; this method is useful at representing behavior at both the macro and micro scale without sacrificing a significant amount of computation time, but it cannot directly incorporate the influence of localized behavior on the overall structure. A more accurate method is substructuring, in which local areas of refined modeling are condensed into 'superelements', which can be directly incorporated into a global simplified model. This technique allows one to consider the effects of local phenomena on the entirety of the structure. While substructuring is an attractive option to many, concerns about how to couple the multiple modeling layers merit further investigation; as such, only a small number of FEA programs have the capability to substructure.

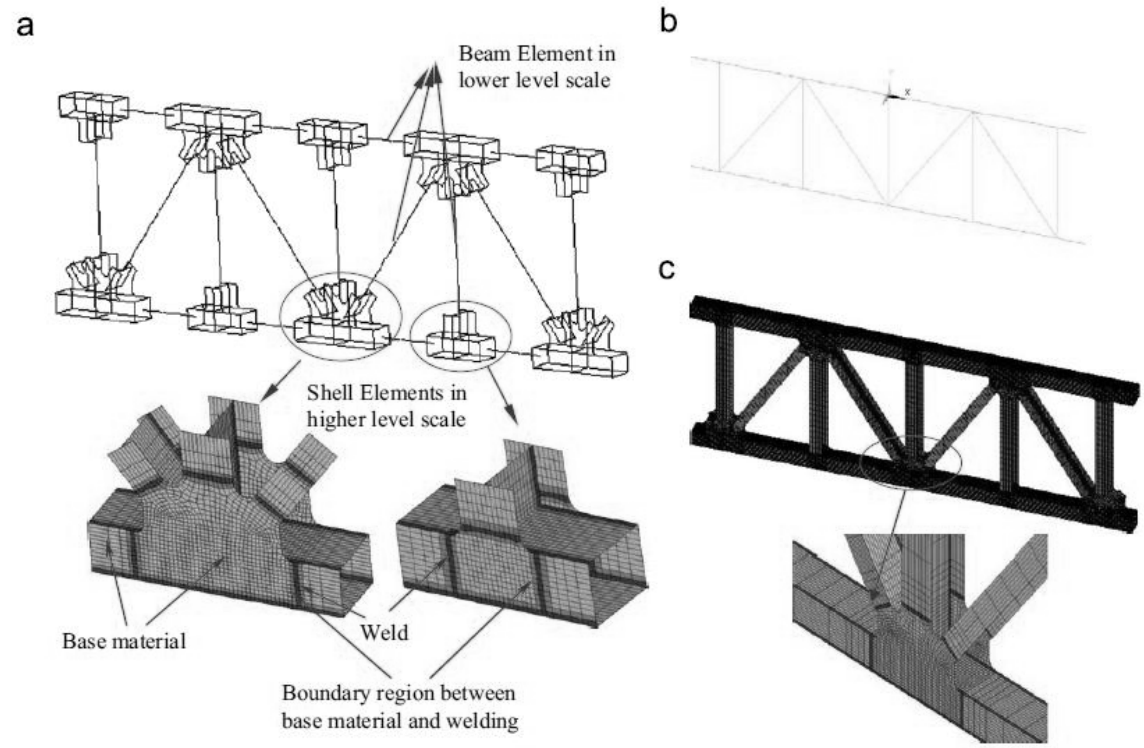

Figure 6: Three models showing (b) beam elements (c) solid elements and (a) multi-scale model with both beam and substructured solid elements (Chan, et al., 2009)

The concepts of simplified, refined, or multi-scale modeling can also be extended to the consideration of boundary conditions or constraints. In traditional structural analysis techniques, end constraints of the structural assembly are most often simulated as fully fixed (no translation or rotation), pinned (no translation) or rolled (translation in one dimension). In addition, it is common practice to assume the loads are concentric as they are transmitted from one element to another. While these approximations are necessary simplifications for manual calculations, (and are often employed in simplified models) they are not necessarily realistic representations of the actual structure; this is a common consideration in the analysis of steel connections which are often designed to be fully fixed or fully pinned, but in practice are rarely either. FEA allows for increased complexity in the modeling of constraints, adding springs, friction and contact restraints, among others to the simple list of fixed, pinned and roller connections. In conjunction with more refined modeling capabilities, the effects of material imperfections (such as splits, cracks, or material loss) or eccentricities can all be considered to more accurately represent connection details. These subtleties can be valuable in cases of failure analysis or damage detection in which connections are often areas of vulnerability, or where localized stress concentrations may influence the behavior of the complete structural assembly.

Equally as important as the geometric representation of the structure is the appropriate designation of material properties. Material properties are a critical but complicated aspect of modeling; while geometry can be recorded and modeled, material properties may be difficult to obtain (particularly in protected historic structures) and their non-homogeneity may make sample testing imprecise or unrepresentative. When sampling and/or testing are not viable options, one must rely on published data or informed assumptions for values. Additionally, many materials will exhibit anisotropic or composite behavior, such as timber or masonry. In simplified models, it is common to assume isotropic behavior or to idealize a composite system (such as mortar and masonry) as a uniform material of some resultant property values. While this may add convenience, it may not always accurately represent the structure.

Perhaps one of the most common shortfalls in the use of FEA is the emphasis of geometric modeling without due consideration of plausible loading scenarios. Determination of load inputs requires understanding of plausible and probable load configurations resulting from the environment as well as occupancy and use of the building. Past loads may be difficult to quantify; while current codes often prescribe load requirements based on probabilistic models, their application to existing structures has its limitations, particularly when actual loads, (rather than code prescribed ones) are needed to assess performance or remaining capacity.

The last area of concern when modeling a structure is the type of analysis that should be performed. The analysis is often dependent on the behavior of the applied loads, which are often categorized as static or dynamic. Static loads are based on the assumption that the structure is at rest (static equilibrium). Static analyses do not consider the time it takes for loads to transfer through elements and reactions are considered instantaneous, rendering them very appropriate for the analysis of dead loads or any other semi-permanent loads. However, dynamic loads (i.e. seismic, vibrational, moving equipment, pedestrian, vehicular, or wind gust loads) change with time and enact considerably different effects on structures due to their short duration and variable intensity[31]. Dynamic analyses are used to determine dynamic displacements, time history and modal frequencies.[32]

Material behavior must also be considered when selecting an analysis method. It has been customary to represent materials as exhibiting elastic behavior; this implies that when loaded, they exhibit a linear correlation between stress and strain, and return back to their original geometric configuration after unloading[33]. This elastic or linear modeling is particularly attractive because it requires a relatively basic understanding of actual material behavior, and leaves less room for the misinterpretation of analytical results. In addition, linear modeling is quite practical if the structure is subject to lower levels of stresses which do not approach the yield strength of the material, past which deformation occurs. However, if the material is loaded beyond its elastic limit, the relationship between stress and strain becomes nonlinear, demonstrated by irreversible deformation known as plasticity. The current understanding of plastic behavior is considerably less developed than the understanding of elasticity, resulting in difficulties in the application of nonlinear analysis techniques. Though nonlinear analysis has the potential for much more accurate modeling of material behavior, its current state of

[31] Dynamic loads can have a significantly larger effect on a structure than a static load of the same magnitude, due to the structure's resistance to deflection (stiffness).
[32] It is useful to know the modal frequencies of a structure as it allows you to ensure that the frequency of any applied periodic loading will not coincide with a modal frequency and hence cause resonance, which leads to large oscillations.
[33] This concept of elasticity was first characterized in Hooke's Law.

development often makes it impractical when not accompanied by adequate parallel efforts of prototype testing, load testing and/or performance data collection.

The availability of FEA as an analysis tool has allowed many disciplines to explore structural behavior in ways that were previously not possible. However, despite the vast capabilities of the tool, it is important that the user be aware of its limitations. Maintaining a healthy skepticism towards computer results is essential when using computer analyses, since engineering or clerical errors in data input or misunderstanding of software limitations may result in catastrophic error. Not only are proper user defined inputs essential to the accuracy of the results, but a thorough understanding of structural behavior is crucial to their interpretation.

3 Historical Background of the Wagner Institute

The Wagner Institute was founded in 1855 by Philadelphia merchant, philanthropist, and amateur scientist William Wagner for the purpose of providing free scientific lectures to the public.[34] Originally housed in Spring Garden Hall at Thirteenth and Spring Garden streets, the institution was forced to relocate just four years later after the hall was recalled by the city. Rather than finding another venue, Wagner elected to construct a new building that would house at once a public lecture hall as well as his personal specimen collection. Though the design of the new building was formally attributed to Philadelphia Architect John McArthur, Jr. (1823 -1890)[35], Wagner was instrumental in both its conception and realization, acting at once as "architect and master builder of the structure"[36]. On March 29th, 1859, work began on the foundations and on site kilns were erected for the construction of the brick walls; just six years later on May 11, 1865, the Wagner Free Institute of Science opened its doors to the public.

The design of McArthur was manifested in the form of a classical Greco-Roman temple. Measuring 60 feet in width by 150 feet in length and 52 feet in height, the main building was situated on a rural plot in northern Philadelphia, —"the highest in elevation of any site located between the Delaware and the Schuylkill Rivers".[37] The main façade faced north and was composed in three bays, separated by paired pilasters and pierced by a large arched window. The pedimented roof gable was duplicated at the top of the

[34] For a more thorough description of the institute's significance, please refer to the National Register of Historic Places nomination and the Historical American Buildings Survey entry.
[35] McArthur would later go on to design and construct Philadelphia City Hall.
[36] Jacobs, James A. *Historic American Buildings Survey*, Wagner Free Institute of Science. HABS no. PA 6667 (2000).
[37] Gredell, Gary. Structural Condition Assessment: Roof and Upper Masonry Walls, Exhibition Hall. Gredell & Associates Structural Engineers. 27 Sept 2008.

windows in the exterior bays, which flanked a wooden entrance portico. The east and west elevations were segmented into nine bays separated by single pilasters and pierced by two story windows. The composition was completed by a classical dentil cornice; however, the walls, which were to have been rendered and incised to mimic ashlar, were left unfinished. (Figure 7)

The interior of the main building consisted of two main stories; the first story housed the lecture hall, modeled after that in the Smithsonian[38], and a large hallway, flanked by eight classrooms and two large staircases that led to the second floor. Above this space was the large exhibition hall which housed Wagner's specimens. With the exception of various small offices and laboratory space, the hall measured nearly the full foot print of the building and was encircled by two tiers of gallery space above. The structure was capped by a large barrel vault roof system (Figure 8), supported by eight arched trusses, set on masonry pilasters in the sidewalls, and topped with a tar and gravel surfaced roof membrane laid on a wood deck.

The building's main structural system was typical for the era, consisting of exterior brick bearing walls and an interior iron columns, girders and beams. The layout of the interior cast iron columns mimicked the tripartite division of the main façade, with two rows extending the length of the building. Supported on the columns sat wood girders and floor joists that framed the floor structure. With the exception of a one story brick wall extending to the underside of the exhibition hall floor, flooring assembly and roof deck acted in the form of rigid diaphragms as the building's only lateral restraint.

---

[38] HABS no. PA 6667 (2000).

Figure 7: Southwest Perspective of the Wagner Free Institute (Photograph by Joseph Elliot for the Historic American Building Survey)

Figure 8: Barrel Vaulted Ceiling and Arched Trusses of the Wagner Institute (Photograph by Joseph Elliot for the Historic American Building Survey)

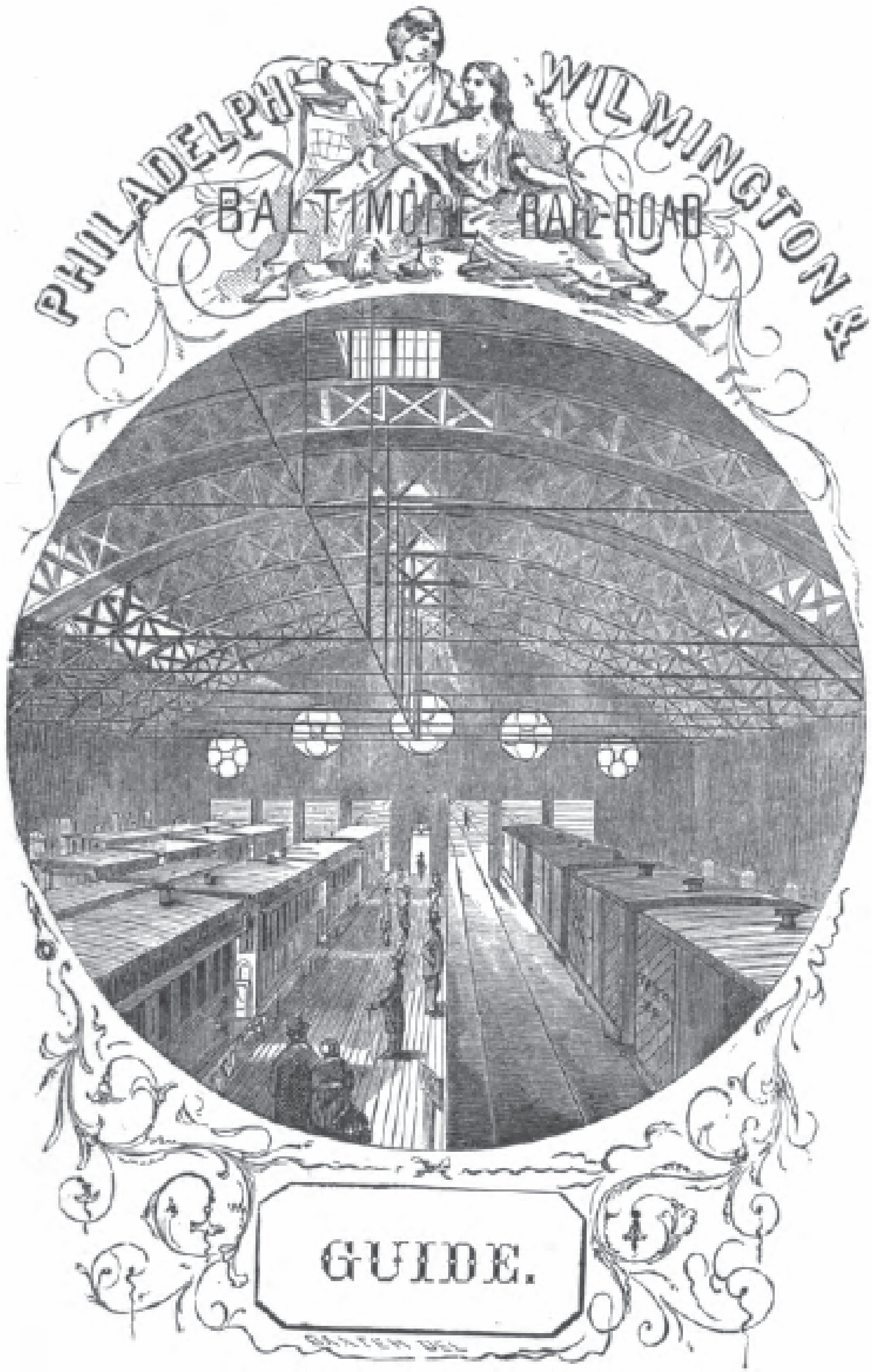

Figure 9: Cover page to the Philadelphia, Wilmington & Baltimore Railroad Guide (Dade, 1856); notice the vaulted ceiling, comprised of arched Howe trusses.

The structure of the building remained for the most part exposed throughout, more akin to an industrial structure than the classical temple of the exterior.

The industrial nature of the exposed columns was reinforced by the use of eight arched trusses that composed the roof structure. In contrast to the more traditional construction of the rest of the building, the trusses represented a nascent, state of the art technology, customarily seen at that era in bridges or train sheds construction. In fact, this particular truss system was based on the patent by Philip Quigley[39], who, prior to becoming a founding partner in the bridge building firm of Stone, Quigley and Burton in 1851, had been chief bridge engineer of the Philadelphia, Wilmington and Baltimore Railroad.[40] Just seven years prior to the construction of the Wagner Institute, this railroad company had completed the nation's first vaulted train shed at the Broad and Prime Street Station in Philadelphia, boasting a curved roof supported by "arched Howe trusses of wood."[41] (Figure 9) Both the Broad Street Station and Wagner roof trusses appear to have been adaptations of the Howe truss[42], a popular system for bridges at the time. (Figure 10) The Howe truss is composed of two identically sized chords which are tied together by a system of vertical rods and diagonal bracing. In the case of the Broad Street station, all of these elements were construction of wood, while the Wagner adaptation employed

---

[39] The patent number for the roof truss could not be obtained.

[40] Stone, Quigley & Burton rebuilt the Orange and Alexandria Railroad, and the aqueduct over the Potomac at Georgetown, and the Georgetown and Alexandria Canal. In 1875 they built Machinery and Agricultural Halls, of the Centennial buildings in Philadelphia.

[41] Dare, Charles P. *Philadelphia, Wilmington and Baltimore Railroad Guide: Containing a Description of the Scenery, Rivers, Towns, Villages, and Objects of Interest along the line of the Road.* Fitzgibbons & Van Ness. Philadelphia. 1856. Earlier references to this type of roof framing system can also be found in Pottstown, PA. "At Pottstown station, 18 miles below Reading, extensive and efficient shops have also been erected…the first shop is covered with a neat and light roof, built of an arched Howe truss, forming a segmented circle, 78 ¼' span by 16' rise." This system would also be duplicated in the construction of the first Grand Central Station in New York in 1869-1871.

[42] The Howe truss was patented by Massachusetts millwright William Howe in 1840.

the more common practice of using iron rods for the vertical elements. Both trusses utilized a system of x-bracing[43], which places the braces in compression and the vertical elements in tension. The main braces are kept full length while the counter bracing is composed of two separate pieces which fit into shallow notches in the main brace. These braces do not rest directly on the chords but rather bear on iron blocks, through which a pair of the iron verticals passes. These verticals are secured by a washer and nut and by tensioning them, the chords are drawn together. These sections of bracing bounded by verticals are referred to as panels.

The Wagner trusses are essentially the Howe truss, but rather than being straight, both chords are arched at a radius of approximately 73 and 75 feet, with the top chord having the greater radius.[44] Both the top and bottom chords measure 2 ½ inches high by 7 ¾ inches wide in cross section and are composed of two pieces which are scarf spliced (see figure) and bolted with three bolts at variable points along the truss. The truss is composed of 28 panels, spaced at approximately 25 inches on center; the cross bracing measures 1 ¾ inches x 6 inches and rests on 6 inch long iron bearing blocks, while the paired verticals measure ⅝ inches in diameter and are spaced at 3 ⅜ inches on center. (Figure 11)

The Wagner arched trusses can be structurally classified as two hinged arch trusses. This type of system essentially requires that the arch be continuous and that it

[43] As opposed to the more traditional use of single braces oriented up toward the center of the top chord. By angling the braces as such, it allows for the braces to act as compression members and the verticals to act in tension. By orienting the braces the other direction, it would place the braces into tension and the chords into compression. This is referred to as the Pratt truss.

[44] It is not known whether the chords were steamed before they were bent, however it would not have been uncommon to do so, given the size of the members and the mechanical force required to bend them.

have restraints at both ends which prevent translational (but not rotational) movement. The ends of the arched trusses must be restrained by means of rigid supports to resist horizontal thrust; due to the statically indeterminate nature of the system, these supports must be generally unyielding as any movement can result in large changes in the stresses in the arch. Often, the horizontal thrust is taken up by means of a tie rod between the two end hinge points; this allows all vertical forces to be transferred through the abutments, while the horizontal forces are taken up by the tie rod.

The Wagner trusses bear on the exterior brick bearing walls and the ends of each truss are tied together with 1 ⅝ inch diameter tie rods, supported at mid-span by a ⅝ inch diameter iron hanger suspended from the bottom chord. The tie rods pass through a 6 inch by 8 inch wooden bearing block, and are secured with a 5 inch square plate and nut at each end; it is tensioned by means of a turnbuckle located at approximately mid-span. The 4 foot long bearing block is notched to receive the bottom chord of the truss, while the upper chord continues unrestrained to the interior side of the non-structural cornice. The brick masonry wall continues up and around the iron verticals and wooden braces that extend into the cornice soffit, providing the only means of lateral restraint (in the direction of the wall line) at the arch ends.[45]

The arched trusses carry the remaining roof structure, which consists of purlins that span in the north-south direction between trusses. The purlins measure approximately 2 ¾ inches wide by 8 inches high and are notched approximately one inch on the bottom

[45] It was common in structures contemporary with the Wagner to anchor one end of the truss to the wall and to leave the other end unrestrained if a tie rod was used. The purpose of this was to ensure that the truss moved with the wall in the event of a lateral load. Conversely, the Wagner trusses rely only on friction between the brick and the wood to restrain the trusses.

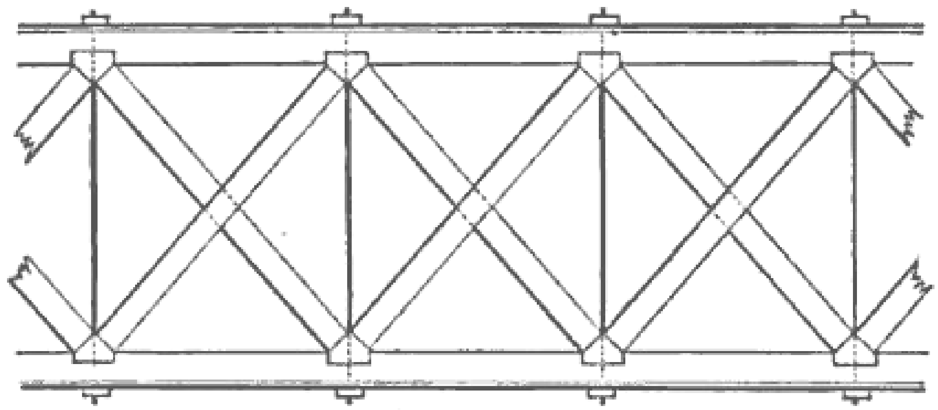

FIG. 187.

Figure 10: Howe Truss (Wheeler, *An Elementary Course of Civil Engineering for the Use of Cadets of the United States Miltary Academy,* 1877. p. 361)

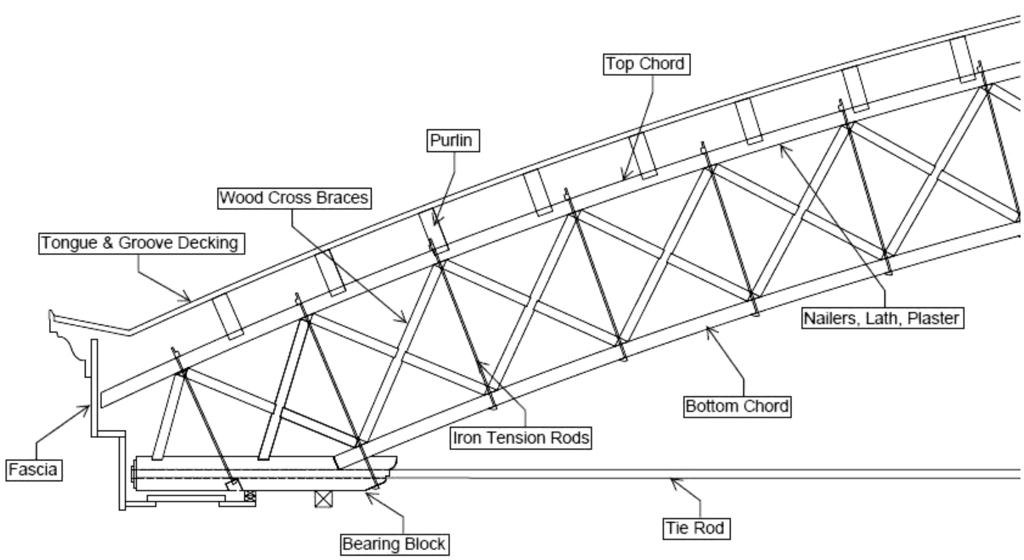

Figure 11: Section of Wagner Institute Roof Assembly at Arched Truss (drawing by author)

where they land on the top chord and are half lap spliced together. The purlins are spaced at 46 inches on center and span two bays; the purlins are toe nailed to the trusses at most intersections, however three bolts are present in each truss which pass through the top chord and the spliced purlins. The purlins transfer loads acting on the roof deck structure to the arched trusses. Fastened to the top of the purlins is the roof deck, composed of 4 inch wide by 1 inch thick tongue and groove boards which curve in the same direction as the arches. Together, the purlins and the tongue and groove decking form a semi-rigid diaphragm, holding the top chords of the arched trusses in their proper spacing. However, because the bottom cords of the arched trusses are unbraced laterally, the roof diaphragm provides is not sufficient to prevent racking.[46]

In addition to their structural function, the purlins support the wood lath and plaster ceiling assembly through a system of 2 ¾ inches wide by 1 ¼ inches thick nailers, spaced 16 inches on center and running parallel to the trusses. Wood lath, measuring 1 ⅜ inches wide and approximately 4 feet in length, is in turn nailed to these nailers, leaving gaps of approximately ⅜ inch for plaster keys. Plaster of variable thickness ranging from ½ inch to ⅝ inch covers the lath.

In 1875, a decade after the completion of the Wagner Institute, the tar and gravel roof was replaced with a new tin sheet roof. Just ten months later, a severe storm struck Philadelphia, accompanied by record wind gusts near 70 miles per hour, which "rooled [sic] up the New Tin Roof of the Hall into a Scroll and carried it off into an adjoining

[46] According to building literature of the day, systems of these trusses were often utilized in larger configurations, and therefore required greater spacing between the arches. This spacing often required the use of framed trusses between the arches. These trusses formed the bracing required for the arches.

lot"[47], allowing for severe interior water damage due to the accompanying rains. Just three years later, the newly replaced roof was damaged once again, when "a tremedious gale[48] passed over our City, tearing off more than half of the tin on the Roof of the Institute building and five of the tere cotta chimneys and demolishing much of the fence around the building."[49] A subsequent rainstorm again caused further damage to the building's interior.

William Wagner's death in 1885 provided the Institute's trustees with a large amount of his estate to be used for the purpose of building improvements.[50] The trustees hired the firm of Collins & Autenrieth[51] to assess and repair the structure as needed. In a letter dated February 28, 1885, Collins and Autenrieth expressed concern over the structural integrity of the building based on their personal observations. Much of the structural cast iron construction appeared to have been undersized and poorly supported; exposure of the exterior walls to the elements (the originally specified stucco had been omitted by Wagner during construction) had resulted in severe deterioration of mortar and the creation of open joints, leading to rot in the floor joists; the east and west walls appeared to have "bulged" 5 ½" inches to the east; and the plaster ceilings through the building were found to be in such poor conditions to merit complete replacement.

---

[47] Collins & Autenrieth. Letter Report. *Conditions Assessment of the Wagner Institute.* 28 Feb 1885.
[48] This time, the wind gust was recorded to be 85 miles per hour, with a 1-minute average speed of 75 miles per hour, the strongest wind ever recorded in Philadelphia.
[49] Ibid.
[50] The timing for this overhaul coincided with tremendous changes in the city. Where the Wagner had previously stood isolated amidst a bucolic landscape of country houses and farms, it was quickly overtaken by the expanding city.
[51] Both Collins and Autenrieth had been under the employ of John McArthur prior to their collaboration in their own firm.

Collins and Autenrieth proposed a number of repairs to the Wagner Institute building. In addition to extensive strengthening of the foundations, and replacement of the undersized iron columns, beams and rotted floor joists, the exterior walls received their originally intended stucco finish.[52] The two interior east-west walls were extended from the first floor to the third, to increase the lateral stability of the building (Figure 12). A number of improvements were also made to the roof structure. Intermediate purlins were introduced between the existing ones, notched and toe nailed into the top chords to match the existing. One row of bridging was added at the midpoint of the arched trusses. Skylights were also added in three of the sections, extending between two trusses and three purlins, measuring 7 ½ feet by 16 feet. The existing plaster ceiling was in such poor condition that it was removed to the purlins, and covered with two thicknesses of felt sheathing paper for insulation, secured by nailing strips to receive the new plaster.[53]

The Wagner Institute building saw its last large scale construction campaign in 1901, when the firm of Hewitt & Hewitt was hired to construct a library addition on the west side of the main structure. The addition measured 47 feet by 56 feet and was designed in a similar classical motif as the original building, complete with a matching stucco finish and large skylight.[54] The impact of this new addition on the original structure was limited, with the exception of some adjustments to the wall where new met

---

[52] This stucco was simply applied and not rendered to look like stone as originally planned.
[53] Collins & Autenrieth. Specifications for the Improvement of the Wagner Institute. 1885.
[54] HABS no. PA 6667 (2000).

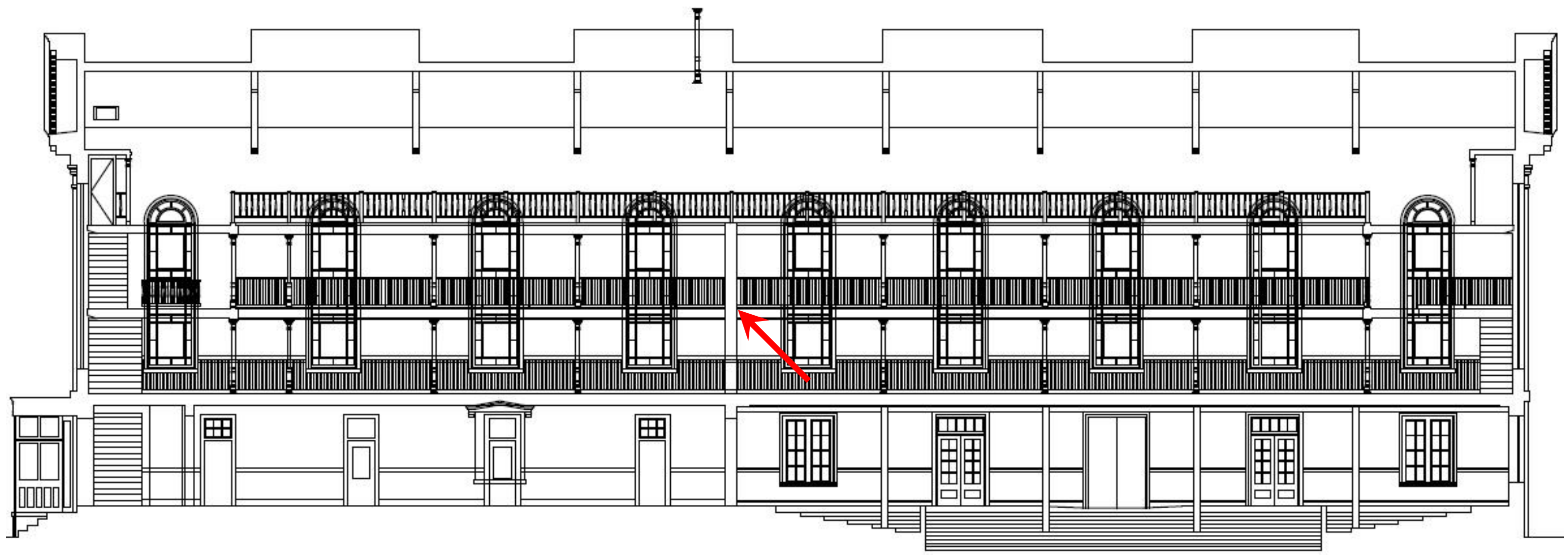

Figure 12: Longitudinal Section of the Wagner Institute Building. Note the interior shear wall, extended by Collins & Autenrieth to the third floor balcony for lateral stability (Drawing by Mark Thompson)

old; here, the two lower window openings were expanded to accommodate doors and the upper windows reduced in size and partially blocked for the roof to wall intersection.[55]

Records of building performance after 1901 show a persistent history of water infiltration, both through the exterior stucco and the skylights, as indicated by a series of repair receipts. However, the record shows little mention of any observed structural movement, with the exception of some wall cracks, and exterior cracks located above the arched windows. In both cases, cracks were considered to be a common occurrence in older buildings, and were attributed to settlement and vibrations from passing traffic. In December 2003, a large section of ceiling plaster detached from the lath and fell to the floor, prompting concerns about the integrity of the roof structure and the stability of the remaining plaster. As a result, structural engineers were consulted to investigate the structural behavior of the roof.

[55] Goeke, Marlene. *Assessment and Analysis of the Plaster Exhibit Hall Ceiling at the Wagner Free Institute of Science, Philadelphia, PA.* MS Thesis, University of Pennsylvania. 2008. p. 55.

4 Summary of Structural Assessments for the Roof of the Wagner Institute

Over the past 15 years, there have been three substantial investigations of the roof structure of the Wagner Institute.[56] The first investigation was completed in 1994 during a restoration campaign which included the replacement of the tin roof. The Philadelphia structural engineering firm of Keast and Hood Company, noted for their experience in historic structures, was hired to perform an evaluation of the arched trusses. Keast & Hood performed a visual inspection for both structural deficiencies and decay, as well as core sampling for wood pathology analysis.[57] Though the scope of the work did not include a detailed structural analysis, Keast & Hood's report discussed the assumed mechanism of the roof framing system. Their report assumes that both chords act entirely in compression, with the highest compressive forces occurring at the crown of the arch in the top chord and at the ends of the arch in the bottom chord. The diagonal braces in the truss panels are also believed to carry compressive forces which gradually increase in magnitude as they approach the ends.

In 2005, two years after the detachment of a portion of the plaster ceiling, Donald Friedman, PE, of Old Structures Engineering PC was hired to investigate the impact of structural movement on the plaster ceiling,.[58] Friedman's investigation included visual observation of existing conditions of both the trusses and the walls above the fourth floor. Friedman analyzed the roof framing system based on five different scenarios of structural action while subject to the expected dead, snow, thermal, and wind loads.

[56] For reports on the plaster ceiling, refer to Marlene Goeke's thesis and Building Conservation Associates findings.
[57] Refer to Appendix III for the full report.
[58] Refer to Appendix II for the full report.

In the first scenario of Friedman's analysis, the arched trusses were assumed to be point loaded by the purlins. The top chord was treated as the principal load-carrying member, with the bracing, vertical members and bottom chord serving as local stiffeners. The tie rod was assumed to be functional, taking up the horizontal thrust of the arch. In this scenario, the analysis indicated overstress in the top chord when both dead and snow loads were applied; in addition, unbalanced wind or snow load would generate an asymmetrical deflection of 1 ½ inch.

In the second scenario, the bottom chord was also considered to be in compression, suggesting true truss behavior. This scenario resulted in similar results to the first scenario, and the stresses were determined to be within acceptable limits for the combined dead and snow loading. In both first and second scenarios, thermal loads on the truss resulted in a maximum downward deflection of ¼ inch.

Friedman's third scenario assumed the same conditions as the first scenario; however, tie rod action is neglected, simulating a situation where the tie rods were installed too loosely, or the tops of the masonry sidewall walls moved toward each other, or the wooden bearing blocks had failed in shear, preventing thrust transfer to the tie rods.. In this third scenario, the unresisted horizontal thrust of the arch creates excessively high shear stresses in the masonry wall. Friedman suggested that if masonry strength were the limiting factor, the roof would be incapable of carrying more than 2 percent of the combined dead and snow load.

Friedman's fourth and fifth scenarios assume vault action of the roof structure. In the fourth scenario, the tongue and groove planking contributes to the load carrying capacity of the roof. Because the roof deck is pierced by the skylights in every other bay, the roof is assumed to display both vaulting action (in the bays where skylights are no present) and simple truss action (in the bays where skylights are present). Though the stresses in all elements were within acceptable limits, the vault areas generate similar end thrusts as in the scenario where the tie rod action is neglected. The fifth scenario is identical to the fourth, however the plaster and lath are also considered to contribute to the diaphragm. Friedman suggested that this scenario is counterintuitive however; if the plaster were in compression in only half of the bays, the cracking in those bays would differ considerably from the cracking in the others.

Friedman concluded that the roof structure is most likely performing as an arched truss, as described in his second scenario. Though his findings indicated that roof structure itself is structurally sufficient in terms of allowable stress, the movement of the roof due to thermal, snow and wind loads would be sufficiently large to crack the plaster ceiling. In a subsequent letter, Donald Friedman indicated that the maximum differential movement under dead and snow loads is approximately 1/8" per foot, or L/100.[59] This exceeds the generally-accepted allowable limit of L/360 (or 2" for a 60 foot span) for structural deflections of members supporting plaster. He follows with a recommendation to incorporate expansion joints to accommodate for this movement rather than stiffening the trusses to limit deflection.

In September of 2008, yet another structural investigation of the roof structure was performed by structural engineers, Gary Gredell & Associates, yet another firm

[59] Friedman, Donald, P.E. Memorandum to William Stivale, Building Conservator: Wagner Museum Design. 7 Jan 2008. See Appedix II for full document.

experienced in historic buildings.[60] The purpose of the Gredell report was to assess the structural condition of the roof and exterior masonry walls above the 4th floor gallery to determine if their structural performance was adversely affecting the plaster ceiling. Gredell performed visual observation, probing and measurements in order to inform their analysis.

Gredell's analysis of the roof structure was based on a two dimensional structural model of a truss, evaluated under conditions which included dead, snow and thermal loads. The results of the analysis indicate behavior similar to that described in both the Keast & Hood and Friedman reports, with the top chord acting in compression with greatest forces occurring at the crown, and the bottom chord also in compression, with the greatest forces occurring at the ends. Under applied dead and thermal loads, the stresses in the truss were deemed acceptable; Gredell's assertion that maximum vertical deflection due to thermal loads is ¼ inch corroborates with Friedman's analysis. In addition, the maximum vertical deflection due to the applied dead and snow load was estimated to be 7/8", indicating a deflection ratio of L/880—considerably lower than the generally accepted value of L/360 —which considerably contrasts Friedman's estimation of L/100.

Though Gredell's analysis deems the truss members themselves to be structurally sufficient, under the combination of dead and snow loads the tie rod was deemed to be overstressed by 10% in tension, and the bearing block overstressed at 40% at the birds mouth notch where the bottom chord intersects the bearing at an angle to the grain. In addition, arched truss load on the bearing block would create excessively high

---

[60] See Appendix I for full report.

compressive stresses in the masonry wall on which it bears. As a repair, Gredell suggests a horizontal mortise at the interface between the bearing block and the bottom chord, and epoxy bonding the two bearing block pieces together, while inserting a bearing plate below them to increase the bearing area. In addition, Gredell suggested tensile reinforcement of the masonry wall by means of glass rods transfer eccentric loads from the bearing block.

Gredell's report also addresses the issue of lateral stability. Per his analysis, the roof deck contributes minimally to the lateral stability of the building with a strength of 20 percent of that required to achieve the desired stiffness; this is governed by the lack of resistance provided by the limited nail connections. The addition of plywood sheathing, glued and nailed to the existing tongue and groove decking and into the purlins is recommended in order to increase stability.

5 Recorded and Observed Conditions

Prior to performing FEA structural analysis, this author performed a conditions assessment of the roof structure. The purpose of this was threefold: first, to validate or challenge the observations indicated in previous reports; second, to build on previous conditions assessment with new observations of conditions that may have occurred since previous observations; and three, to accurately measure the geometry and configuration of the roof structure in order to generate a comprehensive structural model. The conditions described herein are a compilation of those observed in the various reports discussed in the previous section, and those observed and measured by the author. They include data regarding movement and displacement, signs of structural damage or failure, and the general condition of the structural elements.

5.1 Physical Conditions

5.1.1 Alignment

The horizontal and vertical alignment of the brick bearing walls and the roof structure has been studied separately by both Gary Gredell and this author. The horizontal alignment of the roof structure was measured at each of the truss end locations relative to the east and west wall lines of the building. As indicated in Figure 4 of Gredell's report (Figure 13, Woodman) the walls appear to have bowed eastward; the west wall appears to have bowed slightly more, exhibiting a maximum displacement of approximately 6 ¼", while the east wall exhibits a maximum displacement of 5 inches—corroborating with Collins & Autenrieth's reported observations of 1885. The walls both appear to displaced off center from the mid-span of the wall, biased towards the south, with the greatest displacement occurring at truss line 7. Subtracting east wall displacement from the west results in a maximum decrease in truss span of 2 ⅜ inches, occurring at truss 3; though this appears to be a localized outlier, as it is nearly twice the next largest value of 1 ¼ inches, occurring at truss lines 6 and 7.

The vertical alignment of the roof structure at the truss ends was also measured by Gredell (see Figure 14, Woodman). Measurements were taken from the bottom of the tie rod at each end. Generally speaking, the east wall appears to be at a higher elevation than the west, with a maximum difference of approximately 1 inch. In addition, the elevation increases as the wall leans more along one wall; in other words, the elevations of the bottom of the bearing blocks are for the most part ½-1 inch higher in the center of the walls than towards the ends.

Lastly, the lean of the walls was also measured in elevation at varying truss end locations, as indicated in figure 11 from Gredell's report (Figure 15, Woodman). From grade to the second floor level, the misalignment of the walls is relatively small, while above this, lean increases significantly. Gredell attributes this to the lack of lateral stability provided by the floor and roof diaphragms above the fourth floor. While not all of these measurements were field verified, they were spot checked by the author and deemed sufficiently unchanged since their initial measurement by Gredell in the summer of 2008. In addition, there does not appear to be excessive exterior stucco damage, further confirming that the majority of the wall displacement had occurred during the storms of the late 1870s.

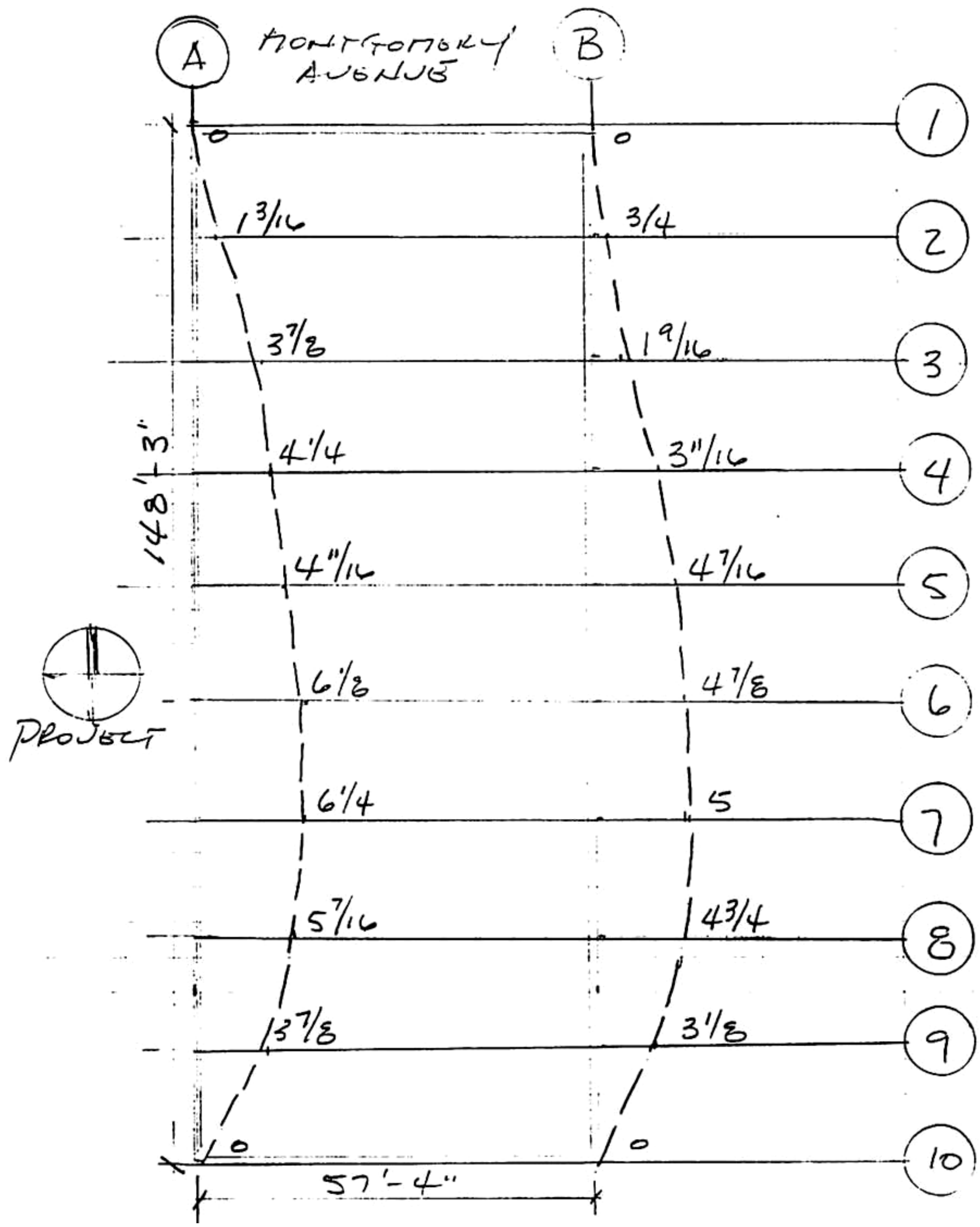

Figure 13: Horizontal Alignment of the East and West Walls (Drawing by Gary Gredell, 2008)

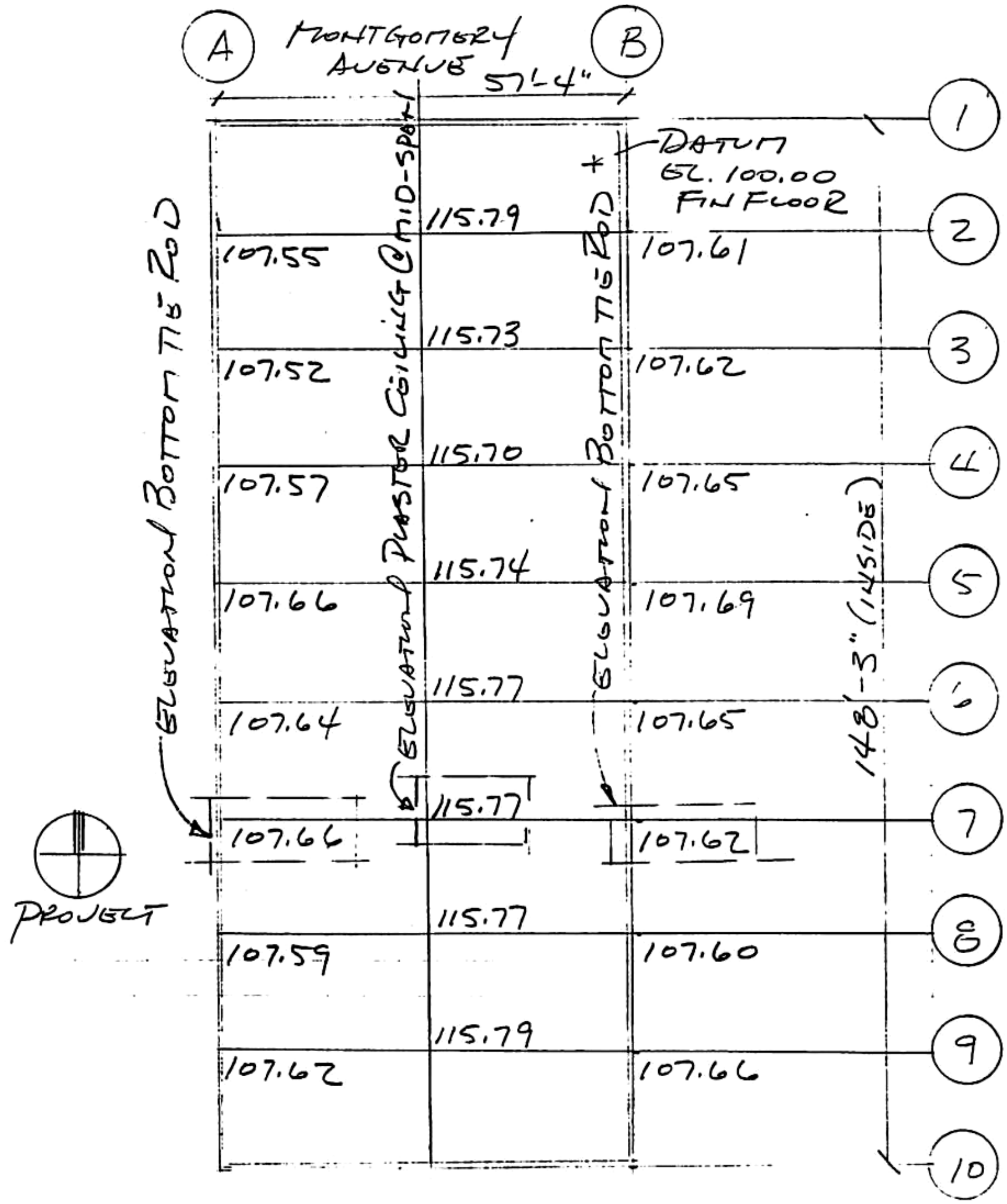

Figure 14: Vertical Alignment of east and West Walls (Drawing by Gary Gredell, 2008)

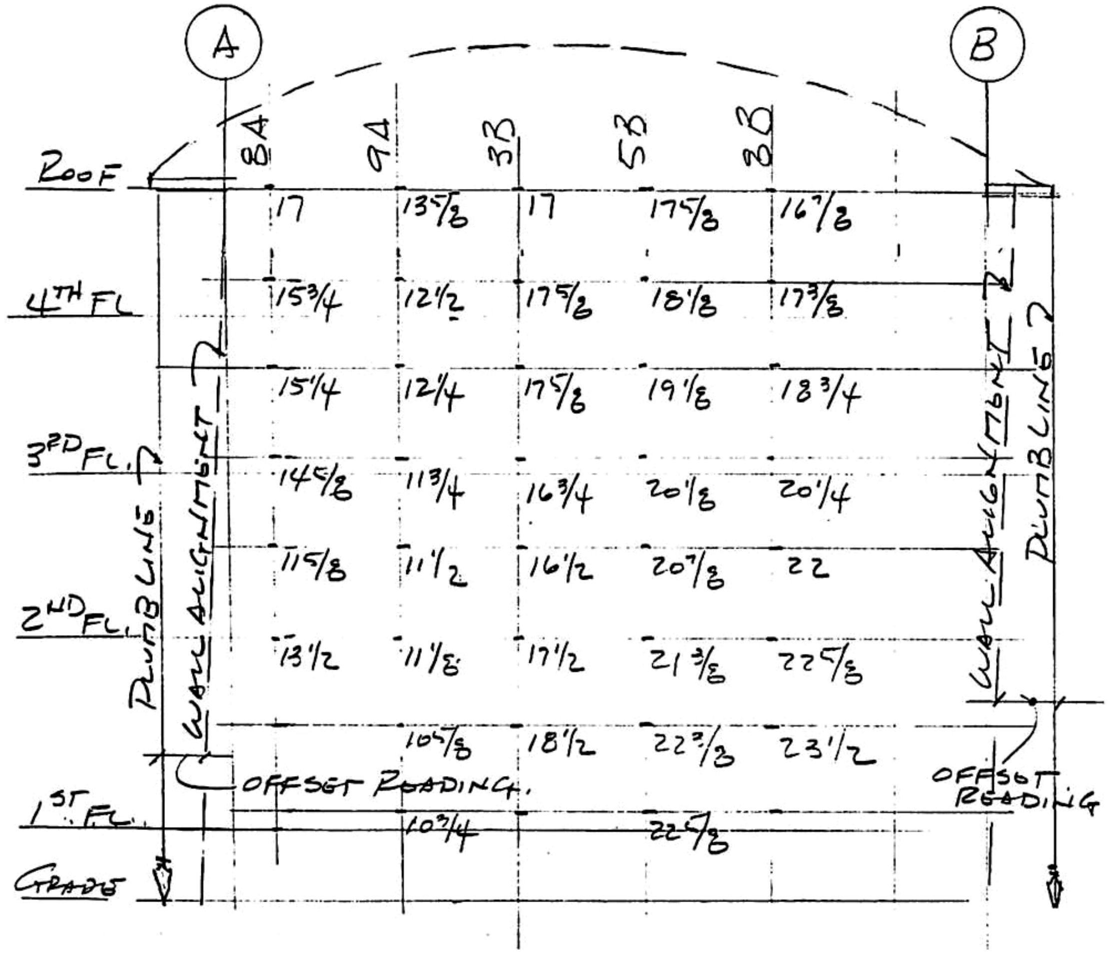

Figure 15: East and West Wall Alignment (Drawing by Gary Gredell, 2008)

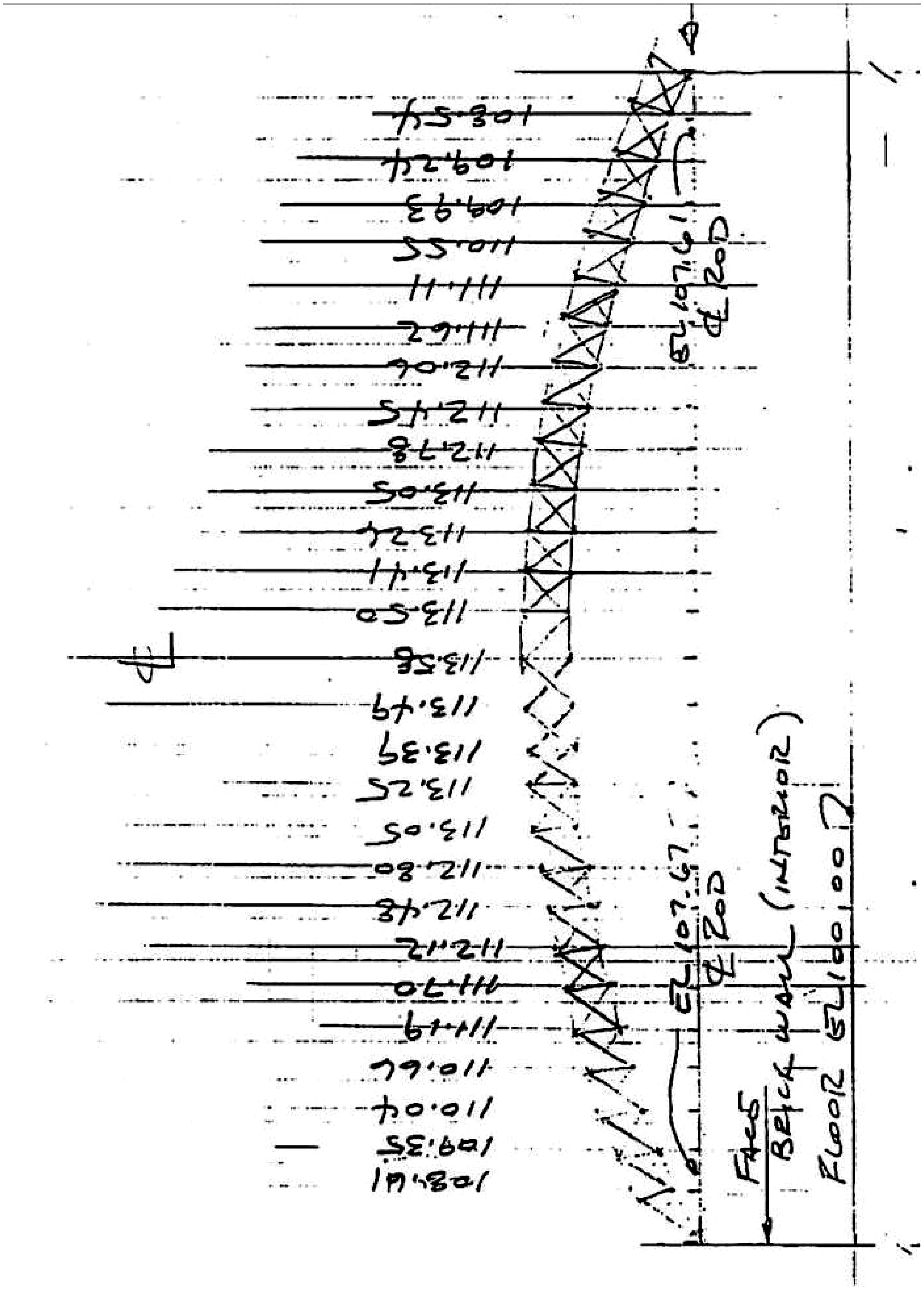

Figure 16: Vertical Alignment of Truss 3 Panel Points (Drawing by Gary Gredell, 2008)

5.1.2 Masonry Walls

In addition to the gross displacement exhibited by the side walls, the masonry itself shows signs of both previous and continuing damage. The Keast & Hood report notes areas of spot masonry repair at the underside of the cornice. Later, the Gredell report describes areas of severe erosion of the brick in the corner. These conditions are most likely linked to the poor condition of the cornice, which exhibits severe decay due to moisture.

5.1.3 Truss Chords

With the exception of some water staining, the chords of the truss appear to be in sound condition. The top chord does exhibit some decay, but according to wood pathologist Joe Clark[61], the decay is superficial and does not extend to areas of high stress or critical joints. However, there are some indications of splitting and crushing at the perpendicular bearing interfaces of the bottom chord splices at almost every truss Figure 18**,** Figure 19). This condition was unconfirmed at the top chords due to the nailing strips fixed to the underside of the member.

Two forms of truss displacement were also noted. Vertical movement was measured by Gredell at truss 3—the truss that exhibited the greatest relative horizontal displacement. As evidenced by Figure 16, the results of the measurements indicate simply that the truss is tilted down towards the east wall. This was later confirmed by the author by the use of a total station. The total station results also revealed rotation of the

[61] Clark, Joe. Letter to Thomas Leidgh, Suzanne Pentz. Wagner Free Institute of Science. 8 October 1994.

truss about its bearing points, as discussed in Friedman's report. However, maximum lateral displacement of the top chord was measured to exceed 2 ½ inches in the worst case (truss 3), which does not corroborate Friedman's assertion that the upper chords appeared to remain straight due to constraint by the purlins and roof deck (Figure 17). The measurements also show that the bottom chord has tilted out of plane in the same direction of the top chord, with the maximum out of plane displacement of the bottom chords measured at approximately 3 inches, which corroborates Friedman's report. This displacement is predominately in the form of a single curve (truss lines 2-5, 8), but also appears as an S curve (truss lines 6, 7), and a double S curve (truss line 9). The direction of the lateral sway appears to alternate, with trusses corresponding to lines 2-5 bowing predominately to the south, while trusses corresponding to lines 6-9 are bowing to the north. **(**Figure 17)

5.1.4 Truss Panel Diagonals

The diagonal cross braces of the truss panels show water stains on their surface, but do not appear to be threatened by decay or structural overstress. In fact, a number of the diagonal spacers were observed to be loose, many of then separated from either the main diagonal or the iron bearing block by up to ¼ inch. In multiple instances, these blocks also appear to be shifted out of the vertical plane of the truss by up to ½ inch. The bracing members also appear to be rotating out of the vertical plane in many instances, corresponding to the lateral displacement of the bottom chords relative to the top chord. (Figure 20)

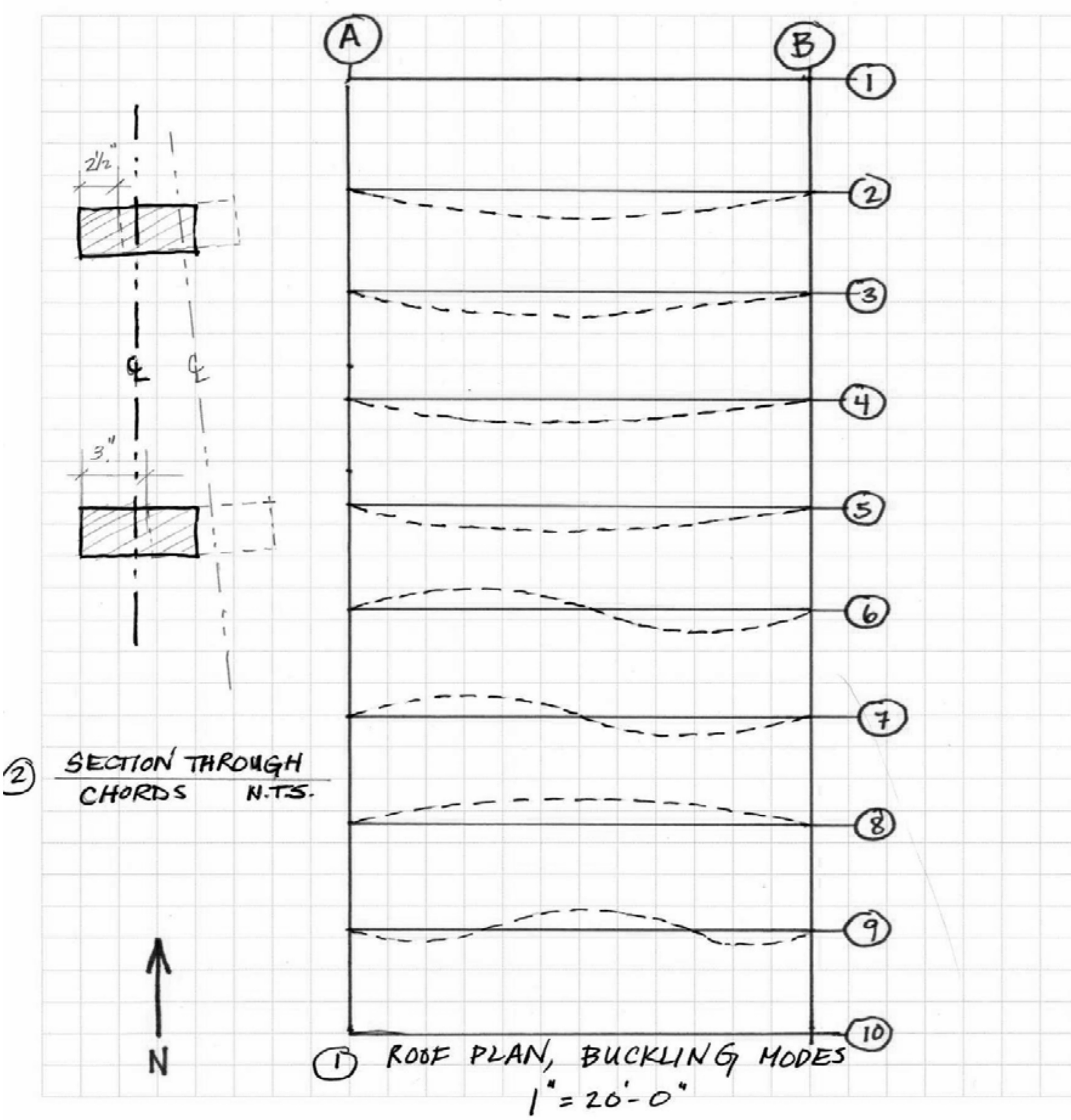

Figure 17: Right--Lateral Displacement and Rotation of Truss Chords. Left--cross section through chords, displaying rotation and displacement from truss centerline.

Figure 18: Typical bottom chord splice. Note water staining and loss of paint. (Photgraph by author)

Figure 19: Detail of typical shear failure parallel to the grain at end of scarf splice. (Photograph by author)

5.1.5 Bearing Blocks

The bearing blocks extend to the cornice fascia, and have therefore been susceptible to roof and gutter leaks. This exposure has resulted in some superficial decay of the outside end of the bearing block. While this is a concern, it does not appear to have any adverse structural implications with respect to vertical bearing on the wall or restraint of the tie rod ends. No overwhelming evidence of crushing of the bearing block due to the tie rod plates was observed. However, in the many instances the two pieces of the bearing block have shifted vertically relative to each other. In trusses 1-4, the southern half of the bearing block appears to be displaced vertically up to ¼ inch relative to the northern bearing blocks at both ends. Conversely, the bearing block pieces display the reverse of this in trusses 5-8. The shifting of these bearing blocks appears to correspond to the direction of lateral rotation of the truss about its bearing points. (Figure 21)

5.1.6 Truss Panel Tension Rods

No adverse conditions or displacements were observed in the iron vertical truss members, aside from the out of plane rotation previously mentioned.

5.1.7 Iron Blocks

No adverse conditions or displacements were observed in the bearing blocks of the panel tension rods, aside from the out of plane rotation previously mentioned.

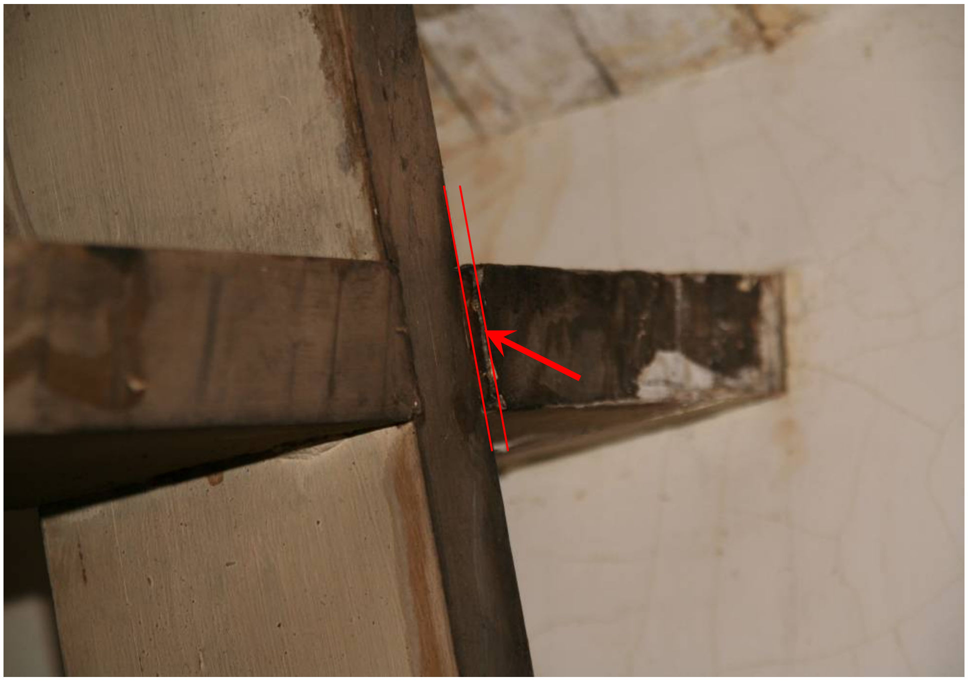

Figure 20: Movement of wood cross braces (Photograph by author)

Figure 21: Shifting of the two bearing block pieces relative to one another (Photograph by author)

5.1.8 Tie Rod

The differential movement of the east and west masonry walls pushes the two truss ends together, which can result in considerable compressive forces in both the arch as well as the tie rod. Under these conditions, the tie rod would be subject to extremely high compressive stresses, well beyond its compressive capacity; as a result, the tie rod would be effectively buckled and the horizontal thrust of the arch resisted predominantly by the wall. The condition of the tie rods suggests that buckling has already occurred to some extent; they are easily moved by hand, and are bowed out of plane in most instances.

5.1.9 Purlins

Purlins were inspected through a combination of roof probes performed by Marlene Goeke in 2008[62], and through an area of plaster loss at bay three of the ceiling. The purlins do not show any adverse structural overstress or displacement. Some water staining is observed, but this does not appear to have resulted in significant water damage. With the exception of the 4 or 6 bolted connections, the purlins are attached to the trusses by means of toe nail connections. According to the Keast & Hood report, a number of these mechanical connections are missing. This raises some concerns as to the lateral stability of the trusses, as well as the performance of the roof due to wind uplift conditions. (Figure 22, Figure 23)

---

[62] Goeke, Marlene. *Assessment and Analysis of the Plaster Exhibit Hall Ceiling at the Wagner Free Institute of Science, Philadelphia, PA.* MS Thesis, University of Pennsylvania. 2008.

Figure 22: Original Purlins. Note lapped splice and lack of mechanical connection. (Photograph by author)

Figure 23: Added intermediate purlins. Note lack of lapped splice and nailed connection. (Photograph by author)

5.1.10 Nailers

No adverse conditions or displacements of the nailers were observed by this author.

5.1.11 Roof Decking

No adverse conditions or displacements of the roof deck were observed by this author.

5.1.12 Lath

The lath is generally in good condition with some minor exceptions. Roof probes taken in the summer of 2008 indicated some warping and twisting of the lath, potentially as a result of water infiltration. In some places gaps exist between the lath and the plaster, possibly caused by shrinkage of the lath or plaster, or some combination of the two.

5.1.13 Plaster

The condition of the ceiling plaster was extensively studied by Marlene Goeke in her thesis on the Wagner Institute (2008). Crack mapping of the plaster ceiling was performed (Figure 24), indicating prominent cracking in both the north-south directions (correlating to the purlins), as well as the east-west directions (correlating to the nailers). Severe cracking at the interface between the plaster and the top chords of the trusses were also identified. In addition, some diagonal cracking at the corners was recorded. In addition to the ceiling, the wall plaster also shows signs of distress, particularly around the ends of the truss where the plaster appears to be cracked and displaced into the wall.

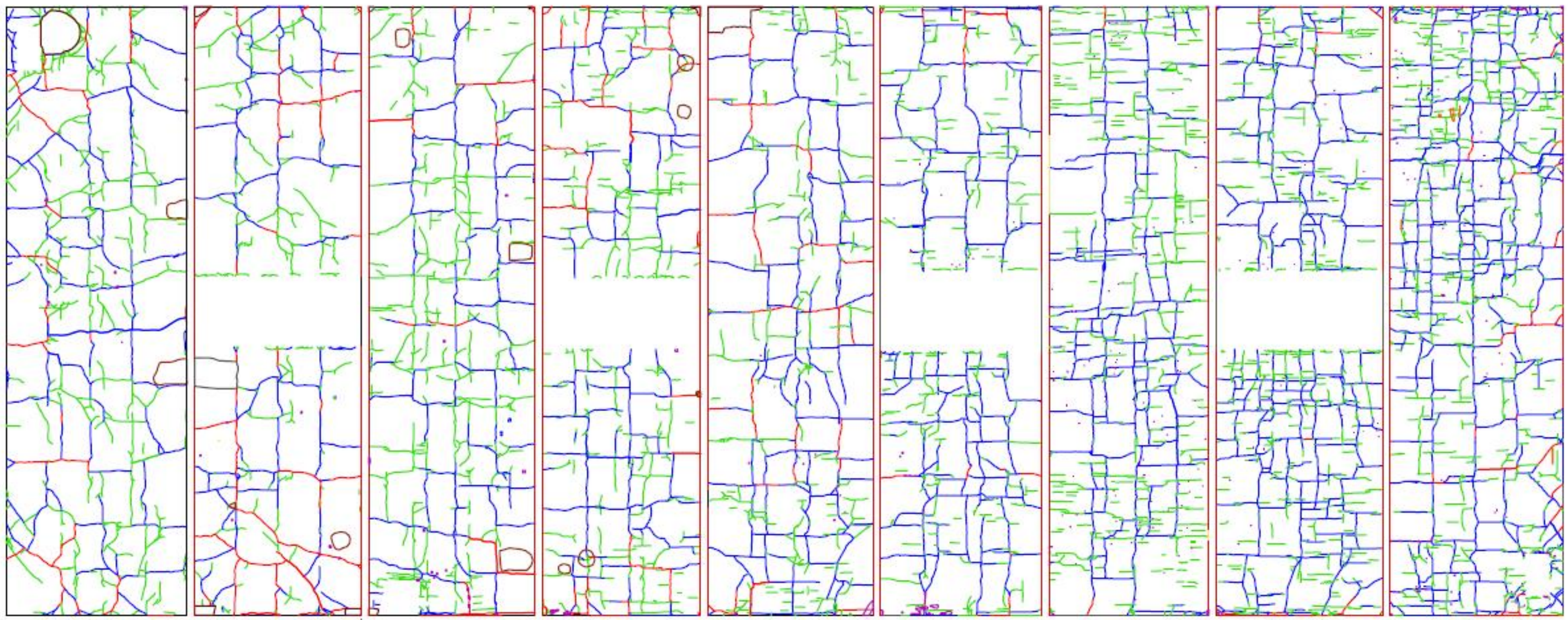

Figure 24: Crack Map of Wagner Institute Plaster Ceiling. Red notation indicates large cracks, blue indicates medium sized cracks and green indicates small cracks. (Image by Marlene Goeke, 2008)

5.2 Material Data

In addition to collecting data concerning the configuration and condition of the roof structure, physical investigation combined with archival research can provide invaluable materials properties data essential to running an accurate analysis. Materials can be classified as either orthotropic (or anisotropic) or isotropic. A material is isotropic if its mechanical or thermal properties are identical in three mutually perpendicular directions; conversely, orthotropic materials have unique and directional properties. Examples of orthotropic materials include wood, crystal, and rolled metal. The mechanical properties of wood, for instance, are described in the longitudinal, radial, and tangential directions. The longitudinal axis is parallel to the grain (fiber) direction; the radial axis is normal to the growth rings; and the tangential axis is tangent to the growth rings. Because of the directional variability of the material properties, wood response to loads is dependent on the load orientation.

5.2.1 *Chords, Braces, Bearing Blocks, Original Purlins*

The majority of the wood elements in the roof framing assembly have been identified in the Joe Clark wood pathology report as old growth Virginia Eastern White Pine. The following table denotes both the published values for actual strength parameters as well as the published allowable values at approximately the time of construction. Data was compiled from the Forest Products Laboratory Wood Handbook[63]

[63] *Wood handbook: wood as an engineering material.* General technical report FPL; GTR-113. Madison, WI: U.S. Department of Agriculture, Forest Service, Forest Products Laboratory, 1991.

and The Architects' and Builders' Handbook of 1921[64], respectively. Allowable safe working stresses are bases on factors of safety of 10, 5, 6 and 4 for tension, compression, flexure and shear, respectively, with a safety factor of one for the modulus of elasticity.

Table 1: Mechanical Properties of Virginia Eastern White Pine

Virginia Eastern White Pine	Actual	Allowable
Tension (psi)[65]		
Parallel to grain	10600	2300
Perpendicular to grain	310	100
Compression (psi)		
Parallel to grain	4800	1300
Perpendicular to grain	440	270
Shear (psi)		
Parallel to grain	900	130
Flexural (psi)	8600	1400
Modulus of Elasticity (psi)	1240000	1000000
Poisson's Ratio (--)	0.344	N/A
Density (pcf)[66]	23	N/A

5.2.2 Intermediate purlins

The intermediate purlins that were added during the Collins and Autenrieth repair campaign of 1885 were identified as Hemlock per the specifications. The following table summarizes actual and allowable working stresses. Data was also compile from the FPL Wood Handbook and the Architects' and Builders' Handbook.

[64] Kidder, Frank and Harry Parker. *Architects' and Builders' Handbook*. New York: J. Wiley and Sons, 1921.
[65] Pounds per square inch
[66] Pounds per cubic foot

Table 2: Mechanical Properties of Hemlock

Hemlock	Actual	Allowable
Tension (psi)		
Parallel to grain	13000	600
Perpendicular to grain	300	50
Compression (psi)		
Parallel to grain	5400	1100
Perpendicular to grain	650	150
Shear (psi)		
Parallel to grain	1060	100
Flexural (psi)	8900	600
Modulus of Elasticity (psi)	1200000	900000
Poisson's Ratio (--)	0.42	N/A
Density (pcf)	27	N/A

5.2.3 Decking, Nailers, Lath

The materials of the nailers and the lath remain unconfirmed. Generally lath is made from white pine, spruce, fir, redwood or some other soft straight grained wood. Because the rest of the structure is made of eastern white pine, these properties will be used for analysis purposes for the nailers and lath. The roof decking has been identified as a general pine but the specific classification remains unknown. It will therefore also be assigned the same values as the eastern white pine.

5.2.4 Verticals, Iron blocks, Tie rod, Plates, Washers

All metal elements of the roof structure have been identified as wrought iron. The actual and allowable strength properties of wrought iron are tabulated below. Allowable values were taken from the Text-Book of the Materials of Engineering, 1917[67].

Table 3: Mechanical Properties of Wrought Iron

Wrought Iron	Actual	Allowable
Tension (psi)	34000	12000
Compression (psi)	34000	11000
Shear (psi)	28000	6000
Flexural (psi)	34000	11000
Modulus of Elasticity (psi)	28000000	28000000
Poisson's Ratio (--)	0.3	N/A
Density (pcf)	490	480

5.2.5 Walls

The exterior bearing walls are common hand-made brick, fired on site and made from the clay excavated for the foundations. The mortar has been identified as lime mortar. While the material properties are likely more consistent throughout the brick, properties of mortar is often highly variable. In addition, the brick and the mortar act as a composite material, resulting in strength properties which don't necessarily correspond to either the brick or the mortar individually. The values tabulated below represent approximate values for both actual and allowable strength properties. Because brick

[67] Moore, Herbert. *Textbook of the Materials of Engineering.* McGraw Hill Book Company, Inc. New York, NY. 1920.

masonry was predominately used in compression only, certain parameters such as tensile or flexural strength are either unknown or highly approximated. As such, analysis should be accompanied by strength testing when feasible in order to ensure accurate results. Both the Text-Book of the Materials of Engineering and A Treatise on Masonry Construction (1914)[68] were consulted for values.

Table 4: Mechanical Properties of Brick Masonry

Brick Masonry	Actual	Allowable
Tension (psi)	75	N/A
Compression (psi)	600	100
Shear (psi)	NA	N/A
Flexural (psi)	150	50
Modulus of Elasticity (psi)	4500000	3000000
Poisson's Ratio (--)	0.25	N/A
Density (pcf)	115	N/A

5.2.6 Plaster

Like brick, the material properties of plaster are extremely variable. Chemical analysis of the Wagner ceiling plaster indicates a high content of magnesium, a 1.3:1 sand to binder ratio and a low level of horse hair for tensile reinforcement. While no mechanical testing values for the Wagner plaster are available, a range of values was taken from Cements, Limes and Plasters: Their Materials, Manufacture and Properties

[68] Kidder, Frank and Harry Parker. *Architects' and Builders' Handbook*. New York: J. Wiley and Sons, 1921.s

(1904)[69]. Because the range is very large, steps should be taken to verify these properties when assessing the results of the analysis.

Table 5: Mechanical Properties of Plaster

Plaster	Actual
Tension (psi)	150-500
Compression (psi)	400-2500
Shear (psi)	N/A
Flexural (psi)	150
Modulus of Elasticity (ksi)[70]	25000-45000
Poisson's Ratio (--)	0.25
Density (pcf)	115

5.2.7 Extraneous Roofing Materials

Roof probes indicate that the current roof deck is covered with two layers of felt sheathing and asphalt roofing, on top of one layer of tin. Though the roofing does not contribute considerably to the structural behavior of the roof system, the materials were nonetheless important to document because they do contribute to the dead load of the structure. The following table lists the weight of the non structural roofing materials, obtained from the Architects' and Builders' Handbook[71].

[69] Eckel, Edwin C. Cements, *Limes, and Plasters: Their Materials, Manufacture and Properties*. New York: John Wiley and Sons, 1928.
[70] Kips per square in; one kip equals 1000 pounds
[71] Kidder, Frank and Harry Parker. *Architects' and Builders' Handbook*. New York: J. Wiley and Sons, 1921.

Table 6: Weight in pounds per square foot of Roofing Materials

Material	Weight (psf)
Tin Roof	1.5
Felt Sheathing	0.3
Gravel Roofing	4
Asphalt Roofing	1

5.3 Load data

Gathering information pertaining to the loads imposed on the structure is necessary to run an effective analysis. For the purposes of this analysis, the loads have been classified as dead, live, wind and displacement loads. Load information is obtained from the aforementioned material properties data, historic weather data, measured conditions, and building codes.

5.3.1 Dead Loads

Dead loads consist of the weights of all materials that comprise the permanent fabric and structure of the building. Generally, these loads are applied vertically to the structure. The table below summarizes the weight of the roofing elements.

Table 7: Weight of Roof Assembly Materials

Material	Weight		
	Lbs	Plf[72]	Psf
Trusses	1700	25.5	--
Purlins			
Pine	120	3.5	--
Hemlock	140	4	--
Furring	3400		0.5

[72] Pounds per linear foot

Lath	3700		0.5
Decking	19000	--	2
Plaster	54000		5.5
Roofing			
Tin	15000	--	1.5
Gravel	45000	--	4.5
Asphalt	15000	--	1.5

5.3.2 Live Loads

Live loads are any loads that may act on a structure for a limited or intermittent duration, such as loads from ponding of rain, accumulations of snow, construction activity, or wind. In order to accurately estimate the environmental live loads applied to the roof structure of the Wagner Institute, historic weather data for the Philadelphia area was researched. According to records, the maximum ground snow load in Philadelphia occurred in 1996, with a maximum of 30.7 inches—the equivalent of between 16 and 48 psf, depending on the moisture content of the snow.[73] Per discussions with Wagner Institute personnel and investigations of the roof after the record-breaking snow storms in February 2010, it was determined that the maximum snow depth on the roof reached 12-16 inches, (equivalent to 20 to 25 psf[74]) —approximately half the depth recorded at the ground; this difference may be attributed to both the curvature of the roof, which allows for sliding of the snow, as well as the lack of insulation in the roof assembly which would contribute to melting. In addition, the curve of the roof in combination with wind gusts, resulted in a non-uniform distribution of the snow. The current building code provides for

[73] Light snow has a density of approximately 10% that of water while heavy wet snow can reach 30% the density of water.
[74] Pounds per square foot

this by allowing the snow load to increase from one half the balanced load (12.5 psf) at the crown to two times the balanced load at the eave (50 psf), distributed over one side of the roof. This case is applicable in roofs with eaves sloped less than 30 degrees.[75]

5.3.3 Wind Loads

As previously stated, the highest wind loads witnessed in Philadelphia were measured at 85 mph gust to the east, with a 75 mph 1-minute sustained wind to the east in the storm of 1878 which tore the roof off of the building. The highest wind load measured since 1878 was a 67 mph 1-minute sustained wind to the east, accompanied by a 73 mph eastward gust in 1955. These values are then utilized in formulas provided by the current building code[76] in order to evaluate the wind pressures on the building. These wind pressures can then be imported into the analysis model.

5.3.4 Displacement Loads

Instead of applying forces or pressures to a structure and obtaining displacement values, the analytical model will also accept imposed displacement values and provide forces. This is important in the case of the Wagner roof frame assembly, particularly for the purpose of evaluating stress in the structure due to the displacement of the side walls. In addition, measured displacement values are also important to compare the results of the analysis with the actual deformations witnessed in the physical investigation. The

[75] The eave slope at the Wagner was measured to be approximately 25 degrees.
[76] Kidder, Frank and Harry Parker. *Architects' and Builders' Handbook*. New York: J. Wiley and Sons, 1921.

following list—while not comprehensive—provides a handful of useful displacement values which will be important in helping to assess the roof structure and evaluate the accuracy of the analytical model. The coordinate system indicated assumes gravity acts in the negative Y direction, the Z axis runs perpendicular to the length of the truss, and the X axis is parallel to the length of the truss.

Table 8: Relevant Displacement Values of Arched Trusses

	Displacement (in)	Direction
Truss end horizontal displacement	-2.5	X
Lateral Displacement (Top Chord)	+/-2.5	Z
Lateral Displacement (Bottom Chord)	+/-3	Z
Sag in Tie Rod	-3	Y

5.3.5 Thermal Loads

In addition to gravitational and lateral loads, the roof assembly is also subjected to thermal loads, induced by temperature fluctuations. These loads allow for the linear and volumetric expansion or contractor of all materials; each material has a unique coefficient of thermal expansion which indicates how much that material moves for a given temperature change. The coefficients of thermal expansion for prevalent materials in the Wagner roof structure are tabulated below.

Table 9: Coefficient of Thermal Expansion

Coefficient of Thermal Expansion (in/in/^{o}F)	
Plaster	9.20E-06
Eastern White Pine	2.80E-06
Hemlock	2.80E-06
Wrought Iron	6.70E-06
Brick Masonry	3.50E-06

Though the exact fluctuation of the temperature of the roof assembly was not measured, an assumed maximum temperature differential of 100 degrees (maximum 50 degree increase/decrease from initial temperature) was assumed in all of the analyses, unless otherwise indicated.

6 Structural Modeling

Once all of the data collection had been completed, structural modeling was begun. Three structural models were created at varying levels of complexity—a simplified arch model, a beam element trussed arch model (both completed using the software RISA3D®)[77], and finally a finite element model, built in SolidWorks/Cosmos®[78]. These models will be discussed in detail in the following section.

6.1 Simple Arch Model

The first step in modeling was to gain a basic understanding of the overall behavior of the structure using a preliminary simplified structural model. This model consisted of two main elements—an arch and a tie rod. The model arch was intended to simulate the arched truss structure; as such, the cross section shares similar area and moment of inertia properties of the combined top and bottom chords of the extant arched truss.[79] Rather than one continuous element, the model arch consisted of segmented beams with fixed end conditions, approximately the length of each arch panel. The tie rod was modeled as a 1 ⅝” diameter wrought iron rod, as it appears in the actual truss. The tie rod ends were assumed to be coincident with the truss ends; on one side, the end was given a pinned

[77] RISA3D 2008® is a registered trademark of RISA Technologies, LLC . It is worth noting that RISA3D® does have some finite element analysis capabilities; however, these were not exercised in this thesis.
[78] SolidWorks Office Premium 2009® and the FEA package CosmosWorks® are registered trademarks of SolidWorks Corporation, a subsidiary of Dassault Systemes (Dassault Systèmes S.A.)
[79] Stress due to axial forces in a beam is dependent on the cross section area normal to the direction of the applied load, and are represented by the formula $\sigma=F/A$ where σ is the stress in pounds per square inch, F is the applied axial force and A is the area. Conversely, the stress in a beam due to bending is a function of the applied bending moment (M), the distance from the neutral axis to the outer surface (c), and the moment of inertia (I), as represented by the formula $\sigma=Mc/I$.

constraint, while the other was modeled with a roller. The model arch joints were also constrained laterally to prevent instability out of the plane of loading.

After the geometry was generated, loads were applied to the simulated structure. Self weight of the model arch was calculated automatically by the software, and distributed accordingly. Dead loads, comprised of the weight of the roofing, framing, plaster, etc. were imposed as point loads at the joints between the arch segments; this approximates the transfer of loads into the truss through the purlins which are spaced at roughly the same intervals as the truss panels. Snow loads were applied in a similar manner. A thermal load was also imposed over the entire structure. Wind loads and unbalanced snow loads were neglected for this particular analysis.

The model arch was subjected to three loading scenarios: dead load only, dead load and snow load, and dead load and thermal load. In all instances, the model arch was found to behave exactly as expected. A summary of the critical parameters is tabulated below:

Table 10: Simplified Model Arch: Calculated Forces and Stresses

		Dead	Dead & Snow	Dead & Temperature	Location
Axial	k	17.75	40.98	17.75	Tie Rod
$Axial_{max}$	k	20.075	46.413	20.075	End
$Axial_{min}$	k	18.415	42.56	18.414	Crown
$Stress_{max}$	ksi	0.169	0.391	0.169	End
% of σ_{allow}	%	13%	30%	13%	--
$Moment_{max}$	Ft-k	3.353	7.307	3.651	Crown
$Displacement_{max}$	in	0.249	0.542	0.239	Crown

The results indicate that model arch acts like a curved beam, with the compressive forces increasingly large towards the ends of the arch and bending moments greatest near the crown. The tie rod acted predominantly in tension (though nominal secondary bending was measured, due to the self weight of the rod), essentially picking up the end thrust of the arch. The tie rod drastically reduced the horizontal components of the end reactions, allowing the arch to transfer almost purely vertical compressive forces into the end constraints. There is a general linear correlation between the magnitude of the forces and the applied load; for instance, the imposed snow load is 2.5 times the applied dead load, and therefore the axial, moment and displacement results are approximately 2.5 times greater than the dead load only case.

This exercise—though simple—is important to perform because it provides a very basic understanding of the structural mechanism without the detail of localized behavior within the structural assembly. However, this level of analysis is certainly not sufficiently informative, particularly when attempting to determine critical deflection values. The model arch geometry does not replicate the actual structural members or their connection conditions. Therefore, a more detailed analysis must follow the preliminary assessment.

6.2 Trussed Arch Model

After the simple model arch was completed, a second, more complex model was generated to better simulate the truss behavior. The purpose of creating this model was twofold. First, by using a model similar to that used in by Gredell, the two methods of analysis – Gredell's RISA® analysis as well as the author's—can be compared and analyzed. Second, by comparing the simplified model arch with the FEA model, differences can be ascertained with respect to: a) whether the FEA model provide more precise results, and b) if the simple model arch is indeed sufficient for purposes of assessing deflection and its impact on plaster cracking.

The geometry of the trussed arch model essentially mimicked that of the actual structure, with both chords, iron ties, cross braces, bearing blocks and tie rod elements all represented. The truss chords were represented as a series of straight segmented sections, with end fixity so as to represent two continuous arches. The wood cross bracing was modeled as it appears in the structure as well—with the main braces continuous from the top to bottom chord and the counter bracing split into two separate pieces which intersect the main brace. The braces were assumed to be pinned at their ends, such that any displacement of the braces is directly linked to that of the chords (or in the case of the counter braces, the displacement of the main brace).

The two iron verticals have been idealized as a single piece, with a resultant cross sectional area equal to the sum of the area of the two verticals.[80] This simplification was due to the method by which the software analyzes the structure. RISA® idealizes all members as two dimensional beam elements and uses classical methods such as elastic theory and mechanics of materials to analyze structures[81]; forces transmitted throughout the structure are therefore assumed to be transmitted through the centroid of each beam, thereby negating any eccentricity. It was therefore more convenient to assume a singular

[80] The verticals are assumed to act predominately in tension and not in bending. Therefore, the cross sectional area is the relevant parameter in terms of analyzing the stress in the vertical ties.
[81] RISA is also capable of basic finite element analysis for plate and shell elements; however, it generally reverts to the more traditional analysis methods for structure composed of beams and columns.

element, rather than two. For similar reasons, the iron bearing block which the cross braces rest on was also omitted from the model. The function of the iron bearing block has been substituted by the pin connection between the cross brace and the chord.

The tie rod was modeled essentially as it exists, except rather than extending through the bearing block, it discontinues where the two intersect. The tie rod ends were modeled as fixed, since they in fact extend through the bearing block for almost four feet. The tie rod hanger was also modeled with the top end pinned to the bottom of the lower chord, and the bottom pinned to the center point of the tie rod. The bearing blocks extend 44 ½ inches from the end of the tie rods towards where the fascia would be located. They are modeled as single 6 inch by 8 inch pieces, rather than two 4 inch by 6 inch pieces bolted together. Because the tie rod in the trussed arch model is not continuous through the bearing block, it does not exert any compressive forces on the bearing block due to the tension in the rod.

The bottom of the bearing block is modeled with compressive spring restraints; in other words, the bearing interaction between the bearing block and the brick wall was simulated by using a compressive spring restraint, which has a spring constant equivalent to the stiffness of the brick wall. By making this spring compressive only, it functioned strictly as a bearing—if the bearing block is pushed down on the spring, it will create a reaction; however, because the spring has no tensile stiffness, there will be no reaction if the bearing block is pulled away from the wall, (i.e. if the bearing block pivots about the front edge of the brick wall and therefore is displaced upward at the back edge).

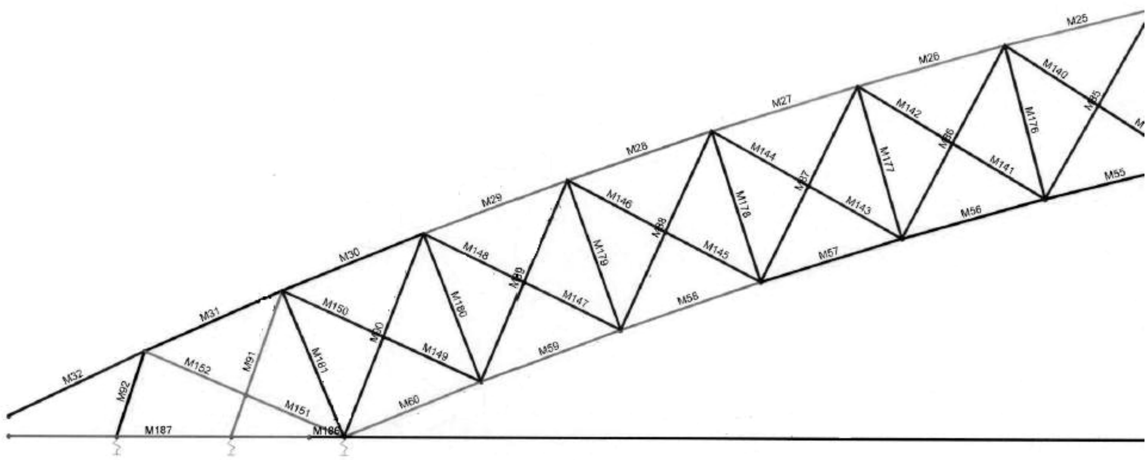

Figure 25: RISA Model, bearing end

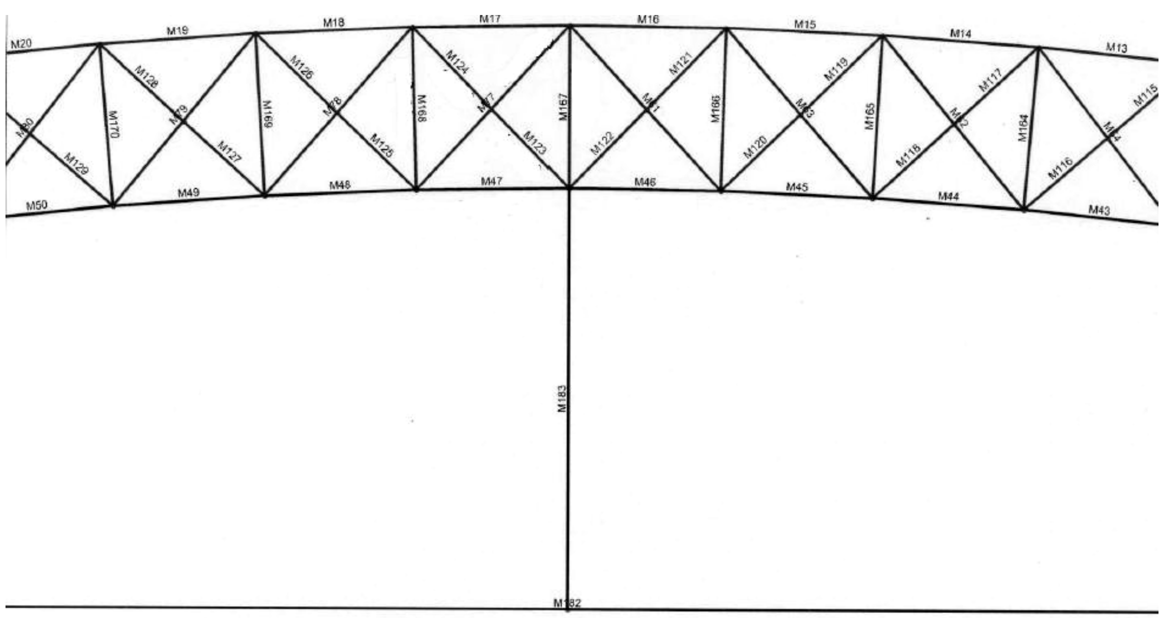

Figure 26: RISA Model, crown

The overall structure was effectively modeled with pinned-roller boundary constraints, much like the simple tied arch model. The bearing block was constrained from movement in the negative Z (vertical) direction by three compression springs. These springs act similarly to full restraints, but rather than being fully rigid, some displacement is possible. The amount of displacement is a function of the spring constant, which has been set to simulate the stiffness of the brick wall the bearing block rests on. By restricting this spring to compression only, the restraint is only applicable in cases where a downward (compressive) force is exerted at the restraint; it has no ability to resist tensile forces, and therefore the member is free to move in the positive Z direction.

In addition to restraining the bearing blocks from vertical displacement, two additional constraints were applied at the interior end of the east bearing block— a spring in the Y (north-south) direction and a rigid restraint in the X (east-west) direction. The spring restraint constrains the truss from any out of plane displacement; again, a spring constant equal to the stiffness of the wall was applied, however by not restricting it to a compression spring, it is constrained in both the positive and negative Y directions. The rigid restraint prevents any displacement of the bearing block into or out of the building; although this is not the actuality of the truss, it must be modeled as such in order for the software to perform the analysis. In actuality, the tie rod as well as the friction and bearing interaction between the truss and the walls prevent any dramatic dislocation of the truss ends (this is known to be at least somewhat effective, given that trusses have displaced with the walls during the 1877-8 wind storms—if not, the trusses would have shifted independently of the walls). In addition to these end constraints, lateral restraint was provided at every top chord joint to limit out of plane movement of the top chord.

The self weight of the structure, dead loads, snow loads and thermal loads were also applied to the arched truss model; wind loads do not govern over these load cases and were therefore omitted from these results. Again, self weight was calculated automatically by the software, with dead and snow loads applied as point loads at the intersection between the chord segments. Two different snow load scenarios were modeled, including both an even distribution as well as an uneven distribution, as discussed in Section 4.3.2. Finally, a horizontal displacement at the roller end of the truss was applied. A total of nine load cases were applied: dead load only; dead + balanced snow load; dead + unbalanced snow load; dead + thermal load; dead + displacement; dead + balanced snow load + displacement; dead + unbalanced snow load (east side) + displacement; dead + unbalanced snow load (west side) + displacement; and dead + thermal load + displacement.

In all load cases excluding those with an imposed horizontal displacement at the roller end, the trussed arch generally behaves exactly as described by Keast & Hood, Friedman and Gredell—the chords act as arches in compression and exert a horizontal thrust at the ends, taken up by the tie rod; the truss panels behave as expected, with the bracing acting in axial compression and the vertical iron ties acting in tension. This is to be expected based on the materials used for the trusswork, with the iron ties tying the two chords together, and the wood bracing resisting the tension in the rods and stabilizing the truss to increase its moment of inertia (omitting the need for a solid web between the flange-like chords). Because of the truss panels, and the application of the vertical loads at the joints at which the wood braces, iron ties and chord segments meet, the structural members are subject to predominately axial forces; in other words, unlike the simple tied arch model, the arch is subject to very little bending.

6.2.1 Load Case 1—Dead Only:

Generally, the arches are acting in compression, with the bottom chord with the highest forces at the end supports and the top chord having the highest forces at the crown. Just beyond the end supports, the top chord starts to exhibit minor tensile forces (with a magnitude of .48 kips, or 480 pounds). The wood cross bracing also appears to be acting in axial compression, with the full braces carrying the majority of the force, and the counter bracing carrying very little. In fact, some tensile forces have developed in some of the counter bracing closest to the support; while these braces are what are referred to as compression only members (they are unable to take any tensile forces because of their lack of end fixity), the analysis results do correlate with field observations of gaps between the braces and the iron bearing blocks, and lateral displacement of some pieces. Though nominal compressive forces were measured in the bearing block, they were assumed to equal the compressive force in the tie rod due to the modeling limitations described previously. All vertical ties are acting in tension, with the exception of the two ties that fix to the top chord and the bearing block; these ties exhibited very small compressive forces.[82]

[82] Refer to Appendix II for graphical display of forces.

The results of the author's analysis generally compare to those obtained by Gary Gredell in magnitude; a comparison of the values is summarized in Table 10. In the author's results, the compressive forces in both chords tend to have a greater range. In addition, Gredell's analysis yields purely compressive forces in all wood members and tensile stresses in all iron members, in contrast to the author's results which indicate tensile forces in some of the wood braces at the ends of the arched truss. The deflection values also indicate a slight discrepancy; Gredell's displacement at the crown of the arch was calculated to be .628 in, compared to the .821 (Woodman). These discrepancies may be a results of one of or any combination of factors, including: geometric/modeling variations; load application (i.e. the use of distributed vs. point loads); and/or load magnitude (i.e. Gredell's report indicates a dead load of 16 psf, compared to 13.25 psf (Woodman)).

Table 11: Arched Truss Model: Summary of Forces and Stresses (Dead Load), Woodman vs. Gredell

Load Case	Gredell		Woodman		
Dead	Mem. No.	Force	Mem. No.	Force	Stress
Bearing End					
Tie Rod	--	12.74	M182	13	14.334
Vertical Tie	M143	2.4	M181	-0.16	0.257
Full Brace 1	M201	-2.7	M91	-0.28	0.027
Full Brace 2	M59	-2.6	M90	-2.6	0.25
Full Brace 3	M60	-2.5	M89	-2.3	0.219
Top Half Brace 1	M141	-0.94	M150	-0.17	0.016
Top Half Brace 2	M139	.-.95	M148	0.04	0.004
Bottom Half Brace 1	M140	-0.94	M149	-0.18	0.018
Bottom Half Brace 2	M138	-0.95	M147	0.02	0.002
Top Chord 1	M57	-1.05	M30	0.48	0.025
Top Chord 2	M56	-1.42	M29	-1.13	0.058
Bottom Chord 1	M29	-11.5	M60	-13.33	0.688

Bottom Chord 2	M28	-10.32	M59	-11.85	0.611
Bearing Block	M203	-12.74	M187	-13	
Midspan					
Bottom Chord 1	M16	-1.39	M47	-0.25	0.013
Bottom Chord 2	M15	-1.39	M46	-0.25	0.013
Top Chord 1	M44	-9.3	M17	-11.44	0.59
Top Chord 2	M43	-9.3	M16	-11.44	0.59
Full Brace	M72	-1.51	M77	-1.08	0.102
Top Half Brace	M114	-1.43	M124	-0.87	0.083
Bottom Half Brace	M115	-1.43	M123	-0.87	0.082
Vertical Tie 1	M169	1.9	M168	1.33	2.168
Vertical Tie 2	M170	1.9	M167	1.38	2.257

The results of the dead load analysis also compare generally to the simple tied arch in that the arch is predominately in compression and the tie rod in tension. However, the magnitudes of the stresses do not truly compare given the geometric discrepancies; in addition the measured displacement is considerably higher in the truss arch analysis (Table 11). The simple analysis therefore appears to provide conservative results which may not be truly indicative of actual behavior.

Table 12: Simple vs. Arched Truss Critical Displacement and Forces Values

Model	Displacement	Force	Location
Simple	0.249	20.075	Crown
Arched Truss	0.821	11.44	Crown

6.2.2 Load Case 2—Dead+Snow:

The relationship between the dead load only and the dead and snow load cases in the trussed arch analysis is similar to that observed in the simple arch analysis. Generally, the forces obtained are approximately 2.5 times those in just the dead load case at bearing end; the same can be said for the midspan. Once again, this represents the ratio of the dead + snow loads to the dead loads. The results are tabulated below.

Table 13: Arched Truss Model: Summary of Forces and Stresses (Dead and Snow Load), Woodman vs. Gredell

Load Case	Gredell		Woodman		
Dead+Snow	Mem. No.	Force	Mem. No.	Force	Stress
Bearing End					
Tie Rod	--	28.3	M182	30.71	15.224
Vertical Tie	M143	5.4	M181	-0.71	1.148
Full Brace 1	M59	-6	M91	-0.27	0.025
Full Brace 2	M60	-5.6	M90	-6.29	0.599
Full Brace 3	M201	-5.44	M89	-5.48	0.522
Top Half Brace 1	M141	-2.16	M150	-0.41	0.039
Top Half Brace 2	M139	-2.16	M148	0.14	0.013
Bottom Half Brace 1	M140	-2.16	M149	-0.43	0.041
Bottom Half Brace 2	M138	-2.16	M147	0.11	0.011
Top Chord 1	M57	-2.23	M30	1.36	0.084
Top Chord 2	M56	-4.07	M29	-2.52	0.13
Bottom Chord 1	M29	-25.5	M60	-31.62	1.632
Bottom Chord 2	M28	-23.08	M59	-28.08	1.449
Bearing Block	M203	-28.3	M187	-30.71	
Midspan					
Bottom Chord 1	M16	-2.85	M47	-0.97	0.064
Bottom Chord 2	M15	-2.85	M46	-0.97	0.064
Top Chord 1	M44	-20.7	M17	-26.55	1.37
Top Chord 2	M43	-20.7	M16	-26.55	1.37
Full Brace	M72	-3.35	M77	-2.43	0.231
Top Half Brace	M114	-3.17	M124	-2.24	0.213
Bottom Half Brace	M115	-3.17	M123	-2.22	0.212
Vertical Tie 1	M169	4.24	M168	3.12	5.083
Vertical Tie 2	M170	4.2	M167	3.01	4.938

6.2.3 Load Case 3—Dead & Thermal:

In the next load case a temperature increase of 70 degrees was applied to the arched truss model, in addition to the preexisting dead load forces. The dead and thermal load case yields similar results to the dead load only case with some differences. As temperature increases, it causes the member to elongate; if the member is constrained at both ends, it generates an internal compressive force to compensate for the lack of movement. When thermal loads are applied to the tie rod, they result in a decrease in the tensile force of the tie rod, allowing the roller end to displace further (.569 inches vs. .186 inches with only dead load). This in turn alleviates some of the compression in the arch; however, it also results in an increase in bending. This results in higher compression values in the top chord and lower compression values in the bottom chord than the dead load only case. The results are summarized below.

Table 14: Arched Truss Model: Summary of Forces and Stresses (Dead and Temperature Loads), Woodman vs. Gredell

Load Case	Gredell		Woodman		
Dead+Temp	Mem. No.	Force	Mem. No.	Force	Stress
Bearing End					
Tie Rod	--	12.6	M182	12.4	14.224
Vertical Tie	M143	1.96	M181	-1.5	2.443
Full Brace 1	M201	-2.74	M91	0.14	0.014
Full Brace 2	M59	-2	M90	-1.54	0.146
Full Brace 3	M60	--	M89	-1.27	0.121
Top Half Brace 1	M141	-0.24	M150	1.23	0.117
Top Half Brace 2	M139	--	M148	1.37	0.131
Bottom Half Brace 1	M140	-0.24	M149	1.22	0.116
Bottom Half Brace 2	M138	--	M147	1.36	0.129
Top Chord 1	M57	-1.5	M30	-0.48	0.052
Top Chord 2	M56	-2.5	M29	-2.25	0.116

Bottom Chord 1	M29	-11.76	M60	-13.53	0.698
Bottom Chord 2	M28	-11.54	M59	-11.78	0.608
Bearing Block	M203	-12.6	M187	-12.4	
Midspan					
Bottom Chord 1	M16	-1.15	M47	1.07	0.055
Bottom Chord 2	M15	-1.15	M46	1.07	0.055
Top Chord 1	M44	-10.25	M17	-13.8	0.712
Top Chord 2	M43	-10.25	M16	-13.8	0.712
Full Brace	M72	-0.9	M77	0.12	0.012
Top Half Brace	M114	-0.8	M124	0.32	0.031
Bottom Half Brace	M115	-0.8	M123	0.33	0.032
Vertical Tie 1	M169	1.03	M168	-0.36	0.587
Vertical Tie 2	M170	1.02	M167	-0.32	0.523

6.2.4 Load Case 4:--Dead+Unbalanced Snow:

The application of an unbalanced snow load, in combination with the dead load of the structure, was also investigated (see Table 15). Due to the asymmetric nature of the load distribution, the resultant stresses and forces were also asymmetric; the arch still acts predominately in compression and bending, though with higher forces expectedly concentrated on the side where the load was applied. In general the bearing end exhibits similar behavior to the dead or dead and snow load cases, with the exception of the counter bracing which exhibits a general increase of tension. By applying the load only to one side, the loaded side is pushed downward; this is countered on the unloaded side by a tendency to bend upward, thus balancing out the differential between compression forces in the top and bottom chords. The vertical displacement measured at the crown of the bottom chord was measured to be 1.314 inches compared to .821 in for dead load only and 1.929 inches for dead and snow.

Table 15: Arched Truss Model: Summary of Forces and Stresses (Dead and Unbalanced Snow Load), Woodman

Load Case	Woodman		
Dead+Usnow	Mem. No.	Force	Stress
Bearing End			
Tie Rod	M182	22.15	15.059
Vertical Tie	M181	-3.01	4.897
Full Brace 1	M91	-0.22	0.021
Full Brace 2	M90	-7.82	0.744
Full Brace 3	M89	-6.25	0.595
Top Half Brace 1	M150	1.86	0.177
Top Half Brace 2	M148	2.15	0.205
Bottom Half Brace 1	M149	1.84	0.176
Bottom Half Brace 2	M147	2.14	0.204
Top Chord 1	M30	1.37	0.102
Top Chord 2	M29	-4.72	0.244
Bottom Chord 1	M60	-23.98	1.238
Bottom Chord 2	M59	-18.32	0.946
Bearing Block	M187	-22.15	
Midspan			
Bottom Chord 1	M47	-2.94	0.152
Bottom Chord 2	M46	-0.99	0.051
Top Chord 1	M17	-16.95	0.875
Top Chord 2	M16	-18.84	0.972
Full Brace	M77	-3.16	0.302
Top Half Brace	M124	-0.16	0.015
Bottom Half Brace	M123	-0.15	0.015
Vertical Tie 1	M168	2.34	3.811
Vertical Tie 2	M167	2.22	3.619

6.2.5 Load Cases 5,6,7,8,9—Load Cases 1,2,3,4+Displacement:

The aforementioned load cases were all repeated with the addition of an applied horizontal displacement of 2. 3125 inches—the maximum displacement differential between the east and west walls, measured by Gredell. As the span of the truss is shortened by net inward displacement of the truss ends due to the walls, the resultant force puts the arch into reverse bending, thus counteracting any forces imposed by vertical loads. In other words the wall displacement cambers the arched truss. Unlike in the case load cases with only vertical loads, under displacement loads the lower chord tends to exhibit higher compressive forces, while the upper chord exhibits lower tensile forces, such that when combined, the forces in each chord tend to be more balanced. However, due to the magnitude of the applied displacement force, the stresses indices are high with regard to the allowable strength of the trusses. Generally speaking, the displacement load cases equal the sum of their respective load cases without displacement, and forces induced by the applied displacement. The results for these load cases are tabulated on the following pages.

Table 16: Arched Truss Model: Summary of Forces and Stresses (Dead and Displacement Loads), Woodman

Load Case	Woodman		
Dead + Disp	Mem. No.	Force	Stress
Bearing End			
Tie Rod	M182	-161.72	77.979
Vertical Tie	M181	3.52	5.737
Full Brace 1	M91	-2.38	0.227
Full Brace 2	M90	0.07	0.007
Full Brace 3	M89	-0.199	0.019
Top Half Brace 1	M150	-2.5	0.238
Top Half Brace 2	M148	-2.76	0.263
Bottom Half Brace 1	M149	-2.51	0.239
Bottom Half Brace 2	M147	-2.76	0.263
Top Chord 1	M30	-9.59	0.495
Top Chord 2	M29	-7.48	0.386
Bottom Chord 1	M60	-7.86	0.405

Bottom Chord 2	M59	-9.46	0.488
Bearing Block	M187	161.72	
Midspan			
Bottom Chord 1	M47	-27.86	1.438
Bottom Chord 2	M46	-27.86	1.438
Top Chord 1	M17	11.89	0.614
Top Chord 2	M16	11.89	0.614
Full Brace	M77	-0.74	0.071
Top Half Brace	M124	-2.65	0.252
Bottom Half Brace	M123	-2.7	0.257
Vertical Tie 1	M168	1.49	2.434
Vertical Tie 2	M167	0.244	0.398

Table 17: Arched Truss Model: Summary of Forces and Stresses (Dead, Snow and Displacement Loads), Woodman

Load Case	Woodman		
Dead + Snow + Disp	Mem. No.	Force	Stress
Bearing End			
Tie Rod	M182	-161.73	77.979
Vertical Tie	M181	6.91	11.261
Full Brace 1	M91	-5.35	0.513
Full Brace 2	M90	-1.86	0.178
Full Brace 3	M89	-2.21	0.212
Top Half Brace 1	M150	-4.4	0.42
Top Half Brace 2	M148	-4.76	0.454
Bottom Half Brace 1	M149	-4.4	0.42
Bottom Half Brace 2	M147	-4.76	0.454
Top Chord 1	M30	-23.3	1.203
Top Chord 2	M29	-20.87	1.077
Bottom Chord 1	M60	-18.09	0.934
Bottom Chord 2	M59	-19.61	1.012
Bearing Block	M187	161.73	

Midspan			
Bottom Chord 1	M47	-35.41	1.828
Bottom Chord 2	M46	-35.41	1.828
Top Chord 1	M17	-2.58	0.133
Top Chord 2	M16	-2.58	0.133
Full Brace	M77	-2.77	0.264
Top Half Brace	M124	-4.26	0.406
Bottom Half Brace	M123	-4.31	0.41
Vertical Tie 1	M168	3.92	6.386
Vertical Tie 2	M167	2.95	4.798

Table 18: Arched Truss Model: Summary of Forces and Stresses (Dead, Temperature and Displacement Loads), Woodman

Load Case	Woodman		
Dead + Temp + Disp	Mem. No.	Force	Stress
Bearing End			
Tie Rod	M182	-189.09	91.174
Vertical Tie	M181	2.28	3.716
Full Brace 1	M91	-1.95	0.186
Full Brace 2	M90	1.39	0.133
Full Brace 3	M89	1.05	0.101
Top Half Brace 1	M150	-1.25	0.119
Top Half Brace 2	M148	-1.6	0.153
Bottom Half Brace 1	M149	-1.26	0.12
Bottom Half Brace 2	M147	-1.61	0.153
Top Chord 1	M30	-10.43	0.539
Top Chord 2	M29	-8.2	0.424
Bottom Chord 1	M60	-7.9	0.408
Bottom Chord 2	M59	-9.5	0.49
Bearing Block	M187	189.09	
Midspan			
Bottom Chord 1	M47	-30.4	1.569
Bottom Chord 2	M46	-30.4	1.569
Top Chord 1	M17	13.66	0.705

Top Chord 2	M16	13.66	0.705
Full Brace	M77	0.64	0.061
Top Half Brace	M124	-1.75	0.167
Bottom Half Brace	M123	-1.81	0.172
Vertical Tie 1	M168	-0.27	0.435
Vertical Tie 2	M167	-1.85	3.028

Table 19: Arched Truss Model: Summary of Forces and Stresses (Dead, Unbalanced Snow-Left, and Displacement Loads), Woodman

Load Case	Woodman		
Dead + Snow(L) + Disp	Mem. No.	Force	Stress
Bearing End			
Tie Rod	M182	-161.73	77.981
Vertical Tie	M181	4.57	7.439
Full Brace 1	M91	-6.14	0.585
Full Brace 2	M90	-3.62	0.345
Full Brace 3	M89	-3.21	0.306
Top Half Brace 1	M150	-1.28	0.122
Top Half Brace 2	M148	-1.99	0.189
Bottom Half Brace 1	M149	-1.27	0.121
Bottom Half Brace 2	M147	-1.97	0.188
Top Chord 1	M30	-23.78	1.227
Top Chord 2	M29	-24.22	1.25
Bottom Chord 1	M60	-6.86	0.354
Bottom Chord 2	M59	-5.5	0.284
Bearing Block	M187	161.73	
Midspan			
Bottom Chord 1	M47	-34.42	1.777
Bottom Chord 2	M46	-31.78	1.64
Top Chord 1	M17	7.27	0.375
Top Chord 2	M16	4.74	0.245
Full Brace	M77	-3.62	0.345
Top Half Brace	M124	-1.63	0.155
Bottom Half Brace	M123	-1.68	0.16

Vertical Tie 1	M168	2.78	4.534
Vertical Tie 2	M167	1.54	2.511

Table 20: Arched Truss Model: Summary of Forces and Stresses (Dead, Unbalanced Snow-Right, and Displacement Loads), Woodman

Load Case	Woodman		
Dead + Snow(R) + Disp	Mem. No.	Force	Stress
Bearing End			
Tie Rod	M182	-161.72	77.981
Vertical Tie	M181	5.84	9.507
Full Brace 1	M91	-2.97	0.282
Full Brace 2	M90	0.9	0.086
Full Brace 3	M89	0.22	0.021
Top Half Brace 1	M150	-4.9	0.468
Top Half Brace 2	M148	-5.12	0.488
Bottom Half Brace 1	M149	-4.93	0.469
Bottom Half Brace 2	M147	-5.14	0.49
Top Chord 1	M30	-11.67	0.602
Top Chord 2	M29	-7.4	0.384
Bottom Chord 1	M60	-17.22	0.889
Bottom Chord 2	M59	-20.79	1.073
Bearing Block	M187	161.72	
Midspan			
Bottom Chord 1	M47	-31.95	1.649
Bottom Chord 2	M46	-34.58	1.785
Top Chord 1	M17	4.89	0.253
Top Chord 2	M16	7.42	0.383
Full Brace	M77	0.12	0.011
Top Half Brace	M124	-5.37	0.511
Bottom Half Brace	M123	-5.42	0.516
Vertical Tie 1	M168	2.72	4.423
Vertical Tie 2	M167	1.54	2.509

6.2.6 Summary Analysis

The load cases that do not include the imposed displacement indicate that the arched truss structure is generally not overstressed based on the allowable strengths indicated previously, with the exception of the balanced snow load case. In this case, the stress due to dead and snow loads is slightly above allowable; however, given that the design factor of safety is considerably high (about 3.5), the stress in the chords is well within the limits of the material's actual capacity of 4800 psi.[83] In the displacement load cases, the balanced snow load case again results in the highest calculated stresses, exhibiting overstress in the bottom chord at midspan. Again, this exceeds the allowable load of 1300 psi, but is just over a third of the estimated actual capacity.

The significance of the displacement load cases does not extend to the plaster cracking, because the ceiling was replaced after the trusses were already permanently displaced as a result of the wall deformation that occurred between 1876-78. Rather, it may help to describe some of the symptoms seen within the trusses, even if they don't correlate to plaster damage.

In addition, the inclusion of displacement loads in the analyses help to understand any residual stresses within the structure than may be exacerbated by any new loading conditions. For example, if we compare deflection due to dead load alone versus dead load and thermal load, the deflection differential is .376 inches; conversely, the differential between both load cases including displacement is .272—an even smaller value than without the displacement load. However, while the dead and temperature load

[83] Look at maximum compressive force needed to achieve the existing geometry.

only case results in stresses well under both the allowable and the actual strength of the wood, the dead, temperature and displacement load case results in a stress of 1569 psi in the top chord—a stress level that exceeds the allowable stress of 1300 psi and may therefore affect post-yielding behavior of the arched truss.

The deflections obtained by the analysis are critical in the understanding of the plaster behavior and are tabulated below. Based on these result, the greatest resultant deflection (not considering those due to the applied horizontal displacement for reasons mentioned above) measures 1.108 inches (dead and snow) downward at the crown of the bottom chord, or L/620 inches. While this ratio exceeds Gredell's measurement of L/880, it is still under the generally accepted value of L/360 for prevention of plaster cracking. This implies that the vertical loads imposed on the structure are not critical enough to damage the plaster. However, this does not consider a number of factors such as displacement due to lateral loads, nor the strength of the plaster. These concerns will be addressed in the following section.

Table 21: Arched Truss Model: Summary of Deflections at Arch Crown, Woodman

Displacement at Crown of Bottom Chord	(in)
Dead	-0.821
Dead+Snow	-1.929
Dead+Temp	-1.197
Dead+Usnow	-1.314
Dead+Disp	3.651
Dead+Snow+Disp	2.787
Dead+Temp+Disp	4.027
Snow	-1.108
Temp	+/-0.376
Disp	4.472

Usnow	-0.493
Snow+Disp	3.608
Temp+Disp	4.744
Temp+Snow	-.732

The arched truss model provides an approximation of the roof truss behavior which generally confers with both the simplified model (and therefore the concepts of structural analysis assumed at the time the truss was designed), and the analyses performed by Gary Gredell and Donald Friedman. However, both the modeling and analytical capabilities of the modeling software raise some concerns which may potentially affect the accuracy of the results. These concerns pertain to the geometry, load application and boundary constraints of the model.

The geometry issues have been comprehensively addressed in the previous paragraphs and will therefore not be reiterated herein. RISA® provides three options for beam end constraints—fully fixed, bending moments released (or pinned), or torsional released. Most boundary conditions except those described as otherwise, are idealized as pinned connections. However, most of the assumed “pinned” connections are in actuality constrained by a combination of friction and compressive forces, such as in the case of the wood braces that bear on the iron blocks. In compression, contact constraint and pinned connections behave similarly; however, if these members were subjected to tensile forces, their behavior would be quite different. The end constraints of the truss also pose some concerns, as previously discussed. In a similar vein, the lateral restraint at the top chord of the truss is also questionable. Though the purlins may provide some lateral restraint, observation in the field and displacement measurements prove this to be somewhat inaccurate.

The forces applied in the model are also idealized to some extent. All downward vertical loads (dead, snow) are assumed to act as point loads at all the purlins. For analysis simplicity, the purlins were assumed to rest at the joints in the top chords; this is convenient because it eliminates any bending stresses within the trusses. However, in actuality the purlins do not align exactly with these joints. As a result, the stresses imposed on the structure may in fact cause secondary bending in the truss elements, which in theory should be solely axial members.

Another factor which has not yet been considered in either analysis is the impact of prestressing forces imposed on the structure during construction. It would have been necessary, for instance, to tension the iron verticals in the web of the trussed arch prior to erection, in order to ensure that the wood cross bracing remained stable when the trusses were hoisted into place. Similarly, the tie rod actually consists of two pieces which feed into either end of a turnbuckle. This turnbuckle would likely have also been tensioned prior to erection to prevent any residual bending forces from acting upon the walls. These pretensioning forces may have a considerable effect on the internal stresses of the structure.

Finally, due to the nature of the load application (assumed to be applied concentrically along the member), the trussed arch analysis does not consider any out of plane movement of the truss due to either any eccentric loads or the applied displacement of the measured wall movement. The out of plane displacement of the trusses may be attributed to buckling—a phenomenon that occurs when a member is subjected to a large compressive force, buckling of that member may occur prior to the point at which the compressive strength of the material is exceeded. This failure, known as Euler buckling, is generally a result of insufficient lateral restraint, which caused the member to bifurcate and curve out of plane.[84] The shape of the buckling curve (referred to as the buckling mode) is a function of the magnitude of the applied load, the geometry of the member, and the end constraints. Different failure characteristics and strengths exist in different buckling modes. Though RISA® is capable of generating several orders of buckling modes for these trusses, it does not return the critical buckling load, nor any displacements or information about post-buckling load carrying capacity.

[84] The load at which buckling occurs is known as the critical buckling load.

7 Finite Element Model

By generating the simple and arched truss models, a general understanding of the structural behavior was ascertained. However, the limitations of both the modeling and analytical capabilities of the tools utilized thus far has raised a number of concerns about the accuracy of these analyses. By utilizing a finite element software, with more precise modeling capabilities and a larger arsenal of analytical methods, a number of these issues may be addressed. The results of the finite element model can then be compared to the simplified models and correlated to the observed conditions of the extant roof system.

7.1 Static Truss Analyses—In-Plane Loading

The finite element model of the truss was generated using the computer aided design (CAD) program SolidWorks®, and analyzed using the integrated design analysis program CosmosWorks®. In SolidWorks/CosmosWorks®, a design study is performed for each loading scenario. Each design study is defined by the following factors: model dimensions, study type, material properties, and loads and boundary conditions. A number of study types are possible, and include: static; frequency; buckling; and thermal loads. This section of the thesis discusses specifically static studies, which provide as an output: displacement, stress, strain, reaction forces, and factor of safety distribution values.

In SolidWorks®, all geometries are defined and modeled as solid bodies, unlike the beam or frame notation employed by RISA®; as a result, more complex configurations can be analyzed. Modeling in SolidWorks® consists of generating individual parts, which are then constructed in an assembly. This method of modeling is convenient for two reasons: from the modeling perspective, it allows each piece (or part) to be manipulated independent of the overall structure; and from the analysis perspective, each part can be assigned unique characteristics such as mesh size or material properties. Once imported into the assembly, the parts are “mated”, or defined spatially relative to one another. This constrains the geometry of the model, which is important in order to run an effective analysis.

The SolidWorks® truss model consists of eight parts: (1) top chord; (2) bottom chord; (3) full wood brace; (4) top wood counter brace; (5) bottom wood counter brace; (6) bearing block (7) iron bearing block; and (8) wall bearing segment (Figure 27). In the model, these parts were assembled as they exist in the extant truss; duplicate parts remain duplicated in this model rather than unified as in previous models, depending on their orientation within the overall geometry. It is important to note the lack of certain elements (such as the iron ties), as well as some geometric simplification (the use of continuous top and bottom chords as opposed to spliced pieces). Though important elements of the truss, the decision was made to simulate these components by alternate means in order to simplify and expedite analyses. This will be discussed in further detail later in this section.

Once the model geometry was generated, the material properties were assigned to each part. In CosmosWorks®, the necessary material properties required are a function of the study type. For static and thermal studies, the applicable properties include modulus of elasticity, shear modulus, coefficient of thermal expansion, Poisson’s ratio, and

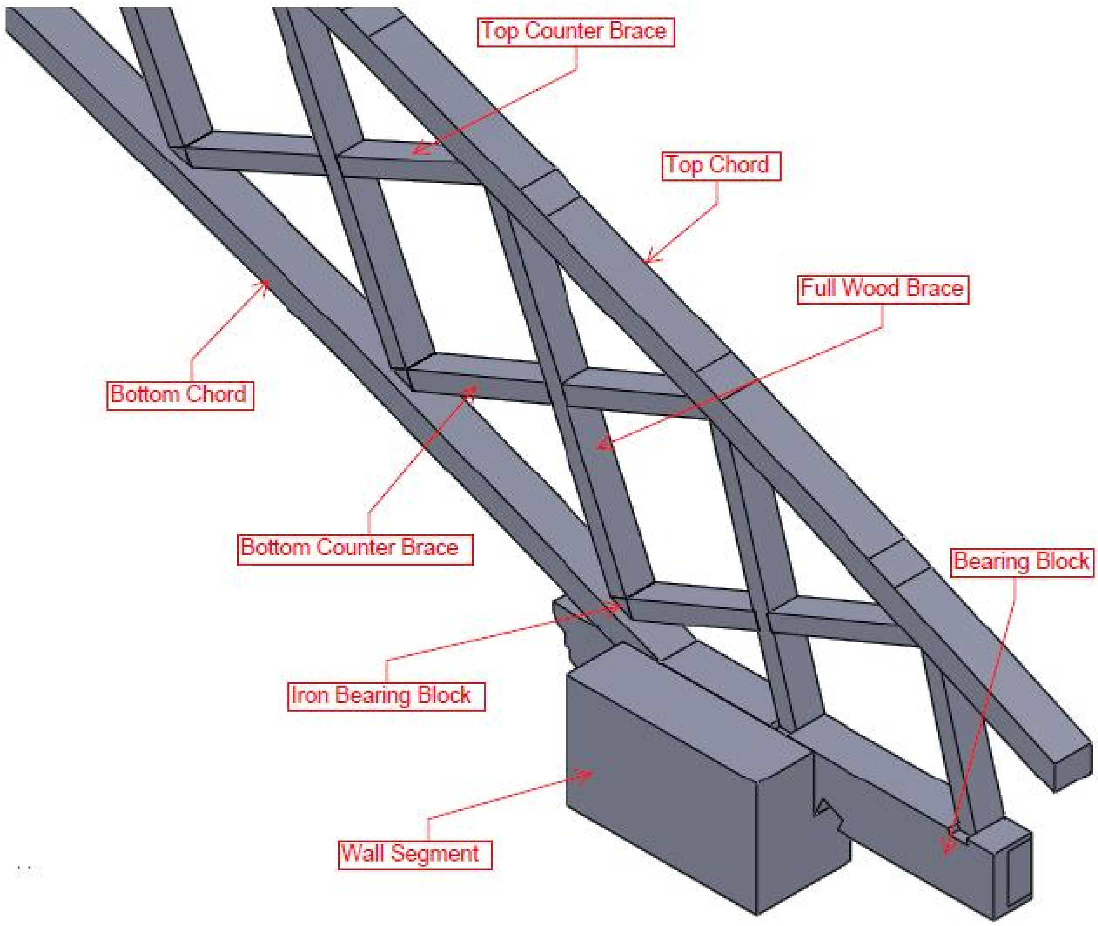

Figure 27: SolidWorks® Truss Assembly at Bearing End

density; these properties have already been tabulated in Section 5.2. These materials may be defined as either orthotropic or isotropic; that is, their properties are either directional or non-directional.

The selection of material properties is also dependent on the type of analysis (linear or nonlinear) selected; the benefits and limitations of these two methods have already been delineated in Section 2.5. Linear analysis was deemed acceptable for the static analysis of the trusses. Though (as previously indicated) the stresses in some load cases may exceed the design strengths, they do not exceed the actual strengths.[85] In addition, the stiffness of the structure is such that the maximum displacements obtained from the simplified analysis are considerably smaller than the characteristic dimension of the model (i.e. the arch cross section).

Once defined geometrically and materially, the model must be loaded and constrained. A number of loading options are provided by CosmosWorks® and include: pressure; force; gravity; thermal; bearing; and centrifugal loads. The self weight of the truss was applied as a gravity load; thermal loads were applied to the whole roof frame assembly as well. In all instances where vertical loads (dead, snow, wind) are imposed on the truss structure, force loads were applied every 23 inches on center—the spacing of the purlins along the truss. By eliminating the purlin geometry from the initial truss model, the analysis becomes considerably simpler to run.

To stabilize the model, displacement restraints must be defined. Restraints can be applied in multiple ways: in the form of defined connectors (i.e. rigid, pin, spring or

[85] Though the actual strength values are idealized to some extent, (they can be lower, given material inconsistencies and/or defects) they have been deemed high enough to justify the use of linear analysis in this application.

elastic supports); prescribed displacements (of zero or non-zero value) which can be applied to faces, edges or vertices; and/or contact conditions which define how individual components interact with one another. Symmetry restraints may also be applied if the model exhibits both geometric and loading symmetry; this allows for only a portion of the structure to be modeled and the results mirrored, cutting down on processing time.

The truss model utilizes a combination of displacement restraints, connections, contact conditions, and symmetry for stabilization. By modeling the spliced chords as continuous parts, it enables us to take advantage of symmetry constraints for all in-plane loading scenarios. The truss exhibits two axes of symmetry—one at the centerline of the truss parallel to its length, and one at the centerline perpendicular to its length. As such, in all instances where in-plane loads are symmetrical, only one quarter of the truss must be modeled; where loads are not symmetrical (such as unbalanced snow load), one half of the truss can be modeled. For solid elements, a face of symmetry is specified by setting normal translation to zero and restraining all internal degrees of freedom.

In order to ensure that symmetry restraints can be applied, the additional restraints must be applied so that they are also symmetric. The purpose of the restraints is to anchor the whole structure so that it is not free to move in space. As such, it must not be allowed to translate or rotate freely in any of the three axes. In order to restrain the truss symmetrically from translation along the (Y) axis, a symmetry restraint was applied at the face perpendicular to the arch length. This restraint allows for movement in both the (X) and (Z) directions so the chords may move both up and down and laterally, but prevents the crown from moving perpendicular to the face towards either truss end.

To restrain the truss from translation in the (X) (lateral) direction and rotation around the (Z) and (Y) axes, a symmetry restraint was applied along the side face of the top chord. This simulates lateral restraint of the top chord by the purlins and the roof deck. Though in actuality the top chords may be only partially restrained by these elements, the application of the in-plane load should not result in any significant out of plane displacement; as a result, this type of restraint is sufficient for this study.[86]

Displacement restraint in the (Z) direction and rotational restraint around the (X) axis was provided at the truss ends where the bearing blocks sit on the wall. Rather than modeling the entire wall (which would substantially increase the analysis time), a small section where it intersects the truss end was modeled instead. This provides a surface for the truss end to bear on, since providing a fixed or roller restraint at the bearing block would over constrain the truss. Instead, the wall component is fixed along its bottom face so the bearing block is free to slide along the top groove.

In addition to constraining the model globally, the interaction and/or interconnection of the individual components must also be defined. This can be done by using connectors or by contact constraints. Connectors are useful in that they simulate desired behavior without having to model complex geometries. The decision was made to substitute spring connectors in place of the vertical iron ties and the tie rod within the truss structure; in so doing, this significantly reduces the amount of time needed to both generate and analyze the model. In addition, the use of springs also allows for the application of preload forces to the structure—an important consideration given that the

[86] Alternative restraints at this area are considered in later studies.

ties were most likely tensioned to hold the chords together prior to installation. The significance of this will be discussed in further detail later.

All other part interfaces were assigned contact conditions. It is important to consider that faces can be initially in contact or they can come into contact due to the effect of applied loads; gaps between faces may exist due to modeling tolerances (i.e. a flat iron bearing block on a curved wood face). Cosmos allows the user to accept these gaps as they are or to ignore them based on user defined tolerances (generally 0.5% of the element size), and assume that a rigid body fills the space between. In the case of the Wagner trusses, it was assumed that no gaps exist between faces initially.

Three options exist for contact conditions between faces: bonded, free or no penetration. These can be set globally (across all parts) or locally (at individual faces). Bonded contact conditions assume that components are fused together and share nodes; in other words, the behavior of the node at one part is indistinguishable from its behavior at the touching part. Free contact conditions assume that all touching faces are free to move in any direction, including into and out of each other under applied loads. This is generally used when the components are not initially touching and are not at risk of interfering with each other. The no penetration (or node-to-node) contact condition creates compatible but separate meshes on both faces, so that the two parts have corresponding nodes. The program creates artificial gap elements which connect these nodes so that the faces are allowed to move away from each other, but do not penetrate one another. No penetration is often the most appropriate contact condition to utilize, but it is also the most computationally expensive. If no penetration contact conditions are utilized, friction may also be considered by applying a coefficient of static friction to the interface. This allows for frictional resistance to be considered in the analysis; however convergence may be problematic and can increase computation time.

For the purposes of this analysis, a combination of contact constraints was used. Because the arched truss model confirmed that the truss exhibited predominately axial compressive forces in both of the chords as well as the braces, interfaces between the iron blocks and the chords, as well as the bird's mouth notch at the bearing block, were globally assigned bonded conditions. No penetration constraints would also have been acceptable; however, because the compressive forces push the two faces together axially, there is minimal threat of either separation or sliding. As such, the behavior of these contact conditions is essentially identical in this situation. Analyses were examined on a case by case basis and if tension forces did arise, no penetration constraints were applied locally as needed.

No penetration conditions were applied at the bearing interface between the bearing block and the wall segment. It was important to model this accurately because the end conditions of the truss are critical in determining the overall behavior of the structure. In addition, because the trusses bear on the wall, any displacements will be dependent on frictional forces that develop at the bearing planes. As such, a static coefficient of friction value of .4 was employed.

After the model was generated and constrained, it was subdivided into discrete elements by a process known as meshing. CosmosWorks® offers two types of meshing: solid and shell. Solid meshing generates three dimensional linear (low order) or parabolic (high order) tetrahedral elements; shell meshing generates two dimensional linear or parabolic triangular elements and the shell thickness is extracted from the model's geometry. Parabolic elements have certain advantages—for the same mesh density they are usually more accurate, and they lend themselves better to curved geometries; however, they require greater computational resources. To compensate for this, coarser meshes are sometimes employed. Parabolic elements were selected for this analysis.

There are a number of options in determining the mesh size for an assembly. The mesh can be defined globally by assigning a uniform element size for all parts and a corresponding tolerance.[87] Automatic transition can be selected as well; this means that CosmosWorks® will automatically assign element sizes based on the corresponding geometry of the model. For instance, finer meshes may be employed around penetrations. Mesh control can be utilized to assign uniform or relative element sizes for individual components based on their geometry and importance within the model. For the purposes of this analysis, automatic meshing was utilized.

Five studies were performed on the FEA truss model. The purpose of these initial truss only studies was to evaluate the stresses within the trusses as well as the deflection resulting from each loading scenario. As such, the following load cases were studied: dead; dead with prestressing; dead, prestressing and temperature; dead, prestressing and snow; and dead, prestressing, snow and displacement. Unbalanced snow loads were omitted from this set of analyses, but will be discussed in later studies.

---

[87] Tolerance refers to how far off the specified global element size individual elements can be.

7.1.1 Dead Load—With/Without Prestress

The first two studies analyzed the truss structure subject to dead load only. In the first load case, no prestressing forces were considered, simulating the arched truss load application for dead load only. In addition to this, a model was generated that included prestressing forces in both the vertical iron ties and the tie rod. Prestressing (or pretensioning) simply refers to the application of a tensile force in order to introduce an internal stress in a member to counteract the effect of applied loads. In this case, prestressing would likely have been applied to all of the iron verticals in order to impose compressive forces in the wood cross bracing and hold the chords together during erection. In addition, pretensioning of the tie rod may have occurred to help alleviate residual thrust on the wall and again stabilize the truss during erection.

Though no historical evidence regarding conventional pretensioning forces in tie rods was ascertained, current standards allow for a force of 70% of the design strength of the material; this allows for a 2.6k tension force in each vertical tie and 17.5k tensions force in the tie rod. Conversely, using maximum forces in the iron ties based on the arched truss analyses (both occurring in the dead + snow load case), and back calculating for allowable remaining force, it was determined that 2.1k per vertical tie and 12.3k in the tie rod are permissible. The lesser of the two values was utilized in both instances.

The results of the dead load only load case yield similar displacement results to the arched truss analysis. Maximum vertical displacement at the crown was measured to be .7177 inches downward, as opposed to the arched truss analysis value of .821 inches. Maximum horizontal displacement was measured at .2054 inches, compared to .186 in the arched truss analysis. Maximum stress levels in the members were measured to be substantially higher than the arched truss analysis indicated; maximum stresses at the top and bottom chords were measured to be 780.5 psi and 1060 psi (22.6k) respectively, exceeding exceed the arched truss results by nearly 50%. However, these values are somewhat misleading—unlike the arched truss analysis, which assumes purely axial behavior, the FEA suggests a stress gradient across the cross section of the chords, consistent with bending behavior. Average values across the cross section of the chord indicate compressive stresses of 496 psi (10.6k) at the top chord and 364 psi (7.8k) at the bottom chord. While these maximum stresses are important to consider as they indicate areas of high concern, they are not necessarily indicative of overall failure if the material strength exceeds the average stress.

The effect of prestressing was also considered in conjunction with dead load. The effect of prestressing on the truss structure is significant. Vertical deflection at the crown of the truss measures .3961 inches—almost half of that obtained in the dead load only analysis. Horizontal deflection is negligible, measuring .014 inches, which suggests that the prestressing force counteracts the axial force imposed on the tie rod by the dead load. While still exceeding the arched truss analysis values, the stresses at the crown and the bottom chord are also less severe than in the case of dead load only (Table 21). It is also worth noting that the stress has decreased by a larger margin in the top chord than in the bottom; this is explained by the fact that the prestressing puts the arch into reverse bending, thereby imposing initial tensile forces into the top chord.

The dead load only and dead & prestress load cases confirm the anticipated behavior of the truss based on the previous analyses. Both the top and bottom chords as well as the wood bracing act in compression, while the tie rod and iron verticals act in tension. Though the measured deflections at the bearing ends and the crown are comparable, the finite element analysis yields considerably higher stress levels than obtained by the frame analysis. These higher stress levels may be attributed to a number of factors such as eccentricities in loading or more accurate constraints. In particular, the frictional end condition at the bearing block introduces an added restraint which may contribute to the decreased movement in the horizontal direction, and result in higher forces in the chords. The sensitivity of the model to this particular factor was examined by removing the frictional constraint and applying a roller, yielding nearly identical results to those obtained in the arched truss analysis.

The introduction of prestressing forces in the truss model also raises an important consideration when investigating historic buildings. The difference between the two models indicates that the capacity of the truss is often dependent on internal stresses, created prior to the installation and loading of the structure. This concept can and should also be extended to the manufacture of the truss, where potential stresses induced by the bending of the chords may also have an impact on the truss capacity. Though these values can not be ascertained with any certainty, the prestressing forces can be predicted, and have thus been included in subsequent analyses.

7.1.2 Dead Load w/Prestress & Temperature

The dead, prestress and temperature load case was also investigated. Unlike the arched truss model which assumed an initial temperature of 0 degrees Fahrenheit and an increase in thermal load of 70 degrees, the FEA model assumed an initial temperature of 300 degress Kelvin (or 80 degrees Fahrenheit) and an imposed temperature drop of 50 degrees. This latter approach may represent more realistic loading conditions, particularly if the plaster were applied under warmer conditions. Because the plaster was also applied after the installation of a central heating system, the temperature differential it is likely to see is closer to 50 degrees than the 70 specified in the arched truss model.

The stresses in the truss subjected to a temperature drop do not differ significantly from the dead load and prestress case. In contrast to the arched truss analysis in which the increase in temperature resulted in negative vertical deflection at the crown, the decrease in temperature in the finite element analysis resulted in shortening of the tie rod and a positive vertical deflection at the crown. In effect, the temperature drop and resultant decrease in length of the tie rod simulates a prestressing force, alleviating the deflection impact due to gravitational loads. Average stresses are tabulated in Table 21.

7.1.3 Dead Load w/Prestress & Snow

The effect of dead load, prestress and snow load was also analyzed using FEA. The resultant stresses and forces are approximately 2.5 times those obtained from the dead load and prestress only load cases; this again correlates to the relationship between dead and dead and snow load cases of the arched truss analysis. Average stresses (Table

21) do not exceed the allowable design strengths of the members, and the stress in the top chord governs the capacity of the truss. Vertical deflection at the crown of the arch was calculated to be 1.34 inches down.

7.1.4 Dead Load w/Prestress, Displacement & Snow

The first three load cases examined indicate that the truss behavior is as predicted, yielding comparable displacement and stress values as the arched truss analysis. In addition, the truss was analyzed again assuming an applied displacement of 1.25 inches (direction) at the end of the bearing block. This is in contrast to the value 2.3125 inches analyzed in the arched truss model; though this was the maximum value measured by Gredell, it may be characterized as a statistical outlier—the 1.25 inch value is much more representative of the typical displacement values observed at the truss ends. The decision was made to evaluate only the dead, prestress & snow load case, as the arched truss analysis indicates that this scenario yields the most critical stresses. The effect of temperature was neglected for this analysis.

The displacement applied at the truss end results in a combination of compressive and bending forces in the arched truss, counteracting the forces imposed by the vertical loads. Unlike the previous load cases, the bottom chord exhibits the most severe average compressive stress, in excess of the design strength by 4%, but significantly below the actual capacity (Table 21). The tie rod exhibits excessive overstress in this load case; due to the extremely large length to cross sectional area ratio, this force is likely to result in buckling of the tie rod before it can contribute greatly to the stiffness of the structure.

7.1.5 Analysis

For comparable loading scenarios, FEA results are generally analogous to those obtained by previous analyses. Similar conclusions may be drawn regarding the strength of the truss, which appears to be limited by the capacity of the top and bottom chords. The trusses experience the most severe stresses when subjected to a combination of dead and snow loads; these stresses are exacerbated by an applied displacement at the truss ends. Maximum vertical displacement of the truss occurs at the crown of the arch, with a resultant value of 1.45 inches due to the combination of snow and thermal loads. A summary of the stresses and deflections are tabulated below.

Table 22: Summary of Stresses and Forces, Finite Element Analysis

Member	Stress (psi)		Force (k)
	Max	Average	Equiv.
Top Chord			
Dead	780.5	496	10.6
Dead+Prestress	615	410	8.7
Dead+Snow+Prestress		1099	23.4
Dead+Temp+Prestress	675	495	10.5
Dead+Snow+Prestress+Disp		620	13.2
Bottom Chord			
Dead	1060	364	7.8
Dead+Prestress	890	440	9.4
Dead+Snow+Prestress		913	19.5
Dead+Temp+Prestress	801	352	7.5
Dead+Snow+Prestress+Disp		1350	28.8
Bearing Block			
Dead	10315	900	19.2
Dead+Prestress	9670	575	12.3
Dead+Snow+Prestress		970	20.7

Dead+Temp+Prestress	511	10.9
Dead+Snow+Prestress+Disp	1600	34.1
Tie Rod		
Dead	4800	10.0
Dead+Prestress	7000	14.5
Dead+Snow+Prestress	8750	18.1
Dead+Temp+Prestress	4720	9.8
Dead+Snow+Prestress+Disp	17650	36.6

Table 23: Summary of Displacements at Bottom Chord Crown of Arch

Displacement	y (in)	x (in)
Dead	-0.7177	0.1027
Dead+Prestress	-0.3961	0.014
Dead+Snow+Prestress	-1.34	0.2694
Dead+Temp+Prestress	-.3126	0.0033
Dead+Snow+Prestress+Disp	0.8196	1.25
Snow	-0.9439	0.2554
Temp	-0.16	-0.0107
Disp	1.2157	1.236
Snow+Disp	0.2718	1.4914
Temp+Disp	1.0557	1.2253
Temp+Snow	-1.0274	0.2447

While the overall stresses and deflections computed by the finite element analysis differ only marginally from previous analyses, the FEA points to areas of high localized stresses which previous analyses did not reveal. These stresses may not be significant enough to impact the overall integrity of the structure, but may suggest points of localized weakness and areas for potential failure if loading exceeds conditions previously witnessed by the structure. Such areas include the bearing blocks and chord splices which have already exhibited some signs of distress.

In addition, the finite element analyses addressed some of the geometric, loading and constraint nuances that could not be employed previously. For instance, the impact of prestressing in the vertical iron panel ties and the tie rod on the overall structural capacity was examined. In addition, the contribution of friction at the bearing block to brick wall interface was also examined. These changes in input parameters help to gauge the sensitivity of not only the model but also the actual structure to variability in conditions.

7.2 Buckling

In addition to static analyses, the truss was also subjected to a buckling analysis. Buckling is an axial instability phenomenon that tends to occur in structural elements with a significant length to thickness ratio, the length being defined as the distance between lateral supports. It can be defined as the sudden deformation which occurs when the stored (axial) energy is converted into bending energy with no change in externally applied loads. This is often manifested in the form of bowing or out of plane displacement, as previously illustrated in Figure 17. Buckling is of great concern in the Wagner trusses; though the top chord is laterally braced by the purlins and roof deck, the bottom chord is unbraced along the entirety of its length. Because the load that induces buckling (often called the critical load) can be significantly lower than the actual strength of the assembly, it is important to run a buckling analysis to determine if the geometry is at risk of premature deformation.

CosmosWorks® is capable of performing linear eigenvalue[88] buckling analyses. This method estimates a critical load factor output based on the user defined loads. This value is the factor of safety against buckling in a particular mode of buckling, based on end conditions. If the critical load factor exceeds 1, the loads applied are not great enough to induce buckling. Conversely, if the critical load factor is less than 1, the applied loads will result in buckling. In addition, CosmosWorks® also outputs the associated buckling shapes (or modes) and their respective displacements and deformations.

The buckling analysis requires the complete geometry of the truss in order to provide accurate results, since the resultant displacement is often not symmetric. For this analysis, one half of the truss was modeled and constrained symmetrically at the crown it was loaded under dead load and an applied force of 90 kips at both the east and west wall bearings, respectively[89]. This force corresponds to the resultant wind load acting at the top of the wall assuming the same wind speed and direction that occurred during the 1876 storm. Because it has already been observed that the tie rod is severely overstressed in the case of the imposed displacement, the tie rod has been omitted from the buckling analysis model.

The critical load factor obtained by the buckling analysis was .89; this corresponds to a critical load of 80 kips (or an equivalent wind speed of 74 miles per hour). The analysis also provides the mode shapes of the structure. In the first mode

---

[88] Eigenvalues are a special set of scalars associated with a linear system of equations (i.e., a matrix equation). The determination of the eigenvalues and of a system is extremely important in physics and engineering, where it is equivalent to matrix diagonalization and arises in such common applications as stability analysis.

[89] The highest wind speed recorded between 1876 and 1878 was approximately 78 mph; this corresponds to a net pressure of 33 psf. Assuming the wall acts as a cantilevered beam, this or the equivalent of approximately 90 kips acting at the top of the wall.

shape, the arched truss buckles into the shape of a sine half-wave; the second mode shape consists of two sine half-waves, and so on (Figure 28). The first, second and third mode buckling shapes have been identified within the roof structure and are displayed in Figure 17. These are manifest as out-of-plane rotation of the arched truss relative to its original vertical plane and bearing points as it spans between the walls.

In addition to confirming buckling would take the form of out of plane wave-like rotation of the trusses, the buckling analysis also sheds some light on the displacement load cases examined in the arched truss analyses. As the arc length of the arched truss shortens due to out of plane displacement, the span of the truss tends to shorten between the truss ends. For the maximum displacement of 2.3125 inches, measured between the truss ends, the displacement analyses indicate a required force of 160 kips to obtain this value. However, the critical buckling load is only 80 kips, indicating that the stresses in the truss due to this displacement may not be as significant as the previous analyses suggest.

While linear eigenvalue buckling analysis serves as a good starting point when attempting to determine whether a structure is prone to buckling, the results must be considered critically. Linear analyses are generally non-conservative in their estimation of buckling, since material imperfections and load eccentricities may significantly decrease the critical loads needed to buckle a member. In addition, linear buckling analysis does not provide any information regarding the load carrying capacity of the structure beyond its buckling point.

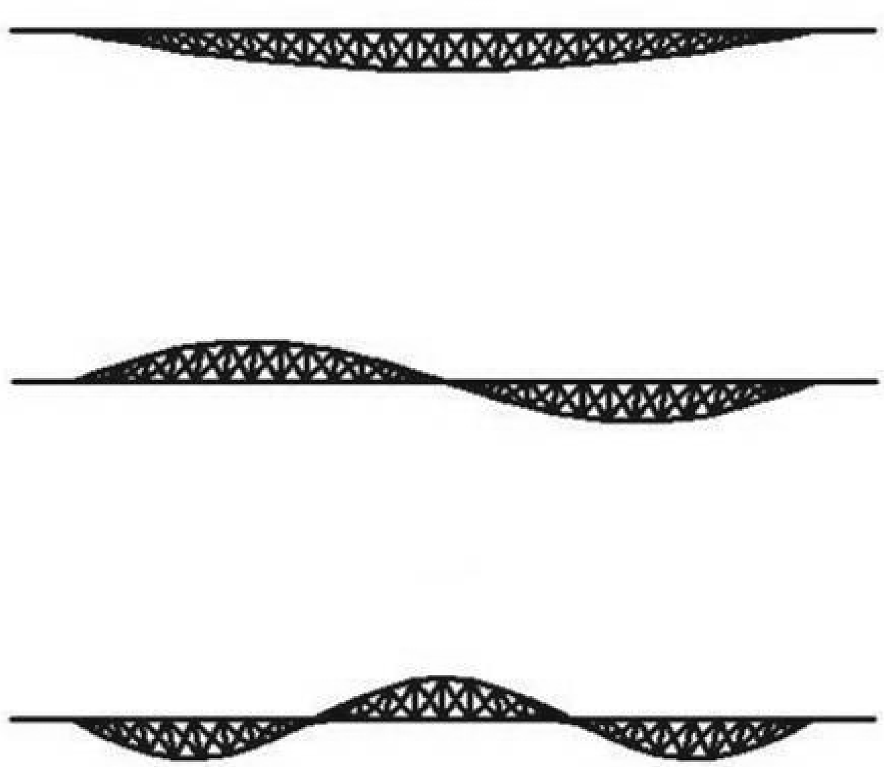

Figure 28: First, Second and Third Order Out of Plane Buckling Modes

A more thorough approach to understanding the buckling behavior of a structure involves the use of geometric nonlinear buckling analysis. This technique can be employed to analyze the behavior of the post-buckled structure subject to additional load; in addition, it aids in understanding the impact of material imperfections, which may exacerbate the instability of the post-buckled structure. However, geometric nonlinear buckling analysis requires both a thorough understanding of the structure's parameters, including boundary conditions, applied imperfections and load eccentricities, as well as considerable computing power since the analyses are difficult and expensive to run.

7.3 Plaster Analysis

The use of FEA has proven to be a useful tool in helping to understand the performance of the arched trusses. However, its capabilities are not limited to the analysis of the trusses; in addition, FEA can be extended in order to evaluate the performance of the remainder of the roof structure—in particular, the plaster ceiling. Four additional studies were performed that incorporated the decking, purlins, nailers and plaster/lath system (the roof/ceiling assembly) into the existing truss assembly model in order to determine how various loading conditions affect the plaster condition. These studies were then compared to the crack mapping of the ceiling, performed by Marlene Goeke in 2008.[90]

---

[90] Goeke, Marlene. *Assessment and Analysis of the Plaster Exhibit Hall Ceiling at the Wagner Free Institute of Science, Philadelphia, PA.* MS Thesis, University of Pennsylvania. 2008.

7.3.1 *Snow Loads—Roof/Ceiling Assembly*

The evaluation of the roof/ceiling assembly required the introduction of additional parts into the truss assembly model. One half of a bay was modeled for this load case. Because this particular analysis was less concerned with the stresses in the truss, the truss geometry was simplified in the model. A number of configurations of the roof structure were modeled to evaluate the impact of certain elements on the overall structural performance of the roof/ceiling assembly (Figure 29, Figure 30).

In addition to the simplified trusses, purlins were modeled at 20 inches on center, notched at 1 inch at the ends where they bear on the truss, and constrained to the truss with a bonded contact condition. Nailers were modeled as well, spaced at 16 inches on center and bonded to the bottom face of the purlins, simulating the nailed connection. Laths were bonded to the bottom of the nailers, spaced at 3/8" inch on center. These parts were all modeled and meshed as solid elements.

The roof deck and ceiling plaster were also modeled as simple shells rather than solid elements which would require prohibitively small meshes[91]. Shells are two-dimensional surfaces with assigned thickness; they are meshed as two dimensional elements (i.e. linear or parabolic triangles), which greatly increases accuracy and speed of analysis. The roof deck and ceiling plaster shells were assigned bonded constraints to the purlins and laths, respectively. Material properties were assigned based on the values tabulated in Section 4.2; a range of plaster values was also employed based on values from Table 5.

---

[91] The decision was made not to model the roof structure as tongue and groove for analytical simplicity.

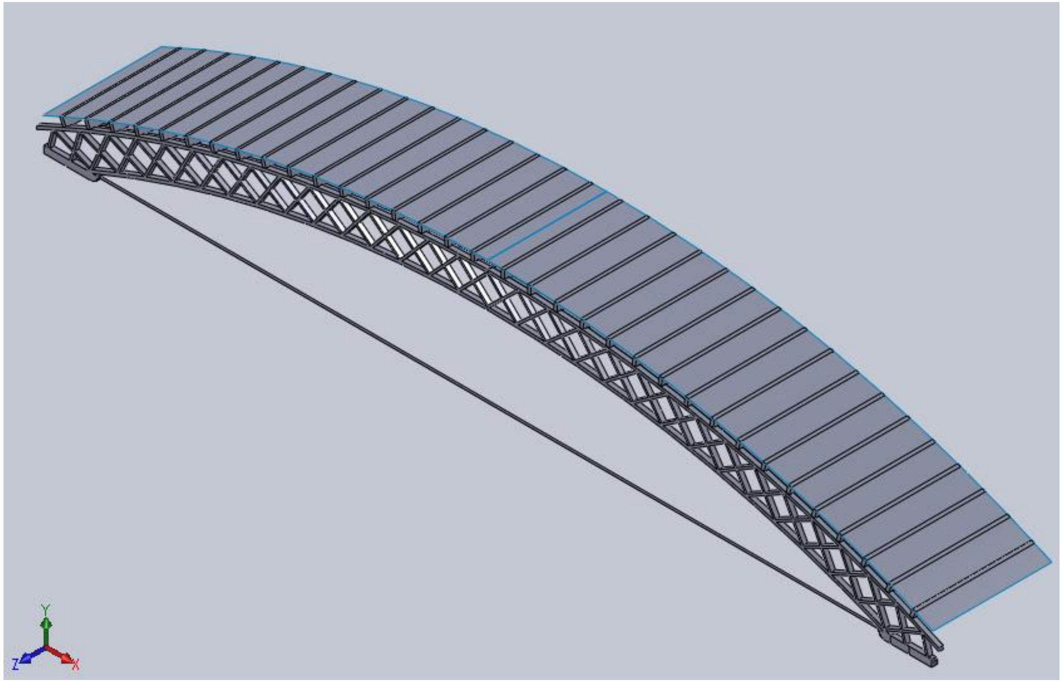

Figure 29: Roof Assembly

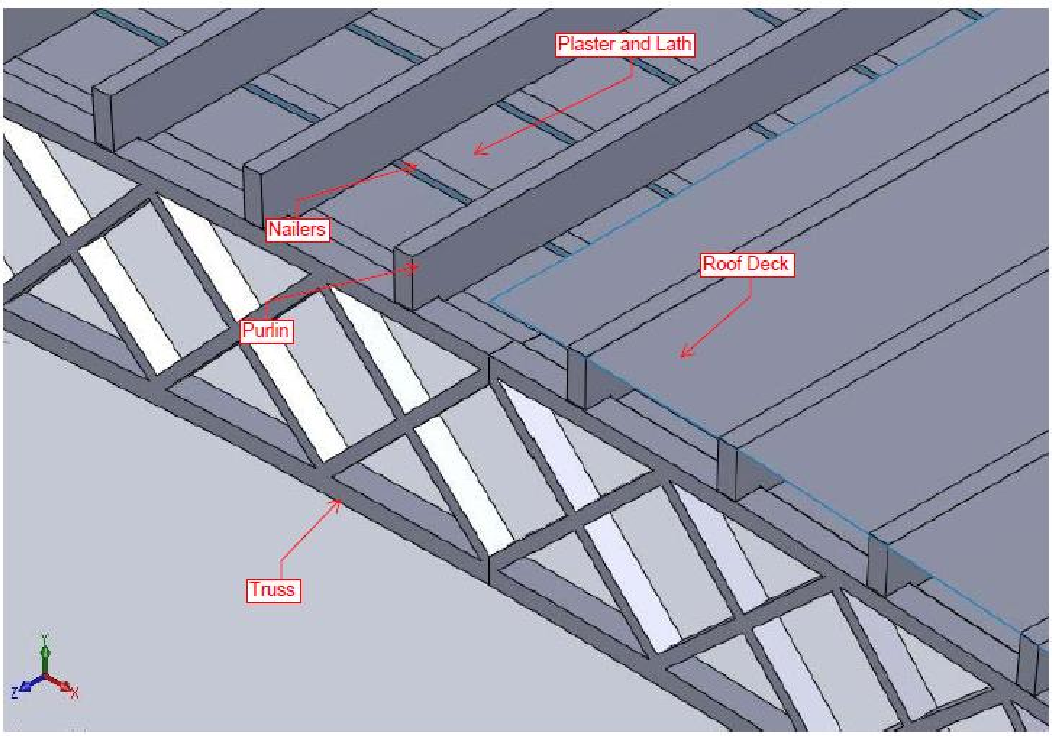

Figure 30: Roof Assembly Detail

The first load case examined for the roof/ceiling assembly considered the effects of snow load on only the truss and purlins, omitting the roof deck, nailers, lath and plaster; snow load had been determined to be the most critical load case in the simple and arched truss analyses. In this load case, it was important to account for the construction sequence of the trusses and the roof/ceiling assembly in developing the applied loads for the analytical model. Because the purpose of this analysis was to ascertain the impact of structural deflection and or deformation on the plaster, and because all of the plaster was applied after the trusses were erected and were self-supporting of their dead loads, the contribution to deflection of gravity and dead load for all parts except the plaster and lath were omitted from the analysis. In addition, the effect of any prestressing in the tie rod was also omitted. As such, only the post-erection loads—the dead load of the plaster/lath system and the live load from snow—were considered. These loads were applied as distributed loads across the top surfaces of the purlins.

The results of the analysis indicate that the predominant deflections occur in the truss, rather than the purlins, with a vertical downward displacement of 1.399 inches at the truss crown (Table 24). The purlins, which span approximately 17 feet between the trusses also exhibit slightly less some vertical displacement, measuring 1.535 inches at mid-span. This differential of .136 inches correlates to a deflection of L/1500—considerably less than the generally accepted deflection limitation of L/360 for plaster and lath ceilings. The analysis also confirms that the majority of the load is ultimately transferred to the trusses themselves, and the auxiliary structural members are considerably less stressed.

Table 24: Finite Element analysis, deflection along purlin

Assembly	Displacement		
	$Vertical_{truss}$	$Vertical_{midbay}$	Deflection Ratio
Truss, Purlins	1.399	1.535	L/1500
Truss, Purlins, Deck	0.7129	0.7257	L/16000
Truss, Purlins, Deck, Nailers (no restraint)	0.6913	0.7047	L/15000
Truss, Purlins, Deck, Nailers (restraint)	0.6903	0.7037	L/15000
Truss, Purlins, Deck, Nailers, Lath, Plaster	0.6584	0.6585	L/2040000

For the next analysis of the roof/ceiling assembly, the roof deck was incorporated into the model structure. The roof deck was assumed to be constrained by symmetry at the midspan of the bay but unconstrained at the ends, where it passes above the plane of the wall. This was in contrast to Friedman's analysis, which assumed constraint of the deck by the wall ends. The results of this analysis indicate that the roof deck acts as a vault, transferring forces in one direction along the arch of the structure, rather than across the curve; this is confirmed by the deflection results, (Table 24). In comparing the vertical deflection results to those obtained in the previous analysis, it is also evident that the roof deck increases the stiffness of the roof structure by almost 100%.

The nailers were included in the next iteration of the analysis of the roof/ceiling assembly. Because the end constraints of the nailers were unknown, two scenarios were investigated. The first scenario assumed that the nailers did not extend to the end walls and were therefore unconstrained at the ends. This scenario yielded similar results to the previous analysis, (Table 24). In this scenario, the nailers merely act as a non-structural surface for adhere the lath and plaster, and contribute minimally to the overall stiffness of the roof structure. The second scenario assumed the nailers abutted the end walls, simulated with an elastic support with the stiffness of the wall. This scenario yielded similar results, (Table 24). This imposes a displacement of .136 inches at the brick wall, and a resultant force of less than 4 pounds at every nailer end—well within the range of acceptable force on the wall.

The next iteration of the analysis incorporated the plaster and lath into the model. The inclusion of the lath does not appear to contribute significantly to deflection or stress within the roof structure. The orientation of the laths perpendicular to the nailers prevents the lath from contributing to the vault action in the bay; rather, they serve merely as a surface for engagement of the plaster. Because the plaster is continuous across the ceiling and down onto the plane of the wall, an elastic constraint—similar to that applied at the nailer end—was applied at the wall edge of the plaster. The inclusion of the plaster contributes marginally to the stiffness of the roof; as indicated by Table 24, the deflection of the roof assembly including all components is negligible, indicating that the structural movement is not severe enough to induce cracking of the plaster.

In addition to examining the deflection of the roof/ceiling assembly, the stresses in the plaster were also analyzed. Critical stresses were evaluated and mapped along the bottom face of the plaster, where they would be evident from the interior of the structure. As evidenced by Figure 31**,** maximum stresses occur the east and west ends, where the plaster turns down from the ceiling to the walls, and at equally spaced intervals along the plaster, spanning north-south, and corresponding to the location of the purlins (with higher stresses at areas where the purlins and nailers intersect). These stresses generally do not exceed 600 psi (compression). If the compressive strength of the plaster is less than this value, it can be concluded the modeled snow loads may induce cracking of the

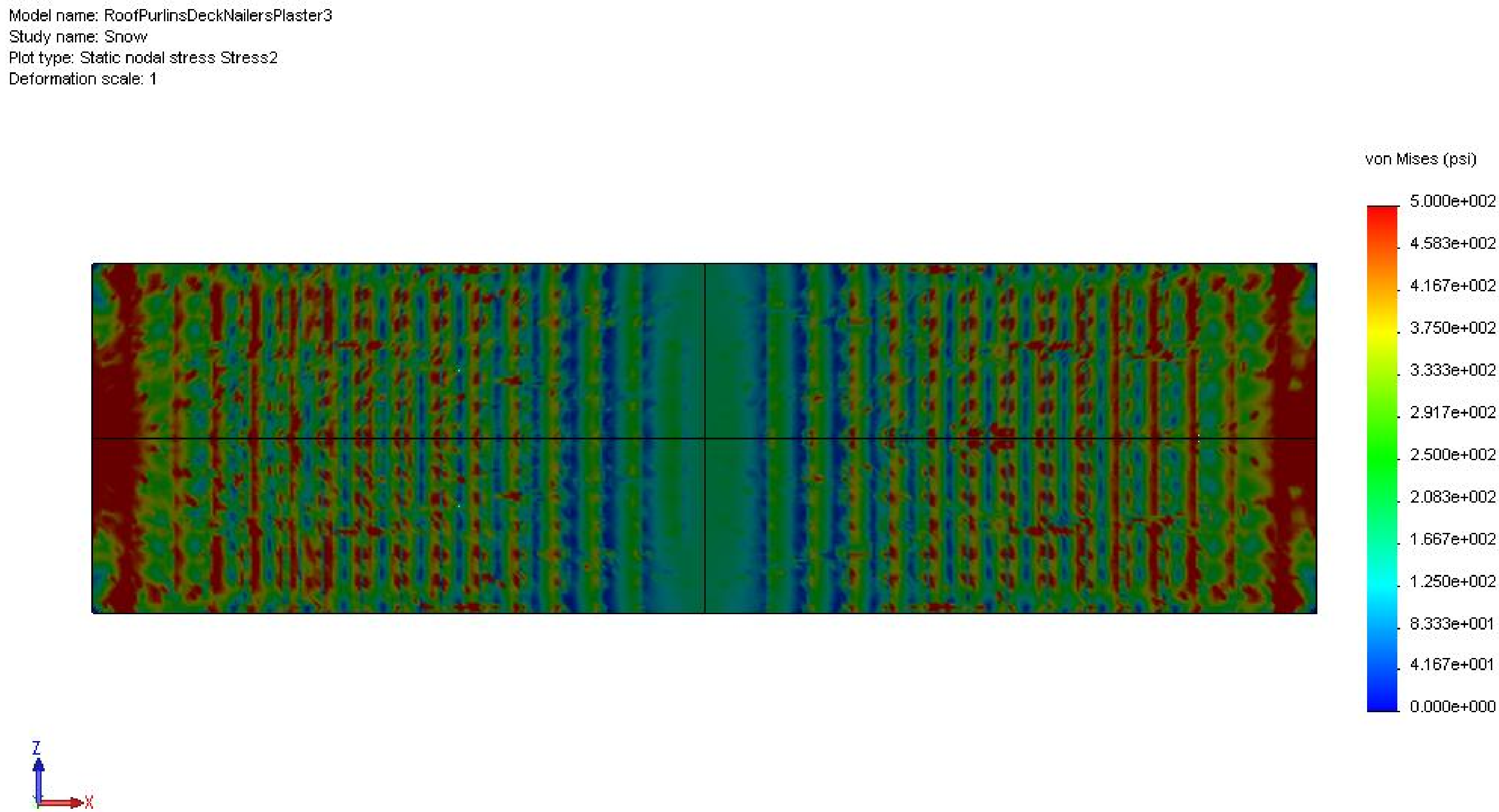

Figure 31: Stress Map of Plaster (Snow Load Only)

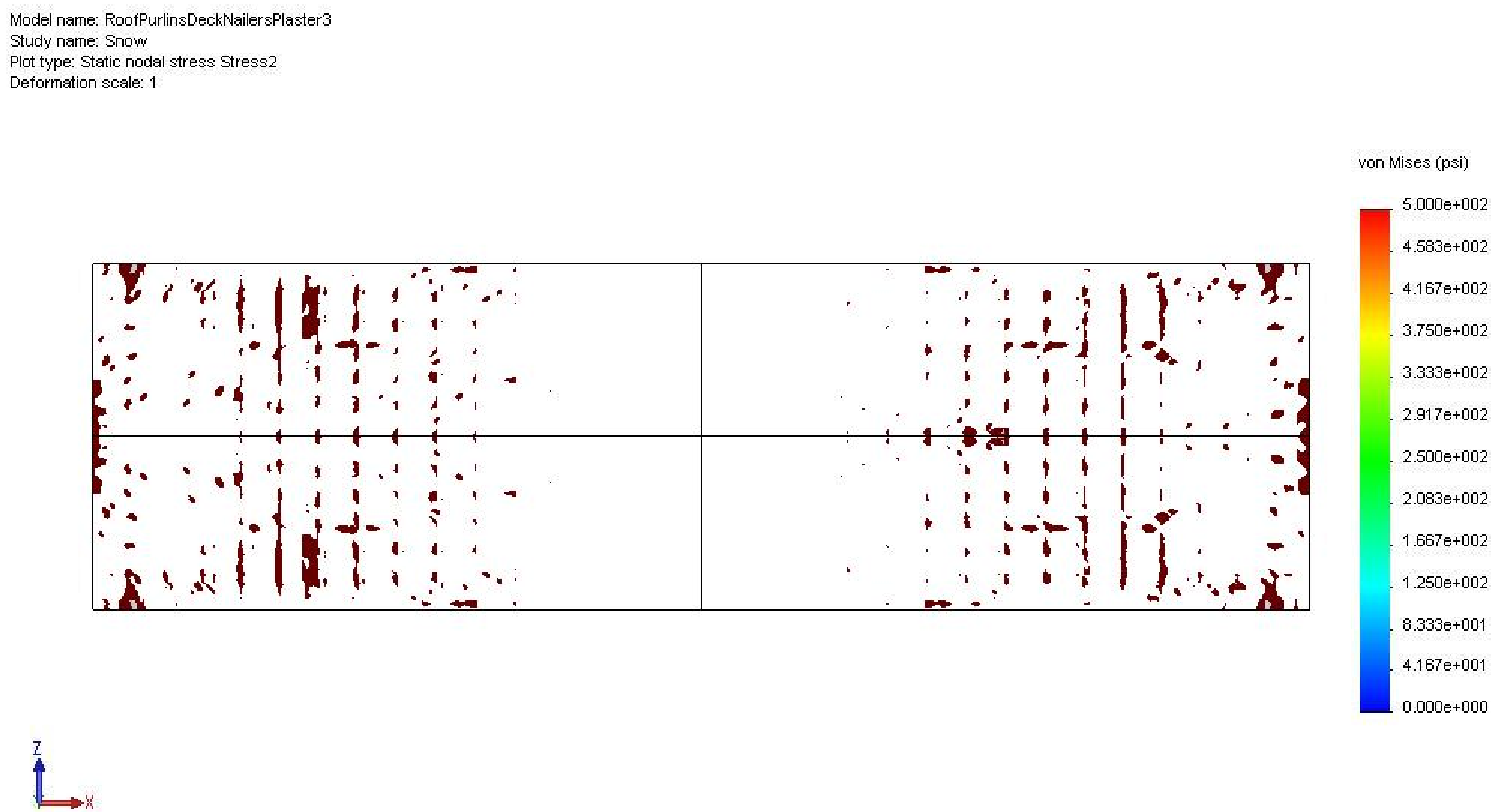

Figure 32: Stress Map with an isolation of 400 psi

plaster. Figure 32 indicated the areas of the plaster overstressed, assuming a compressive strength of 400 psi.[92] However, if the plaster compressive strength exceeds 600 psi, the cracking must be attributable to other factors.

The analysis is significant in that it indicates the areas of concern with regard to high stress concentrations in the plaster. These areas correspond fairly well to the north-south cracks identified in the crack mapping document (Figure 24**).** However, the analysis results are conspicuously devoid of high stress patterns occurring in the east-west direction, as well as high stress concentrations along the long edge where the plaster abuts the truss that the crack map identifies. Alternative load cases may help to explain these phenomena.

7.3.2 Thermal Loads—Roof/Ceiling Assembly

The two following load cases that were modeled considered thermal effects on the roof structure. Though deflection due to thermal loads was not the most severe of the studied load case scenarios, it was nonetheless important to investigate the performance of the plaster subjected to thermal rather than structural loads. In the first load case, an initial temperature of 50 degrees Fahrenheit was assumed, and a thermal increase of 50 degrees was applied.[93] The second load case assumed an initial temperature of 80 degrees

---

[92] The range of compressive strength of plaster is extremely variable, depending on its composition. For the purpose of the analysis, multiple compressive strength values were evaluated to understand their impact on plaster performance.

[93] If the plaster was applied during the spring or fall, temperatures could have averaged 50 degrees Fahrenheit; the maximum temperature of the uninsulated roof during the summer months was assumed to be 100 degrees Fahrenheit. Conversely, the second load case assumed plaster application during the warmer months and a minimum temperature for an uninsulated roof of 30 degrees Fahrenheit.

Fahrenheit and a decrease of 50 degrees. The complete roof geometry was utilized for both analyses.

Accroding to the analysis, a temperature increase from 50 to 100 degrees Fahrenheit applied to the roof structure causes the arched truss to displace vertically downward due to estimated .23 inches elongation of the tie rod; conversely, with a temperature decrease, the roof structure is displaced vertically upward. While these truss deflections are smaller in magnitude in comparison to those induced by snow loading, the stresses measured along the bottom face of the plaster were very high, relative to the compressive strength of the plaster (Figure 33**).** Figure 34 indicates areas overstress, assuming a maximum compressive strength of plaster of 2500 psi. The high imposed stresses are largely attributable to the differential between the thermal expansion coefficients of the wood and the plaster. Because the thermal coefficient of expansion of plaster is greater than that of wood, the plaster is constrained and large internal compressive stresses are induced.

The stress pattern in the thermal analysis indicates that the most critical high stress areas run east-west and correspond to the nailing strips and the constrained faces of the plaster at the truss and at mid-bay (Figure 33). This cracking pattern corresponds strongly to the plaster crack mapping, which indicates pronounced east-west cracks at evenly spaced intervals, and large cracks at the plaster/truss interface. The FEA results indicate more areas of vulnerability, with critical areas occurring along every nailer, rather than approximately every three nailers, as indicated by the crack mapping. Because the FEA analysis is linear, rather than nonlinear, it does not consider failure of the plaster; when the plaster initially cracks, the crack acts as an expansion joint which alleviates some of the stress and allows for further movement of the structure. As such, the plaster may not crack at all locations and may instead occur at areas of weakness; these areas can include discontinuities in the plaster assembly such as locations where the nailers are discontinuous, or where the termination of laths (approximately 4 feet in length) are coincident with a nailer, providing less grip for the plaster keys.

The deflection performance of the roof structure subjected to a thermal decrease from 80 to 30 degrees Fahrenheit is opposite that of the thermal increase. Contraction of the tie rod acts as a prestressing force, pulling the truss ends towards each other and resulting in a vertical upward displacement of the arch; conversely, the remained of the roof structure is displaced vertically down. The plaster exhibits virtually identical stress behavior as in the previous analysis, and the same conclusions can be drawn regarding the correlation between the stress patterns and the crack mapping of the ceiling.

7.3.3 Snow and Thermal Loads—Roof/Ceiling Assembly

The snow load case was revisited after running the thermal analyses to ascertain how the combination of thermal and structural loads would impact that plaster. This time, a more moderate temperature from 70 degrees to 50 degrees Fahrenheit was considered. Deflection results did not differ considerably from those obtained in the snow load only load case. Though the stresses in the plaster did not reach the values obtained in the thermal analyses, they did exceed the snow load only stresses considerably (Figure 35). Average maximum stresses of 1750 psi were measured at high stress locations. Figure 36 and Figure 37 illustrate areas of overstress assuming plaster compressive strengths of 1400 and 2500 psi, respectively.

The results of this analysis correlate remarkably well to the crack mapping. As evidenced by Figure 35, the high stress concentration at the truss edge and the nailers, which was not apparent in the snow load only case area, can be attributed to the thermal load; conversely, the high stresses at the purlins appear to be caused predominately by snow loads. In addition to these perpendicular stress patterns located at nailer and purlin areas, this load case also illustrates some diagonal cracks that occur towards the wall ends of the truss which can also be seen in several bays on the crack map.

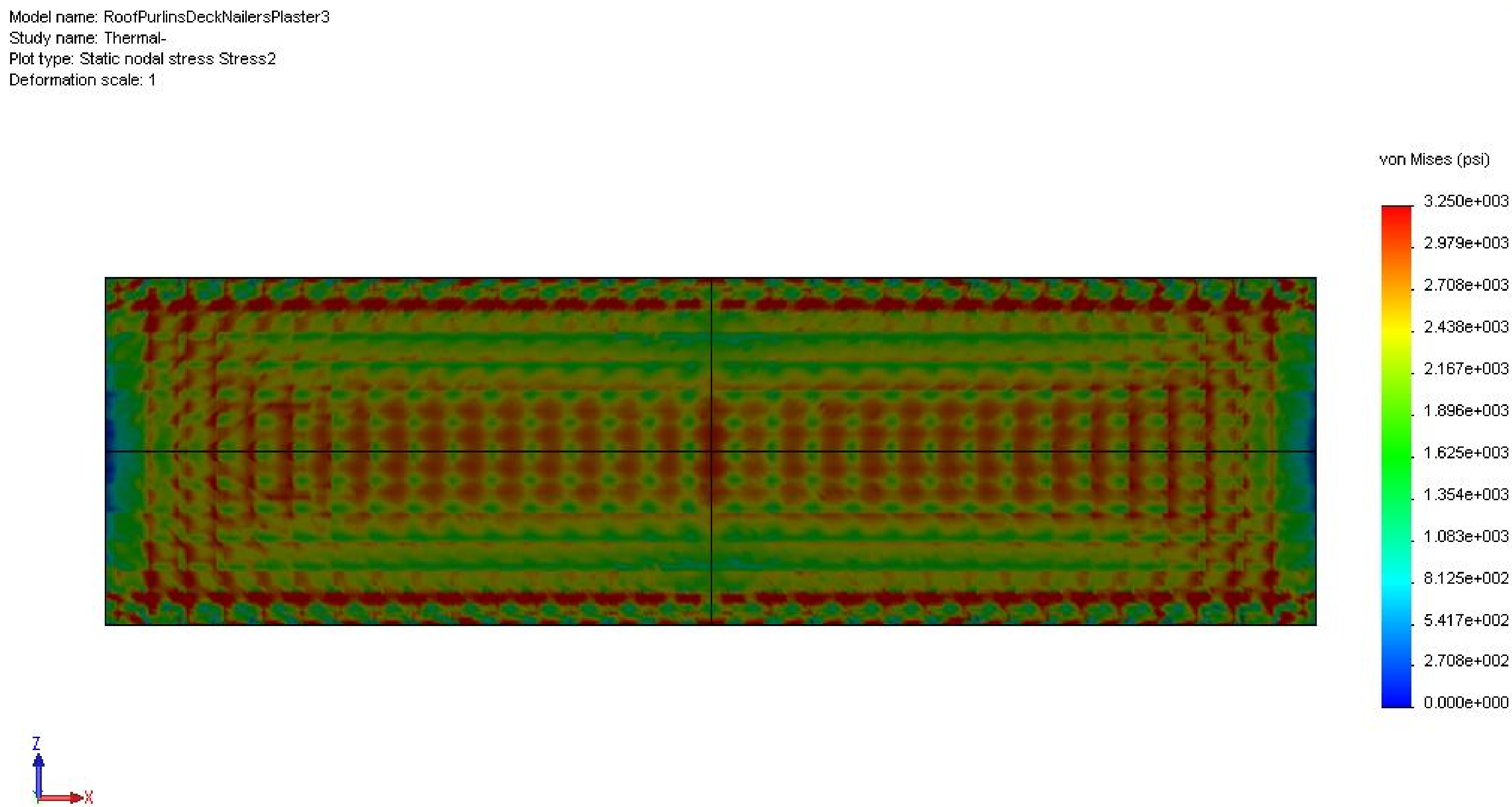

Figure 33: Stress Map of Plaster (Thermal Load Decrease)

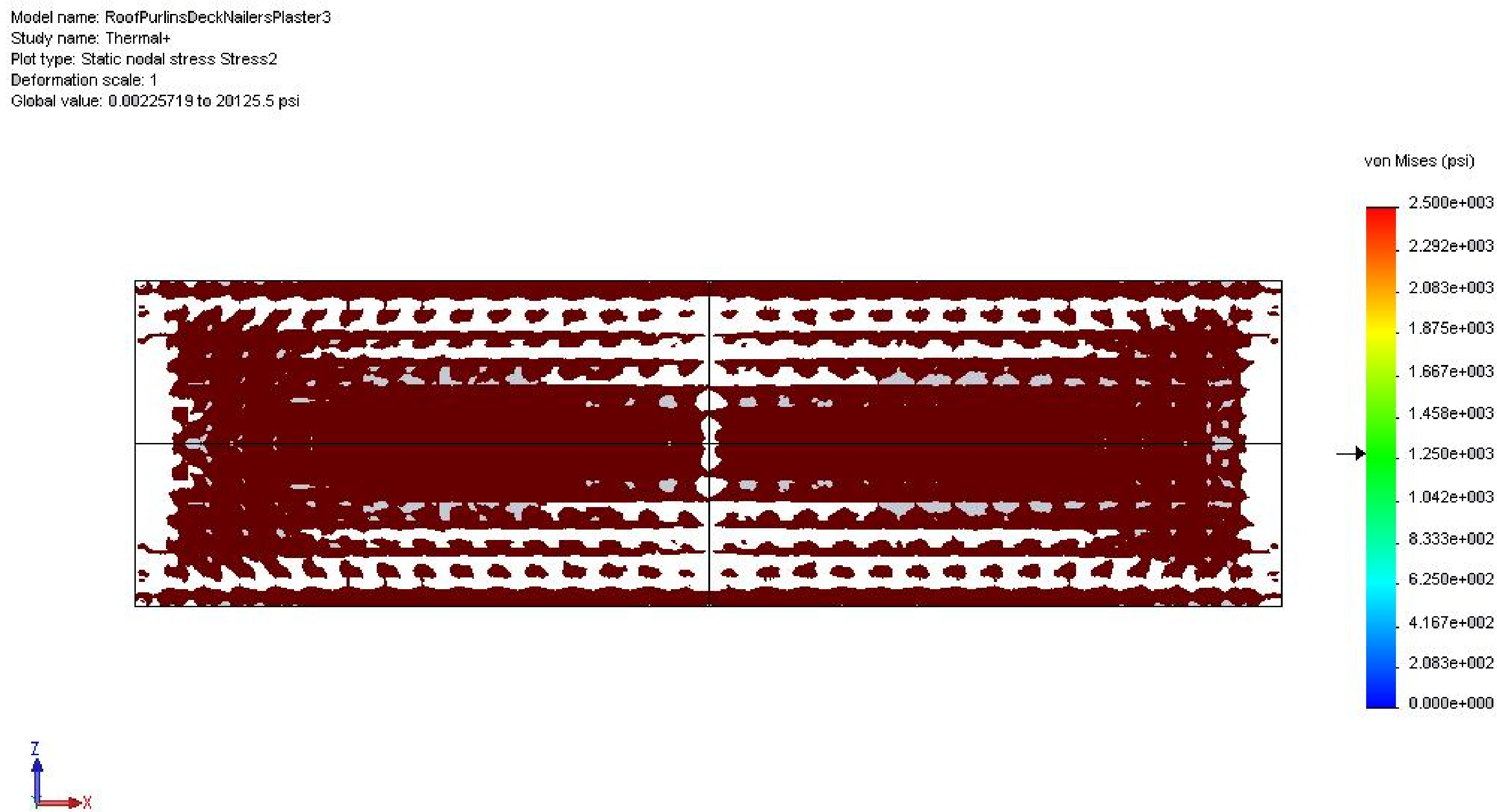

Figure 34: Stress Map of Plaster, with an isolation of 2500 psi (Thermal)

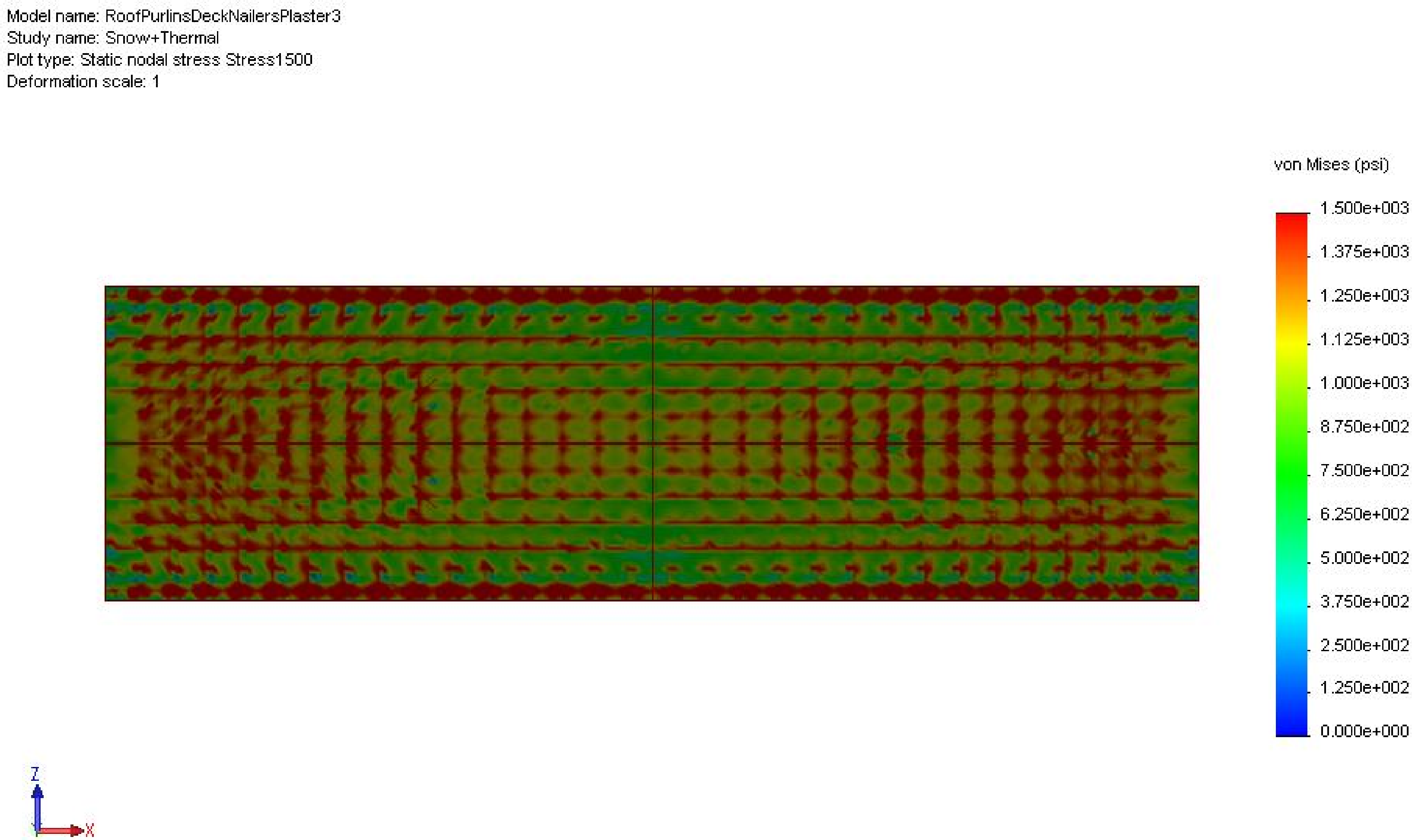

Figure 35: Stress Map of Plaster (Snow and Thermal Loads)

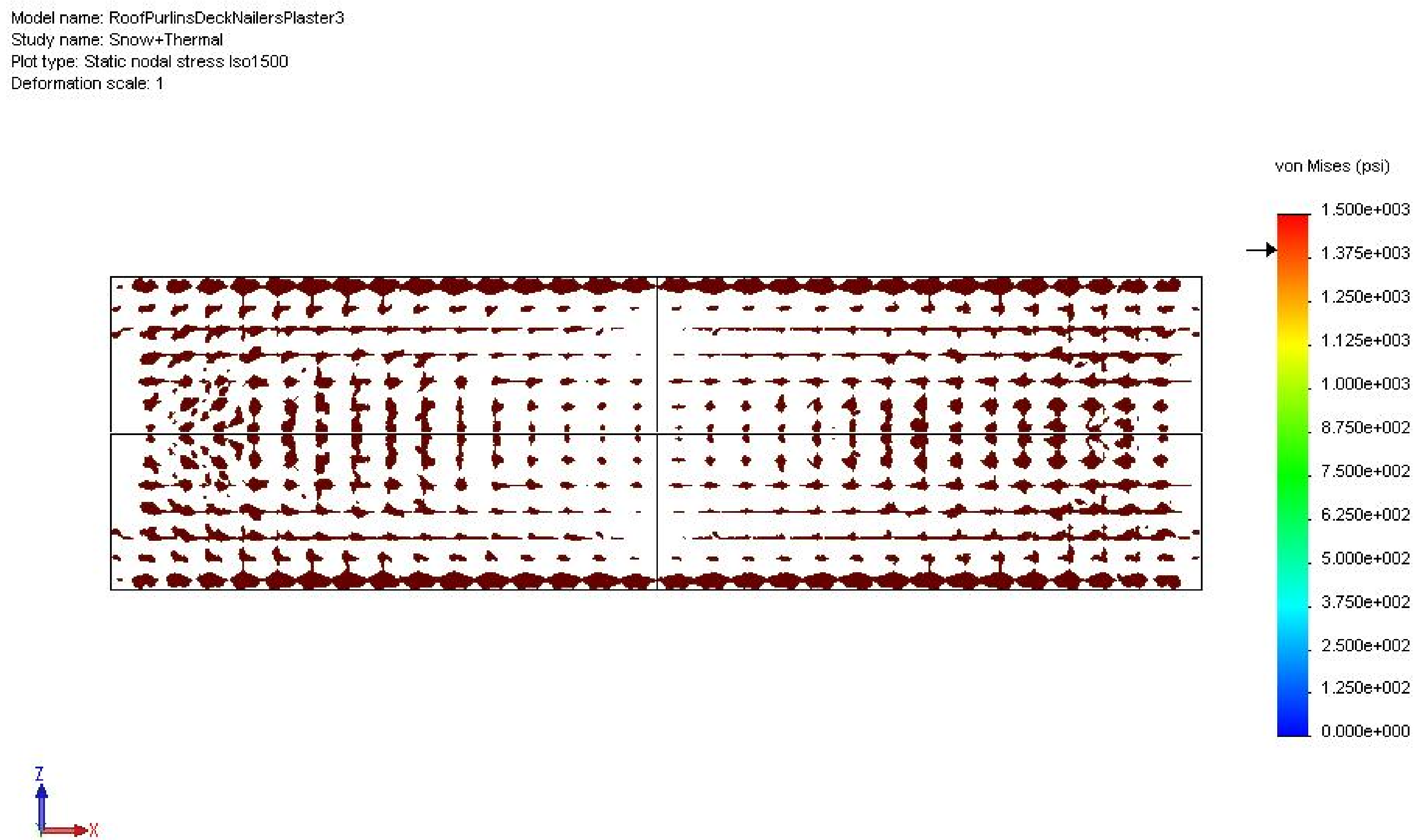

Figure 36: Stress Map of Plaster, with an isolation of stresses greater than 1400 psi

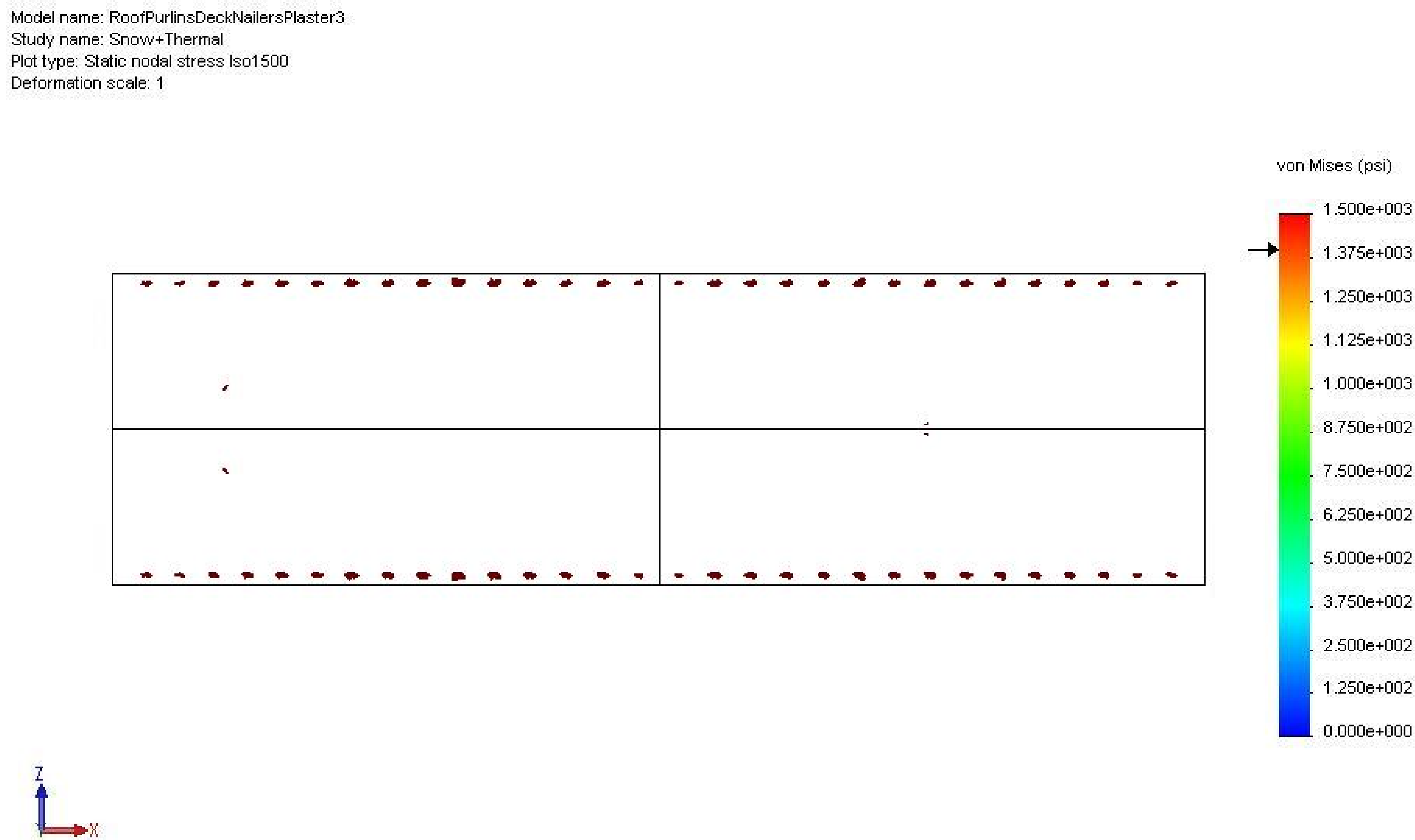

Figure 37: Stress Map of Plaster, with an isolation of stresses over 2500 psi

8 Conclusions

In this thesis, finite element analysis was utilized to investigate the structural performance of the roof structure—inclusive of the arched trusses, the vaulted roof assembly, and the plaster—at the Wagner Free Institute of Science. The purpose of this investigation was to understand structural behavior and to evaluate the impact of structural deflections on the performance of the plaster ceiling. The following section summarizes the results of these analyses and recommendations for further study.

8.1 Truss

The stress and deflections of the arched roof trusses of the Wagner Institute building were studied extensively in this thesis. Three types of analyses were generated for the roof trusses—a simple arch analysis, a trussed arch frame analysis, and a linear elastic finite element analysis. In the simple arch analysis, the arched trusses were simulated as a singe arch with equivalent geometric properties (i.e. moment of inertia, cross sectional area) to the actual structure. The arched truss analysis utilized beam elements assembled in a manner congruent with the actual structure. The finite element analysis simulated the actual geometry of the structure by modeling the structure as an assembly of small finite solid elements.

All three analyses yielded similar results in terms of the structural mechanism of the arch. The arches act in both compression and bending, and loads are transmitted down to the ends of the arches, where vertical load is then transmitted to the exterior brick bearing walls and the horizontal thrust is resisted by the tie rod. Generally, all wood elements of the arched truss are compression members, while the iron elements (with the exception of the panel iron bearing blocks) are in tension. The curved top and bottom chords carry the majority of the load, while the wood cross bracing and the iron tension rods serve to stiffen the structure. Under gravitational (dead) loads, maximum forces in the top chord occur at the crown and gradually diminish towards the end of the arched truss, whereas the forces in the bottom chord are most critical at the ends.

The effects of various dead, live and environmental loads on the structure were examined in all three analyses. In addition, the finite element analysis also incorporated prestressing forces which may have been introduced prior to or during erection of the arched trusses. The combination of dead and snow load generates the most significant forces in the structure. In general, the stresses due to loads generally seem to be within range of the allowable strength of the wood and iron members in most load cases; in all load cases stresses are less than the generally accepted values for "actual" strengths. The bearing blocks are the only instance of marginal capacity relative to estimated stress strength; in this instance, the tension in the tie rod induces high stresses at the plate washer, as well as at the birdsmouth notch where the block receives the lower chord.

The consideration of wall movement also informed the analysis of stresses within the structure. By simulating the post-erection displacement of the walls at the truss ends, and thereby shortening the distance between them, the compression forces in the arched trusses increased, but the bending forces due to gravitational load were countered; in some instances this resulted in a reversal of stresses such that the bottom chord began to exhibit highest stresses at the crown and the top chord exhibited highest stresses at the ends. The combination of dead and snow loads, in conjunction with an applied displacement at the truss ends generated the most significant forces in the structure for this analysis.

Vertical deflections of the truss do not appear to be of great concern as regards the plaster analysis, when compared to the generally accepted deflection ratio limit of L/360 for plaster ceilings. Though maximum displacement of the truss was measured to be 4.027 inches (or L/171) due to the combination of dead, snow and displacement forces, the current plaster would have been installed after the wall movement had occurred and well after the trusses had deflected under their own weight or dead load. Absent the displacements due to truss dead load and post-construction wall movement, the net vertical deflection of the plaster ceiling is calculated as 1.108 inches, or L/620, nearly half the maximum deflection limits for plaster support systems.

The buckling analysis of the arched trusses indicated that the out of plane rotation of the truss was most likely a result of the high winds that hit the building in 1876 and 1878. The addition of the shear wall in 1885 appears to have stabilized the structure from this type of movement, preventing further damage. Furthermore, because buckling occurred prior to the application of the present plaster ceiling, the lateral deflection of the arched trusses is unlikely to have contributed to the plaster cracking. Though further buckling is unlikely, is it important to consider the behavior of the postbuckled structure when considering the effect of additional stresses on the structure and the plaster ceiling. This phenomenon should be analyzed in the future using a nonlinear buckling analysis which considers the arched trusses as well as any contribution of lateral restraint by the remainder of the roof structure.

8.2 Plaster

The extension of the finite element analysis from the roof trusses to the roof/ceiling assembly aids in the further understanding of the deflections, strains and stresses imposed on the plaster ceiling. For these analyses, the impact of snow and thermal loads were investigated, as well as the effects of the remaining roof assembly elements (i.e. purlins, roof deck, nailers, lath and plaster). These analyses indicated that the roof bays act predominately as vaults, transferring the loads from the roof deck through the arched trusses, the horizontal thrust being taken up by the tie rod and the vertical forces being transmitted into the walls. The vaulting action also appears to greatly reduce the deflection in the roof/ceiling assembly.

The effect of structural deflection alone on the plaster does not appear to be severe enough to induce compressive cracking, provided the plaster has a compressive strength of greater than 600 psi. However, thermal loads on the structure and the roof/ceiling assembly were computed to be significant with respect to plaster cracking. Temperature increase from 50 to 100 degrees Fahrenheit were computed to result in severe overstressing of the plaster ceiling; the combination of snow and a 20 degree thermal drop appear to yield intermediate results, with higher stresses than the snow load only case, but less severe stresses than the thermal load cases.

The results of the FEA analysis show that areas of high computed compressive stresses in the plaster correlate strongly to the crack mapping performed by Marlene

Goeke and Building Conservation Associates in 2008.[94] The most significant areas of concern appear to coincide with the roof purlins, the nailers, and the edges of the plaster which are constrained either by the wall of the trusses. The combination of snow and thermal loads suggest that the cracking of the ceiling may be attributed to both structural and thermal loads, and/or the juxtaposition of the two.

The results of the analyses in this thesis must be interpreted with a clear understanding of certain inherent limitations. Certain critical parameters and properties have been assumed in the absence of measured data. . For instance, the temperature range to which the roof structure is subjected must be measured. In addition, the strength properties of the plaster need to be ascertained. These are critical for all structural and thermal load cases.

Given the results of the analyses, some general recommendations can be made regarding the conservation of the plaster ceiling. Because the cracking appears to be the result of active compressive loads (in other words, cracking did not occur as a result of stabilized settlement or shrinkage upon application), these loads will continue to stress the plaster ceiling. As such, repair of the plaster to its original state without the inclusion of some stress relief points will only result in recurring cracking. Moreover, by repairing the plaster with a weaker material, the plaster is likely to crack at the same locations; repair with a stronger material may possibly result in cracking or key failure at new locations within the plaster. It is recommended that a means by which the plaster shell is allowed to accommodate structural movements be provided in the form of a network of expansion joints. The placement of these joints should be designed when more thorough

[94] Ibid.

material properties and environmental data is obtained. In addition, though omitted from this analysis, the integrity of the keys should be thoroughly evaluated in order to inform both the capacity of the plaster as well as the placement of expansion joints.

8.3 Finite Element Analysis

In addition to addressing the concerns associated with the Wagner Institute roof assembly, the purpose of this thesis was to evaluate the efficacy of finite element analysis as a diagnostic tool. Through the various exercises employing FEA, an attempt was made to distinguish both the benefits and the disadvantages that can be associated with the tool, and to critically evaluate some of the specific challenges that the application of FEA to historic structures poses.

The advantages of finite element analysis are numerous; it is powerful, accurate, and allows the user to simulate accurate real world scenarios with powerful analysis techniques. These advantages, which make FEA a favorite tool across many disciples, are equally, if not more, applicable to the investigation of historic structures. FEA allows the user to model complex structural geometries and to evaluate the performance of buildings constructed prior to the understanding of structural mechanics or in multiple phases. It provides a means by which the impact of complex or time dependent loading histories on a structure can be assessed. Its analytical capabilities also allow for the study of structures which exhibit certain failure patterns such as cracking, buckling or yielding.

The application of FEA to the Wagner allowed for the extensive analysis of the roof assembly without threatening the structure. It allowed us to gain an understanding of the overall structural behavior and quantify deflection and stress, using multiple analytical techniques. Its capabilities were above and beyond conventional frame analysis; it allowed us to model accurate geometries rather than idealized concentric beam elements, and to apply a multitude of constraints to simulate real world behavior.

Despite its capabilities, FEA is not without its limitations. In particular, the cost to benefit ratio associated with FEA must also factor in the decision of whether or not it is an appropriate tool for a particular application. Cost can encompass more than just software expense; it can also manifest itself in the form of time—time spent learning how to utilize the software, time spent generating and troubleshooting a model, and/or the actual time required to perform the analyses. Consider, for example, a simple steel frame. It is considerably more laborious to create all of the complex member and connection geometries of this configuration, than it is to create two dimensional lines and automatically select member sizes using a simple frame analysis software or even hand calculations. The cost of time spent generating an FEA model and running an analysis most likely outweighs any nominal increase in accuracy, provided the models are constrained identically. This was manifested in this thesis in the analysis of the truss by both frame analysis and FEA. Though both analyses yielded similar results, the RISA® model took a fraction of the time to model and under 1 minute to analyze; the FEA model took 2 to 4 hours to run comparable load cases, and up to 8 hours for the roof assembly analyses. In this particular scenario, the use of nearly identical properties, geometries and constraints proved that the sometimes the more simple technique may also be the most appropriate.

When employed correctly, the analytical powers of FEA can be applied to historic structures quite effectively. However impressive, there is always a risk in relying on the outputs of the analysis, particularly in historic buildings, where the input parameters such as material properties, constraints and loading patterns are preexisting and not defined by the engineer. Moreover, it is important to recognize that the expense of utilizing such a sophisticated tool may not be warranted if the variability in input parameters outweighs the increase in result resolution. This is of particular important in buildings constructed of materials such as wood, masonry or wrought or cast iron, whose properties are extremely variable by today's standards.

Knowledge of these parameters is important not only to the understanding how sensitive the software is to their variability but also the structure itself. The sensitivity of the Wagner structure to prestressing forces, for example was determined to be quite significant on the deflection results, whereas the use of a bearing constraint in place of a roller was inconsequential with regard to vertical deflection. Furthermore, while some variability in parameters such as thermal loads has minimal impact on results such as deflection of the arched truss, they may have a significant impact on others, like stress in the plaster. By understanding the sensitivity of the model, the user can narrow down on areas of concern which merit further investigation, and can simplify areas which are not critical. Conversely, the comparison of the observed conditions to the FEA may also aid in refining the model for improved accuracy.

The application of the finite element analysis to the roof structure at the Wagner provided valuable information regarding the performance of both the arched trusses as well as the plaster ceiling. Though the study of the arched trusses ultimately proved that more simplified methods can be applied as effectively as FEA, the tool was extremely effective in its prediction of the structural response as evidenced by the pattern plaster damage from high compressive stresses. Through further study of the unknown variables and refinement of the model to accommodate these changes, a conservation plan for the plaster is greatly informed by the results of modeling of the deflection of the structural system that supports the plaster ceiling.

9 Bibliography

2006 International Building Code. Developed by the International Code Council. 2006.

Argyris, J.H."Energy Theorems and Structural Analysis," *Aircraft Eng.*, Vol. 26, October-November 1954, pp. 347–356, 383–387, 394.

ASCE 7-05 Minimum Design Loads for Buildings and Other Structures. Published by the American Society of Civil Engineers. Reston, Virginia. 2006.

Baker, Ira Osborn. *A Treatise on Masonry Construction.* John Wiley & Sons. London. 1914.

Barthel, R.: *Tragverhalten gemauerter Kreuzgewölbe*. Karlsruhe: Universität Karlsruhe. 1993.

Bau, H.H. ©, MEAM 427 Class Notes, "Chapter 2: Interpolation" 21 August 06.

Bau, H.H. © ENM 427/ MEAM 527, Class Notes, "Chapter 1: Introduction to Finite Elements and Applications." 9 Sept 2009.

Brauer, John R. *What Every Engineer Should Know About Finite Element Analysis.* Marcel Dekker Inc. New York, NY. 1993.

Blackburne, E. L. *The mason's, bricklayer's, plasterer's, and decorator's practical guide*. London: J. Hagger, 1850.

Bolt, Eugene, and Susan Glassman. National Historic Landmark Nomination, 4 April 1989.

Boothby, T., Atamturktur, S., (2007), "A Guide for the Finite Element Analysis of Historic Load Bearing Masonry Structures," submitted to 10th North American Masonry Conference, St. Louis, Missouri, USA.

Building Conservation Associates, Inc. "Wagner Free Institute of Science: Exhibit Hall Ceiling Conditions Assessment." February, 2008.

Building Improvements, 1885-1891. ARC 91-035. Wagner Free Institute of Science Archives.

Chan, T.H.T. et al. "Concurrent multi-scale modeling of civic infrastructures for analyses on structural deteriorating—Part II: Model updating and verification." Finite Elements in Analysis and Design 45. 2009. Elsevier Science Publishers. pp. 795-805.

Chan, T.H.T. et al. “Concurrent multi-scale modeling of civic infrastructures for analyses on structural deteriorating—Part I: Modeling methodology and strategy.” Finite Elements in Analysis and Design 45. 2009. Elsevier Science Publishers. pp. 782-794.

Chiostrini, S., Foraboschi, P. and Sorace, S., “Problems connected with the arrangement of a nonlinear finite element method to the analysis of masonry structures.” *Structural Repair and Maintenance of Historical Buildings*, Computational Mechanics Publications, 1989. pp. 525-534

Clark, Joe. Letter to Thomas Leidgh, Suzanne Pentz. Wagner Free Institute of Science. 8 October 1994.

Clough, R.W.“The Finite Element Method after Twenty-Five Years: A Personal View,” *Comput. Structures*, Vol. 12, 1980, pp. 361–370.

Clough, R.W. “The Finite Element Method in Plane Stress Analysis,” *Proceedings of 2nd ASCE Conference on Electronic Computation*, Pittsburgh, PA, September 8–9, 1960.

Collins & Autenrieth. Letter Report. *Conditions Assessment of the Wagner Institute*. 28 Feb 1885.

Collins & Autenrieth. *Specifications for the Improvement of the Wagner Institute.* 1885.

Condit, Carl W. *American Building: Materials and Techniques from the First Colonial Settlements to the Present*. Edited by Daniel Boorstin. Chicago: The University of Chicago Press, 1982.

Construction Drawings; *Wagner Free Institute of Science, Museum Building Restoration Project*, prepared by William Stivali, Building Conservator. 30 January 2007.

Croci, G. *Conservation and Structural Restoration of Architectural Heritage*. Computational Mechanics Publication, 1998.

Dare, Charles P. *Philadelphia, Wilmington and Baltimore Railroad Guide: Containing a Description of the Scenery, Rivers, Towns, Villages, and Objects of Interest along the line of the Road.* Fitzgibbons & Van Ness. Philadelphia. 1856.

Dumortier, S. & W.P. De Wilde. “Finite element study of the Tower of Brussels City Hall”. *Structural Studies, Repairs and Maintenance of Historic Buildings IV. Volume I. Architectural Studies, Materials and Analysis*. 1995. pp. 365-372.

Eckel, Edwin C. Cements, *Limes, and Plasters: Their Materials, Manufacture and Properties*. New York: John Wiley and Sons, 1928.

Eugen-Kurrer, Karl. *The History of the Theory of Structures: From Arch Analysis to Computational Mechanics.* Ernst & Sohn Verlag fur Architektur und technische Wissenschaften GmbH & Co. KG. Berlin. 2008.

Felippa, Carlos. “A Historical Outline of Matrix Structural Analysis: A Play in Three Acts.” Report No. CU-CAS-00-13, University of Colorado, Department of Aerospace Engineering. 2000.

Friedman, Donald, P.E. Letter to William Stivale: Wagner Institute, Main Roof Structure, 19 Sept 2005.

Friedman, Donald, P.E. Memorandum to William Stivale, Building Conservator: Wagner Museum Design. 7 Jan 2008.

Goetke, Marlene. *Assessment and Analysis of the Plaster Exhibit Hall Ceiling at the Wagner Free Institute of Science, Philadelphia, PA.* MS Thesis, University of Pennsylvania. 2008.

Gredell, Gary. Structural Condition Assessment: Roof and Upper Masonry Walls, Exhibition Hall. Gredell & Associates Structural Engineers. 27 Sept 2008.

Heubner, Kenneth, et al. *The Finite Element Method for Engineers.* John Wiley & Sons. New York, NY. 2001.

Heyman, J. *The Stone Skeleton. Structural Engineering of Masonry Architecture*. Cambridge University Press. 1995.

Huerta, Santiago. “The Debate about the Structural Behaviour of Gothic Vaults: From Viollet-le-Duc to Heyman.” Proceedings of the Third International Congress on Construction History, Cottbus, May 2009. p. 837-844.

Hrenikoff, A. “Solution of Problems in Elasticity by the Framework Method,” *J. Appl. Mech.*, Vol. 8, 1941, pp. 169–175.

I.C.S. Reference Library. International Textbook Company. Scranton, PA. 1905.

Jacobs, James A. *Historic American Buildings Survey*, Wagner Free Institute of Science. HABS no. PA 6667 (2000).

Karamchandani, Ashish. “Limitations of Some of the Approximate Structural Analysis Methods that are Used in Structural System Reliability.” Department of Civil Engineering, Stanford University, Stanford, CA. 1989. Structural Safety, 7. 1990. Elsevier Science Publishers. pp. 115-127.

Kidder, Frank and Harry Parker. *Architects' and Builders' Handbook*. New York: J. Wiley and Sons, 1921.

Kübler, L. Computer “Analyse der Statik zweier gotischen Kathedralen.” Architectura 4. 1974. pp. 97-111.

“Lecture 14.5: Space Structure Systems.” WG 14 Structural Systems: Buildings. University of Ljubljana, Slovenia. 2000.

Leidigh, Thomas J., Suzanne M. Pentz. Wagner Free Institute of Science Roof Structure Wood Pathology Investigation. 13 October 1994.

Long, Craig, et al. “Effects of finite element formulation on optimal plate and shell structural topologies.” Finite Elements in Analysis and Design 45. 2009. Elsevier Science Publishers. pp. 817-825.

Mainstone, Roland J. “Structural Analysis, Structural Insights and Historical Interpretation.” The Journal of the Society of Architectural Historians. Vol. 56, No. 3. Sept. 1997. pp. 316-340.

Mark, Robert. *Experiments in Gothic Structure.* MIT Press. Cambridge, MA. 1982.

Mark, Robert, Paul Hutchinson. “On the Structure of the Roman Pantheon.” The Art Bulletin. College Art Association. 1986. pp. 24-34.

Melchers, Robert E. and Richard Hough. *Modeling Complex Engineering Structures.* ASCE Press. Reston, Virginia. 2007.

Minutes of the Board of Trustees of the Wagner Free Institute of Science, 1924. Wagner Free Institute of Science Archives.

Moore, Herbert. *Textbook of the Materials of Engineering.* McGraw Hill Book Company, Inc. New York, NY. 1920.

Morris, Toby E., R. Gary Black, and Stephen O. Tobriner. “Report on the Application of Finite Analysis to Historic Structures: Westminster Hall, London.” Vol. 54, No. 3. Sept. 1995. pp. 336-347.

Newmark, N.M. *Numerical Methods of Analysis in Engineering*, L. E. Grinter (ed.), Macmillan, New York, 1949.

Noor, A.K.“Bibliography of Books and Monographs on Finite Element Technology,” *Appl. Mech. Rev.*, Vol. 44, No. 8, June 1991, pp. 307–317.

Ozkul, Tulay Aksu, Eiichi Kuribayashi. “Structural Characteristics of Hagia Sophia: II—a finite element formulation for dynamic analysis.” Building and Environment 42. 2007. Elsevier Science Publishers. Pp. 2100-2106.

Ozkul, Tulay Aksu, Eiichi Kuribayashi. “Structural Characteristics of Hagia Sophia: I—a finite element formulation for static analysis.” Building and Environment 42. 2007. Elsevier Science Publishers. Pp. 1212-1218.

Rajasekaran, S., G. Sankarasubramanian. *Computational Structural Mechanics.* Prentice Hall of India. New Dehli. 2001.

Records of the Wagner Free Institute of Science, 1885-1949. ARC 90-001. Wagner Free Institute of Science Archives.

Ronca, P., M. Veroli, A. Franchi,. “Deformation Analysis of Joints of a Long Span Trussed Wood Arch: Experimental Tests and Numerical Analyses”. Transactions on the Built Environment vol 15. WIT Press. 1995. pp. 347-356.

Scharf, John Thomas. *History of Delaware 1609-1888: Local History*. L. J. Richards & Co. Philadelphia. 1888.

Szilard, Rudolph. *Theories and Application of Plate Analysis: classical, numerical and engineering methods*. John Wiley & Sons. Hoboken, NJ. 2004.

Testwell, Inc. Historic Masonry Evaluations, Wagner Free Institute of Science. November 2007.

Unay, Ali Ihsan. “Structural Wisdom of Architectural Heritage.” Middle East Technical University, Department of Architecture. Ankara, Turkey. 2000.

Vitruvius. *The Ten Books on Architecture*. Translated by Morris Hicky Morgan. Reprint, Cambridge: Harvard University Press, 1914.

“Wagner Free Institute.” *Philadelphia Inquirer*, 11 January 1861.

“The Wagner Free Institute of Science.” *Philadelphia Press*, 25 October 1860.

Wagner Free Institute of Science, Annual Announcement. Philadelphia, 1911.

Wheeler, Junius Brutus. *An Elementary Course of Civil Engineering for the Use of Cadets of the United States Miltary Academy.* John Wiley & Sons. New York, NY. 1877.

Williams, Judsen, et al. “Failure modeling of sawn lumber with a fastener hole.” Finite Elements in Analysis and Design 36. 2000. Elsevier Science Publishers. pp. 83-98.

Wood handbook: wood as an engineering material. General technical report FPL; GTR-113. Madison, WI: U.S. Department of Agriculture, Forest Service, Forest Products Laboratory, 1991.

Zienkiewicz, O.C. and Y. K. Cheung, “Finite Elements in the Solution of Field Problems,” *Engineer*, Vol. 220, 1965, pp. 507–510.

Zienkiewicz, O.C. and Y. K. Cheung. *The Finite Element Method in Structural and Continuum Mechanics.* McGraw-Hall. London, New York. 1967.

A

B

C

D

M

N

P

Q

R

S

T

V

W

Appendix I—Gary Gredell Structural Assessment

Reprinted with the permission of the Wagner Free Institute of Science

Structural Condition Assessment

Roof and Upper Masonry Walls
Exhibition Hall

The Wagner Free Institute of Science
1700 West Montgomery Avenue
Philadelphia, Pennsylvania

GREDELL
& ASSOCIATES
STRUCTURAL ENGINEERS

PO BOX 357 / NEWARK, DELAWARE 19715-0357 / 302-731-5060 / FAX 302-731-5280 / GGREDELL@GREDELL.COM

GREDELL
& ASSOCIATES
STRUCTURAL ENGINEERS

September 27, 2008

Ms. Susan Glassman
Director
The Wagner Free Institute
1700 West Montgomery Avenue
Philadelphia, PA 19192

WO 2784
CONDITION ASSESSMENT - ROOF STRUCTURE
THE WAGNER FREE INSTITUTE
1700 WEST MONTGOMERY AVENUE
PHILADELPHIA, PENNSYLVANIA

Susan

We have completed our review of the roof structure above the Exhibition Hall of the Wagner Institute building. We understand that the preservation of the plaster ceiling above the Exhibition Hall has become an area of primary concern with regard to the restoration of the building. The concerns have been prompted by the pervasiveness of the cracks and observed misalignment of the plaster ceiling finishes. The stability of the plaster ceiling is currently being studied by representatives of BCA, conservators working for the Institute. The possibility that movement of the roof structure and the supporting brick masonry walls may contribute to the distressed condition of the plaster has been considered. The scope of our work is to assess the structural condition of the building above the level of the 4th floor gallery.

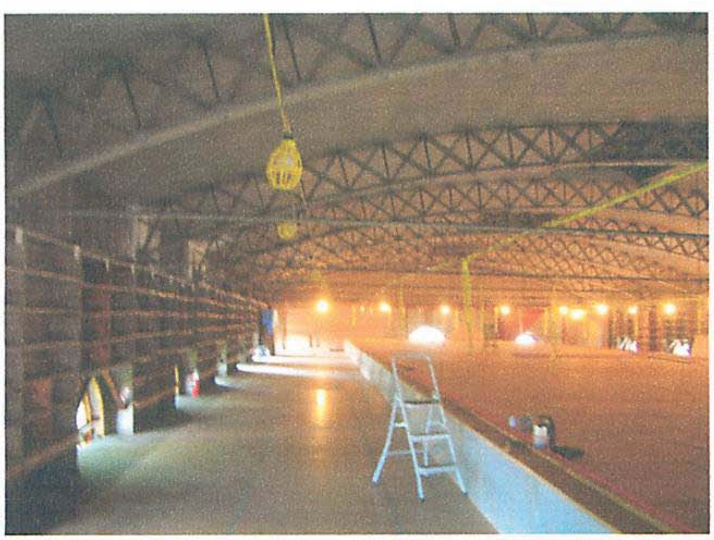

Fourth Level Gallery looking South along 'B'
Gredell & Associates, 8 July 2008

Although our review led us to other areas of the building, the intent of this additional work was to gain a better understanding of the observed misalignment of the east and west exterior walls. This report does not include structural assessment of parts of the building located below the 4th floor gallery. As input for our review and study, the following information was provided by representatives of the Institute:

Construction drawings ,Wagner Free Institute of Science, Museum Building Restoration Project, prepared by William Stivali, Building Conservator, 30 January 2007 (issued for construction cost estimate)

An index identifying the information contained in the Institutes archives

Written Historical & Descriptive Data; Reproduced Copies of Measured Drawings, Historic American Building Survey, HABS No. PA-6667, National Park Service, summer 2000

Letter to William Stivali, Wagner Institute Temporary Deck, Donald Friedman, P.E., November 2007

Letter structural report, Wagner Institute, Main Roof Structure,Donald Friedman, P.E., 19 September 2005

Site visit memorandum, D.G. Cornelius, Keast & Hood, 25 March 2005

Letter to Marianna Thomas, AIA, Roof Trusses, Project No. 95109C, Thomas J. Leidigh, Keast & Hood, 4 December 2001

Roof Structure Wood Pathology Investigation, Keast & Hood, 13 October 1994

Specifications for the Improvement of the Wagner Institute, Collins & Autenrieth, 1885

Letter Report, Condition Assessment of the Wagner Institute, scope of work and construction cost estimate, Collins & Autenrieth, 28 February 1885

The purpose of the review and subsequent evaluation is to assess the structural condition of the roof and to determine whether or not the structure or lack thereof may be adversely affecting the performance of the plaster ceiling which is attached directly to the underside of the secondary roof framing. In addition, our work includes a condition assessment of the brick masonry exterior walls above the 4th floor gallery that support the roof structure. To assist the reader with the orientation of the structural elements discussed, we have enclosed framing plans with superimposed structural grid lines. We have assumed that the entrance to the building faces north towards Montgomery Avenue. Recommendations are highlighted by italicized font.

Historical Background

From historical information, we understand that the building was apparently constructed in phases during the Civil War, from 1859 to 1865. The building work started in 1859 with the clay material excavated for the construction of foundations and basement salvaged for the manufacture of the bricks for the masonry walls of the building- the bricks fired in temporary kilns erected on site. Noteworthy, the site selected for the building was the highest in elevation of any site located between the Delaware and the Schuykill Rivers – a rural setting with full exposure to the elements. History of the building reveals that in February 1876 "a severe storm arose toward midnight accompanied by a tornado which roolled (sic) up the new tin roof on the Hall into a scroll and carried it off into the adjoining lot". Again in October 1878, "a tremenduous (sic) gale passed over our City, tearing off more than half the tin on the roof of the Institute Building and 5 of the tere (sic) cotta chimnies (sic) and demolished much of the fence around the building".

With William Wagner's death in 1885, the Institute Trustees received a sizeable portion of the estate to be used for building improvements. The Trustees retained the architectural and engineering services of Collins & Autenrieth to prepare the necessary plans and specifications for the work. Apparently, during the course of their work, the firm performed an assessment of the condition of the building. In a letter dated February 28, 1885 addressed to the trustees, Collins stated that based on their observations, the building was in "very poor" condition as witnessed by the following:

1. The east and west walls, 150' in length were "too light" laterally, unbraced. As a result they have "bulged 5 ½" eastward. Their solution was to erect masonry shear walls on top of the existing east-west wall separating the lecture hall from the rest of the building. The wall extends upward to the underside of the 4th level gallery on both sides of the building.

2. The faces of the outer masonry walls are laid up with open joints and poor quality mortar. The porosity of the exterior walls had allowed water to enter causing rot to occur in the first floor joists. Collins addressed the concerns regarding the poor condition of the masonry by applying a parge coating to the exterior face of the building; however, the finish appearance was left plain without rendering.

3. The first floor girders located in the front half of the building were determined to be undersized with noticeable distress and misalignment. The structure was repaired by reinforcing the floor beams.

4. The columns located in the lecture room were determined to be undersized. The building was shored and the columns replaced along with extensive foundation work substructure in the basement below the lecture hall.

5. The gallery columns were found to be poorly supported causing overstressing and misalignment of the supporting floors. The gallery floors were apparently shored and framing enhanced by inserting cast iron floor beams and subsequently adjusting the position of the cast iron gallery columns.

6. The plaster ceilings were found to be in such poor condition that they were removed and replaced throughout the building. Wall plaster was left in place and overlaid with new plaster.

In early July 2008, we visited the building on several occasions in order to review the structural condition of the roof and 4th floor exterior walls. The review consisted of visual observations and selective probing of those portions of the structure made safely accessible with staging and uncovering provided by representatives of the Institute. The building is rectangular in plan form measuring approximately 60' east-west by 150' north-south. The structure is founded on stone masonry foundation walls approximately 24" in thickness and extend from the basement level to an elevation approximately 12" below the first floor. The building rises on brick masonry walls 20" thick to the second floor level. Above, the wall reduces to 16" thickness as it rises through the 3rd and 4th floor galleries and upwards to the roof structure.

The primary structure of the roof is comprised of eight (8) tied, two hinged arch timber trusses that clear span east-west approximately 57'-4" and bear on 16" brick masonry exterior walls with integral pilasters. The trusses are on approximately 17' centers with an 8' rise from the bearings to the crown. The truss is framed with 2 ½" x 7 ¾"

Bolster receiving the bottom chord and 1 5/8" tie rod
Gredell & Associates, 8 July 2008

(flat) top and bottom chords, 1 ¾" x 6" diagonals seated on cast iron shoes fixed with 2-5/8" diameter wrought iron rod verticals at approximately 25" centers. The arched truss is tied with a 1 5/8" diameter horizontal rod set in the vertical center of 7 ½"x 6" bolster blocks that bear on the masonry. The blocks extend to the fascia board of the eave construction. The rod is fixed at the exterior end of the blocks with a 5"x 1/2"x 5" plate washers and nut assembly.

GREDELL & ASSOCIATES
STRUCTURAL ENGINEERS
P.O. BOX 357 • NEWARK, DE 19715-0357 • 302-731-5060

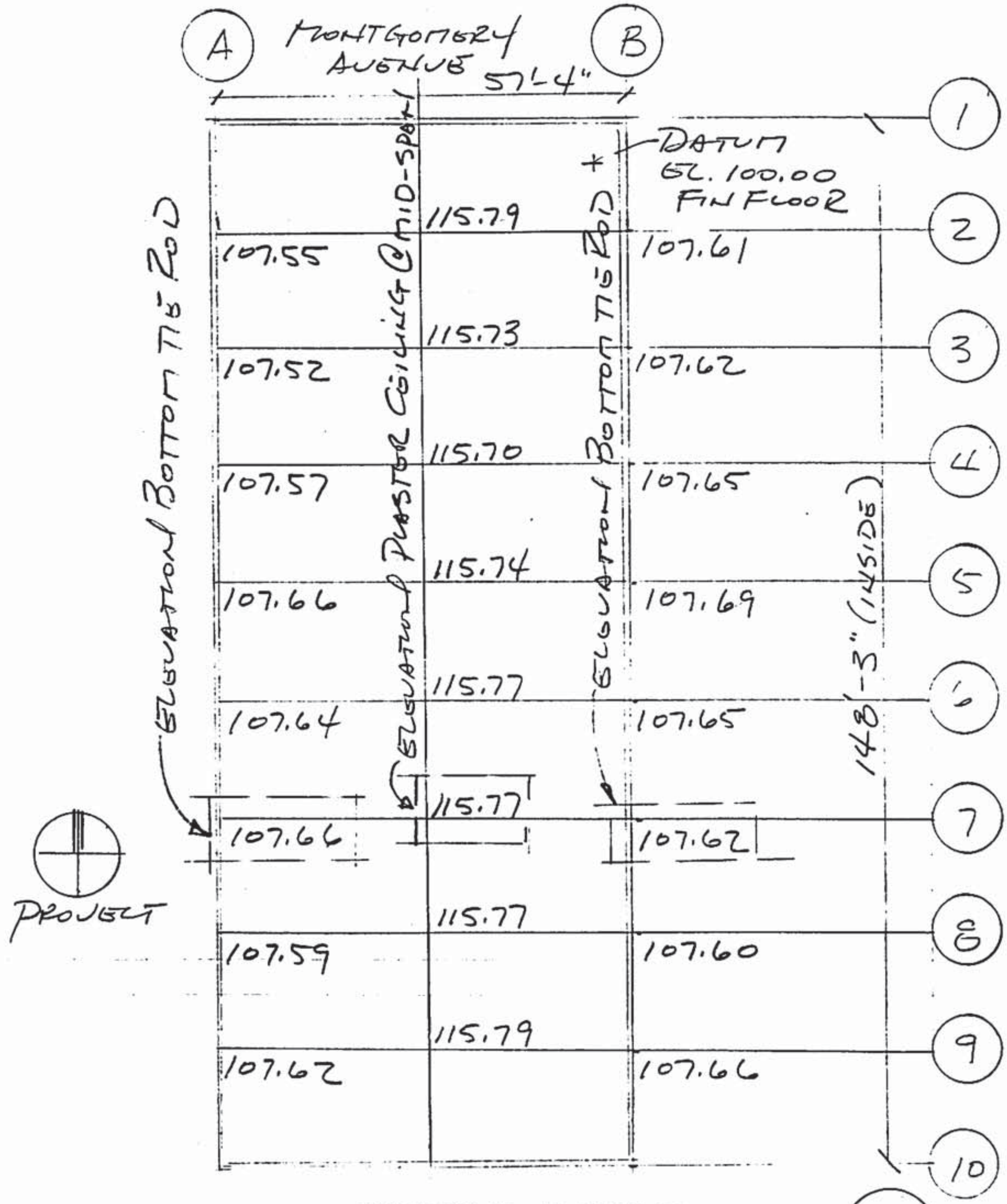

VERTICAL ALIGNMENT
ROOF STRUCTURE
2

GREDELL & ASSOCIATES
STRUCTURAL ENGINEERS
P.O. BOX 357 • NEWARK, DE 19715-0357 • 302-731-5060

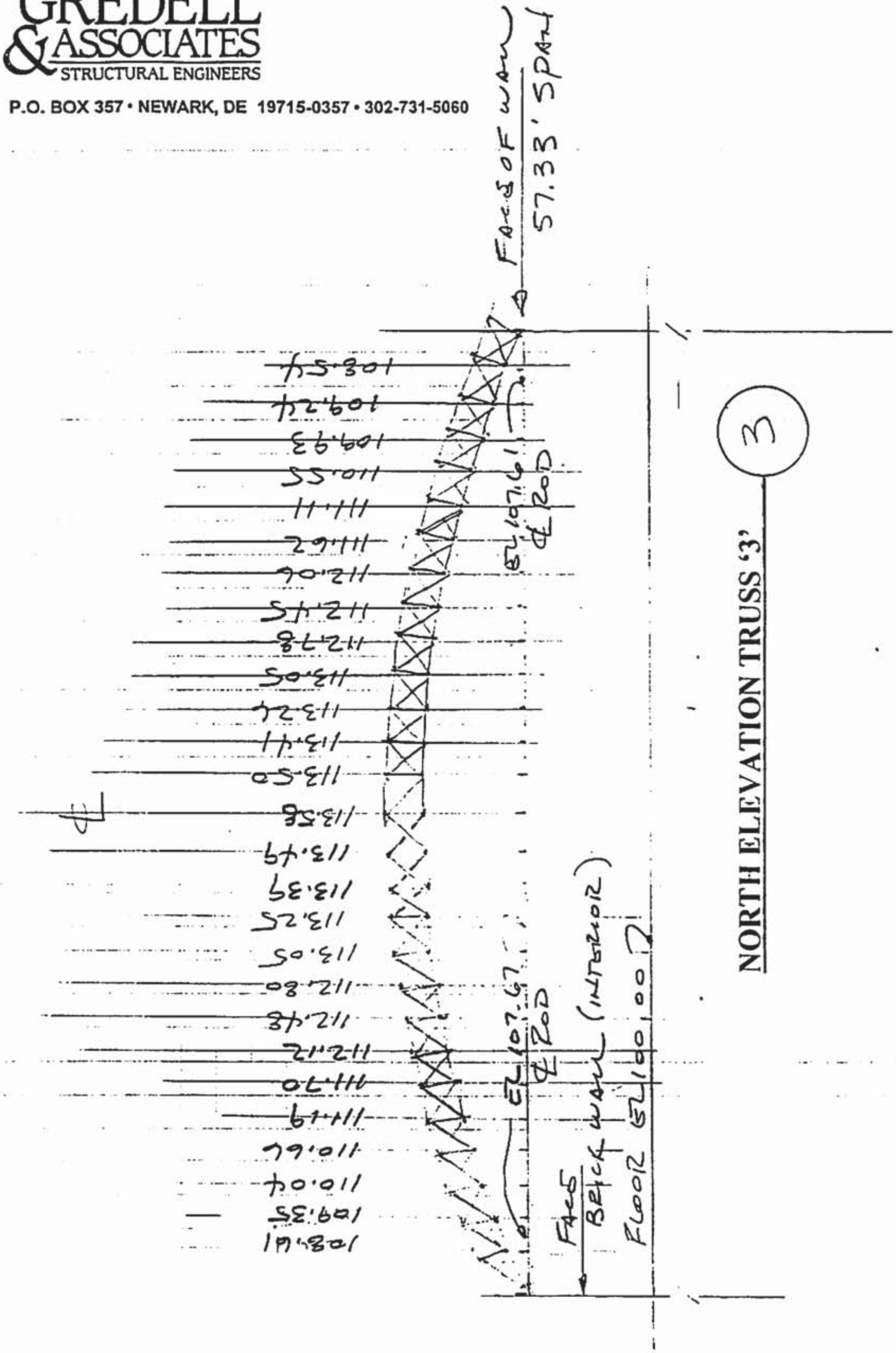

GREDELL & ASSOCIATES
STRUCTURAL ENGINEERS

P.O. BOX 357 • NEWARK, DE 19715-0357 • 302-731-5060

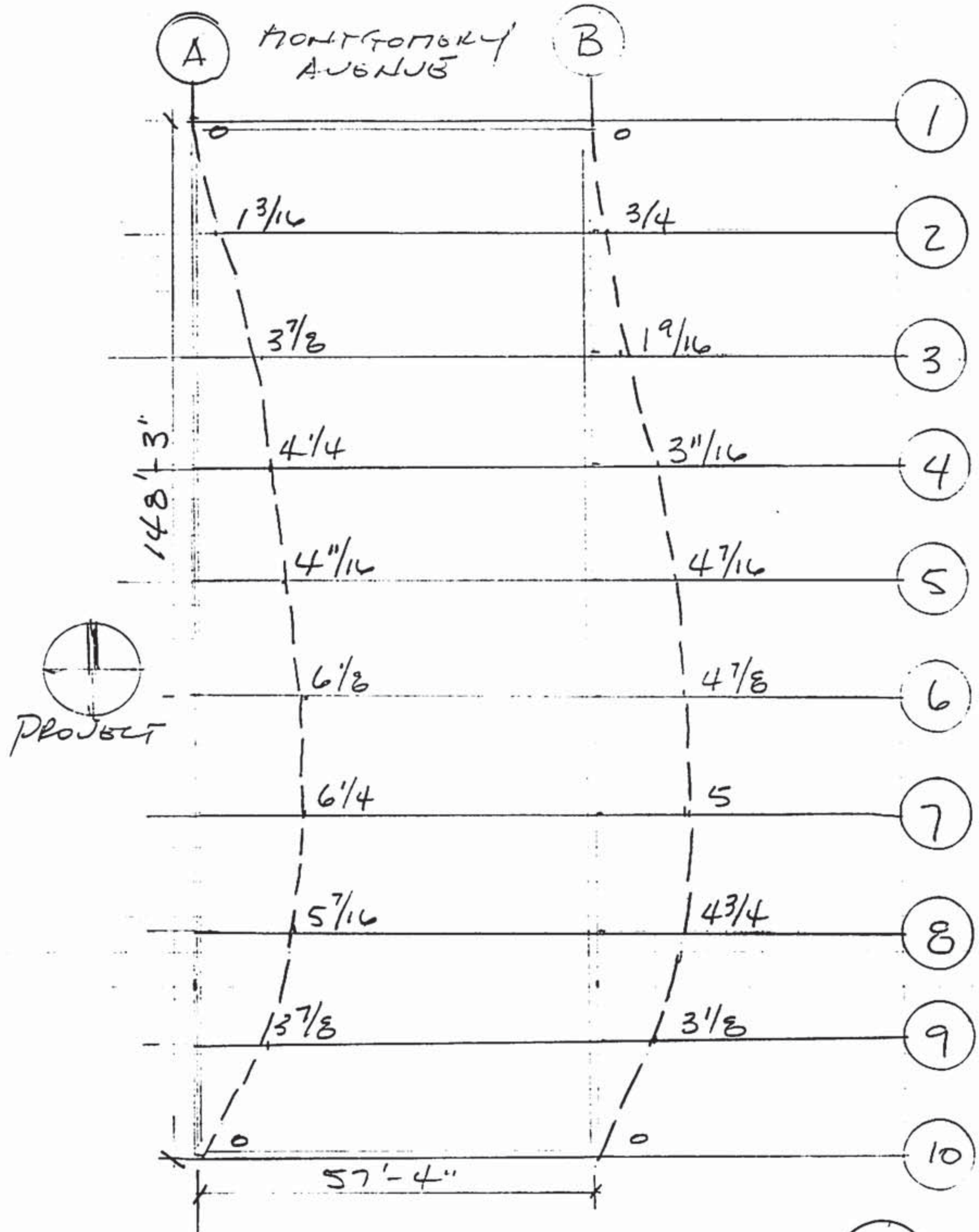

HORIZONTAL ALIGNMENT
ROOF STRUCTURE

4

Truss analysis

Our analysis of the tied, arched trusses is based on a computer model generated in RISA 3D to evaluate the member force distribution throughout the truss under various conditions of load and temperature – dead load only, dead load with an elevated temperature of 110 degrees Fahrenheit, and dead load plus snow loading. The various load conditions impact the truss member forces and therefore the member stresses. Elevated temperatures increase wood stresses and cause elongation of the wrought iron rods. The unit loadings used in the evaluation were as follows:

Description of component	Amount (PSF)
Dead Load	
Roofing	2
Wood decking	3
Framing	2
Furring	1
Lath	2
Plaster	6
Subtotal	16
Snow load	20
Total	36

Based on the findings of the wood pathology report prepared by Dr. Joe W. Clark, dated October 8, 1994, the species of wood used in the construction of the trusses was determined to be Eastern White Pine, old growth, heartwood material. Safe working unit stresses for Eastern White Pine are provided in Architects and Builders Handbook, Kidder-Parker, 1916 as follows:

Classification of Stress	Magnitude (PSI)
Tension (parallel to grain)	2,300
(perpendicular to grain)	1,700
Compression (parallel to grain)	1,300
(perpendicular to grain)	270
Bending (extreme fiber)	1,400
Shear (horizontal)	130
(vertical)	600
Modulus of Elasticity	1,000,000

Based on the computer analysis, we have determined that the distribution of the forces in the truss are such that the greatest axial forces in the bottom chord occur adjacent to the bearing and the intensity of axial loading in the top chord is realized near the crowns of the trusses. The resultant thrusting of the truss is resisted by the tie rod that is inserted in the mid section of the bolster. Under applied dead and dead with elevated temperature conditions, the member stresses are considered to be within acceptable limits. This is consistent with our observations in the field where no visible signs of structural distress or misalignment were detected. Through our analysis, we determined that under dead loading the deflection of the truss was approximately 5/8" at midspan. Under dead load and elevated temperature the deflection at midspan was determined to be 7/8". The dead load of the structure has been essentially unchanged since construction in 1865 – perhaps even less with a gravel roof having been removed according to the historical records. The additional deflection caused by changes in temperature should be no more than 1/4". In the case of dead plus snow load the deflection at midspan was determined to be 1 7/16". Accordingly, the total downward movement at the midspan of the truss due to snow loading is estimated to be 7/8" from the position in 1885. This relatively small amount of deflection under snow loading indicates that the truss is extremely stiff with a deflection ratio of approximately L/ 880. Normal practice regarding stiffness and plaster finishes sets the maximum deflection of the member to 1/360th of the span due to the tributary live loading. This is the amount of deflection above which plaster finishes may be adversely affected due to movement of the ceiling structure. This is considerably more than the 1/880 ratio determined for the Wagner trusses. The amount of deflection is inversely proportional to the modulus of elasticity of the material. Based on this finding, the relatively small amount of deflection in the truss does not adversely affect the performance of the plaster ceiling.

The following table provides a summary of the forces and stresses in the truss members where the highest loading is encountered. Enclosed are sketches of these portions of the structure with the members numbered for reference (see Figures 5,6,7, 8, 9 and 10, Member Forces at Bearings and Midspan). For each critical member we have determined a factor of safety which is the ratio of the allowable stress in the member divided by the actual stress determined by the analysis. Safety factors of less than unity indicate the member is technically overloaded.

Member designation	**Size**	**Force (pounds)**	**Stress (PSI)**	**Safety factor**
Dead loading				
Bearing assembly				
M29	2 ½"x 7 3/4"	11,500	590	2.2
M142	5/8" rod	1,200	4000	3.0
Tie	1 5/8" rod	12,740	6,150	1.9
N85 (1)			590	1.4
Crown assembly				
M44	2 ½"x7 ¾"	9,300	480	2.7
Dead load & snow				
Bearing assembly				
M29	2 ½'x 7 ¾"	25,500	1,310	1.0
M142	5/8" rod	2,700	8,700	1.4
Tie	1 5/8" rod	28,300	13,670	0.9
N85 (1)			1,310	0.6
Crown assembly				
M44	2 1/2"x7 3/4"	20,700	1,070	1.2

1. Critical stressing at node N85 where bottom chord of truss M29 intersects the bolster at an angle to the grain. Since the wood is less strong perpendicular to the grain than parallel, a reduction in the allowable stress at the critical bird mouth connection has been considered.

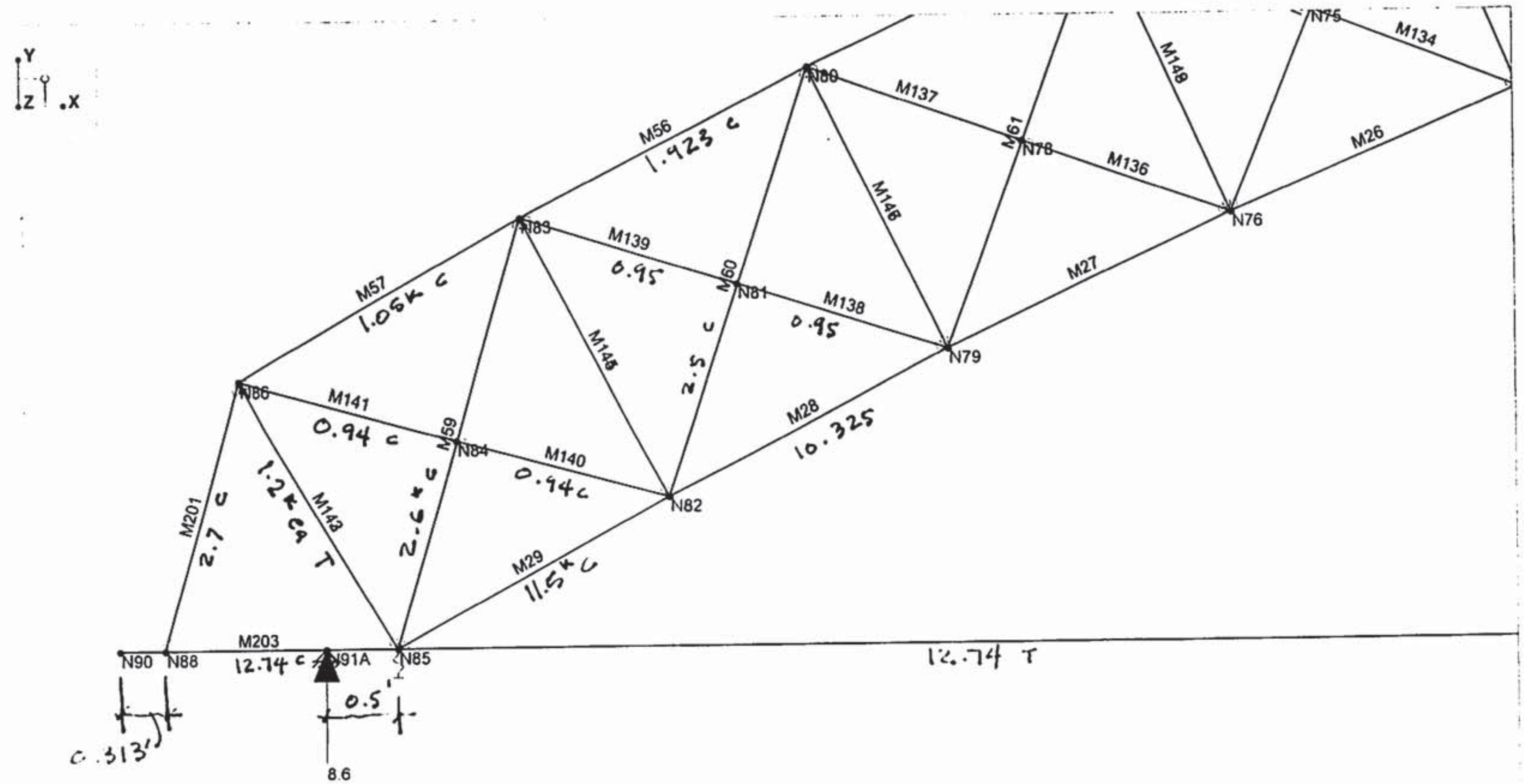

DEAD LOAD MEMBER FORCES
BEARING END

5

Results for LC 1, DL
Reaction units are k and k-ft

Sept 9, 2008 at 3:01 PM
truss rev1.r3d

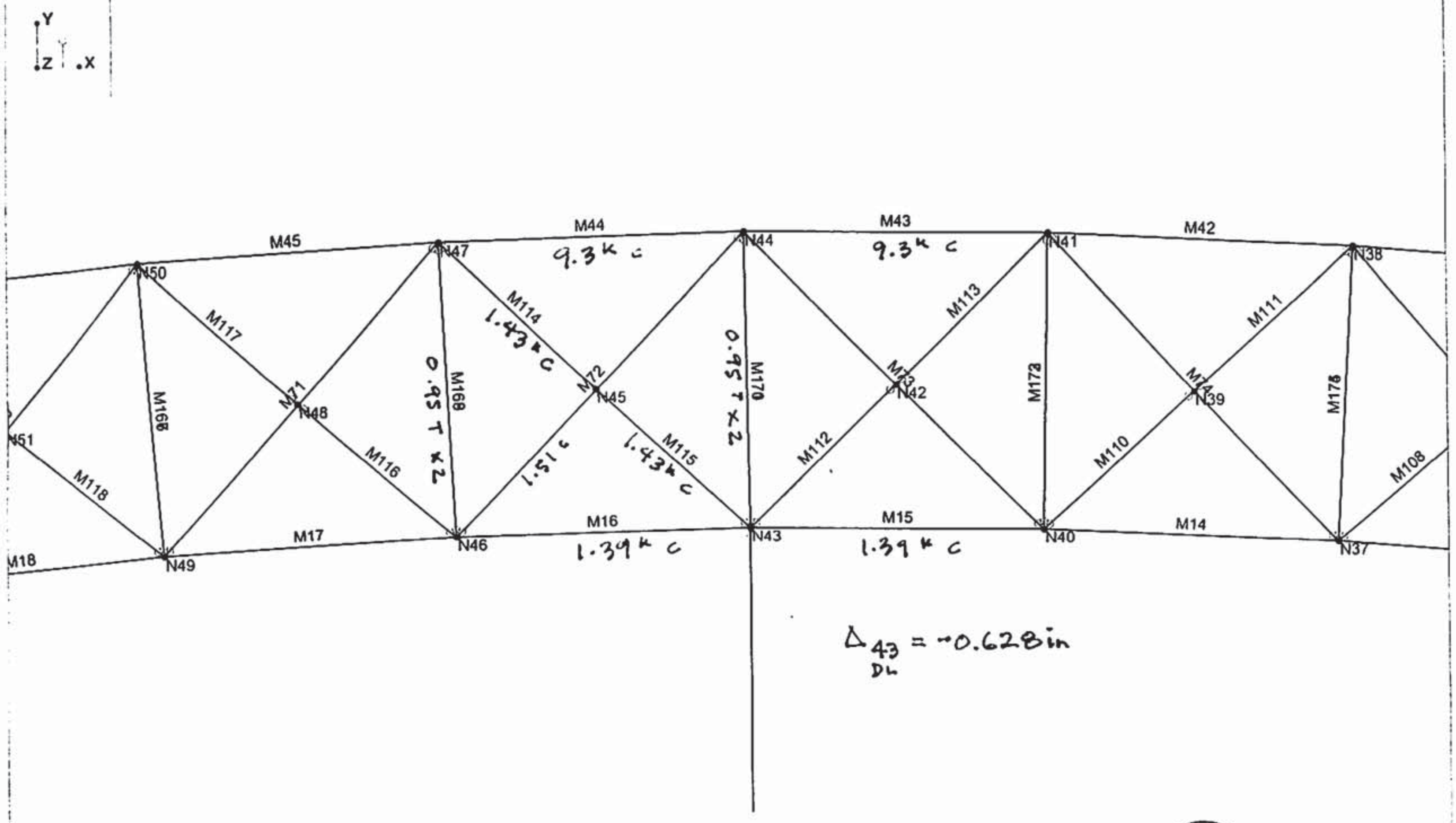

$\Delta_{43_{DL}} = -0.628 in$

DEAD LOAD MEMBER FORCES

MIDSPAN

6

Results for LC 1, DL
Reaction units are k and k-ft

Sept 9, 2008 at 3:13 PM
truss rev1.r3d

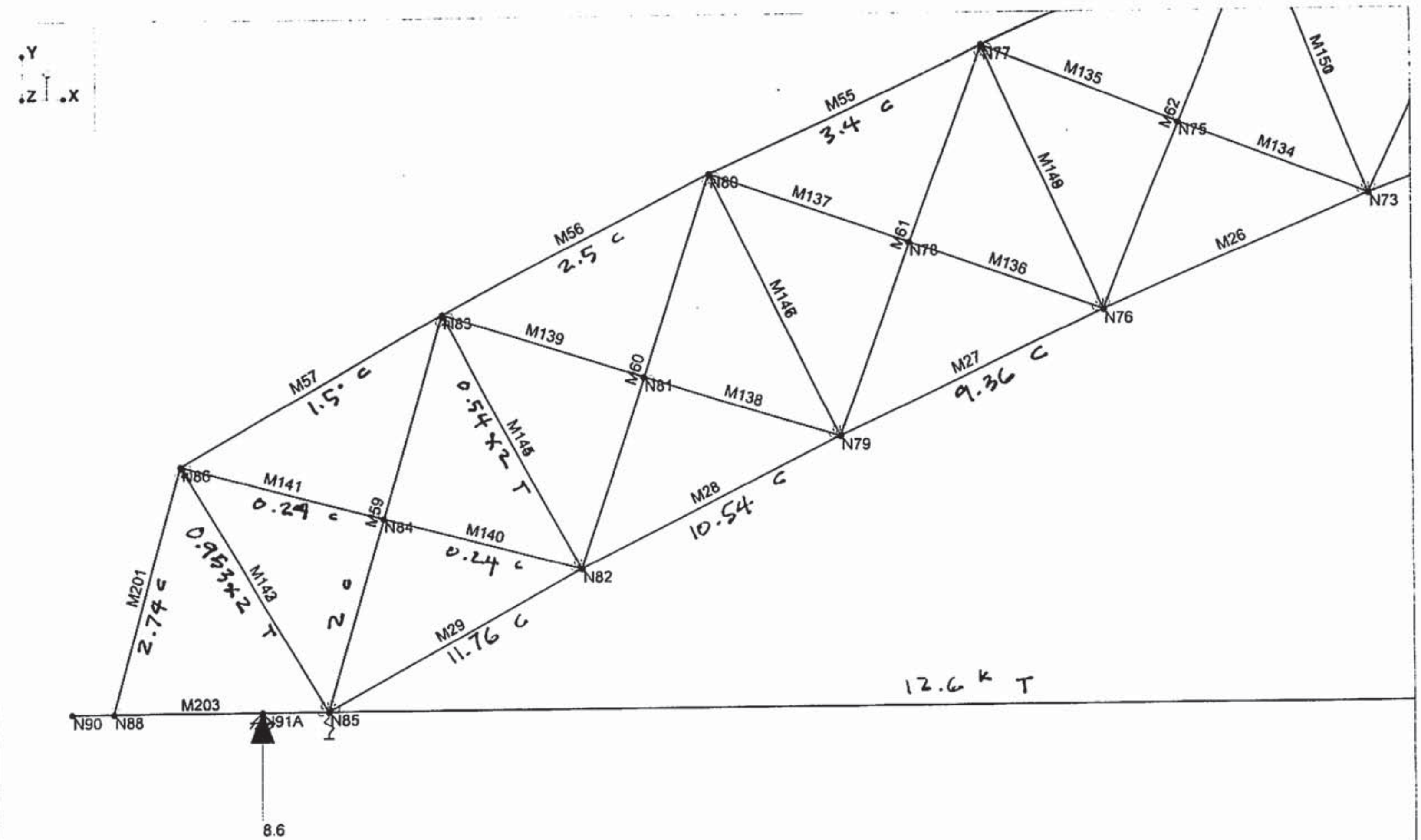

MEMBER FORCES
DEAD LOAD / ELEVATED TEMPERATURE
BEARING END

7

Results for LC 3, temp 110
Reaction units are k and k-ft

DL+ ELEVATED TEMP@ 110°

Sept 9, 2008 at 3:29 PM

truss rev1.r3d

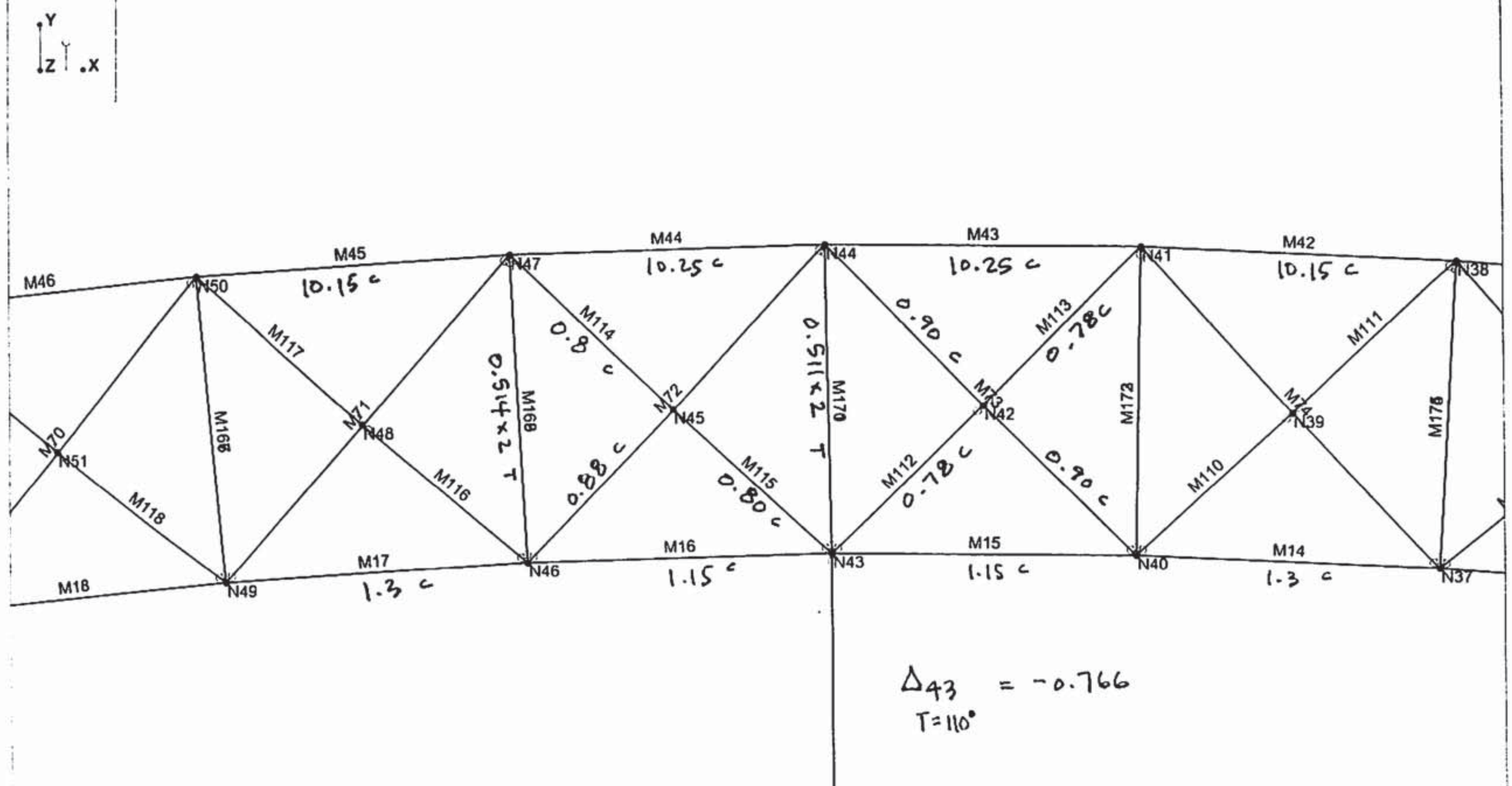

MEMBER FORCES

DEAD LOAD / ELEVATED TEMPERATURE

MIDSPAN

8

Results for LC 3, temp 110
Reaction units are k and k-ft

Sept 9, 2008 at 3:39 PM
truss rev1.r3d

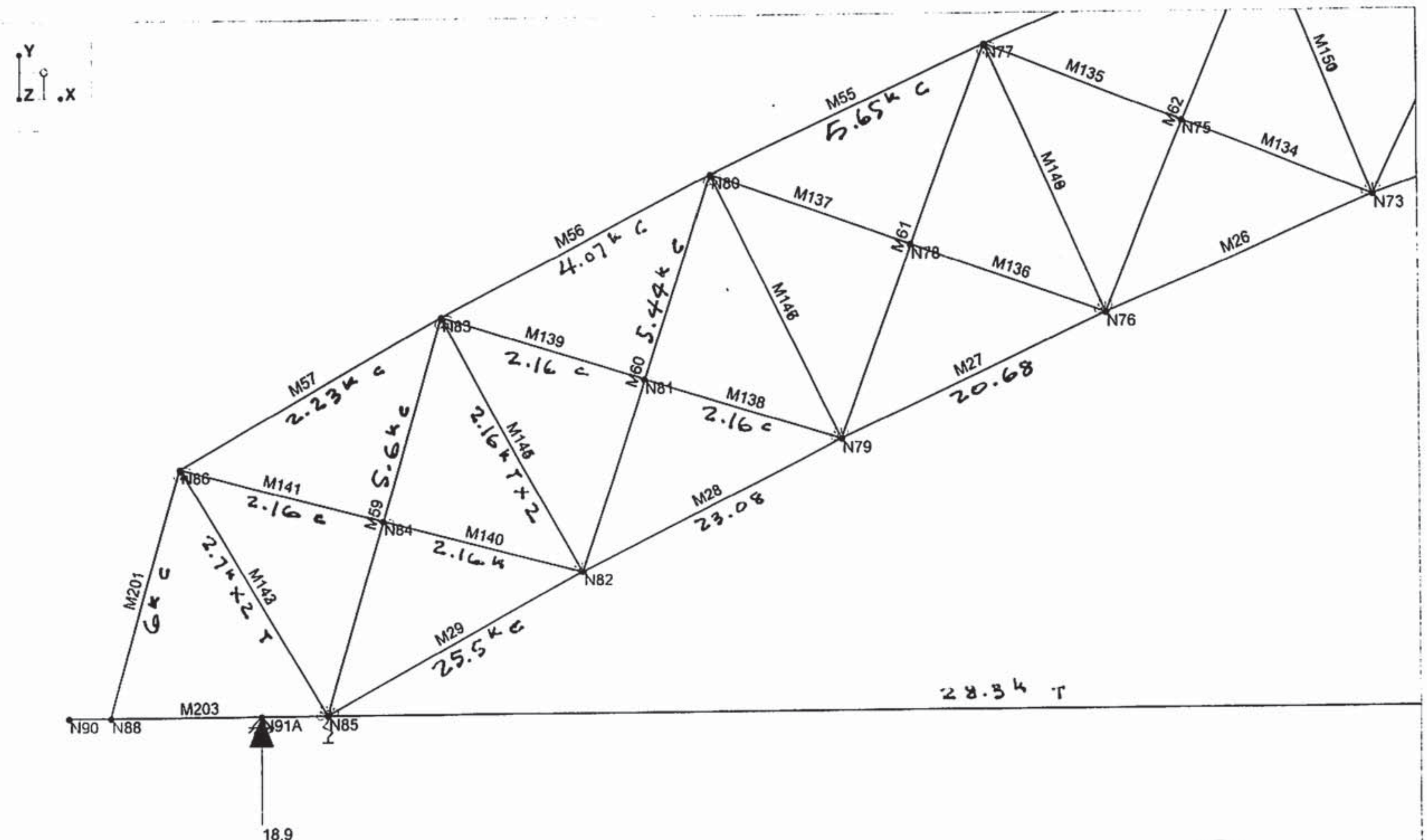

DEAD AND SNOW LOAD MEMBER FORCES
BEARING END

9

Results for LC 2, DL+SL
Reaction units are k and k-ft

Sept 9, 2008 at 3:22 PM
truss rev1.r3d

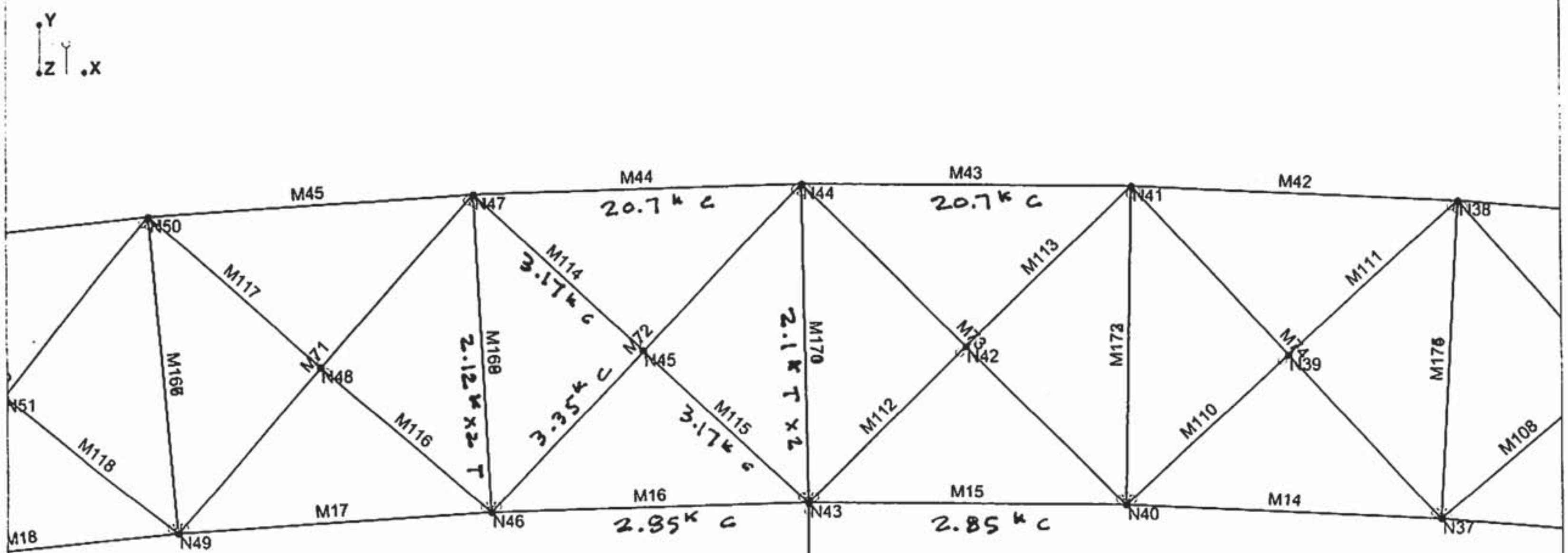

$\Delta_{43_{DL+SL}} = -1.405 \text{ in}$

$\therefore \Delta_{43_{SL}} = -1.405 - (-0.623)$

$= -0.775 \text{ in}$

DEAD AND SNOW LOAD MEMBER FORCES
MID SPAN

10

Results for LC 2, DL+SL
Reaction units are k and k-ft

Sept 9, 2008 at 3:18 PM
truss rev1.r3d

The overstressing of the tie rod is relatively small – 10% overload. Non-destructive testing of the rod is recommended in order to determine actual capacity. The overstress of the timber bolster at N85 requires structural reinforcement. Shore the truss and alternatively provide a horizontal mortise below N85. Insert a steel plate bonded into the timber mortise with high modulus epoxy.

Floor and Roof Diaphragms

The lateral stability of the building in the east-west direction is provided by the brick masonry shear walls forming the gable ends of the building '1' and '10' as shown on the enclosed roof plan (see Figure 2). Tributary wind loading on the east and west walls is distributed to the floors and the roof. These horizontal structures serve as structural diaphragms and must be stiff enough to transfer the wind loading of the east and west walls to the shear walls located on the north and south ends of the building without excessive deflection. Otherwise, the resultant misalignment and distress may adversely affect the structural performance of the exterior masonry walls.

The floor and roof diaphragms are framed with sawn lumber joists and purlins (roof) and 1" thick decking boards nailed to the framing. The decking is laid perpendicular to the framing and appears to be 6" in width as observed through an opening in the ceiling. This type of sheathing is called transverse or straight sheathing. Straight sheathing diaphragms are relatively limited with regard to structural effectiveness since the strength and stiffness depend on the resistance provide by a couple of nails at each joist / purlin crossing. Assuming 2- 10d nails at each crossing of the purlins, we have determined that the strength of the existing roof adjacent to the north and south shear walls is less than 20 % of that required to achieve the desired stiffness and strength provided the only diaphragm mechanism is the nailed flooring. Floors, especially the galleries at the 3rd and 4th levels are technically deficient with regard to both strength and stiffness. The shear walls constructed in 1885 by extending the first floor masonry wall between the lecture hall and the office areas up through the 3rd and 4th level galleries provided increased stiffness to the gallery diaphragms at the 3rd and 4th levels. Unfortunately, it appears that extreme winds reported in February 1876 and October 1878 had already caused the central section of the building to drift eastward approximately 5 ½" at the level at the eaves.

To provide the required stiffness and strength to the roof diaphragm, remove all roofing down to the level of the wood sheathing; glue and screw a structural plywood overlay to the entire roof area. In addition open portions of the 3rd and 4th floor galleries to verify the actual strength of floor diaphragm.

Exterior Masonry Walls

The exterior walls of the building are constructed of brick masonry founded on 24" stone masonry walls below the level of the first floor as viewed from the basement. From the first to the second floor, the brick masonry measures 20". At the second floor level the wall thickness reduces to 16" which extends to the level of the roof.
The transition is provided by a 4" wide watertable which is featured on the exterior face of

the wall. Above the watertable and midway between the windows, brick masonry pilasters approximately 20" x 36" are integral with the wall construction and project 4" from the exterior face of the wall. The pilasters stiffen the walls against the eccentricity of the roof truss bearings and lateral loading by wind. The exterior face of the brick received a parge coating of mortar as part of the 1885 renovations to the building. The parging was applied to enhance service life of the masonry which was reported by the architect, Collins, to be in poor condition- soft bricks and weak mortar. At the interior, plaster finishes are applied directly to the face of the masonry except where millwork (baseboards and wainscoting) were installed prior to plastering. In order to review the condition of the brick masonry at the interior face of the walls, small areas of wainscoting were removed at the west wall of the lecture hall and above on the second floor. At both
locations observed, bricks and mortar appeared in good condition with no signs of moisture, efflorescence or sloughing. Review of the interior face of the brick masonry in the first floor joist envelope revealed some moisture damage - soft , sloughing masonry most probably the result of subflorescence. Site drainage is poor, with areas subject to ponding. As a result water lays against the building, soaking the walls and causing damage due to moisture.

Measurements staged from a high lift and working with a plumb line determined the amount of eastward lean in the exterior walls. Wall leans from the second floor to the roof of 5" were witnessed. (see figure 11, East and West Wall Alignment). From grade to the second floor level, the misalignment is relatively small compared to the remaining height of the walls. Above, flexible gallery and roof diaphragms allowed the building to drift eastward apparently due to the extreme winds that were observed circa 1876. The introduction of the shear walls which were part of Collins work provided the needed stiffness in the building to resist further movement of the structure.

Above the 4th floor gallery, the masonry section is 16" thick with a 36"wide x 20" deep brick masonry pilaster integral with the wall construction. The analysis was based on the assumption that the concentrated roof loads from the trusses and lateral wind loading are supported and resisted by the pilaster section. Below the 4th level gallery, the roof and floor loads are distributed over the full section (pilasters and integral masonry) of the wall. Several loading conditions were considered- dead; dead / wind; dead / snow load; and dead / snow / wind. The following table provides a summary of loading type and calculated compressive stresses encountered in the masonry:

Type of loading	**Compressive stress (PSI)**	
	Mid- level	**4th floor**
Dead		45
Dead / wind	34	95
Dead / snow		94
Dead / snow / wind	57	138

Our analysis of the exterior brick masonry walls above the 4th level gallery was based on allowable compressive stresses established by the Building Code of Philadelphia dated 1929. For medium fired, somewhat porous brick with a compressive stress ranging from

GREDELL & ASSOCIATES
STRUCTURAL ENGINEERS
P.O. BOX 357 • NEWARK, DE 19715-0357 • 302-731-5060

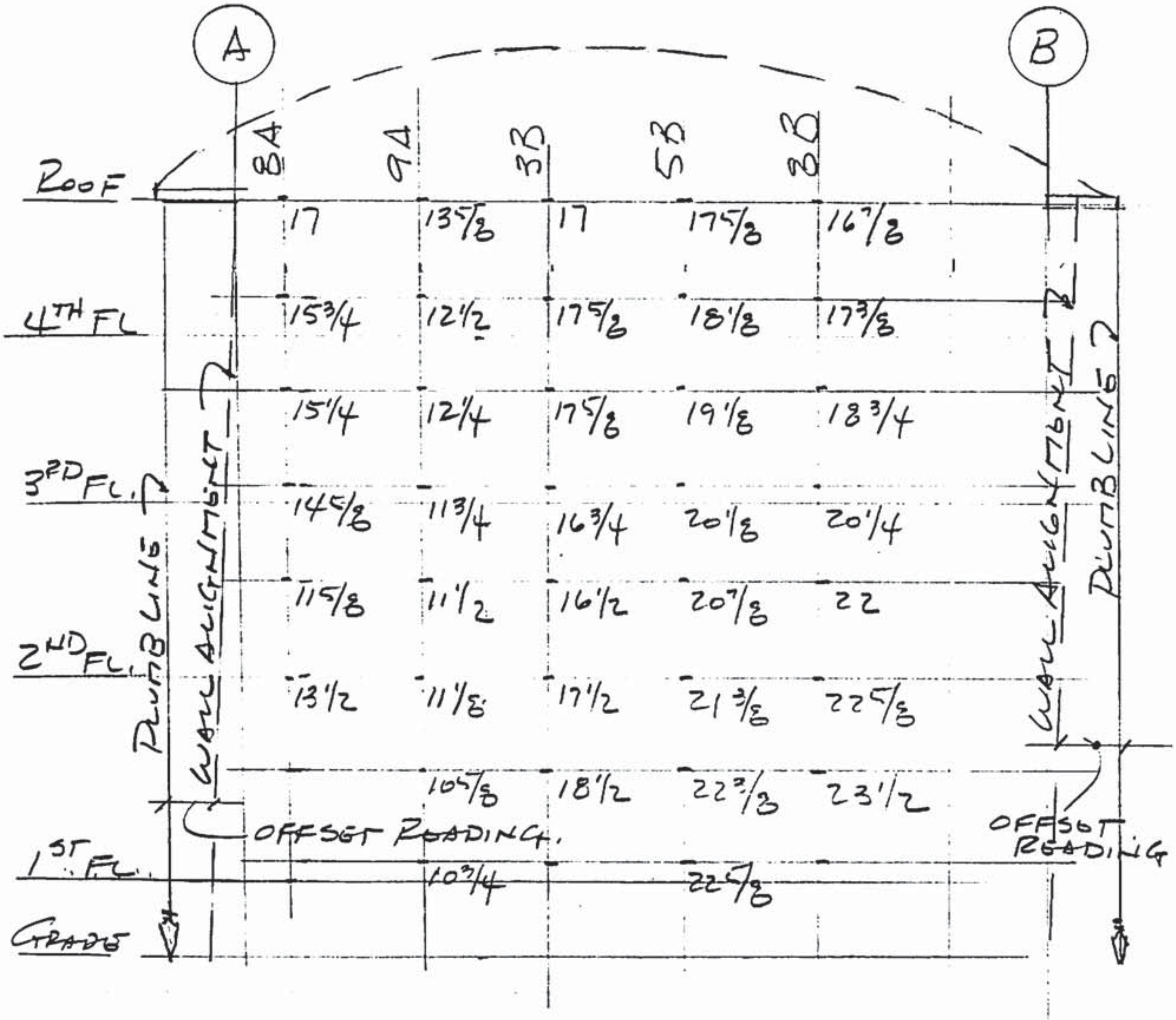

EAST AND WEST WALL ALIGNMENT
NORTH ELEVATION

11

1500-2500 PSI laid up with lime mortar a non-conservative allowable compressive stress of 75 PSI was selected for our evaluation. Eccentricities caused by various combinations of gravity and lateral loading determine the distribution of stress throughout the pilaster cross section. Where the location of resultant forces occur outside the "middle one-third" of the section, tensile stress occur thereby reducing the section available for compression loading. The values presented are maximum compressive stresses determining in light of the reduced section.
In order to maintain compressive stresses to below 75 PSI, the outer face of the pilaster at the 4th level must be reinforced. Reinforcement may be achieved by inserting fiber reinforced glass rods into vertical grooves cut into the exterior face and bonding the assembly with epoxy paste. Complete the work by repairing the parge coating to match color and texture of adjacent finishes.

The timber roof trusses each bear on bolsters that are perpendicular to and set on the brick masonry wall. The bolsters measure 7 1/2" x 6" and are made up of two pieces that are symmetric about the 1 5/8" tie rod that passes through their center and is fixed at the outer end by a large plate washer and nut assembly. The structural capacity of the bolster was considered in this analysis. Under dead loading it was determined that shear and bending stresses occurring in the bolster and the compressive stresses in the masonry are within acceptable limits. Snow loads more than double the bearing reaction on the wall from that of dead load only.
In order to accommodate the resultant overstressing of the bolster section, the two piece bolster block must be bonded together with epoxy paste. Open the masonry walls on both sides of the block and cut a longitudinal slot for the full length of the bolster block that passes through the masonry. Inject epoxy to the depth of the tie rod. Rebuild the masonry to match original configuration.

In addition, the compressive stresses in the masonry must be reduced due to the increased snow load.
Shore the truss bearings and install galvanized steel bearing plates below each truss that would more than double the bearing area of the timber bolster.

In summary, we offer the following comments for your review and consideration:

- The scope of our work features the building structure above the 4th floor gallery. As additional work, we recommend that the structure of the 3rd and 4th floor galleries be uncovered in order to gain confidence that the structure of these floors can safely transfer wind loads to the original end walls and the shear walls constructed during the 1885 renovations to the building. In addition, the shear walls constructed in 1885 should be partially uncovered in order to determine the stability of the structure. Excessive deflection of either the gallery floor diaphragms or the interior shear wall will adversely affect the alignment of the roof and cause additional distress in the plaster ceiling.

- It is reasonable to assume that the high winds experienced by the building approximately 12 years after the construction was completed were responsible for the lateral drift of the building. Collins structural assessment documented in a letter dated February 1885 addresses the poor condition of the building. Lateral stability has always been an issue in this building as has the poor materials and workmanship that characterize the exterior masonry wall. It is critical to the service life of the building to ensure that lateral systems are adequate and that the exterior walls remain water proof. Poor site drainage should be addressed so that water flows freely away form the building with no opportunity to collect against the walls.

- The roof structural diaphragm lacks stiffness and strength as witnessed by the amount of movement that occurred early in the life of the building. To our knowledge the sheathing that exists on the roof is original with no efforts having been made to date to reinforce the assembly. Prior to any remedial work being performed on the plaster ceiling above the Exhibition Hall, the roof diaphragm should be reinforced and stiffened by overlaying the entire roof area sheathing with a layer of structural plywood securely attached to the existing purlins.

- The eight roof trusses are in good structural condition and capable of safely supporting the weight of the roof. However, it was determined that snow loads cause certain portions of the structure to be overstressed – the tie rod 10% and the bolster block 40%. Since the roof of the building has never been insulated, it is unlikely that much snow accumulates prior to being melted by the building heat that escapes through the roof envelope. If improvements add insulation to the roof , the effects of Code recommended snow loadings must be considered. Accordingly, reinforcement of the overstressed elements in the truss will be required.

- Exterior masonry walls are constructed of low to medium strength bricks and lime mortar. Good practice dictates that the maximum allowable compressive stress in the brick masonry should be approximately 75 PSI. Our analysis reveals that wind and snow loading causes theoretical compressive stresses in excess of this amount – reinforcement of the masonry pilasters at the 4th floor level will be required.

- The bearing of the trusses supporting snow loads on the brick masonry walls cause the bolster to be overstressed in bending. Strengthening can be achieved by bonding the two bolster sections with epoxy. In addition, the truss bearings will require shoring in order to install steel bearing plates to distribute the truss reactions to a larger area of the supporting masonry.

After you have the opportunity to review the findings and recommendations of this report, please call so that we might discuss how you plan to proceed.

GREDELL & ASSOCIATES

Gary W. Gredell, P.E.

Cc: Steve Nonnemaker
Aegis Property Group

Appendix II—Donald Friedman Structural Assessment and Memorandum

Reprinted with the permission of the Wagner Free Institute of Science

DONALD FRIEDMAN, P.E.
CONSULTING ENGINEER

159 Madison Avenue #2A
New York, NY 10016
T: 917-494-1586
F: 917-591-2189
DFriedman@OldStructures.com

September 19, 2005

William Stivale, Building Conservator
50 Commerce Street #5C
New York, New York 10014

Re: Wagner Institute
Main Roof Structure

Dear Mr. Stivale:

The following is a report on my investigation of conditions at the Wagner Institute roof. This letter is based on visual observation performed during our site visits on July 20, July 27, and August 23, including observation of conditions at probes in the interior ceiling and wall finishes; review of existing documentation including your photographs taken before the site visits, the HABS report, and the Keast & Hood report by D. G. Cornelius dated March 17, 2005; and my analysis of the conditions, including structural analysis of various roof structures as described below and empirical analysis of damage observed.

General Description

The main building of the Institute has a mixed structural system, including brick exterior bearing walls, interior cast-iron columns, and wood-joist floors. The building has three nominal floors, consisting of the office and theater space at the ground floor, the main gallery floor above, and a partial gallery floor at the top. The barrel-vaulted roof clear-spans the full width of the building (60 feet out to out) and consists of a waterproofing over a wood deck, wood purlins (spanning perpendicular to the vault curve), and a plaster ceiling on wood lath. The obvious structural support for the roof is a set of eight arched trusses which are located below the roof so that the truss top chords are just barely embedded in the plaster. (See Figures 1 and 2.) This investigation was, in part, triggered by partial failure of the plaster ceiling and concerns (as described in the Keast & Hood memo) over the safety and load capacity of the trusses.

The trusses represent the technology of the mid-nineteenth century. The top and bottom chords each consist of a single wood member with one scarf-type splice. (See Figure 9.)These splices have each half of the chord tapered and connected by three horizontal bolts. Similarly, the wood cross-bracing within each truss panel is not connected to the chords but simply bears on prismatic bearing blocks and the wrought-iron verticals that define the panels are simply bolted through the chords. (See Figure 10.) In other words, the verticals are capable of resisting tension but no compression, and the braces are capable of resisting compression but no tension. Finally, the wrought-iron tie rod at each truss passes through wood bearing blocks at each end to plate washers. Both chords are fastened into the end bearing block through birds-mouth cuts.

The wood deck and ceiling lath are simply nailed to the purlins. Most of the purlin-to-truss connections are simple bearing with toe-nails; four of these connections per truss are reinforced with vertical bolts that extend through the purlins and truss top chord.

Conditions Observed

There are several dominant patterns of damage visible at the roof, but no gross deformation or deterioration of structural material. The most visible damage is the presence of numerous plaster cracks across the ceiling and side walls, typically running parallel or perpendicular to the vault and fairly regularly spaced at 3 to 5 feet on center. In almost all cases, there is little separation or out-of-plane movement at the cracks; the only cracks observed with significant movement were vertical cracks on the side walls.

The side walls are out of plumb, with their tops tilted away from the interior. The tilt varies from zero to several inches. There is no corresponding damage to the stucco on the exterior face of the walls; in most cases there is no difference between the interior plaster damage at the most-tilted and least-tilted areas.

Two forms of truss movement were observed: lateral sway and open joints. The first is the sideways movement of the bottom chord of the trusses accompanied by out-of-vertical-plane tilting of the cross-braces and verticals. The upper chords are restrained against lateral movement through their embedment in the plaster ceiling and the bolted purlins, while the remainder of the truss is free to move laterally. The lower-chord movements are in the form of a single curve or a double ("S") curve along the chord length. The maximum lateral movement appears to be roughly three inches.

Open joints in the trusses were observed at the lower-chord splices, which show separations from hairline to 3/8 inches. The one upper-chord splice observed was tight. In addition, as many as a third of the cross-brace to bearing-block joints show separation from hairline to ¼ inches.

Much of the information gained by probing was negatively useful, in that damage that might be expected was not found. There was no sign of rot or other weathering damage at the three truss ends exposed, nor was any splitting or crushing observed at the truss end probes or the center top chord probe. Old weathering damage (deteriorated mortar) and repairs to the brick, including rebuilding and repointing, were observed at some locations. Given that the interior finish was observed to be wet-applied plaster over wood and expanded-metal lath, the repairs were probably made between the 1880s and 1930s.

Analysis

Because the structure was built before accurate truss and arch analysis methods were widely known and because the one-direction-force nature of the vertical and cross-bracing connections suggests that the trusses were not designed (in the modern sense of that term), structural analysis of the roof encompassed analysis of both the expected structural mechanism (the trusses working as tied arches that support the purlins) and several alternates. While the analysis results showed that the alternates could not work, they help to explain some of the damage noted.

The dead load of the roof, including the wood structure, plaster ceiling, and waterproofing, totals approximately 25 pounds per square foot (psf). Using the standard ASCE 7, *Minimum Design Loads for Buildings and Other Structures*, the maximum snow load is 22 psf and the maximum wind pressure 10 psf downward or 15 psf upwards. Since the maximum downward wind pressure will not act simultaneously with the maximum snow load and the wind uplift is less than the dead weight of the roof, the governing load combination is the sum of the dead and snow loads. The analyses below were performed for both this combination and for dead load only, which is the most common load condition.

Tied Arch 1 (Figure 3)

The roof was analyzed using the purlins as simple-span beams from truss to truss, and the trusses as arches consisting of the top chords only. The tie rods were assumed to end in plate washers that cover the rear of the end bearing blocks, in order to distribute the concentrated load from the tie rods over enough wood area to prevent crushing of the wood. (See Figure 5.) In this scenario, the truss verticals, cross-bracing, and lower chord serve only as local stiffeners to prevent small areas of unbalanced load from creating significant bending in the top chord arch. Under dead load only, this analysis provided acceptable results in terms of stress. The tie rods would lengthen approximately 3/8 inches under dead load and ¾ inch under full load. Under full dead and snow load, the top chord would be overstressed in compression. Under a 60° temperature change, the truss center moves vertically roughly ¼ inches. Under wind load from the side or unbalanced snow load caused by a combination of wind and snow, the arches could deflect asymmetrically as much as an 1½ inches.

Tied Arch 2 (Figure 4)

The roof was analyzed in a similar manner to Tied Arch 1, but using both the top and bottom chords as compression members. The only different result is that the stresses were within acceptable limits for the combined dead and snow load.

Untied Arch (Figure 6)

The roof was analyzed in a similar manner to Tied Arch 1, but neglecting the action of the tie rods. (This approximates the conditions if (a) the tie rods were installed too loose to take up the outward thrust created by the arch or (b) the plate washers on the ends of the tie rods are too small, thus creating unacceptably high bearing stress in the wood end blocks that would crush the wood immediately adjacent to the plate washers and therefore allow outward movement of the truss ends.) The stresses in the truss itself are the same as in Tied Arch 1 and Tied Arch 2, however the bending stresses in the masonry wall are unacceptably high. Under the maximum allowable stress in the masonry, the roof can support less than 2 percent of the combined dead and snow load.

Vault 1 (Figure 7)

The wood plank that makes up the roof top surface was analyzed as a vault. Since skylights interrupt the half of the vault panels between the trusses, this would be a combined mechanism, where the vault action takes place in the uninterrupted panels and the interrupted panels are carried by the trusses as tied arches. This type of load sharing is common when deflection from load in a primary structural member (in this case, the trusses) allows load to fall onto secondary members (the vaults). The stress in the wood was high, but not necessarily unacceptably so. However, the vaults create end thrust similar to the untied arch that creates unacceptably high bending stress in the walls.

Vault 2 (Figure 8)

The combination of the wood plank and plaster ceiling was analyzed as a vault, similar to Vault 1. The stress in the wood and plaster was acceptable, however the thrust problem is identical. It should also be noted that this mechanism contradicts empirical observation: if the plaster were in compression in half of the panels, the cracking in those panels would be noticeably less, which is not true.

CONCLUSIONS

The roof is most likely working in exactly the manner that it appears to, with the trusses working as tied arches that carry the purlins above. Given the lack of insulation, it is likely that the snow load has never reached the code maximum; the nature of code maximum snow loads is that they are rare events even if the roof is a cold surface. In addition, the absence of parapets means that there are no valleys to collect snow. For most of the building's 140-year life, the roof load has been the dead load plus small live loads from less-than-maximum wind and snow. It is likely that the ordinary and maximum load-carrying mechanisms are not identical: under ordinary load, the top chord is sufficient as an arch; as load increases during snowfall, the trusses will deflect downward and therefore shorten. When the lower chords shorten sufficiently to close the gaps at the splices, the lower chord will begin to carry load as an arch as well, effectively doubling the arch strength.

The gaps at the lower-chord splices may represent nothing more threatening than wood shrinkage. Sixty feet of timber can be expected to shorten several inches along the grain from drying in service. As the trusses shrank after their installation, the entire curve of the arches would have lowered, but not all pieces of lumber shrink equally. The difference between the gaps may represent different original rates of shrinkage between the various top and bottom chord pieces. Recent gaps, such as that mentioned in the Keast & Hood memo are not shrinkage, and may relate to the masonry movement described below.

Because the tie rods elongate under load and the masonry walls are too weak to resist the arch thrust, there would have been outward movement of the walls (equal to the tie-rod elongation) as the roof was completed and the dead load increased from zero to its current maximum. The truss ends are the wood tie-rod bearing blocks, which are embedded in the masonry walls. As the trusses were loaded during construction, the tie rods would gradually stretch, allowing the horizontal reaction caused by the arch form to push apart the bearing blocks. This reaction, transferred from the bearing blocks to the surrounding masonry,and applied more than 7 feet above the upper gallery floor, quickly caused bending in the walls too large for the capacity of masonry and therefore caused outward rotation of the walls. Any slack in the tie rods or looseness in their end connections would have similarly caused outward movement of the wall top. On those occasions when significant snow load increased the truss loads, the tie rods would have temporarily lengthened, likely causing additional permanent outward tilt. Forced outward rotation of the masonry would crack the mortar joints on the interior face and possibly crush them on the outside face and therefore would tend to be one-way motion. This type of ratchet mechanism in walls, where they move in only one direction after they have first moved, is common in old, unreinforced masonry. The amount of movement observed was far less than would be required to create instability in the walls and is therefore not dangerous as long as the condition of the masonry is maintained.

The upward motion of the roof on hot days, the downward movement on cold days and when snow or high winds load the roof, and the distortion caused by asymmetrical loads are sufficient to crack the plaster. Cracks in the wall plaster can be caused by similar thermal movement. The visible cracks, by themselves, are not dangerous but may be a sign that the plaster keyed through the lath is cracked. The fact that a portion of ceiling collapsed indicates that some keys are damaged; the presence of water damage from old roof leaks suggests this damage may be fairly widespread. As the structural motion of the roof will continue under changing load and temperature, the damage can only get worse.

In summary, there is no evidence of or analytical result showing structural overstress. In order to maintain the conditions under which the roof has performed adequately, material deterioration must be addressed in the roof and the walls. Finally, the plaster damage, while not a structural issue per se, can create hazardous conditions and can only be addressed through removal and replacement.

Recommendations

As there is no damage that can be attributed to structural defect, emergency structural repairs are not required. However, there is structural weather deterioration (the weakened mortar) and finish damage from structural action (the cracked plaster). These conditions must be addressed as soon as possible: the masonry damage can only grow worse and can potentially cause damage to other building elements such as the exterior stucco, while the damaged plaster can detach from the lath and injure people below. Until the repair work is complete, the temporary platform currently in place at the upper gallery level is retained and the upper level left vacant.

Trusses: No work is indicated at this time. Any rotted wood exposed by ceiling demolition must be replaced.

Walls: The damaged upper portions of wall must be repointed. Any cracked or severely eroded bricks exposed by plaster demolition should be replaced. This will require that the roof trusses be shored, and for this reason should be performed in stages. As long as only one truss is affected by the work at any given moment – meaning that the masonry work must proceed in stages down the length of the building – the upper gallery floor is capable of supporting shoring to support the trusses.

Finishes: All plaster at the upper gallery level, including the walls and vaulted ceiling, must be replaced. Replacements can be made in plaster or gypsum board; in either case, provision for movement must be made to prevent recurring cracks. Expansion joints in the plaster or gypsum board should be located at the truss side faces and at no more than 30 feet on center perpendicular to the trusses.

If you have any questions or I can be of further assistance, please call.

Sincerely,

Donald Friedman

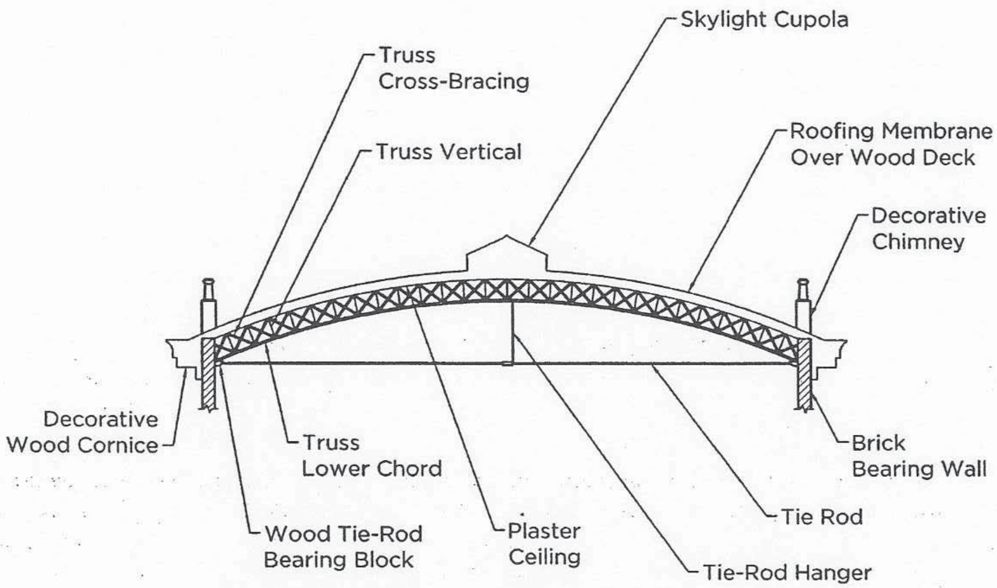

Figure 1: Roof Section, Visible Structure

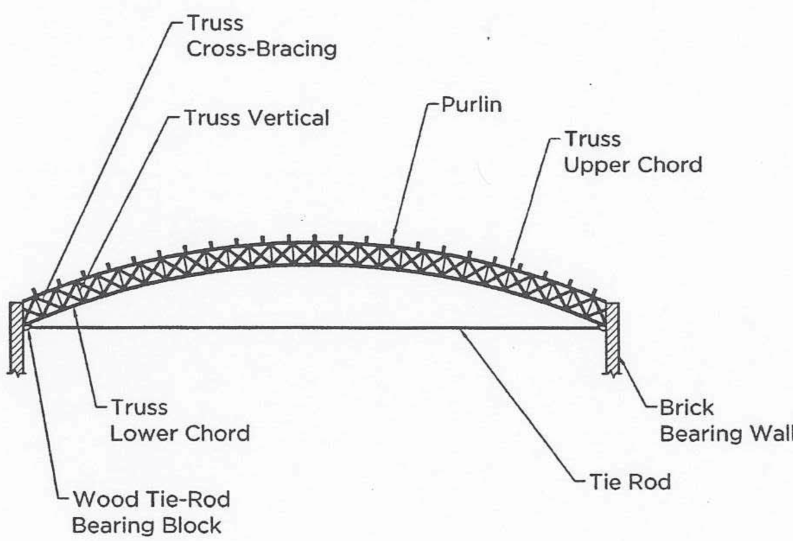

Figure 2: Roof Section, Major Structure

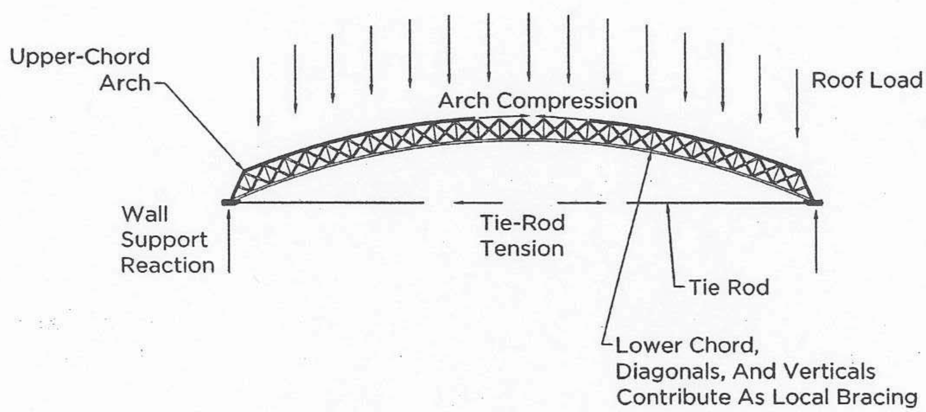

Figure 3: Tied Arch 1 Structural Model

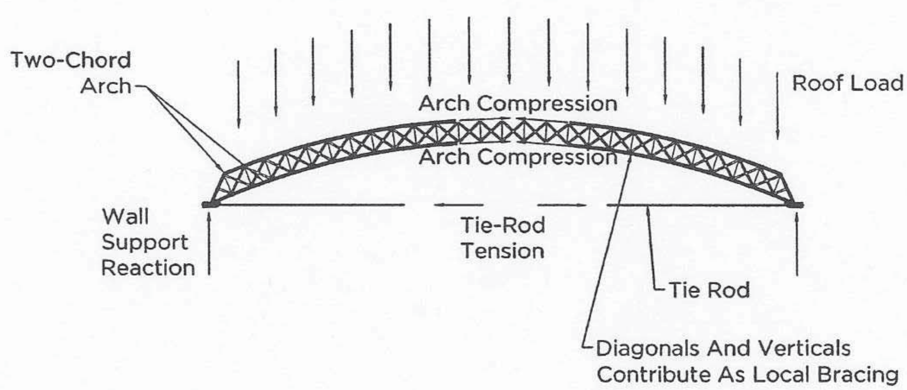

Figure 4: Tied Arch 2 Structural Model

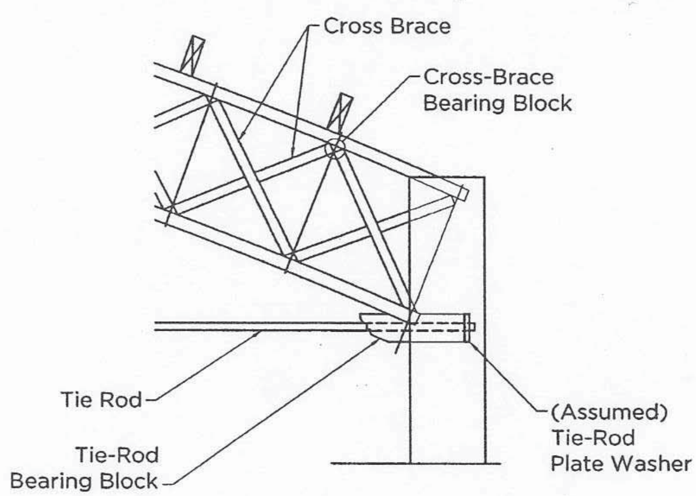

Figure 5: Truss End Detail

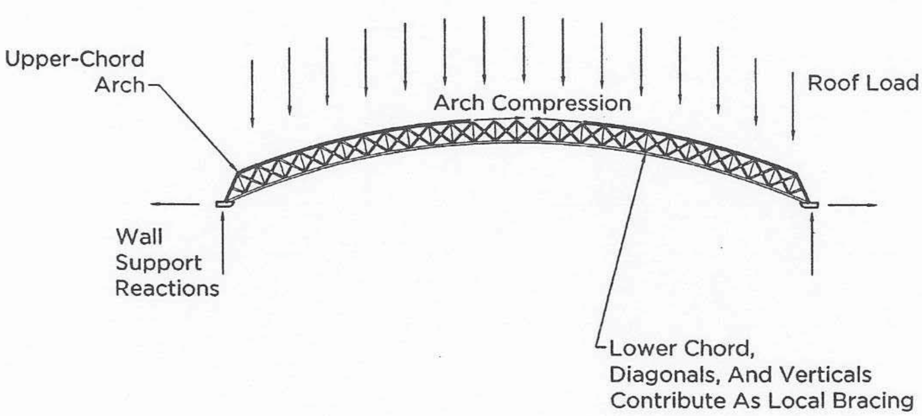

Figure 6: Untied Arch Structural Model

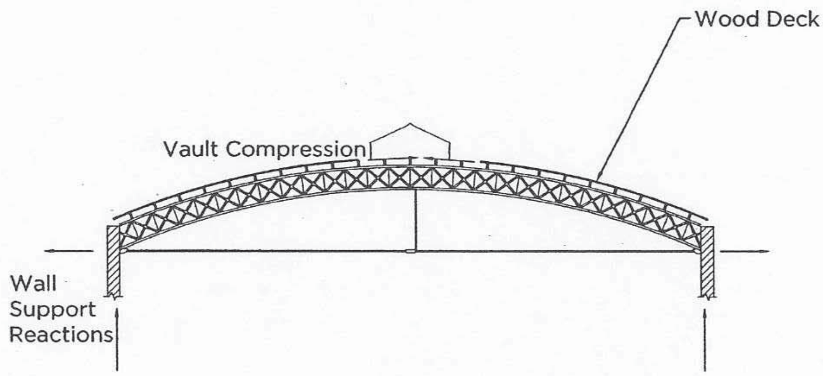

Figure 7: Vault 1 Structural Model

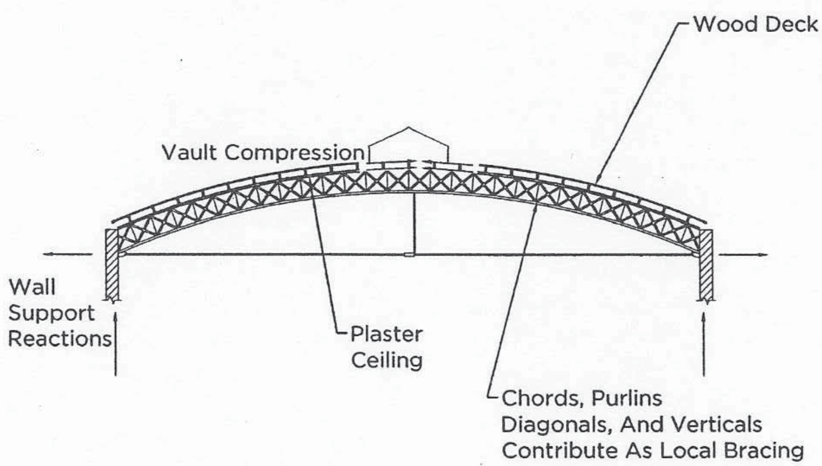

Figure 8: Vault 2 Structural Model

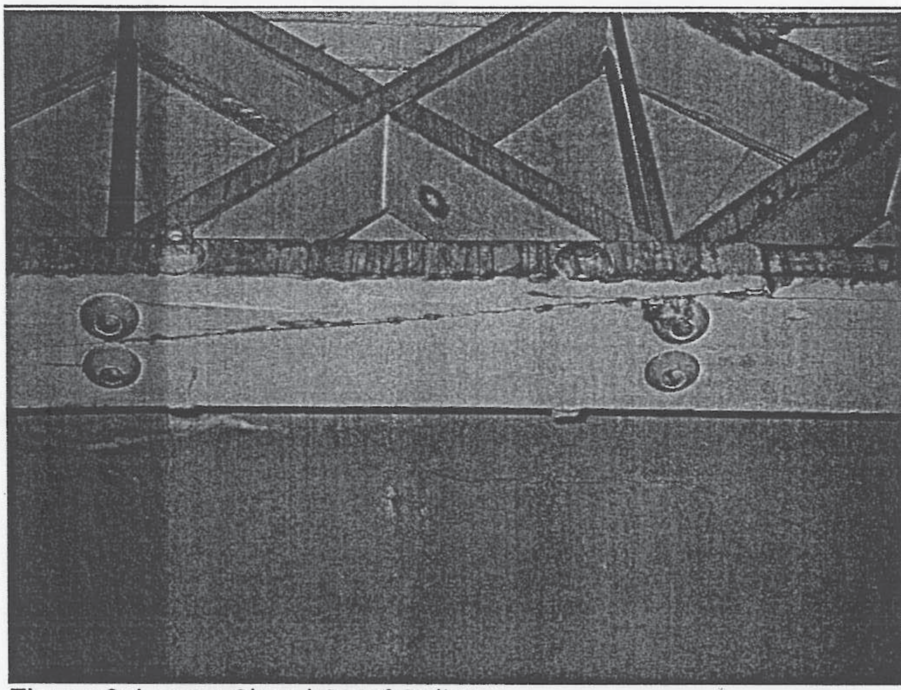
Figure 9: Lower Chord Scarf Splice

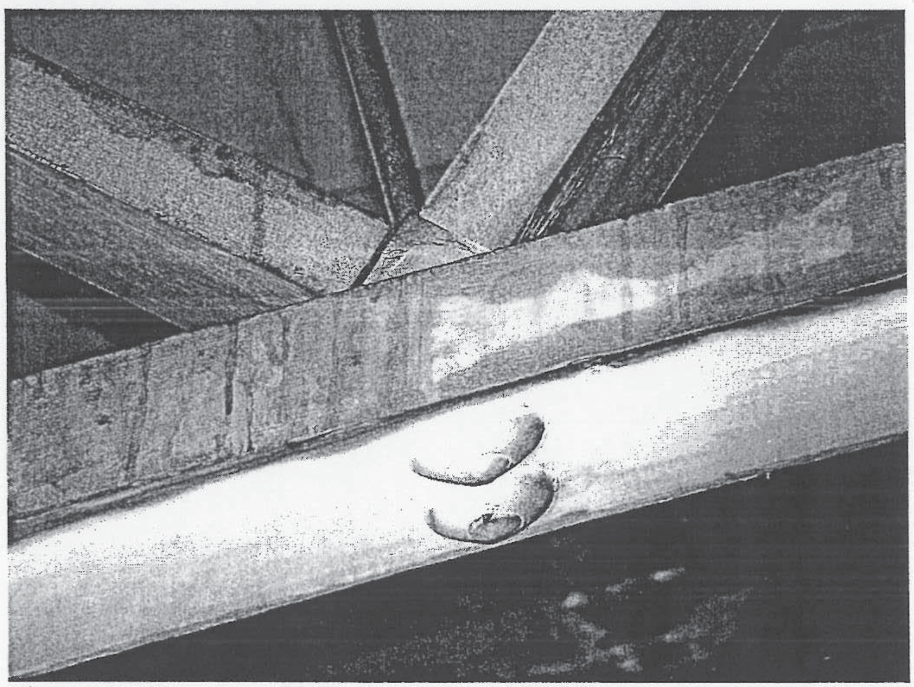
Figure 10: Cross-Bracing and Bearing Block

OLD STRUCTURES

260 West 35th Street, Suite 501 | New York, NY 10001 | T: 212-244-4546 | F: 917-591-2189 | www.oldstructures.com

Memorandum

From:	Donald Friedman	Date:	January 7, 2008
To:	Bill Stivale	Company:	William Stivale, Building Conservator
c:			
Project #	J1386.02	Project:	Wagner Museum Design

Per our discussion, I have reviewed the movement of the roof trusses and purlins under load. The load cases compared were dead load only, dead load and uniform snow load, unbalanced wind load, and dead load and unbalanced snow load (wind drift).

Note that the dead load is in range of 22 to 25 pounds per square foot (psf) depending on the variable thickness of plaster, the uniform snow load is 22 psf, the wind load is negligible (less than 1 psf), and the unbalanced snow load varies from 0 to 44 psf.

The maximum differential movement is approximately 1/8" per foot, which is equivalent to movement of roughly 1/100 a given span. Note that the typical guideline for structural deflections of ceiling members supporting plaster is L/360.

Per my comments at the meeting on November 28, I believe this movement is too large to be accommodated without expansion joints in the plaster and too large for the existing cracked plaster under any circumstances.

Appendix III—Keast and Hood Roof Structure Investigation

Reprinted with the permission of the Wagner Free Institute of Science

WAGNER FREE INSTITUTE OF SCIENCE

ROOF STRUCTURE WOOD PATHOLOGY INVESTIGATION

By

Keast & Hood Co.
Thomas J. Leidigh
Suzanne M. Pentz

October 13, 1994

INTRODUCTION AND BACKGROUND

As consultants to John Blatteau Associates, architects, Keast & Hood Co. was asked to perform an inspection of the historic timber roof arches at the Wagner Free Institute of Science. The Institute is planning a restoration program that will include replacing the original tin roof which is now in very poor condition. The purpose of the inspection was to determine if there were any deficiencies in the roof structure which could affect planning and budgeting for the future roof restoration program.

Where timber structures have been subjected to prolonged wetting from roof leaks, such as has occurred at the Wagner Institute, there is a high potential for fungal decay infections to develop, resulting in severe material strength loss. Recent experience has shown that the traditional methods of visual inspection and ice-pick probing are not adequate to detect hidden internal or early decay infections which, although not apparent on the visible external surfaces, can seriously weaken a structure. For these reasons, Keast & Hood Co. recommended that core samples from the Wagner Institute roof arches should be taken and examined by Wood Products Pathologist Dr. Joe Clark.

DESCRIPTION OF ROOF ARCHES

There are 8 tied timber lattice arches supporting the roof and plaster ceiling of the Wagner Institute. The arches span about 58 feet horizontally and are spaced at approximately 17 feet center-to-center. We do not believe that there are any arches buried within the end walls of the building.

Each arch is a semicircular segment with a bottom chord rise of about 6 feet and a radius of roughly 72 feet. The arches are tied together at the base with 1-5/8 ϕ tie rods which are supported vertically at the center with sag rods hung from the arches. The curved arch members are constructed of concentric 2-1/2 x 8 timber top and bottom chords which were most likely bent and formed through a steaming and heating process. This type of process plasticizes the material so that the timber can be bent without inducing significant residual stresses. The bent timber will then tend to hold its shape once the material has cooled and dried. If, on the other hand, the timbers were not plasticized through steaming or other means, bending would produce large stresses in the material which would still be present today. The magnitude of this initial stress is of potentially great significance in evaluating the structural capacity of the arches. However, the process that was used to produce the curvature remains unconfirmed (and is probably unconfirmable). Considering the years of successful performance, we presume that the residual stress from bending to the arch configuration must be relatively low.

Between the curved top and bottom chords are 1-7/8" x 6" diagonal timber lattice members forming an "X" panel pattern. These diagonals are seated at the top and bottom into triangular cast iron bearing blocks which are bolted into the chords with radial iron tie bolts. Of the diagonal members, those which slope downwards towards the walls carry compression forces, while those which slope in the opposite direction are considered to be spacers which help the arch hold its shape, and may also carry compression forces under unbalanced loading conditions. Several of these diagonal spacers were observed to be loose.

Each of the curved chords is composed of two lengths of timbers spliced somewhere within the inner 1/3 of the span. The splice joints are scarfed with long diagonal cuts and fastened with 3 horizontal through bolts. At the ends of the long diagonal cut, there are perpendicular return cuts of about 1/2" on either side of the chord, providing very little effective bearing area for the transfer of compressive forces. Several of these chord splice joints were observed to be split.

Where the arches bear on the exterior wall, the ends of the bottom chords are seated into birdsmouth notches in short horizontal abutment pieces called bolster blocks. The bolster blocks are composed of paired 4 x 5-1/2 members sandwiched around the 1-5/8" ϕ tie rods. The tie rods resist the thrust of the arches and are restrained at the outer ends of the bolster blocks with end plates and nuts.

MECHANICS OF THE ARCH

While a detailed structural analysis of the roof arch has not been part of the scope of work of this project, we are familiar with the mechanics of similar historical arch forms. Under normal uniform gravity loading conditions, we would expect that the curved arch members act entirely in compression, with top chord compression stresses highest near the center of the span, and bottom chord compression stresses highest at the ends of the span. The diagonal web members also would be expected to carry increasing compression forces towards the ends of the span.

Our overall impression of the Wagner Institute roof arches is that they are technologically sophisticated structures built of high quality material (clear, virgin Eastern White Pine) and featuring well-executed joinery and craftsmanship. Perhaps the only shortcoming in the form is the scarf splices, which although finely crafted and fitted, might be considered to be poorly conceived from a modern engineer's viewpoint of the transfer of forces. Reportedly, the roof arch design was patented[1], although efforts to locate the patent have so far been unsuccessful.

---

[1] Ledger and Transcript, Philadelphia, PA., October 24, 1860

A rough analysis of the roof arches discloses that the basic stress level in the timber chords and iron tie rods is rather high. Indeed, the small member sizes that were used (2-1/2" x 8" chords, 1-5/8" ϕ tie rods) suggest that, in an era of increasing engineering sophistication and mechanization, this reportedly patented design pushed the materials towards the limits of their safe working use. The tradeoff in engineering sophistication and economy of form and materials is that the highly stressed members cannot tolerate much physical deterioration and strength loss due to decay. Furthermore, there is little redundancy available in the structure, so that the undiminished condition and performance of every element becomes critical.

DECAY INVESTIGATION

Because the wall-bearing ends of the arches carry the highest stress and are also the location which is most susceptible to water intrusion from failures in gutters, flashings, and rainwater conductors, we were very concerned about the potential for decay deterioration in ends of the arches. Fortunately, the decay investigation as conducted by Dr. Joe Clark did not disclose any significant deterioration in the principal structural members comprising the roof arches. Decay in the arch members was confined to the non-critical free end of the top chord in the cornice, or superficial external infection in the outer portion of the bolster block. However, the secondary structural members (cornice outrigger supports and roof rafters) did not fare as well, and many of these will require replacement. (See Dr. Clark's report, attached, for additional information on the decay investigation).

RECOMMENDATIONS

The following itemized list of recommended structural repairs is submitted for planning, budgeting, and estimating purposes:

1. **Splices**

   Because several of the top and bottom chord scarf splices exhibit splitting and crushing at the perpendicular bearing interfaces, we recommend that all splice joints be provided with new steel reinforcements. The reinforcements may entail new steel shear pins and/or side plates and will necessitate scaffolding over the center of the hall for installation access. Shoring of the trussed arches will probably not be required; however, protection of the museum collections and building finishes below the scaffold working platform is expected to be a significant budgetary component of this work.

2. **Cornice and Outriggers**

   We concur with Dr. Clark's recommendation that the cornice outrigger structure should be completely rebuilt with new light framing replicating the original structure. The new outrigger framing should be built of seasoned, preservative-treated material.

3. **Rafter Tie-Downs**

The rafters which span from arch to arch are typically spiked down to the top chords, although in some cases the mechanical connection appeared to be missing. The means of anchoring the rafters down to the arches becomes an important consideration in a wind uplift situation, which, in this type of roof, is most critical around the roof edges. We recommend that the roof sheathing should be removed in a strip at the rafter/arch junctures for about 15' back from the east and west walls, so that the perimeter rafter ends can be inspected, and the rafter/arch connections reinforced with new anchors as required. Improvement of the rafter/arch connections will also help to laterally brace the chords of the arches. Bottom chord bracing is derived from the top chord/rafter connection and the stiffness of the diagonal web members to provide the necessary lateral restraint.

4. **Rafter and Sheathing Replacement**

Generally, roof sheathing and roof rafters appeared to be in fair-to-good condition, although the area available for inspection was limited to the east cornice edge, one location adjacent to a skylight at the center of the roof, and one location (with a totally decayed rafter) at the west roof edge. It is difficult to develop an allowance for rafter/sheathing replacement based on such a small sample, but one might expect that there will be additional decayed rafters found around the roof edges where leaks are most likely to have occurred. The perimeter rafter ends can be inspected when the sheathing is removed for the tiedown inspection (item 3 above). In the absence of more definitive information, we suggest that an allowance for replacement-in-kind of 10% of the rafters and sheathing should be budgeted.

5. **Plaster Ceiling**

The plaster ceiling exhibits many (old) cracks, but it does not seem to be presently falling or flaking. However, there is always the risk that the impact of construction activities on the roof could further weaken or damage the ceiling. First, we recommend that the present condition of the ceiling should be evaluated by an experienced plaster conservator. If the ceiling is determined to be sound, the reroofing project could proceed as planned using careful, minimal-impact construction techniques. However, the risk of inadvertent damage to the historic ceiling should be recognized, and a contingency should be allowed in the budget for ceiling repair/ replacement.

Alternatively, if the present condition of the ceiling is determined to be poor or marginal, the opportunity for replacing the ceiling from the vantage of the full scaffolding that will be available during this project should be carefully considered.

During the investigation, a section of ceiling plaster was removed for weighing in order to calculate the magnitude of the dead loads available to resist wind uplift forces. We note for the record that the plaster (without the wood lath) weighs 6 PSF, which is slightly lighter than the normal density for historic ceiling plaster.

6. **Wall Studs and Sill**

Near the top of the east and west brick bearing walls, the walls step in with a 4 inch ledge and are furred out with plaster on wood studs. These studs and the wood sill they sit on were found in some instances to be totally decayed to the point of complete disintegration. However, the studs and sill do not carry roof or wall loads, and there is no compelling structural reason to replace them. To the extent that they can continue to serve the purpose as a substrate for the upper plaster wall surface, there may be no need to disturb the historic plaster to replace the studs.

ADDITIONAL CONSIDERATIONS

It should be noted that during this overview investigation, we have not had the opportunity to fully measure the existing roof construction, nor have we performed a detailed load and stress analysis of the structure. Our conclusions regarding the roof structure may need to be modified later when these steps are taken.

The scope of the present assessment has been limited to investigation of the roof structure only; the condition and capacity of the floor structures, balconies, columns, bearing walls, and foundations have not been considered. However, based on our experience with historic buildings of similar age and construction, we anticipate that a structural assessment of the whole building system would most likely disclose certain elements that are deficient or not code-conforming. If limited funds are available for further study, we suggest that priority should be given to the structural assessment and strengthening/ stabilization of those areas of the building which are accessible to the general public, particularly, the area under the lecture hall.

CONCLUSIONS

We are pleased to report that the wood pathology investigation indicates a "clean bill of health" for the principal load-bearing elements of the trussed roof arches at the Wagner Free Institute of Science. Fortunately, the decay that was found was limited to areas or elements of secondary structural importance. However, decay can spread or resume at any time that water from roof leaks is available to fuel the infections. The provision of new water-tight roofing, with adherence to a rigorous schedule of maintenance, will be the most important preservation measures that can be taken to protect this distinctive historic structure.

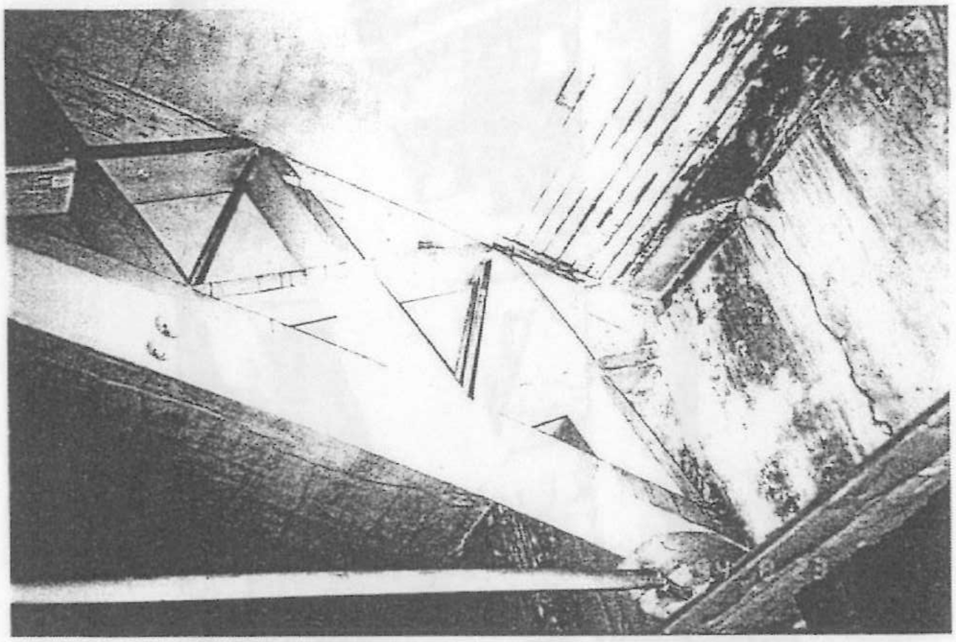

1. *Typical trussed arch at the Wagner Free Institute of Science, showing curved bottom chord, diagonal web members, and paired radial tie bolts. The curved solid top chord, identical in size to the bottom chord, is hidden above the plaster ceiling. The 1-5/8" ϕ tie rod which restrains the thrust of the arch is visible at the bottom of the picture.*

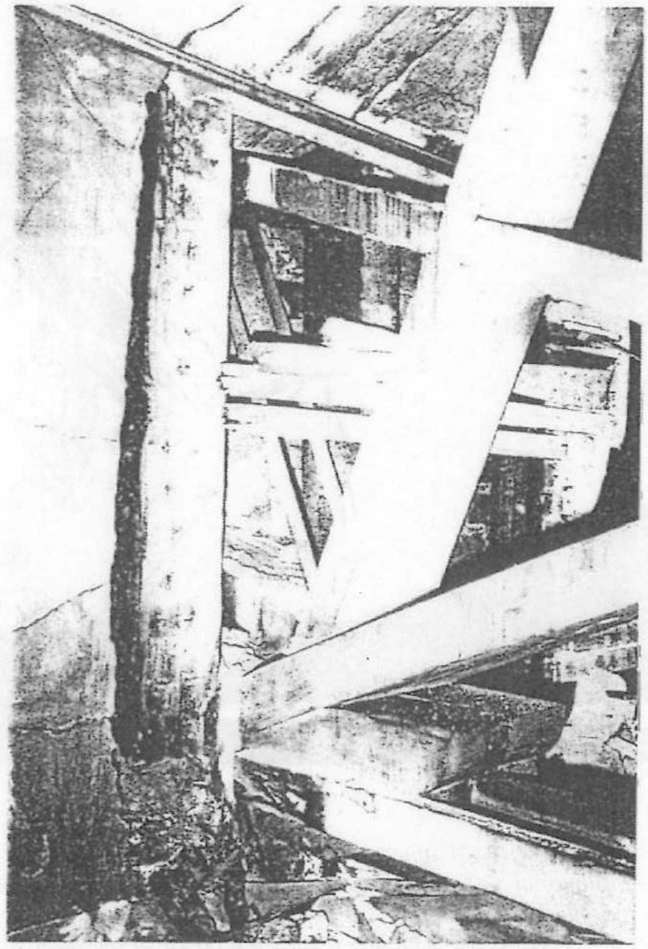

2. *View of typical arch end at bearing wall showing birdsmouth notch of bolster block to receive bottom chord. A core sampling hole is visible in the side of the bolster block. The critical load-bearing members of the arch ends were found to be generally sound.*

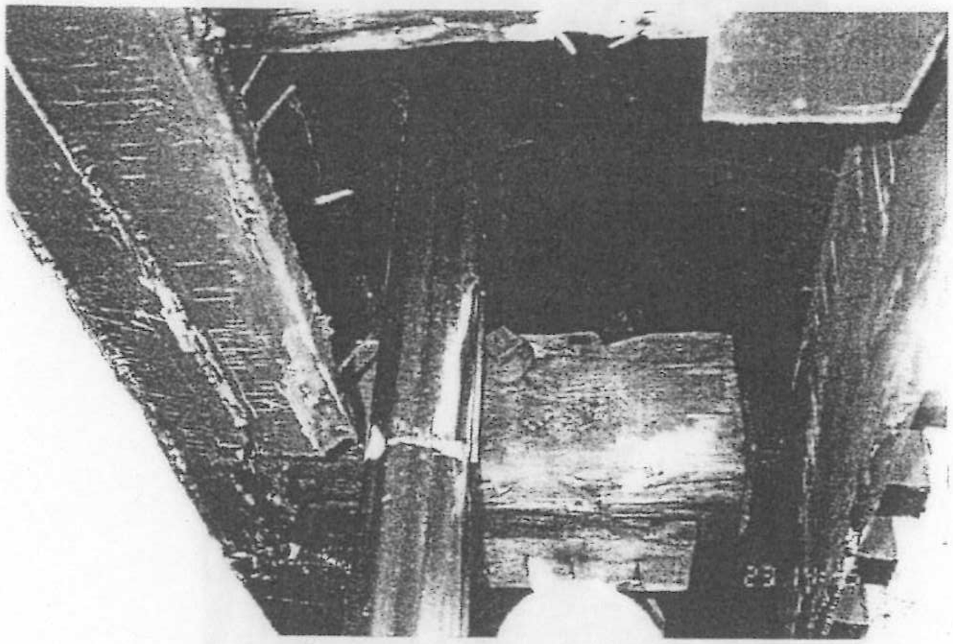

3. *View of typical extension of arch end into cornice. Some decay was found on the surfaces of the bolster block and the free ends of the top chords, although the decay was not structurally significant.*

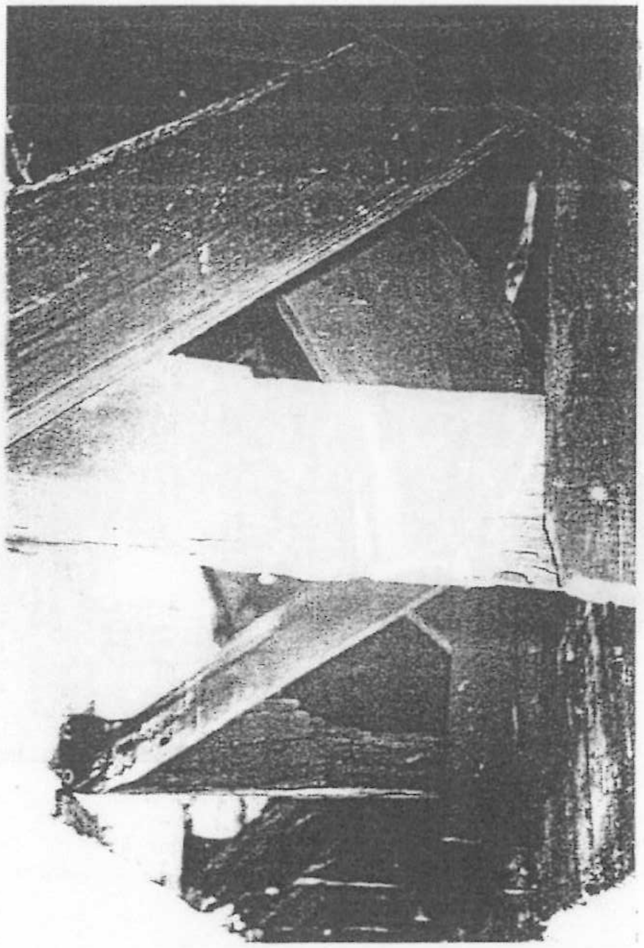

4. View of outriggers and nominal one-inch framing members supporting cornice fascia and soffit. These materials were found to be in a highly deteriorated condition.

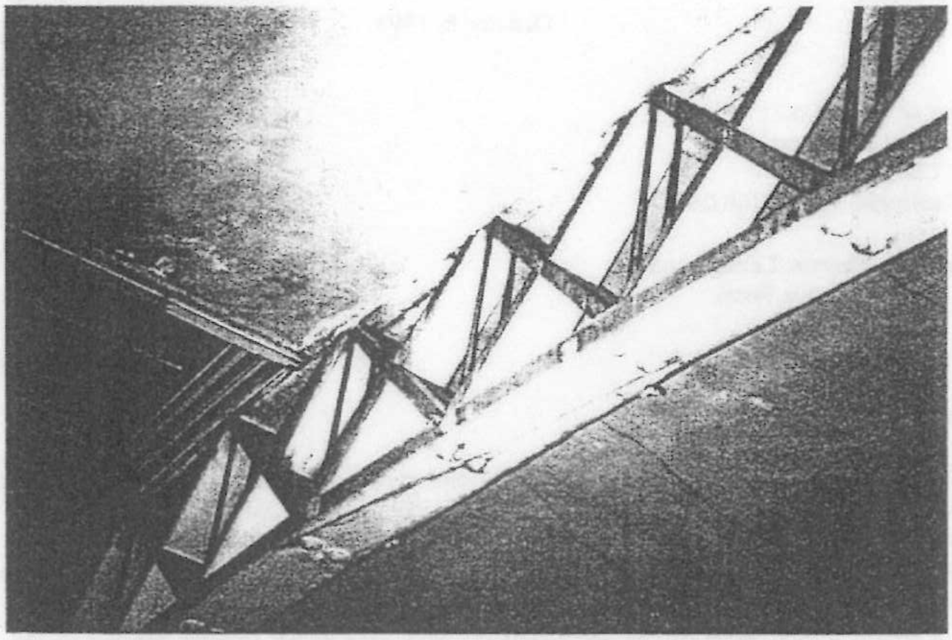

5. *Typical scarf splice in curved chord. Closer inspection of the 1/2" perpendicular bearing interfaces at the ends of the long diagonal cut reveals several instances of crushing and splitting of the wood fibers.*

DR. JOE W. CLARK, CONSULTANT
WOOD PRODUCTS PATHOLOGY
8076 LONE OAK CT. (608) 798-3889
CROSS PLAINS, WI 53528

October 8, 1994

Keast & Hood Co.
Structural Engineers
325 Chestnut Street
Philadelphia, PA 19106-2605

Attention: Thomas Leidigh and
Suzanne Pentz

Project: Wagner Free Institute of Science

Dear Tom and Suzanne:

Following is a summary of my findings during our recent investigation of the roof arches at the Wagner Free Institute of Science. I understand the present plans call for new roofing, and the question I was to look into was the condition of the arches and the attached soffit framing with emphasis on the parts of the arch ends extending to and beyond the exterior walls. The upper and lower chords of the arches are the most critical members along with the bolster blocks that form the extensions of the arches where they are supported by the exterior walls.

Arches were selected for investigation where interior water stains on the walls under or adjacent to arch ends indicated probable wetting from roof or gutter leakage of rain or snow melt. Such wetting would be expected to allow sufficient moisture build-up in some framing members that would permit decay fungus infections and consequent decay in such members. Another factor considered in the selection of arches for investigation was the deterioration of the exterior fascia and soffit materials along the cornice as viewed exteriorly.

Exterior or surface decay of selected arch or associated framing members was examined by probing the wood with an awl-like tool to determine the presence of decay and its depth and extent. Interior decay in the heavier members such as upper and lower chords, bolster blocks, and outrigger supports was determined by the removal of 3/8 inch diameter cores from areas of the wood that appeared most likely to have interior decay.

The examination at ten arch ends showed the following:

1. <u>The gutter system</u> along both long sides of the roof is leaking water into the cornice area because of holes in the tin roofing material that extends to form the gutter. Leaf blockage of drainage via the downspouts has increased the amount of leakage. A new gutter system is essential and of a design to include protective devices that will prevent leaf clogging.

2. Nominal one inch material that form the framing for the fascia and soffit boards in the cornice spaces was found to be decayed severely. This has resulted in very significant wood strength loss, a loss of nail holding capacity, and the active decay now present will continue to spread until these members are replaced or the wood is thoroughly dried.

3. Both the fascia and soffit boards show severe decay in small to large areas. In my view these boards should not be retained for use in the rebuilding of a new cornice structure.

4. The lower chord members of the arches do not extend into the cornice space but terminate in a notched joint in the upper surface of the bolster block; and, although water marked frequently on their surfaces, these members were found free of decay and can be continued in use in cases that were examined.

5. The upper chord members do extend into the cornice space with their ends positioned under the leaky gutters. These ends have been subjected to sufficient wetting so that decay, in some instances, is severe. However, the severe decay and the associated moderate and early stages of decay do not extend upward in these members to areas of critical joints or significant stress-loading. In my view these members may be continued in service although some outer ends may need replacement to support the light framing members for the cornice.

6. The bolster block members which transfer the arch loads into the tie rods do extend over the supporting exterior wall and into the full extension of the cornice. Wetting of these members has occurred commonly which has permitted decay fungus infections and consequent decay. The observed decay has occurred at the outer surfaces of these members and has only penetrated a small proportion of the block cross sections. In the cases observed, these bolster blocks can be continued in service if new gutters and cornice replacement will assure dry conditions that will permit thorough drying of these members. To assure this drying, and the necessary future dry conditions needed in the cornice enclosed areas, the new cornice construction should provide spaced vents in the soffit to assure adequate ventilation.

7. The outrigging framing members that are set into nine inch "sockets" in the brick wall form intermediate horizontal frame members between the bolster blocks. The outriggers were commonly found to be severely decayed and should be replaced during the replacement of the cornice.

8. Cross brace members of the trussed arches do show water stains on the painted surfaces. However, examination of the wood at and adjacent to the joints between the lower ends of the cross braces and the upper sides of the lower chord members showed no decay. The joints examined were limited to those above the fourth floor balcony that were accessible from a rolling platform or ladder. The absence of decay in these members in the building interior is attributable to the fact that the wood wetting which has occurred has dried soon

after wetting, and to the comparatively good natural decay resistance of the eastern white pine old growth heartwood material used for these members.

9. The brick wall in the cornice at some openings shows severe erosion and may require evaluation of the damage to date and a consideration of possible control measures by someone knowledgeable in this subject area.

I have had no opportunity as yet to do a laboratory examination of the cores removed from the various structural members. However, I feel confident of this report regarding the areas sampled. Further, I believe these samplings represent the most probable areas for serious degrade from decay.

Should you have any questions regarding this report, please contact me.

Yours truly,

Joe W. Clark

JWC:tl
File: Wagner.108

Appendix IV—Simple Arch Analysis

Basic Load Cases

	BLC Description	Category	X Gravity	Y Gravity	Z Gravity	Joint	Point	Distributed	Area (Me...	Surface (...
1	sw	DL		-1		29				
2	snow	None				29				
3	temperature	None						30		

Joint Boundary Conditions

	Joint Label	X [k/in]	Y [k/in]	Z [k/in]	X Rot.[k-ft/rad]	Y Rot.[k-ft/rad]	Z Rot.[k-ft/rad]	Footing
1	N29		Reaction	Reaction	Fixed	Fixed		
2	N30	Reaction	Reaction	Reaction	Fixed	Fixed		
3	N1			Reaction				
4	N15			Reaction				
5	N16			Reaction				
6	N2			Reaction				
7	N3			Reaction				
8	N4			Reaction				
9	N5			Reaction				
10	N6			Reaction				
11	N7			Reaction				
12	N8			Reaction				
13	N9			Reaction				
14	N10			Reaction				
15	N11			Reaction				
16	N12			Reaction				
17	N13			Reaction				
18	N14			Reaction				
19	N17			Reaction				
20	N18			Reaction				
21	N19			Reaction				
22	N20			Reaction				
23	N21			Reaction				
24	N22			Reaction				
25	N23			Reaction				
26	N24			Reaction				
27	N25			Reaction				
28	N26			Reaction				
29	N27			Reaction				
30	N28			Reaction				
31	N31			Reaction				

Load Combinations

	Description	Solve	PD...	SR...	BLC	Factor	BLC	Factor	BLC	Factor	BLC	Factor	BLC	Factor	BLC	Factor	BLC	Factor	BLC	Factor
1	sw	Yes	Y		1	1														
2	dead+snow	Yes	Y		1	1	2	1												
3	dead+thermal	Yes	Y		1	1	3	1												

Member Distributed Loads (BLC 3 : temperature)

	Member Label	Direction	Start Magnitude[k/ft,d..	End Magnitude[k/ft,d...	Start Location[ft,%]	End Location[ft,%]
1	M3	T	70	70	0	0
2	M4	T	70	70	0	0
3	M5	T	70	70	0	0
4	M6	T	70	70	0	0
5	M7	T	70	70	0	0
6	M8	T	70	70	0	0

Member Distributed Loads (BLC 3 : temperature) (Continued)

	Member Label	Direction	Start Magnitude[k/ft,d..	End Magnitude[k/ft,d...	Start Location[ft,%]	End Location[ft,%]
7	M9	T	70	70	0	0
8	M10	T	70	70	0	0
9	M11	T	70	70	0	0
10	M12	T	70	70	0	0
11	M13	T	70	70	0	0
12	M14	T	70	70	0	0
13	M15	T	70	70	0	0
14	M16	T	70	70	0	0
15	M17	T	70	70	0	0
16	M18	T	70	70	0	0
17	M19	T	70	70	0	0
18	M20	T	70	70	0	0
19	M21	T	70	70	0	0
20	M22	T	70	70	0	0
21	M23	T	70	70	0	0
22	M24	T	70	70	0	0
23	M25	T	70	70	0	0
24	M26	T	70	70	0	0
25	M27	T	70	70	0	0
26	M28	T	70	70	0	0
27	M29	T	70	70	0	0
28	M30	T	70	70	0	0
29	M31	T	70	70	0	0
30	M2	T	70	70	0	0

Joint Loads and Enforced Displacements (BLC 1 : sw)

	Joint Label	L,D,M	Direction	Magnitude[(k,k-ft), (in,rad), (k*s^2/ft...
1	N28	L	Y	-.481
2	N27	L	Y	-.481
3	N26	L	Y	-.481
4	N25	L	Y	-.481
5	N24	L	Y	-.481
6	N23	L	Y	-.481
7	N22	L	Y	-.481
8	N21	L	Y	-.481
9	N20	L	Y	-.481
10	N19	L	Y	-.481
11	N18	L	Y	-.481
12	N17	L	Y	-.481
13	N16	L	Y	-.481
14	N15	L	Y	-.481
15	N1	L	Y	-.481
16	N2	L	Y	-.481
17	N3	L	Y	-.481
18	N4	L	Y	-.481
19	N5	L	Y	-.481
20	N6	L	Y	-.481
21	N7	L	Y	-.481
22	N8	L	Y	-.481
23	N9	L	Y	-.481
24	N10	L	Y	-.481
25	N11	L	Y	-.481
26	N12	L	Y	-.481
27	N13	L	Y	-.481
28	N14	L	Y	-.481
29	N31	L	Y	-.481

Joint Loads and Enforced Displacements (BLC 2 : snow)

	Joint Label	L,D,M	Direction	Magnitude[(k,k-ft), (in,rad), (k*s^2/ft...
1	N28	L	Y	-.726
2	N27	L	Y	-.726
3	N26	L	Y	-.726
4	N25	L	Y	-.726
5	N24	L	Y	-.726
6	N23	L	Y	-.726
7	N22	L	Y	-.726
8	N21	L	Y	-.726
9	N20	L	Y	-.726
10	N19	L	Y	-.726
11	N18	L	Y	-.726
12	N17	L	Y	-.726
13	N16	L	Y	-.726
14	N15	L	Y	-.726
15	N1	L	Y	-.726
16	N2	L	Y	-.726
17	N3	L	Y	-.726
18	N4	L	Y	-.726
19	N5	L	Y	-.726
20	N6	L	Y	-.726
21	N7	L	Y	-.726
22	N8	L	Y	-.726
23	N9	L	Y	-.726
24	N10	L	Y	-.726
25	N11	L	Y	-.726
26	N12	L	Y	-.726
27	N13	L	Y	-.726
28	N14	L	Y	-.726
29	N31	L	Y	-.726

Member Primary Data

	Label	I Joint	J Joint	K Joint	Rotate(deg)	Section/Shape	Type	Design List	Material	Design Rules
1	M2	N30	N28			4.4375X26.75...	Beam	Rectangular	EWPine	Typical
2	M3	N28	N27			4.4375X26.75...	Beam	Rectangular	EWPine	Typical
3	M4	N27	N26			4.4375X26.75...	Beam	Rectangular	EWPine	Typical
4	M5	N26	N25			4.4375X26.75...	Beam	Rectangular	EWPine	Typical
5	M6	N25	N24			4.4375X26.75...	Beam	Rectangular	EWPine	Typical
6	M7	N24	N23			4.4375X26.75...	Beam	Rectangular	EWPine	Typical
7	M8	N23	N22			4.4375X26.75...	Beam	Rectangular	EWPine	Typical
8	M9	N22	N21			4.4375X26.75...	Beam	Rectangular	EWPine	Typical
9	M10	N21	N20			4.4375X26.75...	Beam	Rectangular	EWPine	Typical
10	M11	N20	N19			4.4375X26.75...	Beam	Rectangular	EWPine	Typical
11	M12	N19	N18			4.4375X26.75...	Beam	Rectangular	EWPine	Typical
12	M13	N18	N17			4.4375X26.75...	Beam	Rectangular	EWPine	Typical
13	M14	N17	N16			4.4375X26.75...	Beam	Rectangular	EWPine	Typical
14	M15	N16	N15			4.4375X26.75...	Beam	Rectangular	EWPine	Typical
15	M16	N15	N1			4.4375X26.75...	Beam	Rectangular	EWPine	Typical
16	M17	N1	N2			4.4375X26.75...	Beam	Rectangular	EWPine	Typical
17	M18	N2	N3			4.4375X26.75...	Beam	Rectangular	EWPine	Typical
18	M19	N3	N4			4.4375X26.75...	Beam	Rectangular	EWPine	Typical
19	M20	N4	N5			4.4375X26.75...	Beam	Rectangular	EWPine	Typical
20	M21	N5	N6			4.4375X26.75...	Beam	Rectangular	EWPine	Typical
21	M22	N6	N7			4.4375X26.75...	Beam	Rectangular	EWPine	Typical
22	M23	N7	N8			4.4375X26.75...	Beam	Rectangular	EWPine	Typical
23	M24	N8	N9			4.4375X26.75...	Beam	Rectangular	EWPine	Typical
24	M25	N9	N10			4.4375X26.75...	Beam	Rectangular	EWPine	Typical

Member Primary Data (Continued)

	Label	I Joint	J Joint	K Joint	Rotate(deg)	Section/Shape	Type	Design List	Material	Design Rules
25	M26	N10	N11			4.4375X26.75...	Beam	Rectangular	EWPine	Typical
26	M27	N11	N12			4.4375X26.75...	Beam	Rectangular	EWPine	Typical
27	M28	N12	N13			4.4375X26.75...	Beam	Rectangular	EWPine	Typical
28	M29	N13	N14			4.4375X26.75...	Beam	Rectangular	EWPine	Typical
29	M30	N14	N31			4.4375X26.75...	Beam	Rectangular	EWPine	Typical
30	M31	N31	N29			4.4375X26.75...	Beam	Rectangular	EWPine	Typical
31	M31A	N30	N29			1 5/8	Beam	Wide Flange	A36 Gr.36	Typical
32	M32	N1	N32			fiveeights	Beam	Wide Flange	A36 Gr.36	Typical

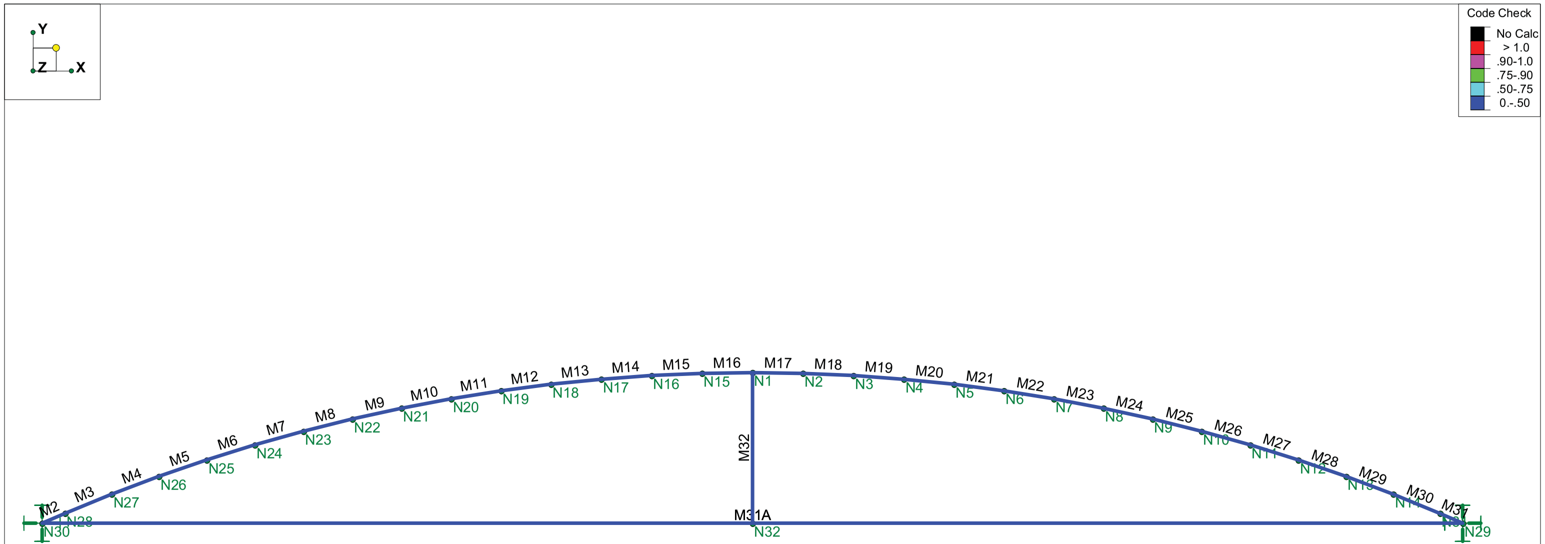

Results for LC 3, dead+thermal

SK - 1

Apr 21, 2010 at 2:54 PM

wagnersimpletiedarch.r3d

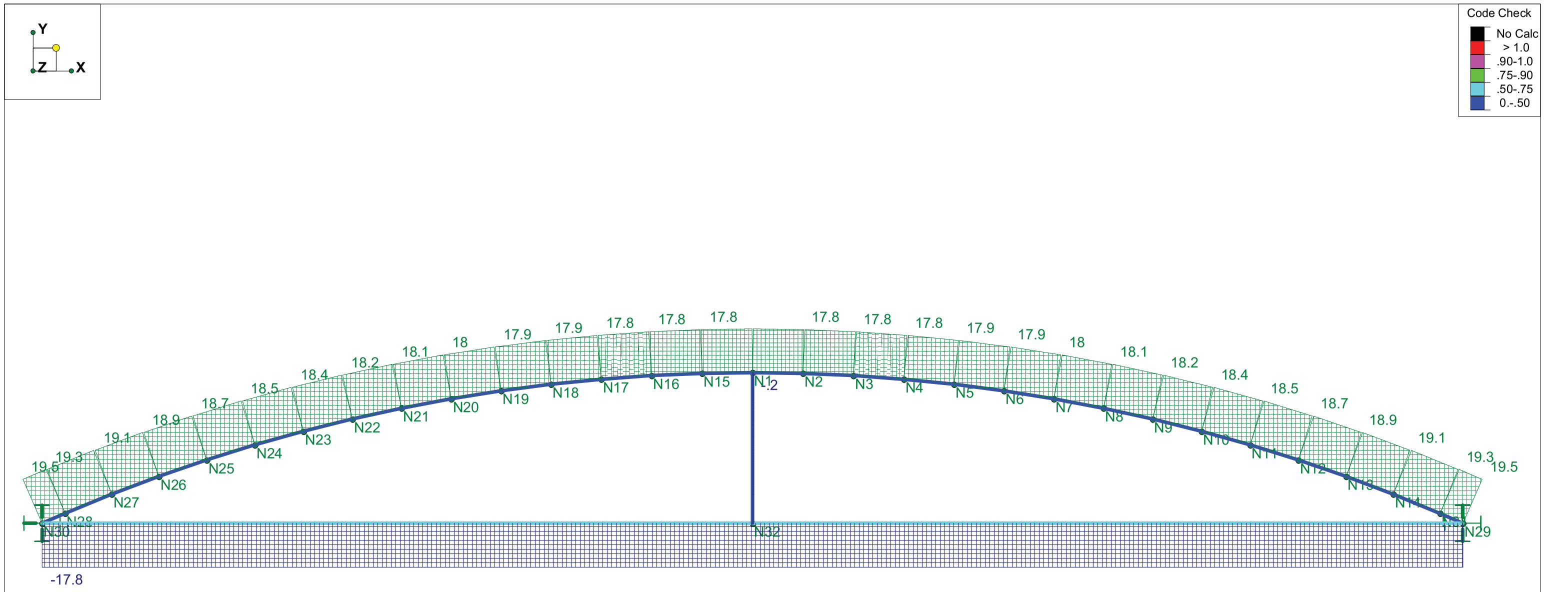

Results for LC 1, sw
Member Axial Forces (k)

SK - 6

Apr 21, 2010 at 2:59 PM

wagnersimpletiedarch.r3d

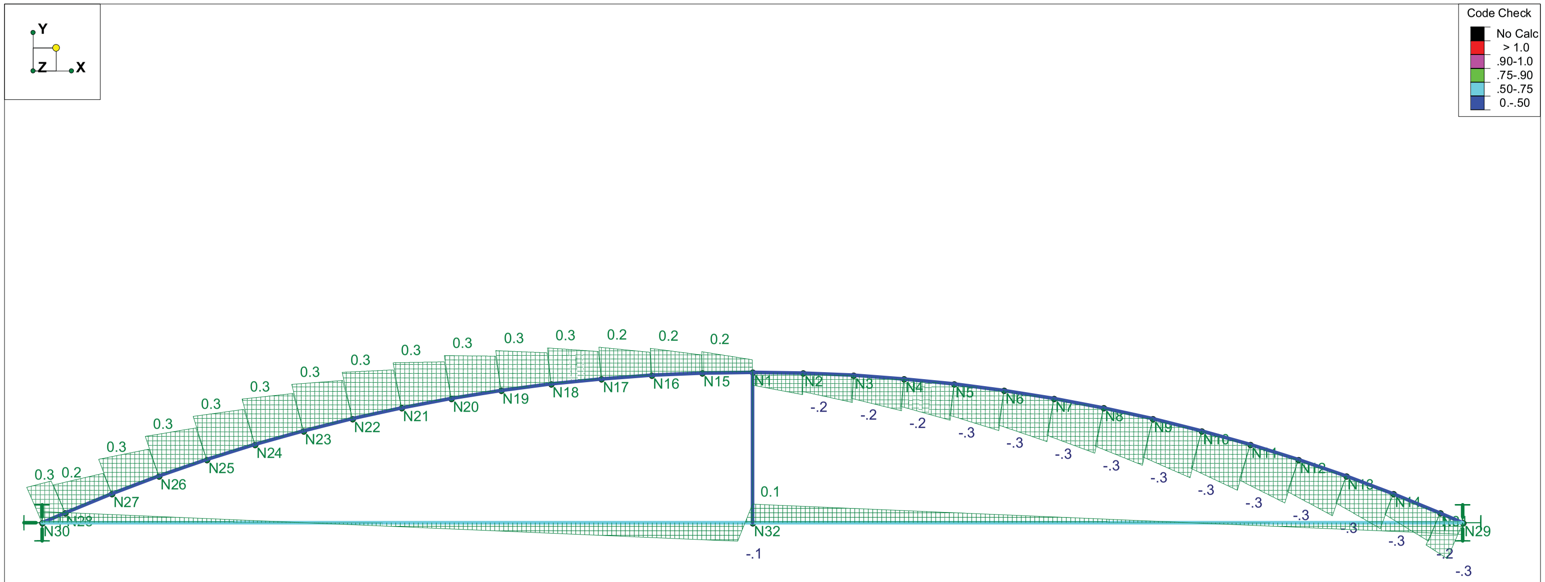

Results for LC 1, sw
Member y Shear Forces (k)

SK - 5

Apr 21, 2010 at 2:58 PM

wagnersimpletiedarch.r3d

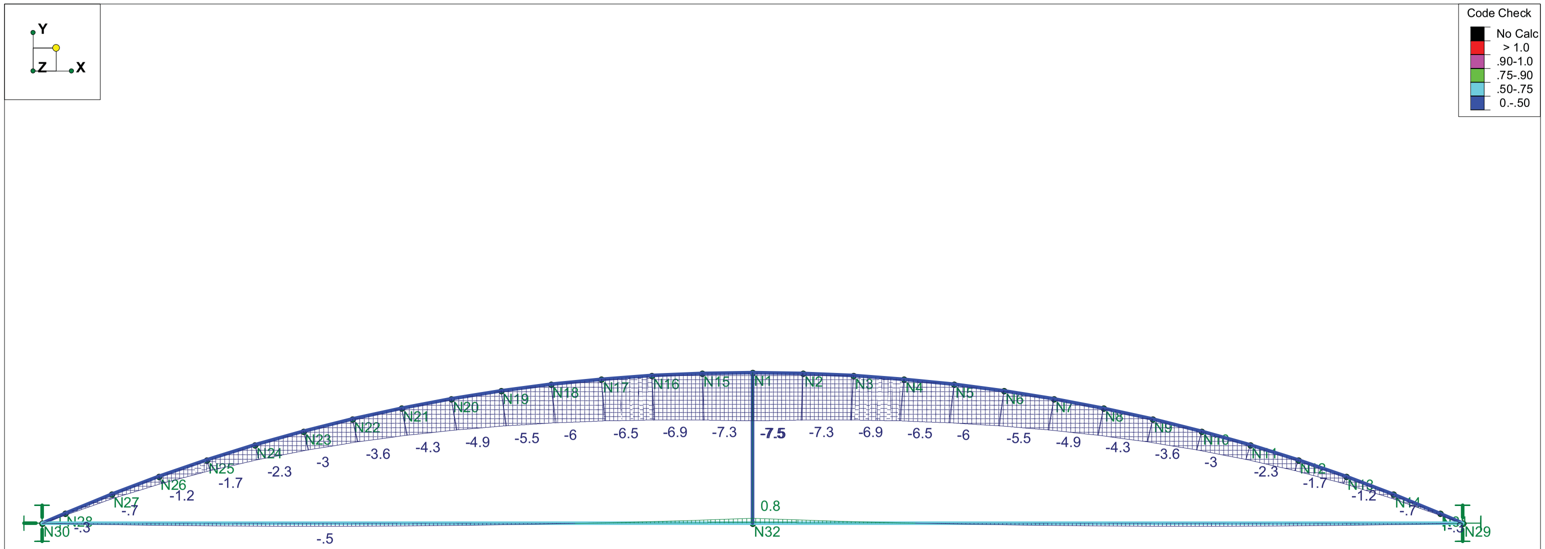

Results for LC 1, sw
Member z Bending Moments (k-ft)

SK - 7

Apr 21, 2010 at 2:59 PM

wagnersimpletiedarch.r3d

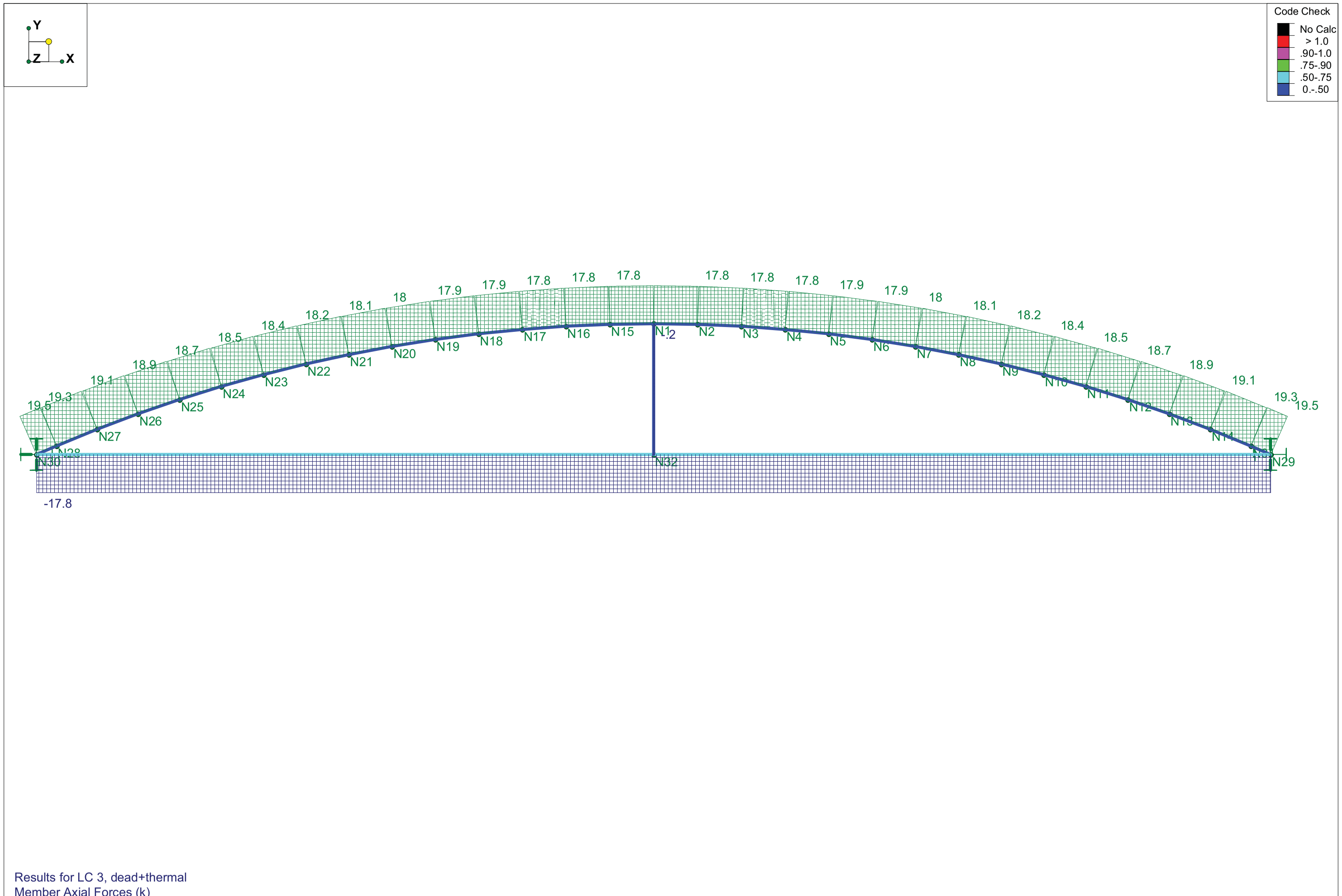

Results for LC 3, dead+thermal
Member Axial Forces (k)

SK - 2

Apr 21, 2010 at 2:56 PM

wagnersimpletiedarch.r3d

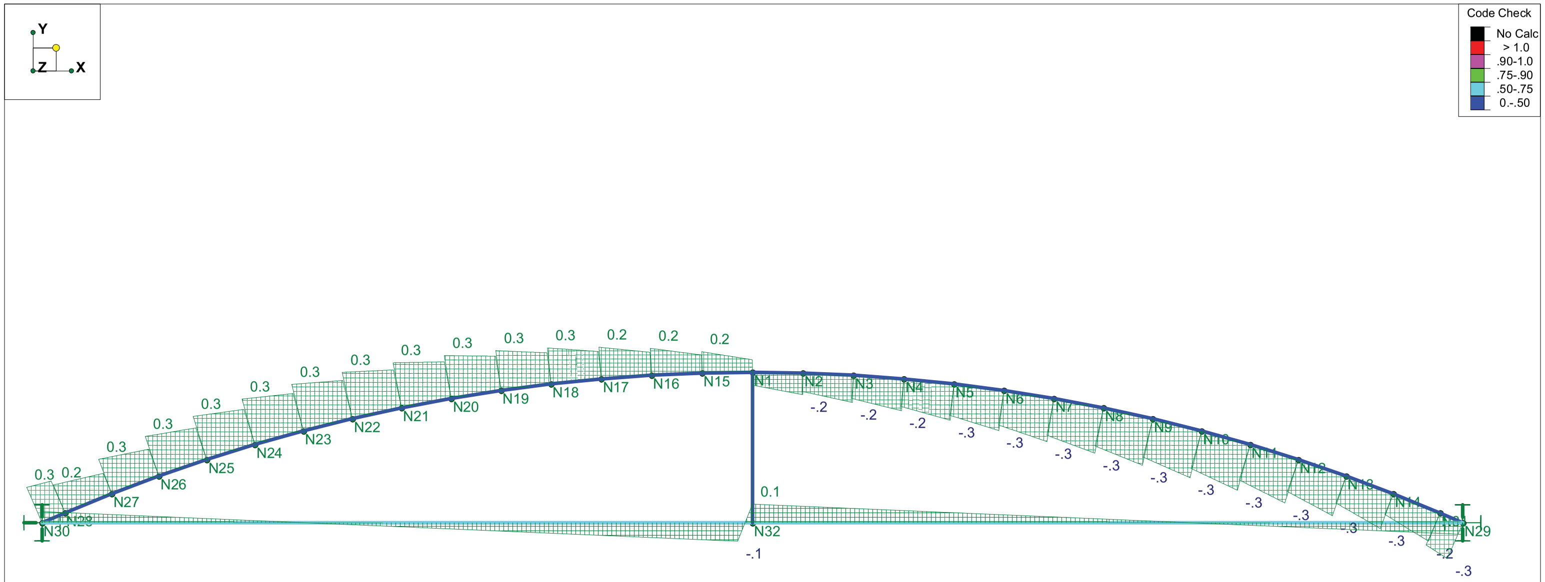

Results for LC 3, dead+thermal
Member y Shear Forces (k)

SK - 4

Apr 21, 2010 at 2:57 PM

wagnersimpletiedarch.r3d

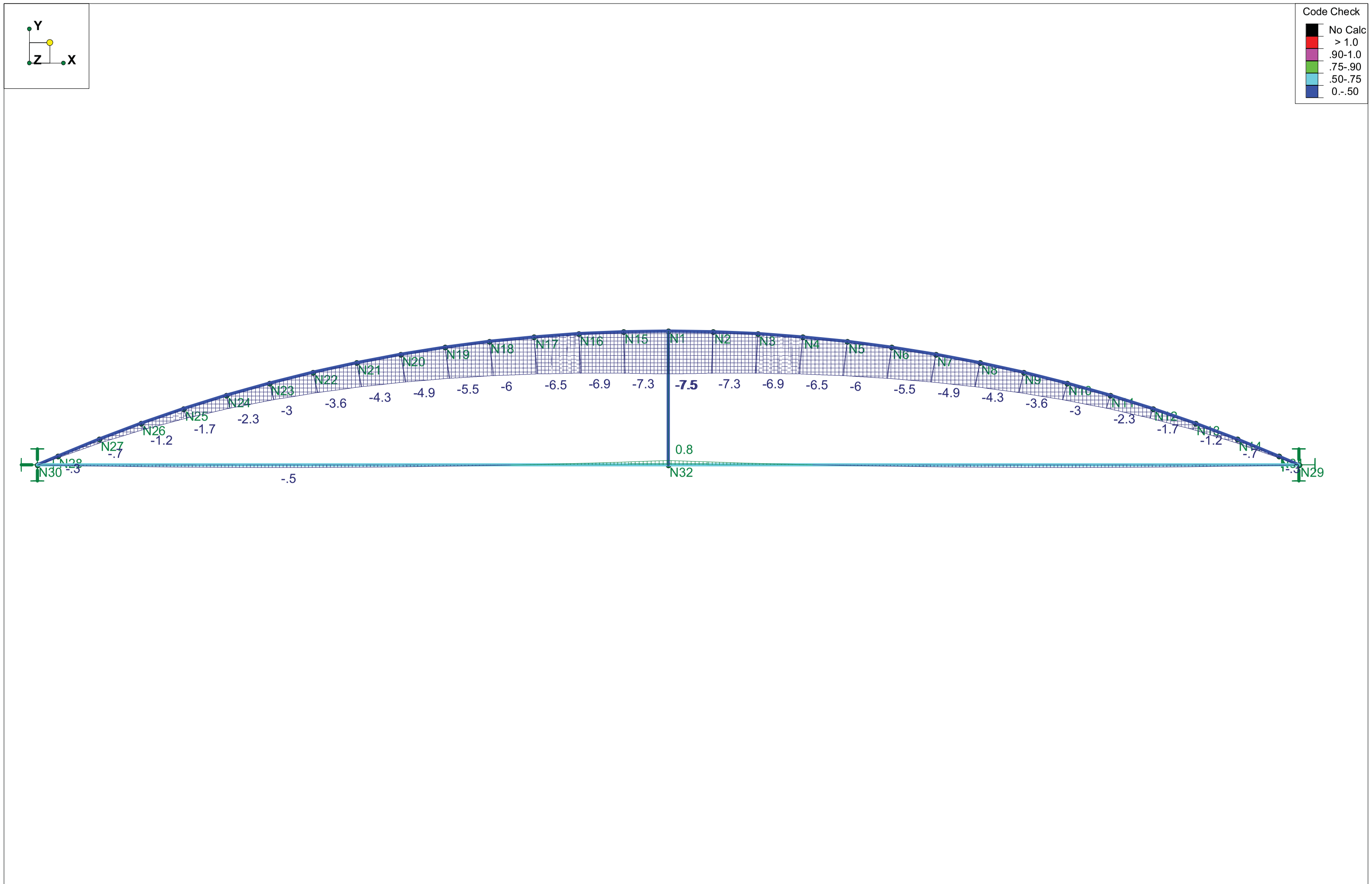

Results for LC 3, dead+thermal
Member z Bending Moments (k-ft)

		SK - 3
		Apr 21, 2010 at 2:57 PM
		wagnersimpletiedarch.r3d

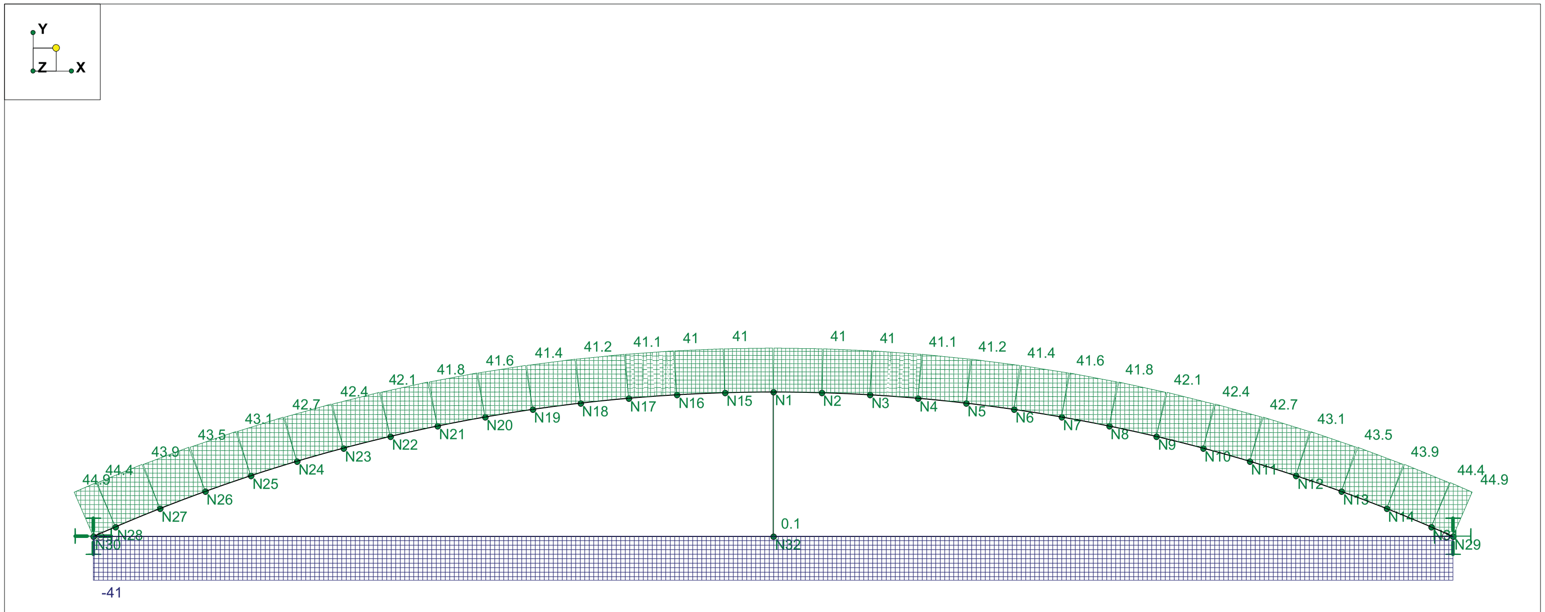

Results for LC 2, dead+snow
Member Axial Forces (k)

		SK - 9
		Apr 21, 2010 at 3:07 PM
		wagnersimpletiedarch.r3d

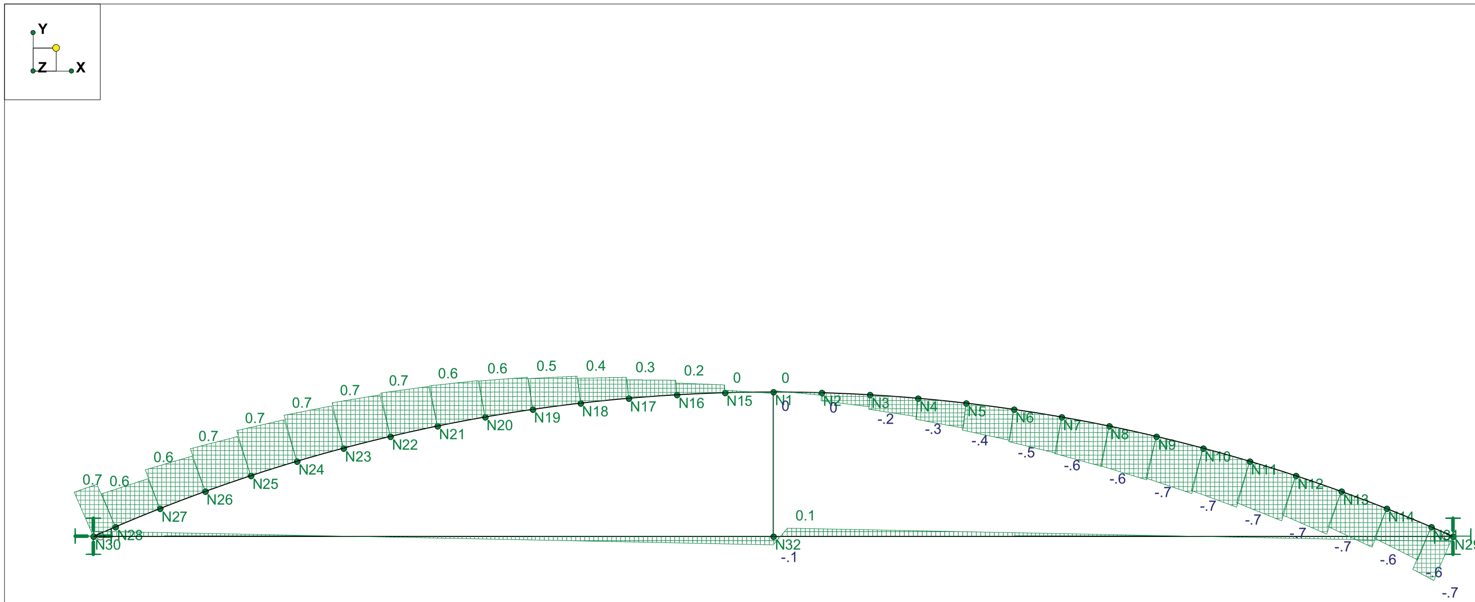

Results for LC 2, dead+snow
Member y Shear Forces (k)

SK - 10

Apr 21, 2010 at 3:07 PM

wagnersimpletiedarch.r3d

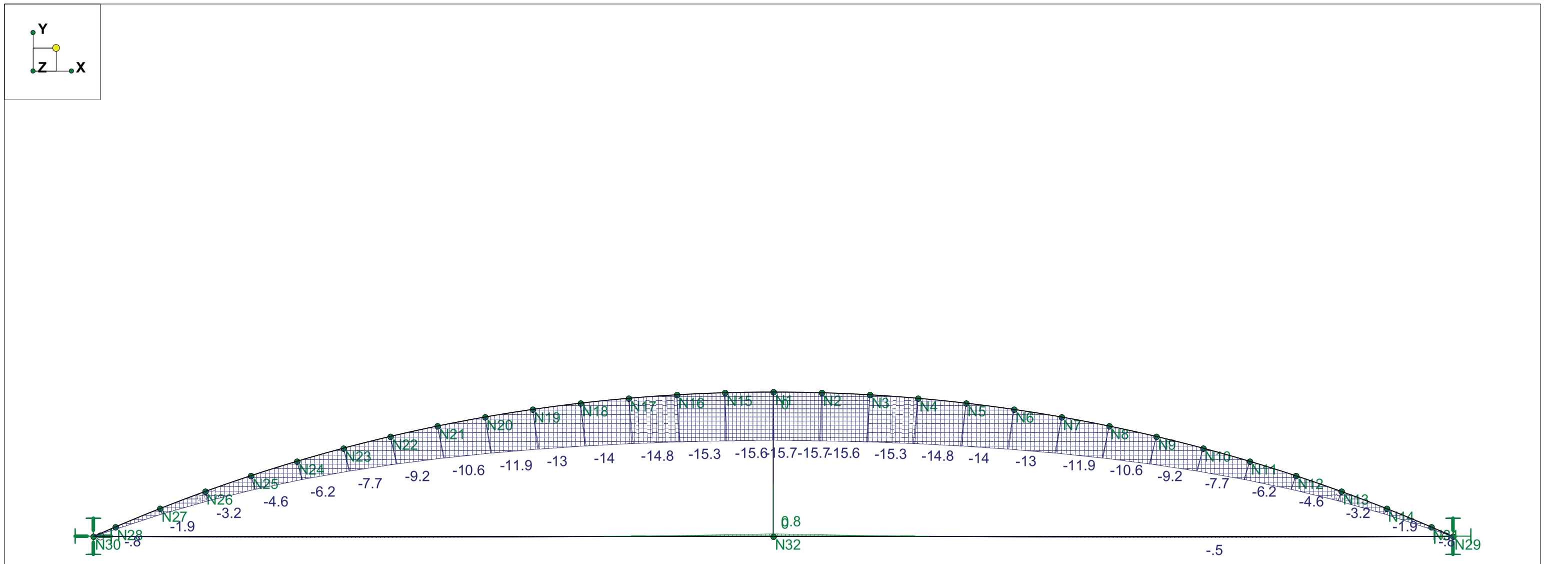

Results for LC 2, dead+snow
Member z Bending Moments (k-ft)

		SK - 8
		Apr 21, 2010 at 3:06 PM
		wagnersimpletiedarch.r3d

Appendix V—Arched Truss Analysis Results

Basic Load Cases

	BLC Description	Category	X Gravity	Y Gravity	Z Gravity	Joint	Point	Distributed	Area (Me...	Surface (...
1	Dead Load	DL				31				
2	Self Weight	DL		-1						
3	Displacement	DL				1				
4	Snow	SL				31				
5	Thermal	TL						187		
6	Unbalanced Snow R	SL				16				
7	Unbalanced Snow L	SL				16				
8	Disp2	None				1				

Load Combinations

	Description	Solve	PD...	SR...	BLC	Factor	BLC	Factor	BLC	Factor	BLC	Factor	BLC	Factor	BLC	Factor	BLC	Factor	BLC	Factor
1	Dead	Yes	Y		1	1	2	1												
2	D+Disp	Yes	Y		1	1	2	1	3	1										
3	D+Snow	Yes	Y		1	1	2	1	4	1										
4	D+Snow+Disp	Yes	Y		1	1	2	1	3	1	4	1								
5	D+T	Yes	Y		1	1	2	1	5	1										
6	D+T+Disp	Yes	Y		1	1	2	1	3	1	5	1								
7	D+USnow	Yes	Y		1	1	2	1	6	1										
8	D+USnow (l...	Yes	Y		1	1	2	1	3	1	6	1								
9	D+USnow(ri...	Yes	Y		1	1	2	1	3	1	7	1								
10	D+Disp2	Yes	Y		1	1	2	1	8	1										
11	D+Snow+Di...	Yes	Y		1	1	2	1	8	1	4	1								

Joint Loads and Enforced Displacements (BLC 1 : Dead Load)

	Joint Label	L,D,M	Direction	Magnitude[(k,k-ft), (in,rad), (k*s^2/ft...
1	N63	L	Y	-.244
2	N58	L	Y	-.488
3	N56	L	Y	-.488
4	N54	L	Y	-.488
5	N52	L	Y	-.488
6	N50	L	Y	-.488
7	N48	L	Y	-.488
8	N46	L	Y	-.488
9	N44	L	Y	-.488
10	N42	L	Y	-.488
11	N40	L	Y	-.488
12	N38	L	Y	-.488
13	N36	L	Y	-.488
14	N34	L	Y	-.488
15	N32	L	Y	-.488
16	N1	L	Y	-.488
17	N3	L	Y	-.488
18	N5	L	Y	-.488
19	N7	L	Y	-.488
20	N9	L	Y	-.488
21	N11	L	Y	-.488
22	N13	L	Y	-.488
23	N15	L	Y	-.488
24	N17	L	Y	-.488
25	N19	L	Y	-.488
26	N21	L	Y	-.488
27	N23	L	Y	-.488
28	N25	L	Y	-.488
29	N27	L	Y	-.488

Joint Loads and Enforced Displacements (BLC 1 : Dead Load) (Continued)

	Joint Label	L,D,M	Direction	Magnitude[(k,k-ft), (in,rad), (k*s^2/ft...
30	N29	L	Y	-.488
31	N61	L	Y	-.244

Joint Loads and Enforced Displacements (BLC 3 : Displacement)

	Joint Label	L,D,M	Direction	Magnitude[(k,k-ft), (in,rad), (k*s^2/ft...
1	N31	D	X	2.313

Joint Loads and Enforced Displacements (BLC 4 : Snow)

	Joint Label	L,D,M	Direction	Magnitude[(k,k-ft), (in,rad), (k*s^2/ft...
1	N63	L	Y	-.369
2	N58	L	Y	-.737
3	N56	L	Y	-.737
4	N54	L	Y	-.737
5	N52	L	Y	-.737
6	N50	L	Y	-.737
7	N48	L	Y	-.737
8	N46	L	Y	-.737
9	N44	L	Y	-.737
10	N42	L	Y	-.737
11	N40	L	Y	-.737
12	N38	L	Y	-.737
13	N36	L	Y	-.737
14	N34	L	Y	-.737
15	N32	L	Y	-.737
16	N1	L	Y	-.737
17	N3	L	Y	-.737
18	N5	L	Y	-.737
19	N7	L	Y	-.737
20	N9	L	Y	-.737
21	N11	L	Y	-.737
22	N13	L	Y	-.737
23	N15	L	Y	-.737
24	N17	L	Y	-.737
25	N19	L	Y	-.737
26	N21	L	Y	-.737
27	N23	L	Y	-.737
28	N25	L	Y	-.737
29	N27	L	Y	-.737
30	N29	L	Y	-.737
31	N61	L	Y	-.369

Joint Loads and Enforced Displacements (BLC 6 : Unbalanced Snow R)

	Joint Label	L,D,M	Direction	Magnitude[(k,k-ft), (in,rad), (k*s^2/ft...
1	N1	L	Y	-.369
2	N32	L	Y	-.438
3	N34	L	Y	-.507
4	N36	L	Y	-.577
5	N38	L	Y	-.646
6	N40	L	Y	-.715
7	N42	L	Y	-.784
8	N44	L	Y	-.853
9	N46	L	Y	-.923
10	N48	L	Y	-.992
11	N50	L	Y	-1.061
12	N52	L	Y	-1.13
13	N54	L	Y	-1.2

Joint Loads and Enforced Displacements (BLC 6 : Unbalanced Snow R) (Continued)

	Joint Label	L,D,M	Direction	Magnitude[(k,k-ft), (in,rad), (k*s^2/ft...
14	N56	L	Y	-1.268
15	N58	L	Y	-1.338
16	N63	L	Y	-1.407

Joint Loads and Enforced Displacements (BLC 7 : Unbalanced Snow L)

	Joint Label	L,D,M	Direction	Magnitude[(k,k-ft), (in,rad), (k*s^2/ft...
1	N1	L	Y	-.369
2	N3	L	Y	-.438
3	N5	L	Y	-.507
4	N7	L	Y	-.577
5	N9	L	Y	-.646
6	N11	L	Y	-.715
7	N13	L	Y	-.784
8	N15	L	Y	-.853
9	N17	L	Y	-.923
10	N19	L	Y	-.992
11	N21	L	Y	-1.061
12	N23	L	Y	-1.13
13	N25	L	Y	-1.2
14	N27	L	Y	-1.268
15	N29	L	Y	-1.338
16	N61	L	Y	-1.407

Joint Loads and Enforced Displacements (BLC 8 : Disp2)

	Joint Label	L,D,M	Direction	Magnitude[(k,k-ft), (in,rad), (k*s^2/ft...
1	N31	D	X	1.25

Member Distributed Loads (BLC 5 : Thermal)

	Member Label	Direction	Start Magnitude[k/ft,d..	End Magnitude[k/ft,d...	Start Location[ft,%]	End Location[ft,%]
1	M1	T	70	70	0	0
2	M2	T	70	70	0	0
3	M3	T	70	70	0	0
4	M4	T	70	70	0	0
5	M5	T	70	70	0	0
6	M6	T	70	70	0	0
7	M7	T	70	70	0	0
8	M8	T	70	70	0	0
9	M9	T	70	70	0	0
10	M10	T	70	70	0	0
11	M11	T	70	70	0	0
12	M12	T	70	70	0	0
13	M13	T	70	70	0	0
14	M14	T	70	70	0	0
15	M15	T	70	70	0	0
16	M16	T	70	70	0	0
17	M17	T	70	70	0	0
18	M18	T	70	70	0	0
19	M19	T	70	70	0	0
20	M20	T	70	70	0	0
21	M21	T	70	70	0	0
22	M22	T	70	70	0	0
23	M23	T	70	70	0	0
24	M24	T	70	70	0	0
25	M25	T	70	70	0	0
26	M26	T	70	70	0	0

Member Distributed Loads (BLC 5 : Thermal) (Continued)

	Member Label	Direction	Start Magnitude[k/ft,d..	End Magnitude[k/ft,d...	Start Location[ft,%]	End Location[ft,%]
27	M27	T	70	70	0	0
28	M28	T	70	70	0	0
29	M29	T	70	70	0	0
30	M30	T	70	70	0	0
31	M31	T	70	70	0	0
32	M32	T	70	70	0	0
33	M33	T	70	70	0	0
34	M34	T	70	70	0	0
35	M35	T	70	70	0	0
36	M36	T	70	70	0	0
37	M37	T	70	70	0	0
38	M38	T	70	70	0	0
39	M39	T	70	70	0	0
40	M40	T	70	70	0	0
41	M41	T	70	70	0	0
42	M42	T	70	70	0	0
43	M43	T	70	70	0	0
44	M44	T	70	70	0	0
45	M45	T	70	70	0	0
46	M46	T	70	70	0	0
47	M47	T	70	70	0	0
48	M48	T	70	70	0	0
49	M49	T	70	70	0	0
50	M50	T	70	70	0	0
51	M51	T	70	70	0	0
52	M52	T	70	70	0	0
53	M53	T	70	70	0	0
54	M54	T	70	70	0	0
55	M55	T	70	70	0	0
56	M56	T	70	70	0	0
57	M57	T	70	70	0	0
58	M58	T	70	70	0	0
59	M59	T	70	70	0	0
60	M60	T	70	70	0	0
61	M61	T	70	70	0	0
62	M62	T	70	70	0	0
63	M63	T	70	70	0	0
64	M64	T	70	70	0	0
65	M65	T	70	70	0	0
66	M66	T	70	70	0	0
67	M67	T	70	70	0	0
68	M68	T	70	70	0	0
69	M69	T	70	70	0	0
70	M70	T	70	70	0	0
71	M71	T	70	70	0	0
72	M72	T	70	70	0	0
73	M73	T	70	70	0	0
74	M74	T	70	70	0	0
75	M75	T	70	70	0	0
76	M76	T	70	70	0	0
77	M77	T	70	70	0	0
78	M78	T	70	70	0	0
79	M79	T	70	70	0	0
80	M80	T	70	70	0	0
81	M81	T	70	70	0	0
82	M82	T	70	70	0	0
83	M83	T	70	70	0	0

Member Distributed Loads (BLC 5 : Thermal) (Continued)

	Member Label	Direction	Start Magnitude[k/ft,d..	End Magnitude[k/ft,d...	Start Location[ft,%]	End Location[ft,%]
84	M84	T	70	70	0	0
85	M85	T	70	70	0	0
86	M86	T	70	70	0	0
87	M87	T	70	70	0	0
88	M88	T	70	70	0	0
89	M89	T	70	70	0	0
90	M90	T	70	70	0	0
91	M91	T	70	70	0	0
92	M92	T	70	70	0	0
93	M93	T	70	70	0	0
94	M94	T	70	70	0	0
95	M95	T	70	70	0	0
96	M96	T	70	70	0	0
97	M97	T	70	70	0	0
98	M98	T	70	70	0	0
99	M99	T	70	70	0	0
100	M100	T	70	70	0	0
101	M101	T	70	70	0	0
102	M102	T	70	70	0	0
103	M103	T	70	70	0	0
104	M104	T	70	70	0	0
105	M105	T	70	70	0	0
106	M106	T	70	70	0	0
107	M107	T	70	70	0	0
108	M108	T	70	70	0	0
109	M109	T	70	70	0	0
110	M110	T	70	70	0	0
111	M111	T	70	70	0	0
112	M112	T	70	70	0	0
113	M113	T	70	70	0	0
114	M114	T	70	70	0	0
115	M115	T	70	70	0	0
116	M116	T	70	70	0	0
117	M117	T	70	70	0	0
118	M118	T	70	70	0	0
119	M119	T	70	70	0	0
120	M120	T	70	70	0	0
121	M121	T	70	70	0	0
122	M122	T	70	70	0	0
123	M123	T	70	70	0	0
124	M124	T	70	70	0	0
125	M125	T	70	70	0	0
126	M126	T	70	70	0	0
127	M127	T	70	70	0	0
128	M128	T	70	70	0	0
129	M129	T	70	70	0	0
130	M130	T	70	70	0	0
131	M131	T	70	70	0	0
132	M132	T	70	70	0	0
133	M133	T	70	70	0	0
134	M134	T	70	70	0	0
135	M135	T	70	70	0	0
136	M136	T	70	70	0	0
137	M137	T	70	70	0	0
138	M138	T	70	70	0	0
139	M139	T	70	70	0	0
140	M140	T	70	70	0	0

Member Distributed Loads (BLC 5 : Thermal) (Continued)

	Member Label	Direction	Start Magnitude[k/ft,d..	End Magnitude[k/ft,d...	Start Location[ft,%]	End Location[ft,%]
141	M141	T	70	70	0	0
142	M142	T	70	70	0	0
143	M143	T	70	70	0	0
144	M144	T	70	70	0	0
145	M145	T	70	70	0	0
146	M146	T	70	70	0	0
147	M147	T	70	70	0	0
148	M148	T	70	70	0	0
149	M149	T	70	70	0	0
150	M150	T	70	70	0	0
151	M151	T	70	70	0	0
152	M152	T	70	70	0	0
153	M153	T	70	70	0	0
154	M154	T	70	70	0	0
155	M155	T	70	70	0	0
156	M156	T	70	70	0	0
157	M157	T	70	70	0	0
158	M158	T	70	70	0	0
159	M159	T	70	70	0	0
160	M160	T	70	70	0	0
161	M161	T	70	70	0	0
162	M162	T	70	70	0	0
163	M163	T	70	70	0	0
164	M164	T	70	70	0	0
165	M165	T	70	70	0	0
166	M166	T	70	70	0	0
167	M167	T	70	70	0	0
168	M168	T	70	70	0	0
169	M169	T	70	70	0	0
170	M170	T	70	70	0	0
171	M171	T	70	70	0	0
172	M172	T	70	70	0	0
173	M173	T	70	70	0	0
174	M174	T	70	70	0	0
175	M175	T	70	70	0	0
176	M176	T	70	70	0	0
177	M177	T	70	70	0	0
178	M178	T	70	70	0	0
179	M179	T	70	70	0	0
180	M180	T	70	70	0	0
181	M181	T	70	70	0	0
182	M182	T	70	70	0	0
183	M183	T	70	70	0	0
184	M184	T	70	70	0	0
185	M185	T	70	70	0	0
186	M186	T	70	70	0	0
187	M187	T	70	70	0	0

Member Primary Data

	Label	I Joint	J Joint	K Joint	Rotate(deg)	Section/Shape	Type	Design List	Material	Design Rules
1	M1	N64	N63		90	2.5X7.75FS	Beam	Rectangular	EWPine	Typical
2	M2	N63	N58		90	2.5X7.75FS	Beam	Rectangular	EWPine	Typical
3	M3	N58	N56		90	2.5X7.75FS	Beam	Rectangular	EWPine	Typical
4	M4	N56	N54		90	2.5X7.75FS	Beam	Rectangular	EWPine	Typical
5	M5	N54	N52		90	2.5X7.75FS	Beam	Rectangular	EWPine	Typical
6	M6	N52	N50		90	2.5X7.75FS	Beam	Rectangular	EWPine	Typical

Member Primary Data (Continued)

	Label	I Joint	J Joint	K Joint	Rotate(deg)	Section/Shape	Type	Design List	Material	Design Rules
7	M7	N50	N48		90	2.5X7.75FS	Beam	Rectangular	EWPine	Typical
8	M8	N48	N46		90	2.5X7.75FS	Beam	Rectangular	DF/SPine	Typical
9	M9	N46	N44		90	2.5X7.75FS	Beam	Rectangular	EWPine	Typical
10	M10	N44	N42		90	2.5X7.75FS	Beam	Rectangular	EWPine	Typical
11	M11	N42	N40		90	2.5X7.75FS	Beam	Rectangular	EWPine	Typical
12	M12	N40	N38		90	2.5X7.75FS	Beam	Rectangular	EWPine	Typical
13	M13	N38	N36		90	2.5X7.75FS	Beam	Rectangular	EWPine	Typical
14	M14	N36	N34		90	2.5X7.75FS	Beam	Rectangular	EWPine	Typical
15	M15	N34	N32		90	2.5X7.75FS	Beam	Rectangular	EWPine	Typical
16	M16	N32	N1		90	2.5X7.75FS	Beam	Rectangular	EWPine	Typical
17	M17	N1	N3		90	2.5X7.75FS	Beam	Rectangular	EWPine	Typical
18	M18	N3	N5		90	2.5X7.75FS	Beam	Rectangular	EWPine	Typical
19	M19	N5	N7		90	2.5X7.75FS	Beam	Rectangular	EWPine	Typical
20	M20	N7	N9		90	2.5X7.75FS	Beam	Rectangular	EWPine	Typical
21	M21	N9	N11		90	2.5X7.75FS	Beam	Rectangular	EWPine	Typical
22	M22	N11	N13		90	2.5X7.75FS	Beam	Rectangular	EWPine	Typical
23	M23	N13	N15		90	2.5X7.75FS	Beam	Rectangular	EWPine	Typical
24	M24	N15	N17		90	2.5X7.75FS	Beam	Rectangular	EWPine	Typical
25	M25	N17	N19		90	2.5X7.75FS	Beam	Rectangular	EWPine	Typical
26	M26	N19	N21		90	2.5X7.75FS	Beam	Rectangular	EWPine	Typical
27	M27	N21	N23		90	2.5X7.75FS	Beam	Rectangular	EWPine	Typical
28	M28	N23	N25		90	2.5X7.75FS	Beam	Rectangular	EWPine	Typical
29	M29	N25	N27		90	2.5X7.75FS	Beam	Rectangular	EWPine	Typical
30	M30	N27	N29		90	2.5X7.75FS	Beam	Rectangular	EWPine	Typical
31	M31	N29	N61		90	2.5X7.75FS	Beam	Rectangular	EWPine	Typical
32	M32	N61	N62		90	2.5X7.75FS	Beam	Rectangular	EWPine	Typical
33	M33	N60	N57		90	2.5X7.75FS	Beam	Rectangular	EWPine	Typical
34	M34	N57	N55		90	2.5X7.75FS	Beam	Rectangular	EWPine	Typical
35	M35	N55	N53		90	2.5X7.75FS	Beam	Rectangular	EWPine	Typical
36	M36	N53	N51		90	2.5X7.75FS	Beam	Rectangular	EWPine	Typical
37	M37	N51	N49		90	2.5X7.75FS	Beam	Rectangular	EWPine	Typical
38	M38	N49	N47		90	2.5X7.75FS	Beam	Rectangular	EWPine	Typical
39	M39	N47	N45		90	2.5X7.75FS	Beam	Rectangular	EWPine	Typical
40	M40	N45	N43		90	2.5X7.75FS	Beam	Rectangular	EWPine	Typical
41	M41	N43	N41		90	2.5X7.75FS	Beam	Rectangular	EWPine	Typical
42	M42	N41	N39		90	2.5X7.75FS	Beam	Rectangular	EWPine	Typical
43	M43	N39	N37		90	2.5X7.75FS	Beam	Rectangular	EWPine	Typical
44	M44	N37	N35		90	2.5X7.75FS	Beam	Rectangular	EWPine	Typical
45	M45	N35	N33		90	2.5X7.75FS	Beam	Rectangular	EWPine	Typical
46	M46	N33	N2		90	2.5X7.75FS	Beam	Rectangular	EWPine	Typical
47	M47	N2	N4		90	2.5X7.75FS	Beam	Rectangular	EWPine	Typical
48	M48	N4	N6		90	2.5X7.75FS	Beam	Rectangular	EWPine	Typical
49	M49	N6	N8		90	2.5X7.75FS	Beam	Rectangular	EWPine	Typical
50	M50	N8	N10		90	2.5X7.75FS	Beam	Rectangular	EWPine	Typical
51	M51	N10	N12		90	2.5X7.75FS	Beam	Rectangular	EWPine	Typical
52	M52	N12	N14		90	2.5X7.75FS	Beam	Rectangular	EWPine	Typical
53	M53	N14	N16		90	2.5X7.75FS	Beam	Rectangular	EWPine	Typical
54	M54	N16	N18		90	2.5X7.75FS	Beam	Rectangular	EWPine	Typical
55	M55	N18	N20		90	2.5X7.75FS	Beam	Rectangular	EWPine	Typical
56	M56	N20	N22		90	2.5X7.75FS	Beam	Rectangular	EWPine	Typical
57	M57	N22	N24		90	2.5X7.75FS	Beam	Rectangular	EWPine	Typical
58	M58	N24	N26		90	2.5X7.75FS	Beam	Rectangular	EWPine	Typical
59	M59	N26	N28		90	2.5X7.75FS	Beam	Rectangular	EWPine	Typical
60	M60	N28	N31		90	2.5X7.75FS	Beam	Rectangular	EWPine	Typical
61	M61	N1	N33		90	1.75X6FS	Beam	Rectangular	EWPine	Typical
62	M62	N34	N37		90	1.75X6FS	Beam	Rectangular	EWPine	Typical
63	M63	N32	N35		90	1.75X6FS	Beam	Rectangular	EWPine	Typical

Member Primary Data (Continued)

	Label	I Joint	J Joint	K Joint	Rotate(deg)	Section/Shape	Type	Design List	Material	Design Rules
64	M64	N36	N39		90	1.75X6FS	Beam	Rectangular	EWPine	Typical
65	M65	N38	N41		90	1.75X6FS	Beam	Rectangular	EWPine	Typical
66	M66	N40	N43		90	1.75X6FS	Beam	Rectangular	EWPine	Typical
67	M67	N42	N45		90	1.75X6FS	Beam	Rectangular	EWPine	Typical
68	M68	N44	N47		90	1.75X6FS	Beam	Rectangular	EWPine	Typical
69	M69	N46	N49		90	1.75X6FS	Beam	Rectangular	EWPine	Typical
70	M70	N48	N51		90	1.75X6FS	Beam	Rectangular	EWPine	Typical
71	M71	N50	N53		90	1.75X6FS	Beam	Rectangular	EWPine	Typical
72	M72	N52	N55		90	1.75X6FS	Beam	Rectangular	EWPine	Typical
73	M73	N54	N57		90	1.75X6FS	Beam	Rectangular	EWPine	Typical
74	M74	N56	N60		90	1.75X6FS	Beam	Rectangular	EWPine	Typical
75	M75	N58	N97		90	1.75X6FS	Beam	Rectangular	EWPine	Typical
76	M76	N63	N99		90	1.75X6FS	Beam	Rectangular	EWPine	Typical
77	M77	N1	N4		90	1.75X6FS	Beam	Rectangular	EWPine	Typical
78	M78	N3	N6		90	1.75X6FS	Beam	Rectangular	EWPine	Typical
79	M79	N5	N8		90	1.75X6FS	Beam	Rectangular	EWPine	Typical
80	M80	N7	N10		90	1.75X6FS	Beam	Rectangular	EWPine	Typical
81	M81	N9	N12		90	1.75X6FS	Beam	Rectangular	EWPine	Typical
82	M82	N11	N14		90	1.75X6FS	Beam	Rectangular	EWPine	Typical
83	M83	N13	N16		90	1.75X6FS	Beam	Rectangular	EWPine	Typical
84	M84	N15	N18		90	1.75X6FS	Beam	Rectangular	EWPine	Typical
85	M85	N17	N20		90	1.75X6FS	Beam	Rectangular	EWPine	Typical
86	M86	N19	N22		90	1.75X6FS	Beam	Rectangular	EWPine	Typical
87	M87	N21	N24		90	1.75X6FS	Beam	Rectangular	EWPine	Typical
88	M88	N23	N26		90	1.75X6FS	Beam	Rectangular	EWPine	Typical
89	M89	N25	N28		90	1.75X6FS	Beam	Rectangular	EWPine	Typical
90	M90	N27	N31		90	1.75X6FS	Beam	Rectangular	EWPine	Typical
91	M91	N29	N98		90	1.75X6FS	Beam	Rectangular	EWPine	Typical
92	M92	N61	N100		90	1.75X6FS	Beam	Rectangular	EWPine	Typical
93	M93	N63	N93		90	1.75X6FS	Beam	Rectangular	EWPine	Typical
94	M94	N93	N60		90	1.75X6FS	Beam	Rectangular	EWPine	Typical
95	M95	N58	N78		90	1.75X6FS	Beam	Rectangular	EWPine	Typical
96	M96	N78	N57		90	1.75X6FS	Beam	Rectangular	EWPine	Typical
97	M97	N56	N77		90	1.75X6FS	Beam	Rectangular	EWPine	Typical
98	M98	N77	N55		90	1.75X6FS	Beam	Rectangular	EWPine	Typical
99	M99	N54	N76		90	1.75X6FS	Beam	Rectangular	EWPine	Typical
100	M100	N76	N53		90	1.75X6FS	Beam	Rectangular	EWPine	Typical
101	M101	N52	N75		90	1.75X6FS	Beam	Rectangular	EWPine	Typical
102	M102	N75	N51		90	1.75X6FS	Beam	Rectangular	EWPine	Typical
103	M103	N50	N74		90	1.75X6FS	Beam	Rectangular	EWPine	Typical
104	M104	N74	N49		90	1.75X6FS	Beam	Rectangular	EWPine	Typical
105	M105	N48	N73		90	1.75X6FS	Beam	Rectangular	EWPine	Typical
106	M106	N73	N47		90	1.75X6FS	Beam	Rectangular	EWPine	Typical
107	M107	N46	N72		90	1.75X6FS	Beam	Rectangular	EWPine	Typical
108	M108	N72	N45		90	1.75X6FS	Beam	Rectangular	EWPine	Typical
109	M109	N44	N71		90	1.75X6FS	Beam	Rectangular	EWPine	Typical
110	M110	N71	N43		90	1.75X6FS	Beam	Rectangular	EWPine	Typical
111	M111	N42	N70		90	1.75X6FS	Beam	Rectangular	EWPine	Typical
112	M112	N70	N41		90	1.75X6FS	Beam	Rectangular	EWPine	Typical
113	M113	N40	N69		90	1.75X6FS	Beam	Rectangular	EWPine	Typical
114	M114	N69	N39		90	1.75X6FS	Beam	Rectangular	EWPine	Typical
115	M115	N38	N68		90	1.75X6FS	Beam	Rectangular	EWPine	Typical
116	M116	N68	N37		90	1.75X6FS	Beam	Rectangular	EWPine	Typical
117	M117	N36	N67		90	1.75X6FS	Beam	Rectangular	EWPine	Typical
118	M118	N67	N35		90	1.75X6FS	Beam	Rectangular	EWPine	Typical
119	M119	N34	N66		90	1.75X6FS	Beam	Rectangular	EWPine	Typical
120	M120	N66	N33		90	1.75X6FS	Beam	Rectangular	EWPine	Typical

Member Primary Data (Continued)

	Label	I Joint	J Joint	K Joint	Rotate(deg)	Section/Shape	Type	Design List	Material	Design Rules
121	M121	N32	N65		90	1.75X6FS	Beam	Rectangular	EWPine	Typical
122	M122	N65	N2		90	1.75X6FS	Beam	Rectangular	EWPine	Typical
123	M123	N2	N79		90	1.75X6FS	Beam	Rectangular	EWPine	Typical
124	M124	N79	N3		90	1.75X6FS	Beam	Rectangular	EWPine	Typical
125	M125	N4	N80		90	1.75X6FS	Beam	Rectangular	EWPine	Typical
126	M126	N80	N5		90	1.75X6FS	Beam	Rectangular	EWPine	Typical
127	M127	N6	N81		90	1.75X6FS	Beam	Rectangular	EWPine	Typical
128	M128	N81	N7		90	1.75X6FS	Beam	Rectangular	EWPine	Typical
129	M129	N8	N82		90	1.75X6FS	Beam	Rectangular	EWPine	Typical
130	M130	N82	N9		90	1.75X6FS	Beam	Rectangular	EWPine	Typical
131	M131	N10	N83		90	1.75X6FS	Beam	Rectangular	EWPine	Typical
132	M132	N83	N11		90	1.75X6FS	Beam	Rectangular	EWPine	Typical
133	M133	N12	N84		90	1.75X6FS	Beam	Rectangular	EWPine	Typical
134	M134	N84	N13		90	1.75X6FS	Beam	Rectangular	EWPine	Typical
135	M135	N14	N85		90	1.75X6FS	Beam	Rectangular	EWPine	Typical
136	M136	N85	N15		90	1.75X6FS	Beam	Rectangular	EWPine	Typical
137	M137	N16	N86		90	1.75X6FS	Beam	Rectangular	EWPine	Typical
138	M138	N86	N17		90	1.75X6FS	Beam	Rectangular	EWPine	Typical
139	M139	N18	N87		90	1.75X6FS	Beam	Rectangular	EWPine	Typical
140	M140	N87	N19		90	1.75X6FS	Beam	Rectangular	EWPine	Typical
141	M141	N20	N88		90	1.75X6FS	Beam	Rectangular	EWPine	Typical
142	M142	N88	N21		90	1.75X6FS	Beam	Rectangular	EWPine	Typical
143	M143	N22	N89		90	1.75X6FS	Beam	Rectangular	EWPine	Typical
144	M144	N89	N23		90	1.75X6FS	Beam	Rectangular	EWPine	Typical
145	M145	N24	N90		90	1.75X6FS	Beam	Rectangular	EWPine	Typical
146	M146	N90	N25		90	1.75X6FS	Beam	Rectangular	EWPine	Typical
147	M147	N26	N91		90	1.75X6FS	Beam	Rectangular	EWPine	Typical
148	M148	N91	N27		90	1.75X6FS	Beam	Rectangular	EWPine	Typical
149	M149	N28	N92		90	1.75X6FS	Beam	Rectangular	EWPine	Typical
150	M150	N92	N29		90	1.75X6FS	Beam	Rectangular	EWPine	Typical
151	M151	N31	N94		90	1.75X6FS	Beam	Rectangular	EWPine	Typical
152	M152	N94	N61		90	1.75X6FS	Beam	Rectangular	EWPine	Typical
153	M153	N58	N60		90	.625x2	VBrace	Wide Flange	A36 Gr.36	Typical
154	M154	N56	N57		90	.625x2	VBrace	Wide Flange	A36 Gr.36	Typical
155	M155	N54	N55		90	.625x2	VBrace	Wide Flange	A36 Gr.36	Typical
156	M156	N52	N53		90	.625x2	VBrace	Wide Flange	A36 Gr.36	Typical
157	M157	N50	N51		90	.625x2	VBrace	Wide Flange	A36 Gr.36	Typical
158	M158	N48	N49		90	.625x2	VBrace	Wide Flange	A36 Gr.36	Typical
159	M159	N46	N47		90	.625x2	VBrace	Wide Flange	A36 Gr.36	Typical
160	M160	N44	N45		90	.625x2	VBrace	Wide Flange	A36 Gr.36	Typical
161	M161	N42	N43		90	.625x2	VBrace	Wide Flange	A36 Gr.36	Typical
162	M162	N40	N41		90	.625x2	VBrace	Wide Flange	A36 Gr.36	Typical
163	M163	N38	N39		90	.625x2	VBrace	Wide Flange	A36 Gr.36	Typical
164	M164	N36	N37		90	.625x2	VBrace	Wide Flange	A36 Gr.36	Typical
165	M165	N34	N35		90	.625x2	VBrace	Wide Flange	A36 Gr.36	Typical
166	M166	N32	N33		90	.625x2	VBrace	Wide Flange	A36 Gr.36	Typical
167	M167	N1	N2		90	.625x2	VBrace	Wide Flange	A36 Gr.36	Typical
168	M168	N3	N4		90	.625x2	VBrace	Wide Flange	A36 Gr.36	Typical
169	M169	N5	N6		90	.625x2	VBrace	Wide Flange	A36 Gr.36	Typical
170	M170	N7	N8		90	.625x2	VBrace	Wide Flange	A36 Gr.36	Typical
171	M171	N9	N10		90	.625x2	VBrace	Wide Flange	A36 Gr.36	Typical
172	M172	N11	N12		90	.625x2	VBrace	Wide Flange	A36 Gr.36	Typical
173	M173	N13	N14		90	.625x2	VBrace	Wide Flange	A36 Gr.36	Typical
174	M174	N15	N16		90	.625x2	VBrace	Wide Flange	A36 Gr.36	Typical
175	M175	N17	N18		90	.625x2	VBrace	Wide Flange	A36 Gr.36	Typical
176	M176	N19	N20		90	.625x2	VBrace	Wide Flange	A36 Gr.36	Typical
177	M177	N21	N22		90	.625x2	VBrace	Wide Flange	A36 Gr.36	Typical

Member Primary Data (Continued)

	Label	I Joint	J Joint	K Joint	Rotate(deg)	Section/Shape	Type	Design List	Material	Design Rules
178	M178	N23	N24		90	.625x2	VBrace	Wide Flange	A36 Gr.36	Typical
179	M179	N25	N26		90	.625x2	VBrace	Wide Flange	A36 Gr.36	Typical
180	M180	N27	N28		90	.625x2	VBrace	Wide Flange	A36 Gr.36	Typical
181	M181	N29	N31		90	.625x2	VBrace	Wide Flange	A36 Gr.36	Typical
182	M182	N60	N31		90	1.625	VBrace	Wide Flange	A36 Gr.36	Typical
183	M183	N2	N101		90	.625	VBrace	Round Default	A36 Gr.36	Typical
184	M184	N59	N95		90	6X7.75FS	Beam	Rectangular	EWPine	Typical
185	M185	N60	N59		90	6X7.75FS	Beam	Rectangular	EWPine	Typical
186	M186	N31	N30		90	6X7.75FS	Beam	Rectangular	EWPine	Typical
187	M187	N30	N96		90	6X7.75FS	Beam	Rectangular	EWPine	Typical

Joint Boundary Conditions

	Joint Label	X [k/in]	Y [k/in]	Z [k/in]	X Rot.[k-ft/rad]	Y Rot.[k-ft/rad]	Z Rot.[k-ft/rad]	Footing
1	N1			Reaction				
2	N64			Reaction				
3	N63			Reaction				
4	N58			Reaction				
5	N56			Reaction				
6	N54			Reaction				
7	N52			Reaction				
8	N50			Reaction				
9	N48			Reaction				
10	N46			Reaction				
11	N44			Reaction				
12	N42			Reaction				
13	N40			Reaction				
14	N38			Reaction				
15	N36			Reaction				
16	N34			Reaction				
17	N32			Reaction				
18	N3			Reaction				
19	N5			Reaction				
20	N7			Reaction				
21	N9			Reaction				
22	N11			Reaction				
23	N13			Reaction				
24	N15			Reaction				
25	N17			Reaction				
26	N19			Reaction				
27	N21			Reaction				
28	N23			Reaction				
29	N25			Reaction				
30	N27			Reaction				
31	N29			Reaction				
32	N61			Reaction				
33	N62			Reaction				
34	N95							
35	N96							
36	N59							
37	N30							
38	N31		CS3500	S3500				
39	N60	Reaction	CS3500	S3500				
40	N98		CS3500					
41	N100		CS3500					
42	N97		CS3500					
43	N99		CS3500					

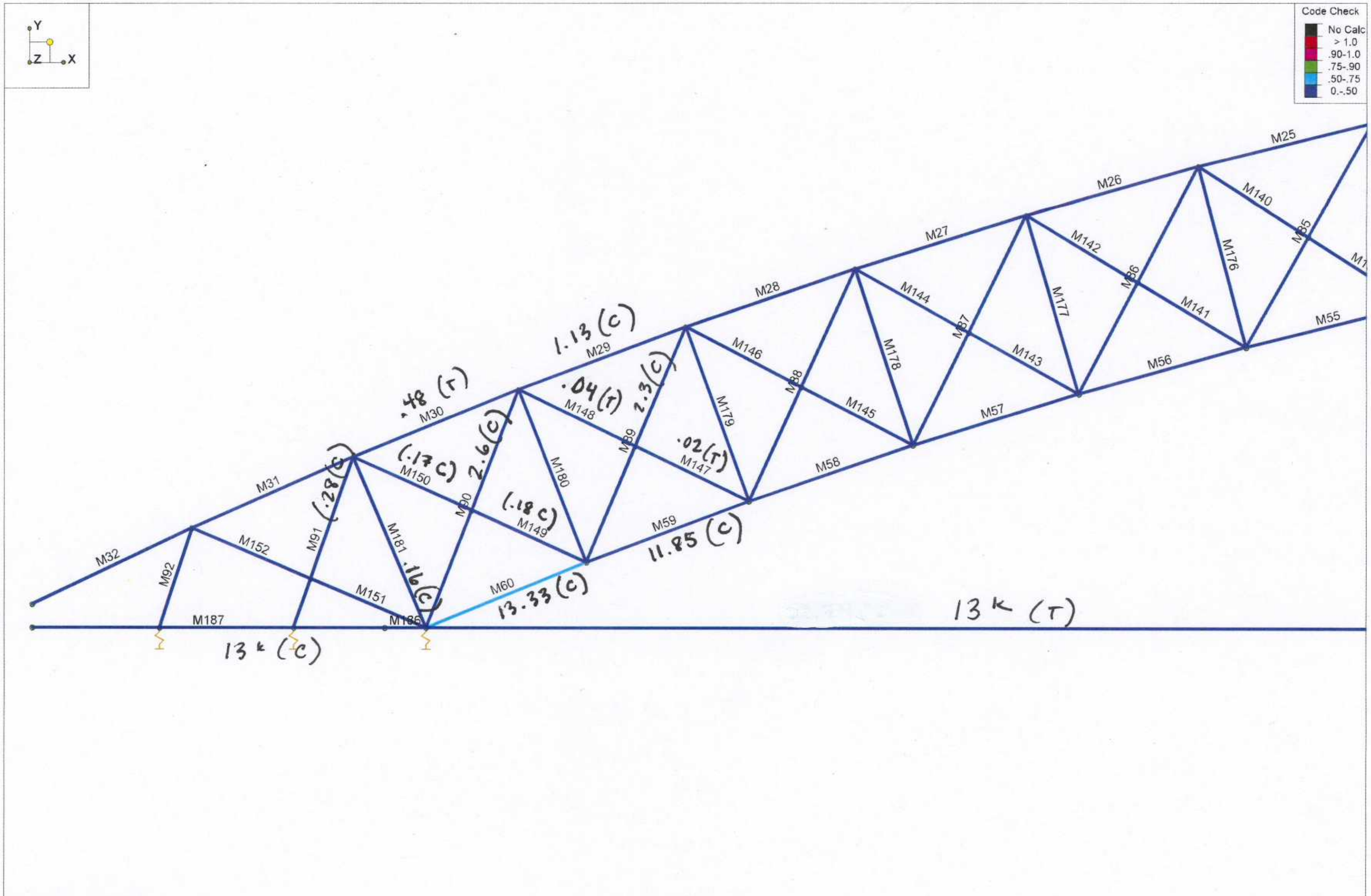

Results for LC 1, Dead

SK - 1

Mar 23, 2010 at 5:59 PM

wagner_tied_2hinge_pr2.r3d

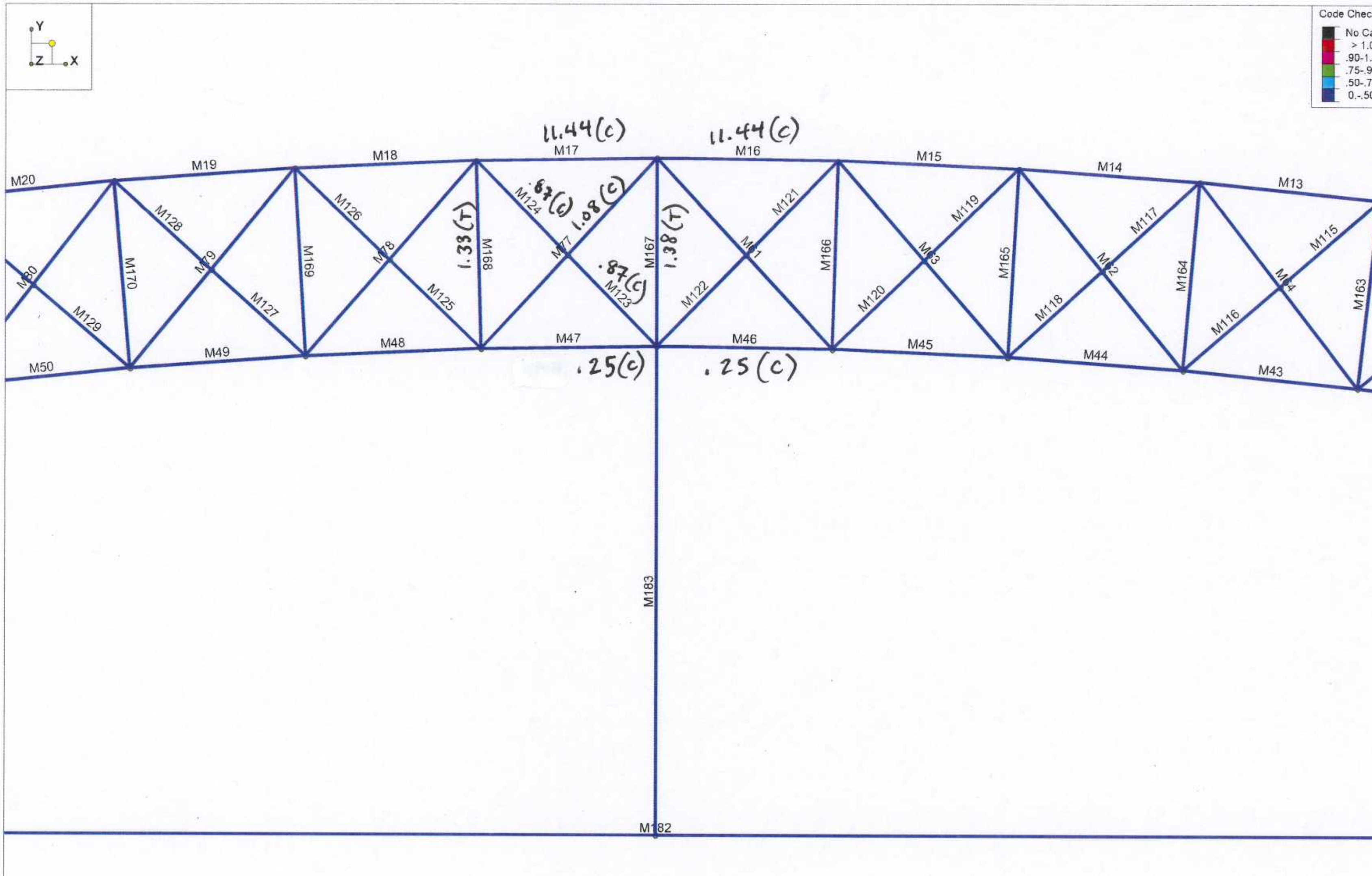

Results for LC 1, Dead

SK - 12

Mar 23, 2010 at 6:05 PM

wagner_tied_2hinge_pr2.r3d

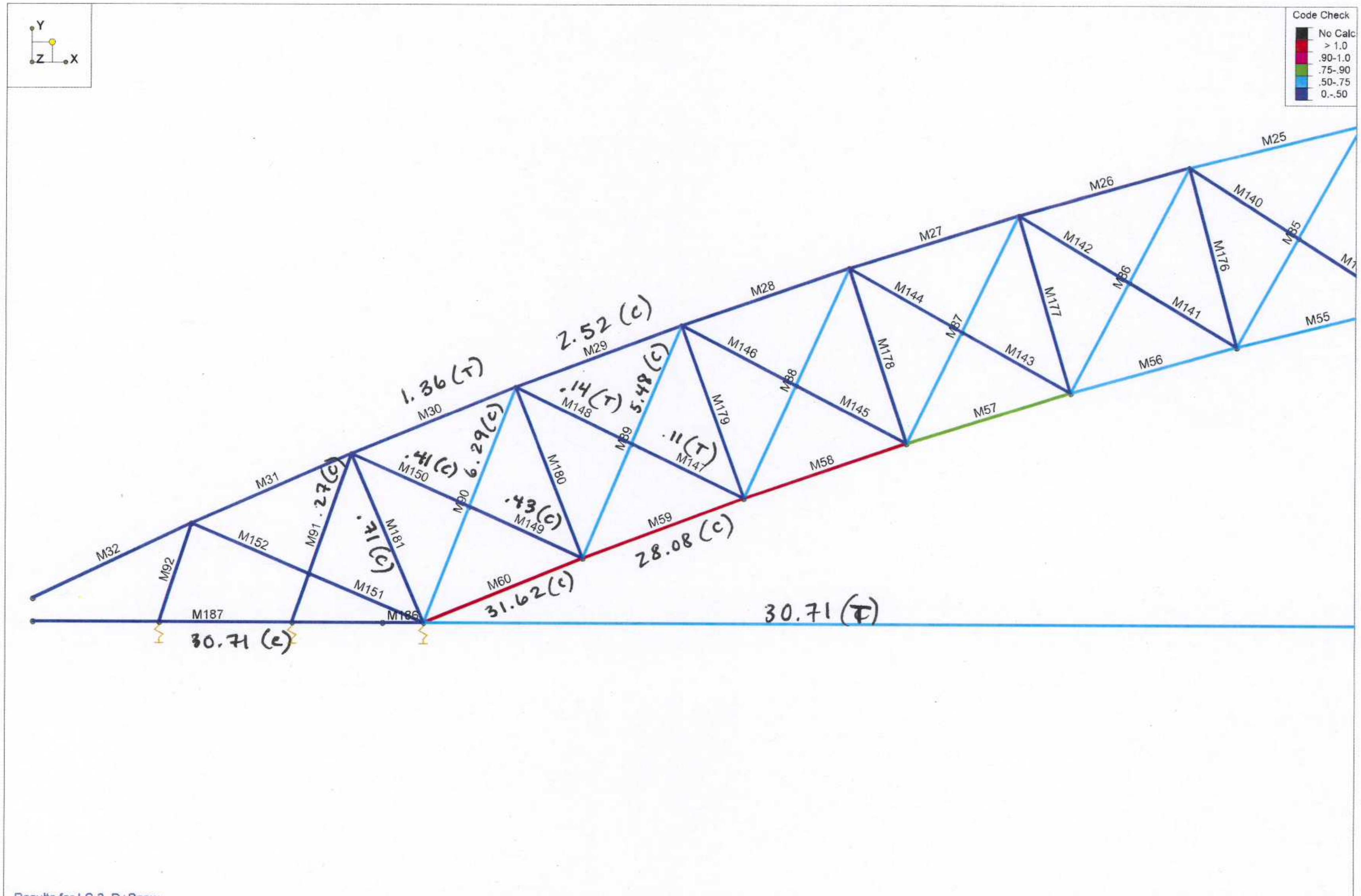

Results for LC 3, D+Snow

SK - 3

Mar 23, 2010 at 6:00 PM

wagner_tied_2hinge_pr2.r3d

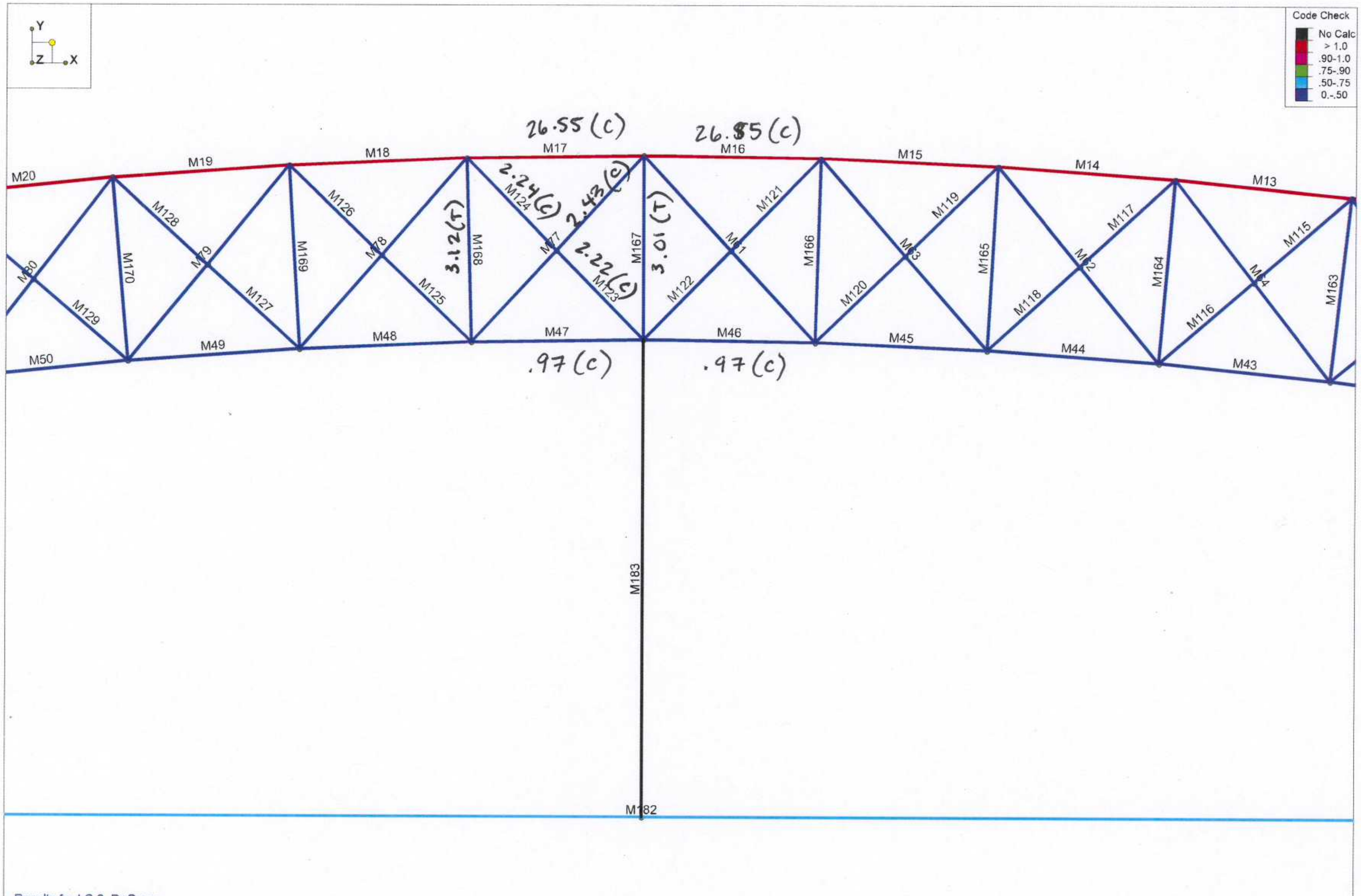

Results for LC 3, D+Snow

SK - 10

Mar 23, 2010 at 6:04 PM

wagner_tied_2hinge_pr2.r3d

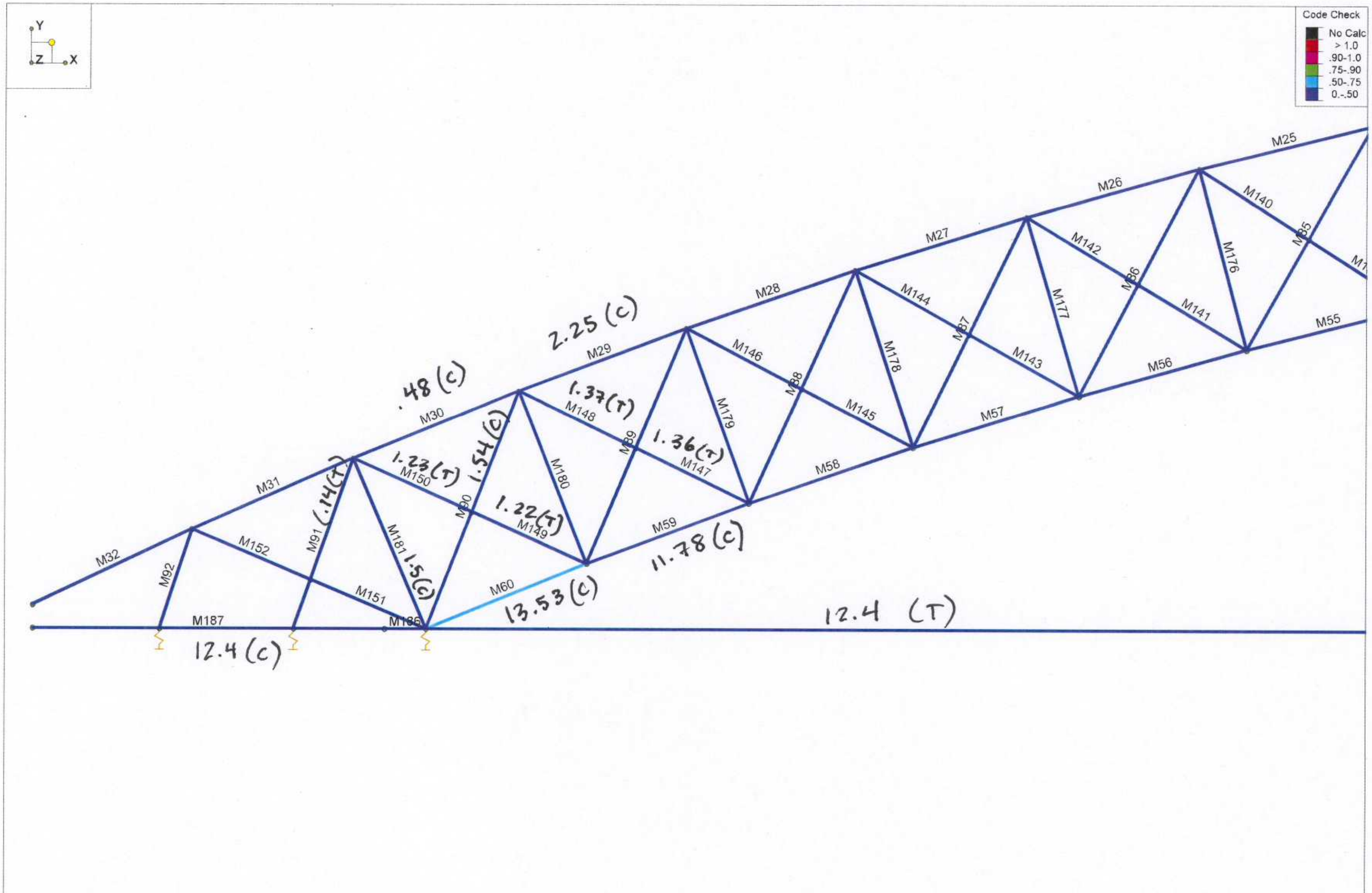

Results for LC 5, D+T

SK - 5	
Mar 23, 2010 at 6:02 PM	
wagner_tied_2hinge_pr2.r3d	

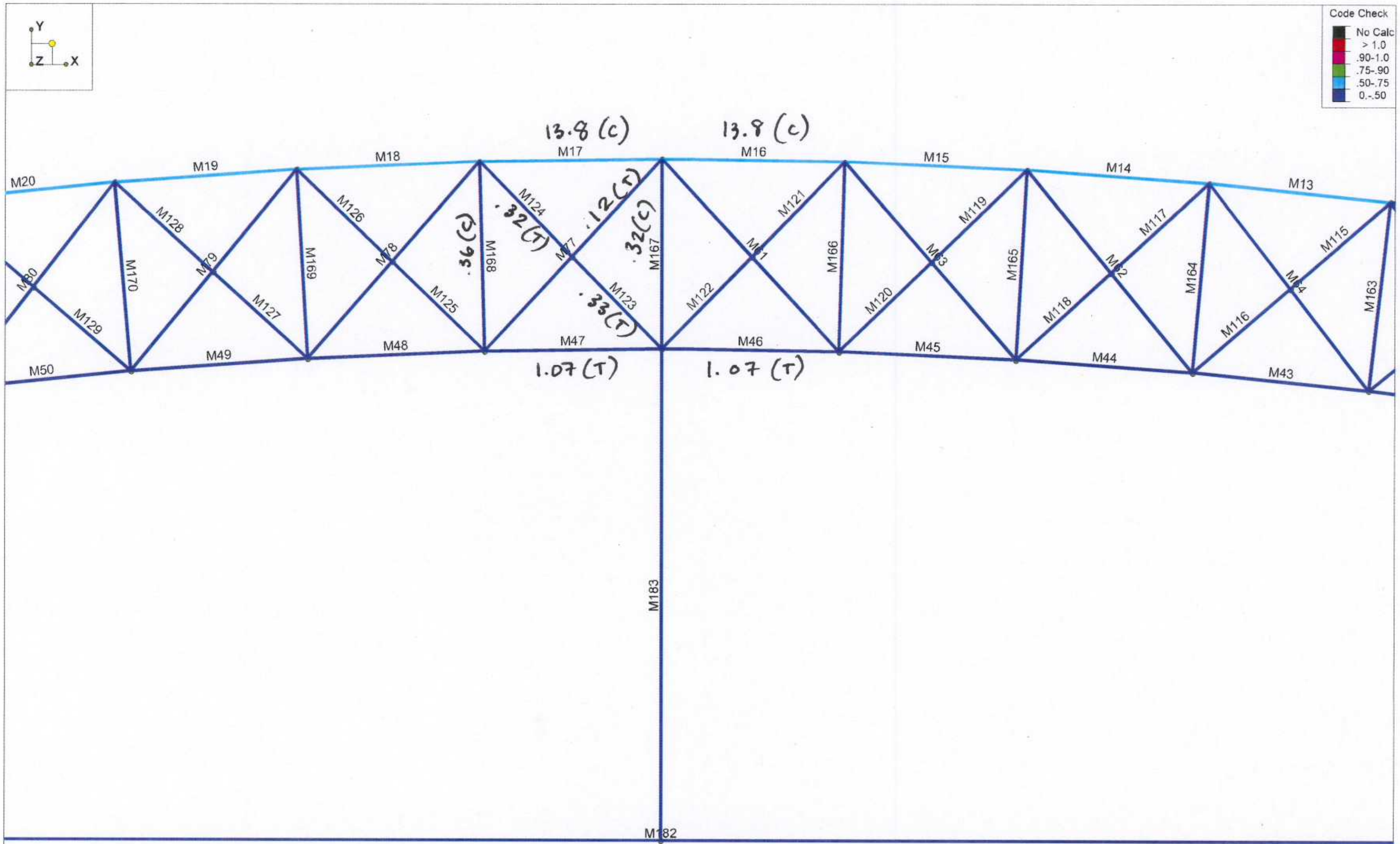

Results for LC 5, D+T

	SK - 8
	Mar 23, 2010 at 6:03 PM
	wagner_tied_2hinge_pr2.r3d

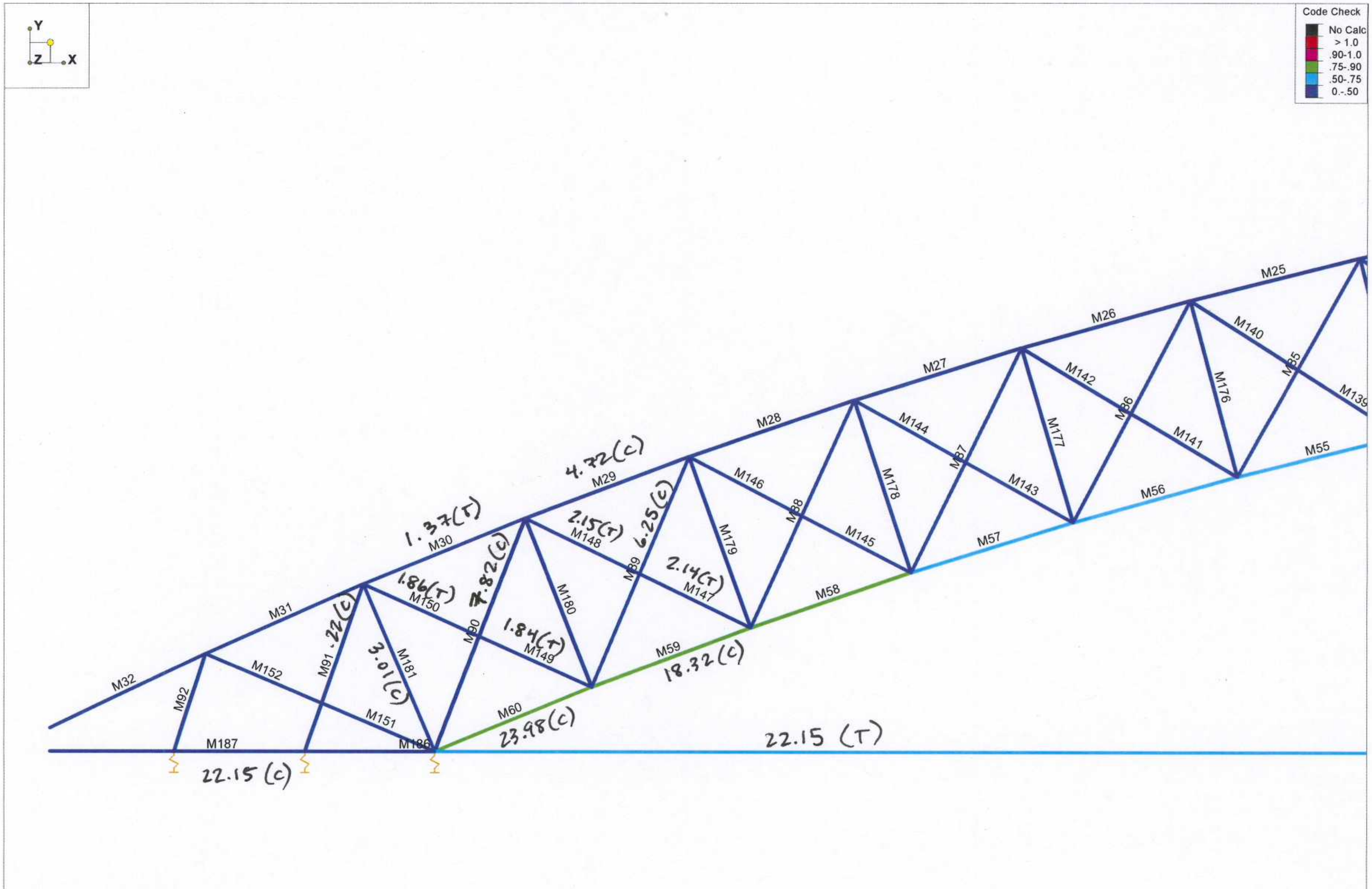

Results for LC 7, D+USnow

SK - 10

Apr 21, 2010 at 2:08 PM

wagner_tied_2hinge_pr2.r3d

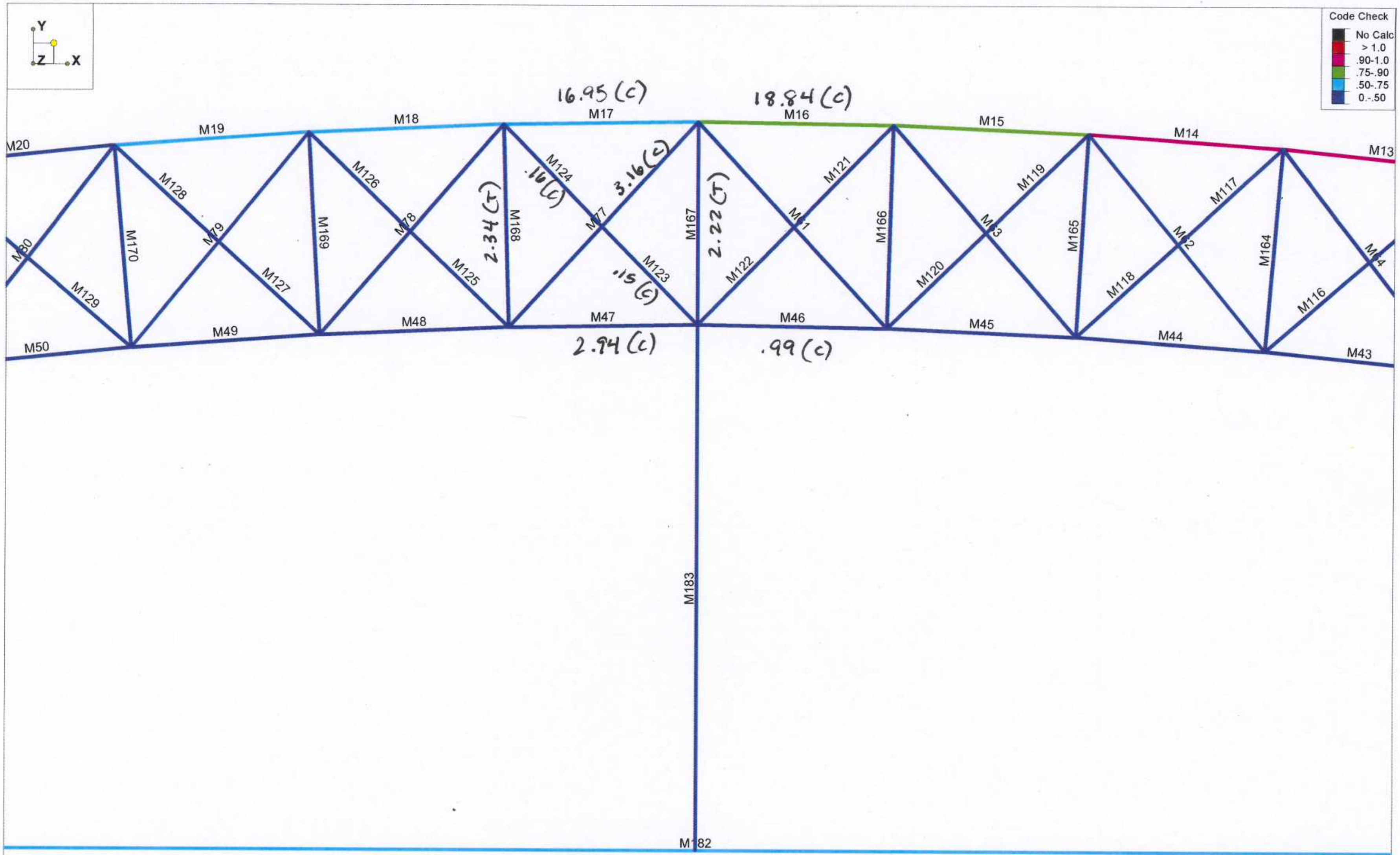

Results for LC 7, D+USnow

SK - 9

Apr 21, 2010 at 2:07 PM

wagner_tied_2hinge_pr2.r3d

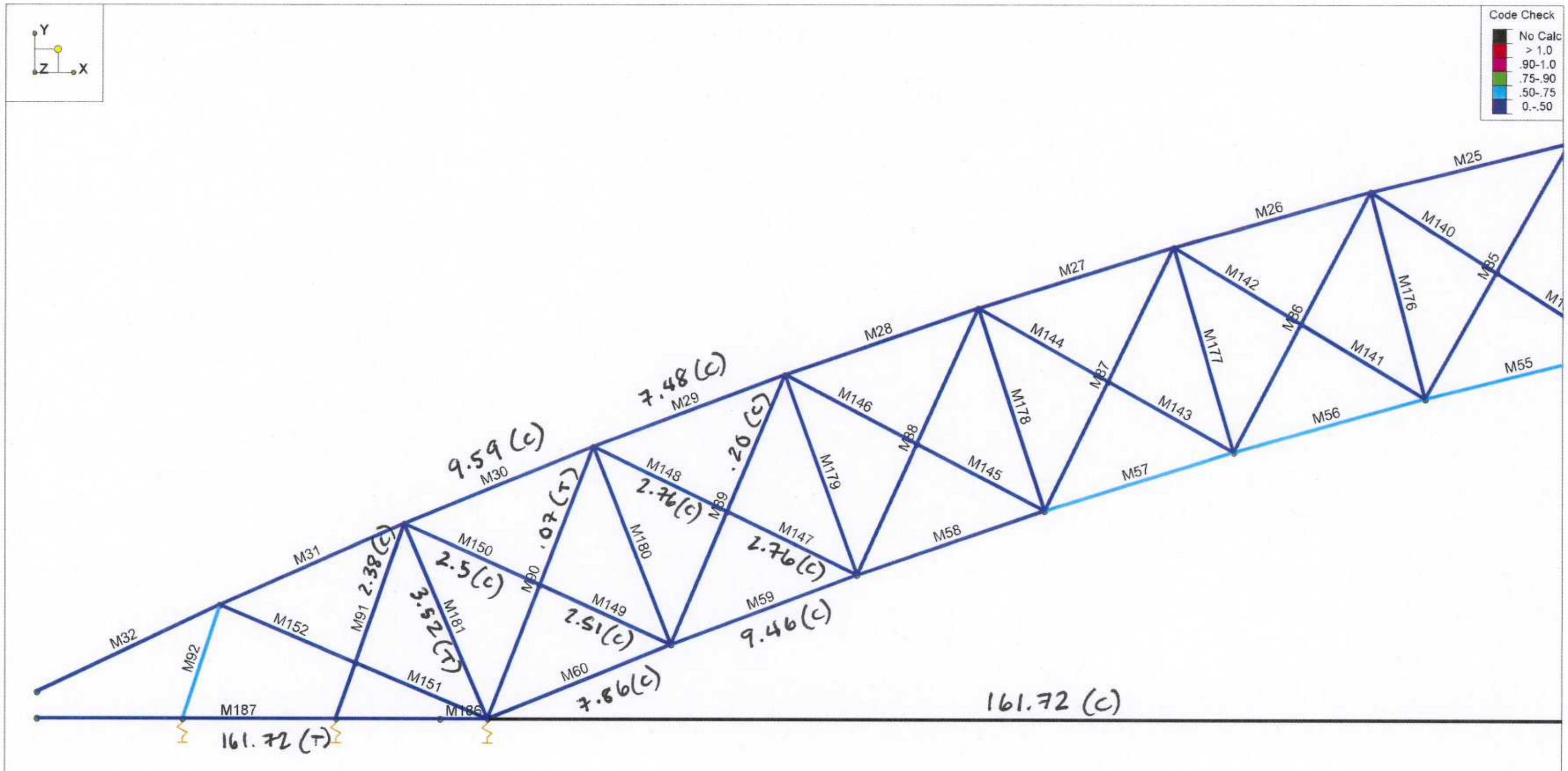

Results for LC 2, D+Disp

		SK - 2
		Mar 23, 2010 at 6:00 PM
		wagner_tied_2hinge_pr2.r3d

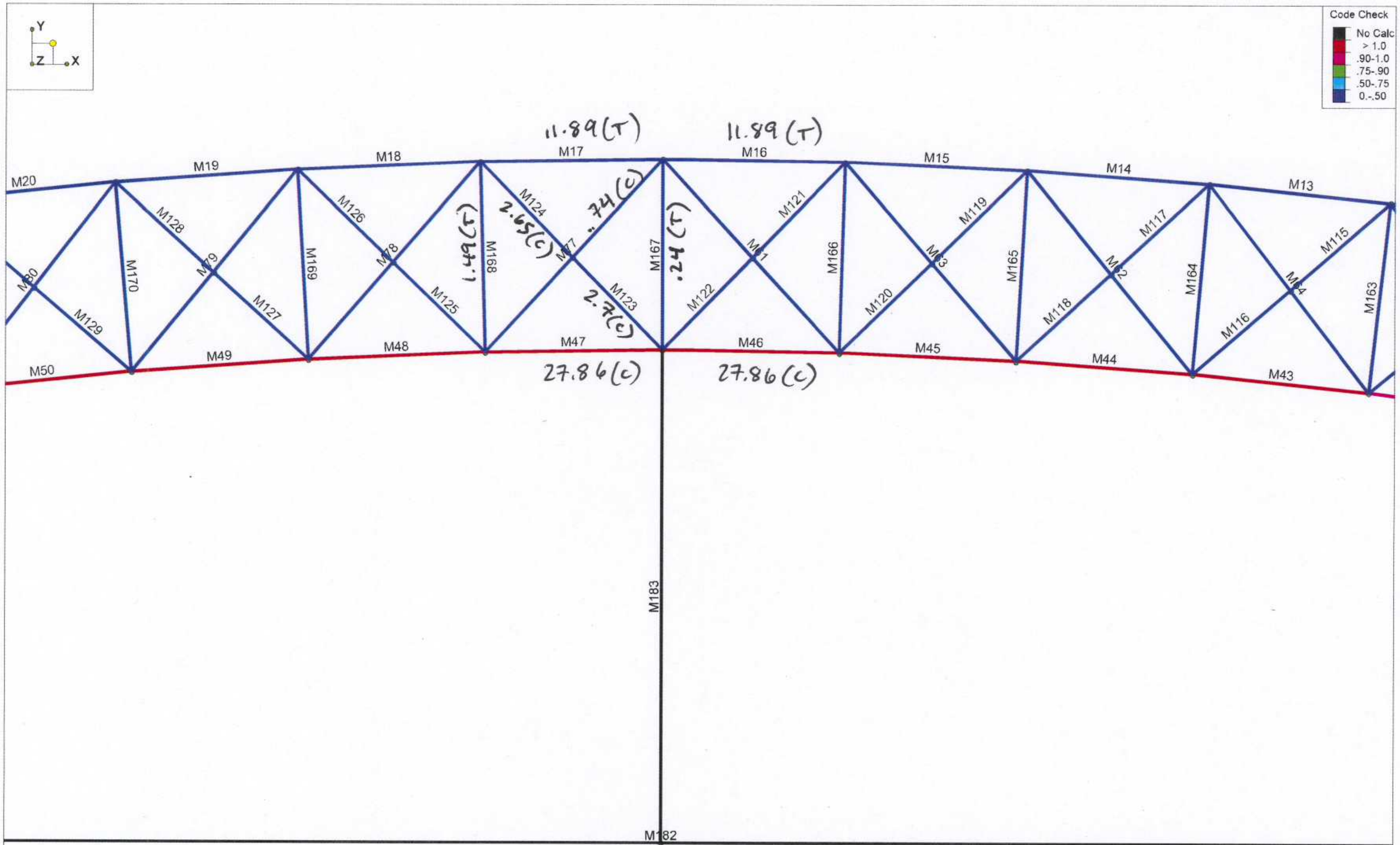

Results for LC 2, D+Disp

SK - 11

Mar 23, 2010 at 6:05 PM

wagner_tied_2hinge_pr2.r3d

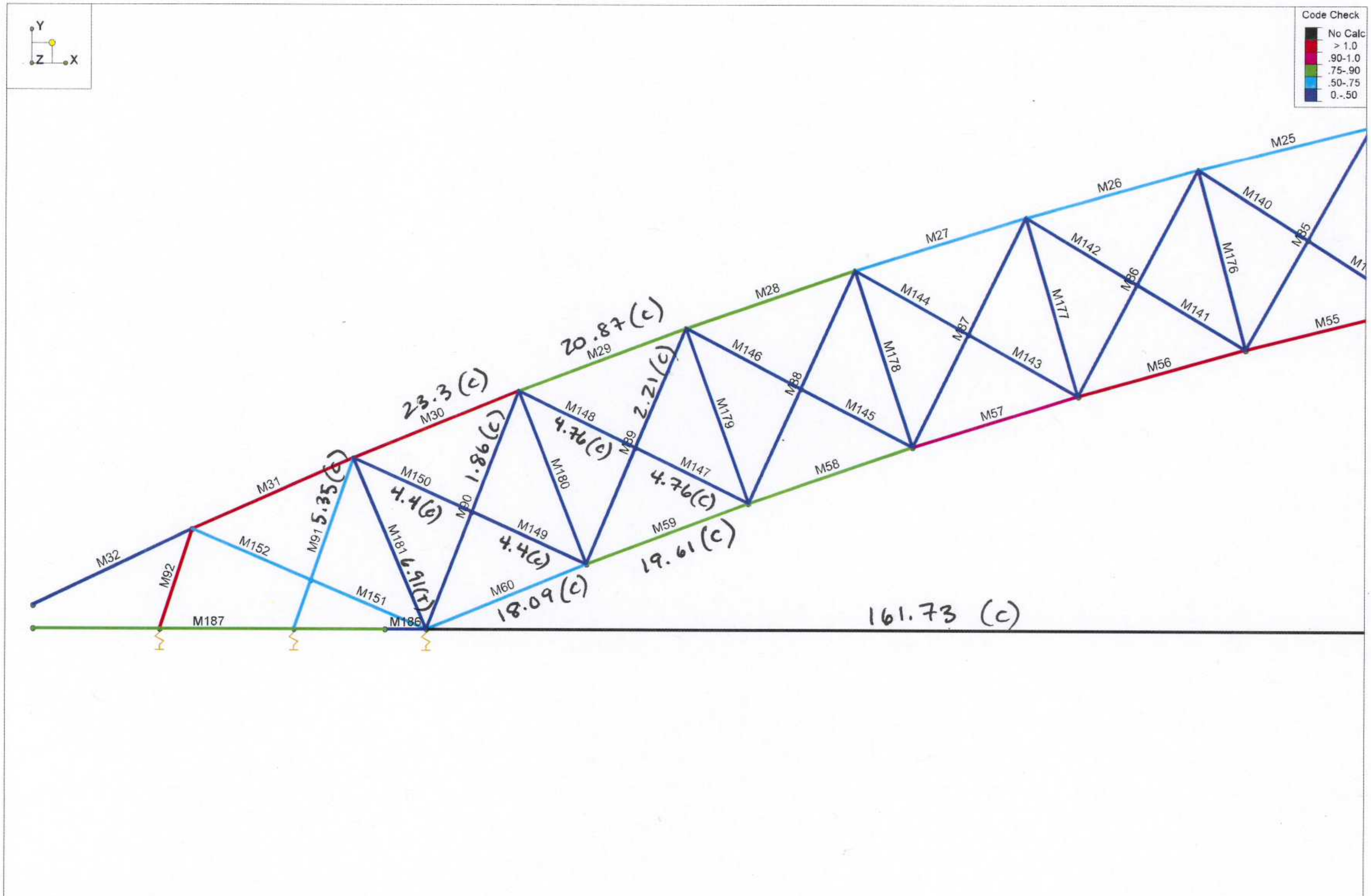

Results for LC 4, D+Snow+Disp

SK - 4	
Mar 23, 2010 at 6:01 PM	
wagner_tied_2hinge_pr2.r3d	

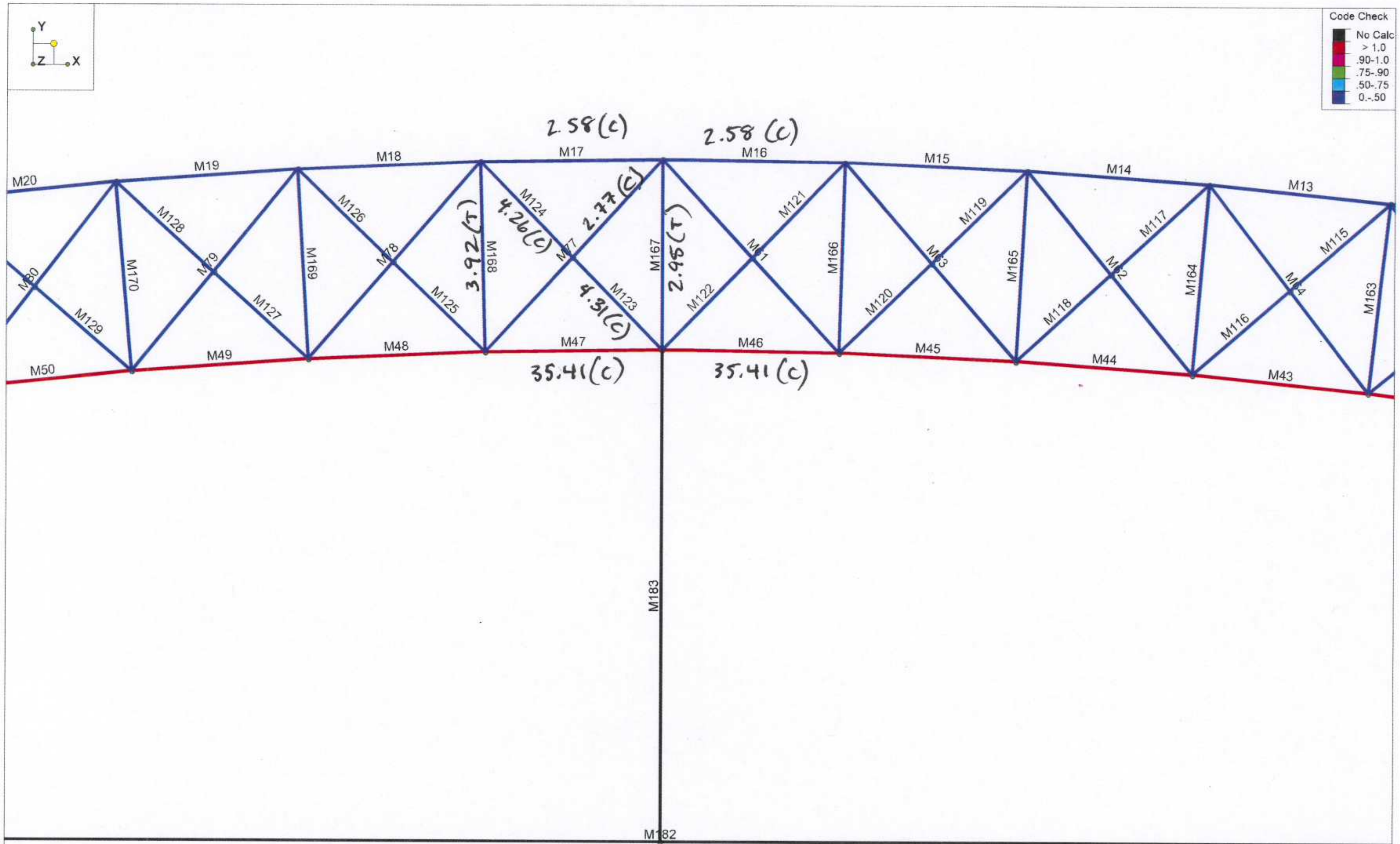

Results for LC 4, D+Snow+Disp

SK - 9

Mar 23, 2010 at 6:04 PM

wagner_tied_2hinge_pr2.r3d

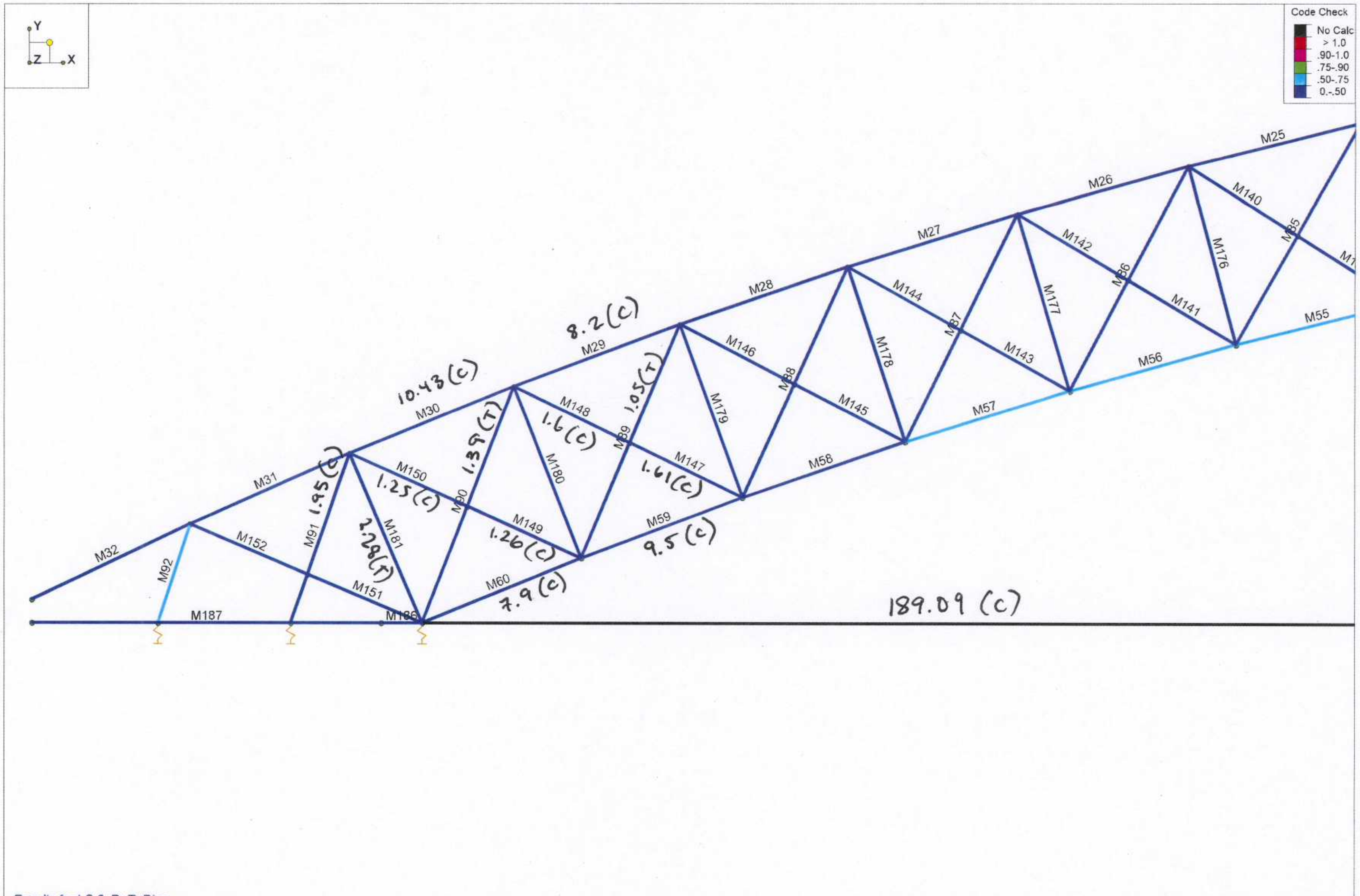

Results for LC 6, D+T+Disp

SK - 6

Mar 23, 2010 at 6:02 PM

wagner_tied_2hinge_pr2.r3d

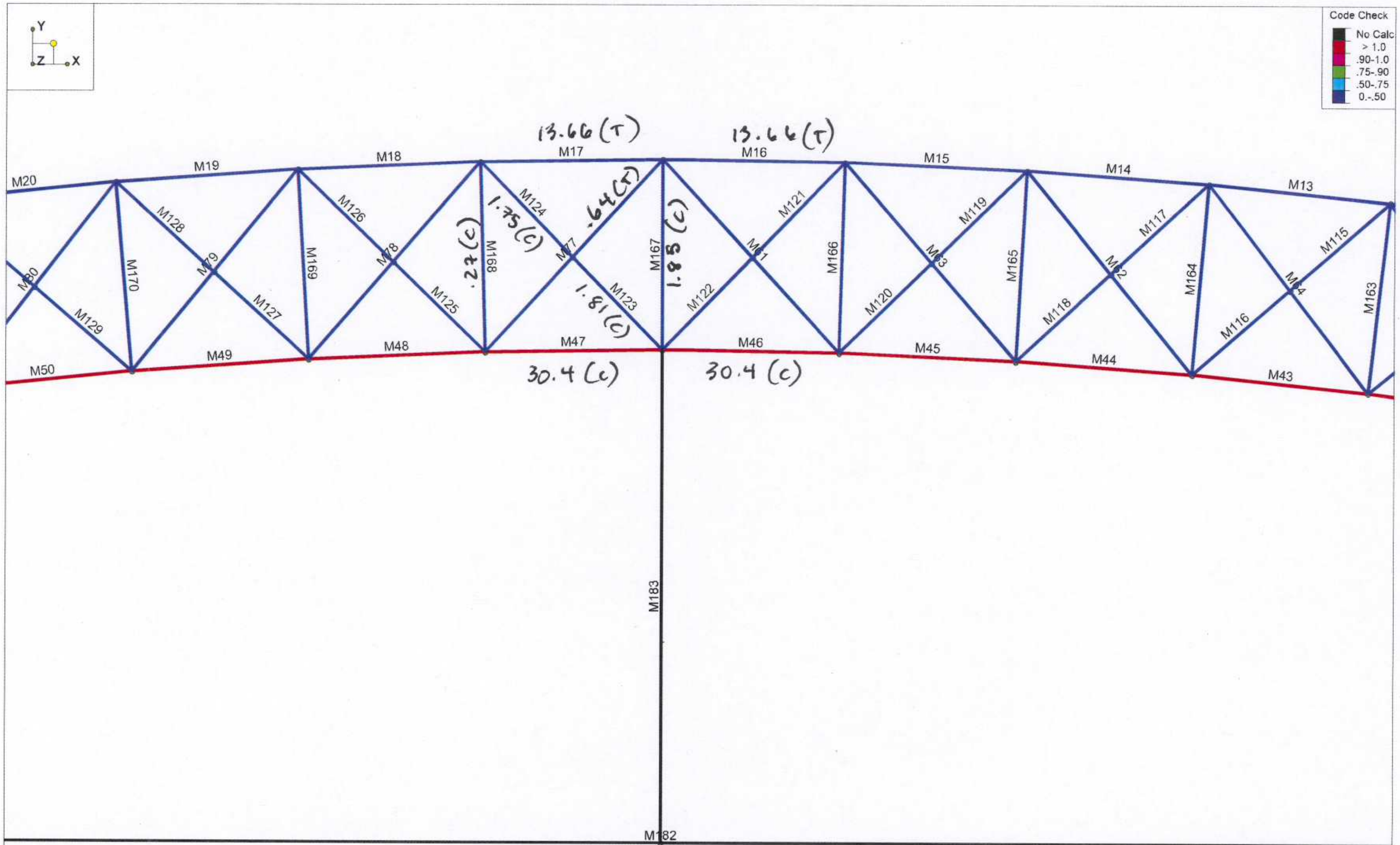

Results for LC 6, D+T+Disp

SK - 7

Mar 23, 2010 at 6:03 PM

wagner_tied_2hinge_pr2.r3d

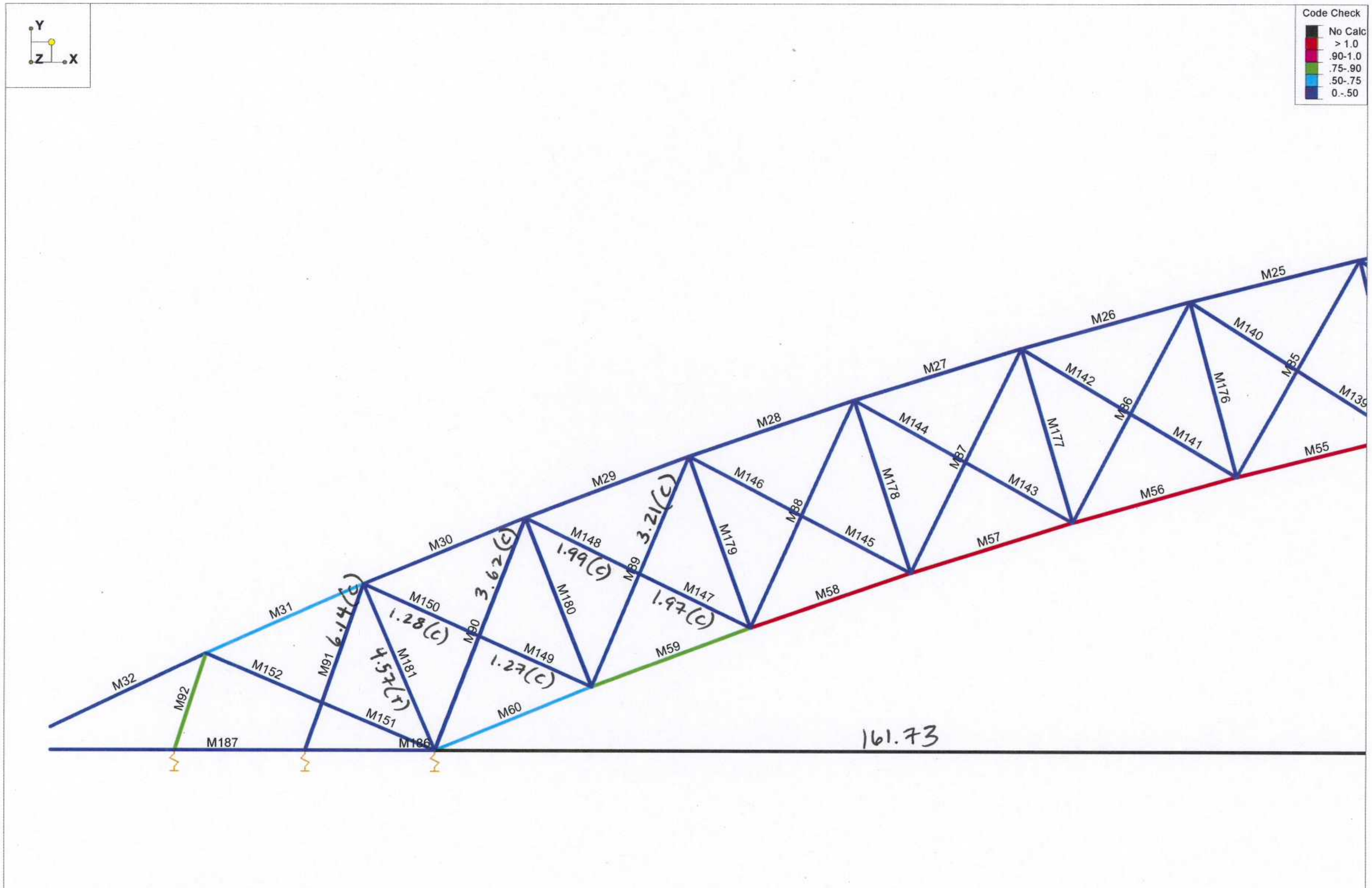

Results for LC 8, D+USnow (left)+Disp

SK - 11

Apr 21, 2010 at 2:08 PM

wagner_tied_2hinge_pr2.r3d

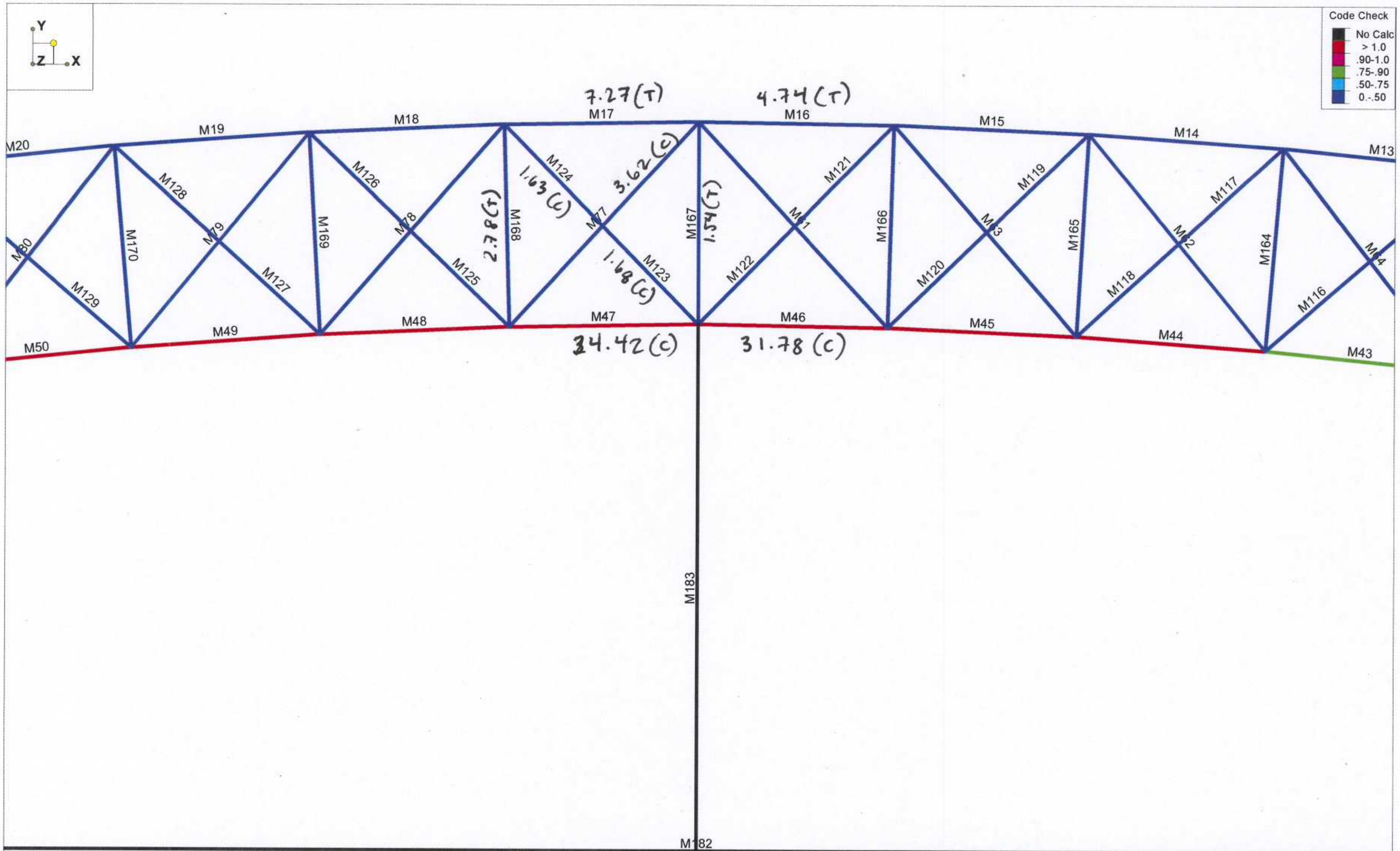

Results for LC 8, D+USnow (left)+Disp

	SK - 8
	Apr 21, 2010 at 1:57 PM
	wagner_tied_2hinge_pr2.r3d

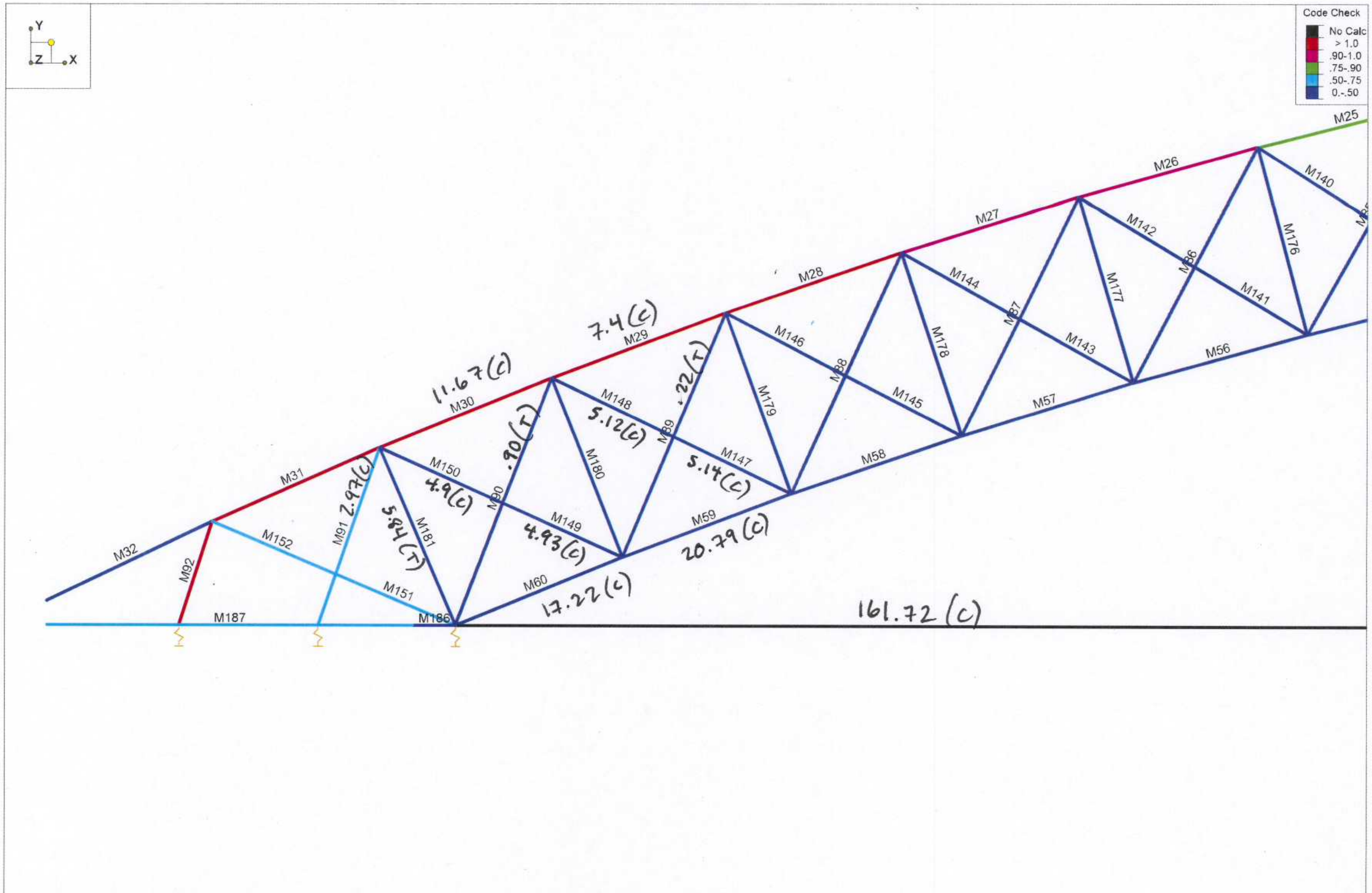

Results for LC 9, D+USnow(right)+Disp

SK - 2

Apr 21, 2010 at 1:50 PM

wagner_tied_2hinge_pr2.r3d

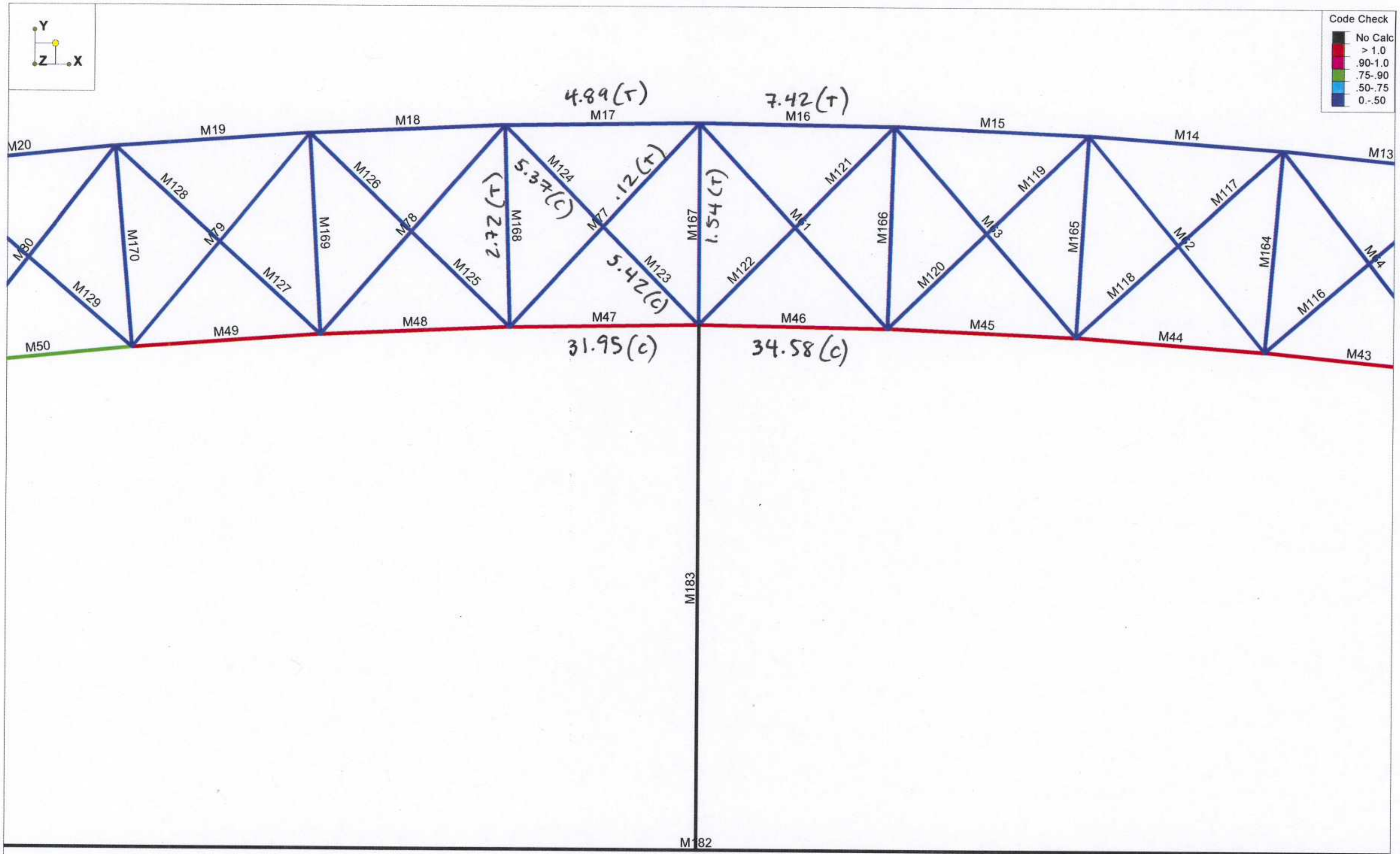

Results for LC 9, D+USnow(right)+Disp

SK - 6

Apr 21, 2010 at 1:56 PM

wagner_tied_2hinge_pr2.r3d

Appendix VI—Finite Element Analysis Results

Stress analysis of QuarterTruss Dead

Table of Contents

List of Figures

Description

Summarize the FEM analysis on QuarterTruss

Study Properties

Study name	Dead Load
Analysis type	Static
Mesh Type:	Solid Mesh
Solver type	FFEPlus
Inplane Effect:	Off
Soft Spring:	Off
Inertial Relief:	Off
Thermal Effect:	Input Temperature
Zero strain temperature	298.000000
Units	Kelvin
Include fluid pressure effects from COSMOSFloWorks	Off
Friction:	Off
Ignore clearance for surface contact	Off
Use Adaptive Method:	Off

Units

Unit system:	English (IPS)
Length/Displacement	in
Temperature	Fahrenheit
Angular velocity	rad/s
Stress/Pressure	psi

Material Properties

No.	Body Name	Material	Mass	Volume
1	Bearing_Block3-1	Eastern White Pine	13.5989 lb	1022.47 in^3
2	BothChordsQ2-1	Eastern White Pine	20.7272 kg	0.0563021 m^3
3	BothChordsQ2-1	Eastern White Pine	23.3735 kg	0.0634903 m^3
4	BraceSimpleFull-1	Eastern White Pine	1.07175 kg	0.00291123 m^3
5	BraceSimpleFull-10	Eastern White Pine	1.07175 kg	0.00291123 m^3
6	BraceSimpleFull-11	Eastern White Pine	1.07175 kg	0.00291123 m^3
7	BraceSimpleFull-12	Eastern White Pine	1.07175 kg	0.00291123 m^3

8	BraceSimpleFull-13	Eastern White Pine	1.07175 kg	0.00291123 m^3
9	BraceSimpleFull-14	Eastern White Pine	1.07175 kg	0.00291123 m^3
10	BraceSimpleFull-2	Eastern White Pine	1.07175 kg	0.00291123 m^3
11	BraceSimpleFull-3	Eastern White Pine	1.07175 kg	0.00291123 m^3
12	BraceSimpleFull-4	Eastern White Pine	1.07175 kg	0.00291123 m^3
13	BraceSimpleFull-5	Eastern White Pine	1.07175 kg	0.00291123 m^3
14	BraceSimpleFull-6	Eastern White Pine	1.07175 kg	0.00291123 m^3
15	BraceSimpleFull-7	Eastern White Pine	1.07175 kg	0.00291123 m^3
16	BraceSimpleFull-8	Eastern White Pine	1.07175 kg	0.00291123 m^3
17	BraceSimpleFull-9	Eastern White Pine	1.07175 kg	0.00291123 m^3
18	BracesSimpleBoth-1	Eastern White Pine	0.500893 kg	0.00136059 m^3
19	BracesSimpleBoth-1	Eastern White Pine	0.515791 kg	0.00140106 m^3
20	BracesSimpleBoth-10	Eastern White Pine	0.500893 kg	0.00136059 m^3
21	BracesSimpleBoth-10	Eastern White Pine	0.515791 kg	0.00140106 m^3
22	BracesSimpleBoth-11	Eastern White Pine	0.500893 kg	0.00136059 m^3
23	BracesSimpleBoth-11	Eastern White Pine	0.515791 kg	0.00140106 m^3
24	BracesSimpleBoth-12	Eastern White Pine	0.500893 kg	0.00136059 m^3
25	BracesSimpleBoth-12	Eastern White Pine	0.515791 kg	0.00140106 m^3
26	BracesSimpleBoth-13	Eastern White Pine	0.500893 kg	0.00136059 m^3
27	BracesSimpleBoth-13	Eastern White Pine	0.515791 kg	0.00140106 m^3
28	BracesSimpleBoth-14	Eastern White Pine	0.500893 kg	0.00136059 m^3
29	BracesSimpleBoth-14	Eastern White Pine	0.515791 kg	0.00140106 m^3
30	BracesSimpleBoth-2	Eastern White Pine	0.500893 kg	0.00136059 m^3
31	BracesSimpleBoth-2	Eastern White Pine	0.515791 kg	0.00140106 m^3
32	BracesSimpleBoth-3	Eastern White Pine	0.500893 kg	0.00136059 m^3
33	BracesSimpleBoth-3	Eastern White Pine	0.515791 kg	0.00140106 m^3
34	BracesSimpleBoth-4	Eastern White Pine	0.500893 kg	0.00136059 m^3

35	BracesSimpleBoth-4	Eastern White Pine	0.515791 kg	0.00140106 m^3
36	BracesSimpleBoth-5	Eastern White Pine	0.500893 kg	0.00136059 m^3
37	BracesSimpleBoth-5	Eastern White Pine	0.515791 kg	0.00140106 m^3
38	BracesSimpleBoth-6	Eastern White Pine	0.500893 kg	0.00136059 m^3
39	BracesSimpleBoth-6	Eastern White Pine	0.515791 kg	0.00140106 m^3
40	BracesSimpleBoth-7	Eastern White Pine	0.500893 kg	0.00136059 m^3
41	BracesSimpleBoth-7	Eastern White Pine	0.515791 kg	0.00140106 m^3
42	BracesSimpleBoth-8	Eastern White Pine	0.500893 kg	0.00136059 m^3
43	BracesSimpleBoth-8	Eastern White Pine	0.515791 kg	0.00140106 m^3
44	BracesSimpleBoth-9	Eastern White Pine	0.500893 kg	0.00136059 m^3
45	BracesSimpleBoth-9	Eastern White Pine	0.515791 kg	0.00140106 m^3
46	IronBlockBottomH-1	Ductile Iron (SN)	0.594697 kg	7.52781e-005 m^3
47	IronBlockBottomH-56	Ductile Iron (SN)	0.594697 kg	7.52781e-005 m^3
48	IronBlockBottomH-57	Ductile Iron (SN)	0.594697 kg	7.52781e-005 m^3
49	IronBlockBottomH-58	Ductile Iron (SN)	0.594697 kg	7.52781e-005 m^3
50	IronBlockBottomH-59	Ductile Iron (SN)	0.594697 kg	7.52781e-005 m^3
51	IronBlockBottomH-60	Ductile Iron (SN)	0.594697 kg	7.52781e-005 m^3
52	IronBlockBottomH-61	Ductile Iron (SN)	0.594697 kg	7.52781e-005 m^3
53	IronBlockBottomH-62	Ductile Iron (SN)	0.594697 kg	7.52781e-005 m^3
54	IronBlockBottomH-63	Ductile Iron (SN)	0.594697 kg	7.52781e-005 m^3
55	IronBlockBottomH-64	Ductile Iron (SN)	0.594697 kg	7.52781e-005 m^3
56	IronBlockBottomH-65	Ductile Iron (SN)	0.594697 kg	7.52781e-005 m^3
57	IronBlockBottomH-66	Ductile Iron (SN)	0.594697 kg	7.52781e-005 m^3
58	IronBlockBottomH-67	Ductile Iron (SN)	0.594697 kg	7.52781e-005 m^3
59	IronBlockBottomH-68	Ductile Iron (SN)	0.594697 kg	7.52781e-005 m^3
60	IronBlockBottomQ-1	Ductile Iron (SN)	0.297348 kg	3.7639e-005 m^3
61	IronBlockTopH-1	Ductile Iron (SN)	0.594697 kg	7.52781e-005 m^3

62	IronBlockTopH-44	Ductile Iron (SN)	0.594697 kg	7.52781e-005 m^3
63	IronBlockTopH-85	Ductile Iron (SN)	0.594697 kg	7.52781e-005 m^3
64	IronBlockTopH-86	Ductile Iron (SN)	0.594697 kg	7.52781e-005 m^3
65	IronBlockTopH-87	Ductile Iron (SN)	0.594697 kg	7.52781e-005 m^3
66	IronBlockTopH-88	Ductile Iron (SN)	0.594697 kg	7.52781e-005 m^3
67	IronBlockTopH-89	Ductile Iron (SN)	0.594697 kg	7.52781e-005 m^3
68	IronBlockTopH-90	Ductile Iron (SN)	0.594697 kg	7.52781e-005 m^3
69	IronBlockTopH-91	Ductile Iron (SN)	0.594697 kg	7.52781e-005 m^3
70	IronBlockTopH-92	Ductile Iron (SN)	0.594697 kg	7.52781e-005 m^3
71	IronBlockTopH-93	Ductile Iron (SN)	0.594697 kg	7.52781e-005 m^3
72	IronBlockTopH-94	Ductile Iron (SN)	0.594697 kg	7.52781e-005 m^3
73	IronBlockTopH-95	Ductile Iron (SN)	0.594697 kg	7.52781e-005 m^3
74	IronBlockTopH-96	Ductile Iron (SN)	0.594697 kg	7.52781e-005 m^3
75	IronBlockTopH-97	Ductile Iron (SN)	0.594697 kg	7.52781e-005 m^3
76	IronBlockTopQ-1	Ductile Iron (SN)	0.297348 kg	3.7639e-005 m^3
77	WallBearingH-1	Eastern White Pine	11.5829 kg	0.0314632 m^3
78	WoodBraceBearingH1-1	Eastern White Pine	0.50275 kg	0.00136564 m^3
79	WoodBraceBearingH2-1	Eastern White Pine	0.819782 kg	0.0022268 m^3
80	WoodBraceBothBearingH-1	Eastern White Pine	0.459656 kg	0.00124858 m^3
81	WoodBraceBothBearingH-1	Eastern White Pine	0.541041 kg	0.00146965 m^3
82	tie2-1	Ductile Iron (SN)	0.240465 lb	0.842539 in^3

Material name:	**Eastern White Pine**
Description:	
Material Source:	Library files
Material Library Name:	ewpine
Material Model Type:	Linear Elastic Isotropic

Property Name	**Value**	**Units**	**Value Type**
Elastic modulus	1.24e+006	psi	Constant
Poisson's ratio	0.344	NA	Constant
Shear modulus	7.346e+005	psi	Constant
Mass density	0.0133	lb/in^3	Constant

Tensile strength	10600	psi	Constant
Compressive strength	4800	psi	Constant
Yield strength	10600	psi	Constant
Thermal expansion coefficient	2.7778	/Fahrenheit	Constant
Thermal conductivity	1.605e-006	BTU/(in.s.F)	Constant
Specific heat	0.59723	Btu/(lb.F)	Constant

Material name:	**Ductile Iron (SN)**
Description:	
Material Source:	Library files
Material Library Name:	cosmos materials
Material Model Type:	Linear Elastic Isotropic

Property Name	Value	Units	Value Type
Elastic modulus	1.2e+011	N/m^2	Constant
Poisson's ratio	0.31	NA	Constant
Shear modulus	7.7e+010	N/m^2	Constant
Mass density	7900	kg/m^3	Constant
Tensile strength	8.617e+008	N/m^2	Constant
Yield strength	5.5149e+008	N/m^2	Constant
Thermal expansion coefficient	1.1e-005	/Kelvin	Constant
Thermal conductivity	75	W/(m.K)	Constant
Specific heat	450	J/(kg.K)	Constant

Loads and Restraints

Restraint

Restraint name	Selection set	Description
Restraint-1 <WallBearingH-1>	on 1 Face(s) fixed.	
Restraint-2 <BothChordsQ2-1, IronBlockTopQ-1, IronBlockBottomQ-1>	on 4 Face(s) symmetry	
Restraint-3 <BothChordsQ2-1, IronBlockBottomQ-1, IronBlockTopQ-1, IronBlockTopH-1, IronBlockBottomH-56, IronBlockTopH-85, IronBlockBottomH-57, IronBlockTopH-87, IronBlockBottomH-58, IronBlockBottomH-59, IronBlockTopH-88, IronBlockTopH-89, IronBlock...	on 78 Face(s) symmetry	
Restraint-4 <WoodBraceBearingH1-1, WoodBraceBothBearingH-1, WoodBraceBearingH2-1,	on 46 Face(s) symmetry	

BraceSimpleFull-14, BracesSimpleBoth-14, BraceSimpleFull-13, BracesSimpleBoth-13, BracesSimpleBoth-12, BraceSimpleFull-12, BraceSimpleFull-11, BracesSimpleBoth-11, Br...		
Restraint-5 <tie2-1>	on 2 Face(s) symmetry	

Load

Load name	Selection set	Loading type	Description
Pressure-1 <BothChordsQ2-1>	on with Pressure - 17.95 psi normal to reference plane Edge< 1 >	Sequential Loading	
Pressure-2 <WallBearingH-1>	on with Pressure - 17.95 psi normal to reference plane Edge< 1 >	Sequential Loading	
Pressure-3 <WallBearingH-1>	on with Pressure - 17.95 psi normal to reference plane Edge< 1 >	Sequential Loading	
Pressure-4 <WallBearingH-1>	on with Pressure - 17.95 psi normal to reference plane Edge< 1 >	Sequential Loading	
Pressure-5 <>	on with Pressure - 17.95 psi normal to reference plane Top Plane	Sequential Loading	
Pressure-6 <>	on with Pressure - 17.95 psi normal to reference plane Top Plane	Sequential Loading	
Pressure-7 <>	on with Pressure - 17.95 psi normal to reference plane Top Plane	Sequential Loading	
Pressure-8 <>	on with Pressure - 17.95 psi normal to reference plane Top Plane	Sequential Loading	
Pressure-9 <>	on with Pressure - 17.95 psi normal to reference plane Top Plane	Sequential Loading	
Pressure-10 <>	on with Pressure - 17.95 psi normal to reference plane Top Plane	Sequential Loading	
Pressure-11 <>	on with Pressure -	Sequential Loading	

	17.95 psi normal to reference plane Top Plane		
Pressure-12 <>	on with Pressure -17.95 psi normal to reference plane Top Plane	Sequential Loading	
Pressure-13 <>	on with Pressure -17.95 psi normal to reference plane Top Plane	Sequential Loading	
Pressure-14 <>	on with Pressure -17.95 psi normal to reference plane Top Plane	Sequential Loading	
Pressure-15 <>	on with Pressure -17.95 psi normal to reference plane Top Plane	Sequential Loading	
Pressure-16 <>	on with Pressure -17.95 psi normal to reference plane Top Plane	Sequential Loading	
Pressure-17 <>	on with Pressure -17.95 psi normal to reference plane Top Plane	Sequential Loading	
Pressure-18 <>	on with Pressure -17.95 psi normal to reference plane Top Plane	Sequential Loading	
Pressure-19 <>	on with Pressure -17.95 psi normal to reference plane Top Plane	Sequential Loading	
Pressure-20 <BothChordsQ2-1>	on 1 Face(s) with Pressure -36.93 psi normal to reference plane Top Plane	Sequential Loading	

Connector Definitions

Connector name	Selection set	Loading type	Description
Spring Connector-1 <IronBlockTopQ-1, IronBlockBottomQ-1>	Spring(Flat parallel faces) Connectors on 2 Face(s); with distributed normal stiffness of 1.12e+006 (lb/in)/in^2 and distributed shear stiffness of 0 (lb/in)/in^2	Sequential Loading	
Spring Connector-2	Spring(Flat parallel	Sequential Loading	

<IronBlockBottomH-1, IronBlockTopH-1>	faces) Connectors on 2 Face(s); with distributed normal stiffness of 1.12e+006 (lb/in)/in^2 and distributed shear stiffness of 0 (lb/in)/in^2		
Spring Connector-3 <IronBlockTopH-85, IronBlockBottomH-56>	Spring(Flat parallel faces) Connectors on 2 Face(s); with distributed normal stiffness of 1.12e+006 (lb/in)/in^2 and distributed shear stiffness of 0 (lb/in)/in^2	Sequential Loading	
Spring Connector-5 <IronBlockTopH-87, IronBlockBottomH-58>	Spring(Flat parallel faces) Connectors on 2 Face(s); with distributed normal stiffness of 1.12e+006 (lb/in)/in^2 and distributed shear stiffness of 0 (lb/in)/in^2	Sequential Loading	
Spring Connector-6 <IronBlockBottomH-59, IronBlockTopH-88>	Spring(Flat parallel faces) Connectors on 2 Face(s); with distributed normal stiffness of 1.12e+006 (lb/in)/in^2 and distributed shear stiffness of 0 (lb/in)/in^2	Sequential Loading	
Spring Connector-7 <IronBlockTopH-89, IronBlockBottomH-60>	Spring(Flat parallel faces) Connectors on 2 Face(s); with distributed normal stiffness of 1.12e+006 (lb/in)/in^2 and distributed shear stiffness of 0 (lb/in)/in^2	Sequential Loading	
Spring Connector-8 <IronBlockBottomH-61, IronBlockTopH-90>	Spring(Flat parallel faces) Connectors on 2 Face(s); with distributed normal stiffness of 1.12e+006 (lb/in)/in^2 and distributed shear stiffness of 0 (lb/in)/in^2	Sequential Loading	
Spring Connector-9 <IronBlockTopH-91,	Spring(Flat parallel faces) Connectors on	Sequential Loading	

IronBlockBottomH-62>	2 Face(s); with distributed normal stiffness of 1.12e+006 (lb/in)/in^2 and distributed shear stiffness of 0 (lb/in)/in^2		
Spring Connector-10 <IronBlockBottomH-63, IronBlockTopH-92>	Spring(Flat parallel faces) Connectors on 2 Face(s); with distributed normal stiffness of 1.12e+006 (lb/in)/in^2 and distributed shear stiffness of 0 (lb/in)/in^2	Sequential Loading	
Spring Connector-11 <IronBlockTopH-93, IronBlockBottomH-64>	Spring(Flat parallel faces) Connectors on 2 Face(s); with distributed normal stiffness of 1.12e+006 (lb/in)/in^2 and distributed shear stiffness of 0 (lb/in)/in^2	Sequential Loading	
Spring Connector-13 <IronBlockTopH-95, IronBlockBottomH-66>	Spring(Flat parallel faces) Connectors on 2 Face(s); with distributed normal stiffness of 1.12e+006 (lb/in)/in^2 and distributed shear stiffness of 0 (lb/in)/in^2	Sequential Loading	
Spring Connector-14 <IronBlockBottomH-67, IronBlockTopH-96>	Spring(Flat parallel faces) Connectors on 2 Face(s); with distributed normal stiffness of 1.12e+006 (lb/in)/in^2 and distributed shear stiffness of 0 (lb/in)/in^2	Sequential Loading	
Spring Connector-15 <IronBlockTopH-97, Bearing_Block3-1>	Spring(Flat parallel faces) Connectors on 2 Face(s); with distributed normal stiffness of 1.12e+006 (lb/in)/in^2 and distributed shear stiffness of 0 (lb/in)/in^2	Sequential Loading	
Spring Connector-16 <IronBlockTopH-44, Bearing_Block3-1>	Spring(Flat parallel faces) Connectors on 2 Face(s); with	Sequential Loading	

	distributed normal stiffness of 1.12e+006 (lb/in)/in^2 and distributed shear stiffness of 0 (lb/in)/in^2		
Spring Connector-17 <IronBlockTopH-94, IronBlockBottomH-65>	Spring(Flat parallel faces) Connectors on 2 Face(s); with distributed normal stiffness of 1.12e+006 (lb/in)/in^2 and distributed shear stiffness of 0 (lb/in)/in^2	Sequential Loading	
Spring Connector-18 <IronBlockTopH-86, IronBlockBottomH-57>	Spring(Flat parallel faces) Connectors on 2 Face(s); with distributed normal stiffness of 1.12e+006 (lb/in)/in^2 and distributed shear stiffness of 0 (lb/in)/in^2	Sequential Loading	
Spring Connector-21 <tie2-1, Bearing_Block3-1>	Spring(Flat parallel faces) Connectors on 2 Face(s); with total normal stiffness of 42203 lb/in and total shear stiffness of 0 lb/in	Sequential Loading	

Contact

Contact state: Touching faces - Bonded

Contact Set-1	Bonded contact pair: Between selected entities of IronBlockTopQ-1 and BothChordsQ2-1
Description:	
Contact Set-2	Bonded contact pair: Between selected entities of IronBlockTopH-1 and BothChordsQ2-1
Description:	
Contact Set-3	Bonded contact pair: Between selected entities of IronBlockBottomH-68 and BothChordsQ2-1
Description:	
Contact Set-8	Bonded contact pair: Between selected entities of BracesSimpleBoth-1 and IronBlockBottomQ-1
Description:	
Contact Set-9	No Penetration contact pair: Between selected entities of WallBearingH-1 and WallBearingH-1 Include friction with Friction Coefficient: 0.4
Description:	
Contact Set-10	No Penetration contact pair: Between selected

	entities of Bearing_Block3-1 and WallBearingH-1 Include friction with Friction Coefficient: 0.4
Description:	

Mesh Information

Mesh Type:	Solid Mesh
Mesher Used:	Standard
Automatic Transition:	On
Smooth Surface:	On
Jacobian Check:	4 Points
Element Size:	52.019 mm
Tolerance:	0.97536 mm
Quality:	High
Number of elements:	93595
Number of nodes:	157907
Time to complete mesh(hh;mm;ss):	00:03:01
Computer name:	PDH-KWOODMAN

Mesh Control Information:

Control-2 <IronBlockBottomQ-1, IronBlockBottomH-1, IronBlockBottomH-56, IronBlockBottomH-57, IronBlockBottomH-58, IronBlockBottomH-59, IronBlockBottomH-60, IronBlockBottomH-61, IronBlockBottomH-62, IronBlockBottomH-63, IronBlockBottomH-64, IronBloc...	Mesh control on 66 Face(s) with seed 0.3125 in, 3 layers and ration 1.5.
Control-4 <WallBearingH-1>	Mesh control on 1 Component(s) with seed 63.4987 mm, 3 layers and ration 1.5.
Control-6 <Bearing_Block3-1>	Mesh control on 2 Face(s) with seed 0.5 in, 3 layers and ration 1.5.

Reaction Forces

Selection set	Units	Sum X	Sum Y	Sum Z	Resultant
Entire Body	lb	-77.4663	5774.58	-0.138704	5775.1

Study Results

Default Results

Name	Type	Min	Location	Max	Location
XDisp	UX: X Displacement	-0.0451471 in Node: 7961	(2210.91 mm, 8981.08 mm, 6240.41 mm)	0.105557 in Node: 156581	(7050.72 mm, 6839.65 mm, 6265.02 mm)
Stress1300	VON: von	0.00228005	(8418.42 mm,	19137 psi	(3044.34 mm,

	Mises Stress	psi Node: 5200	7008.45 mm, 6254.45 mm)	Node: 72176	8121.06 mm, 6166.59 mm)
YDisp25	UY: Y Displacement	-0.717738 in Node: 41427	(-1334.61 mm, 8649.43 mm, 6242.79 mm)	0.0504943 in Node: 769	(8441.86 mm, 7058.84 mm, 6265.02 mm)
Strain	ESTRN: Equivalent Strain	1.64752e-009 Node: 5200	(8418.42 mm, 7008.45 mm, 6254.45 mm)	0.0074518 Node: 115130	(8282.73 mm, 6692.13 mm, 6166.59 mm)

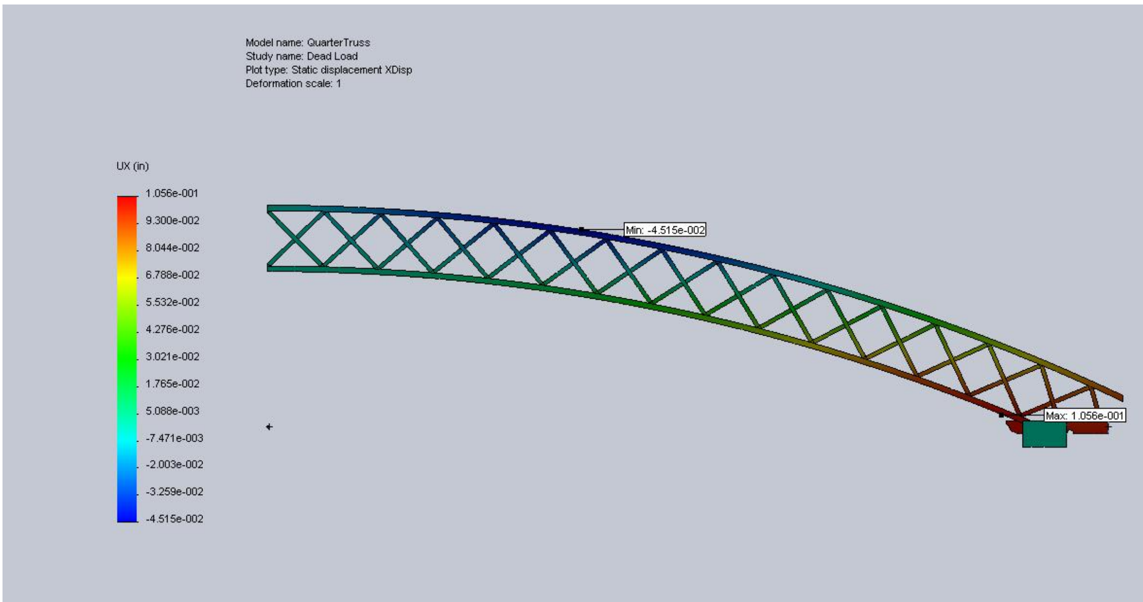

QuarterTruss-Dead Load-Displacement-XDisp

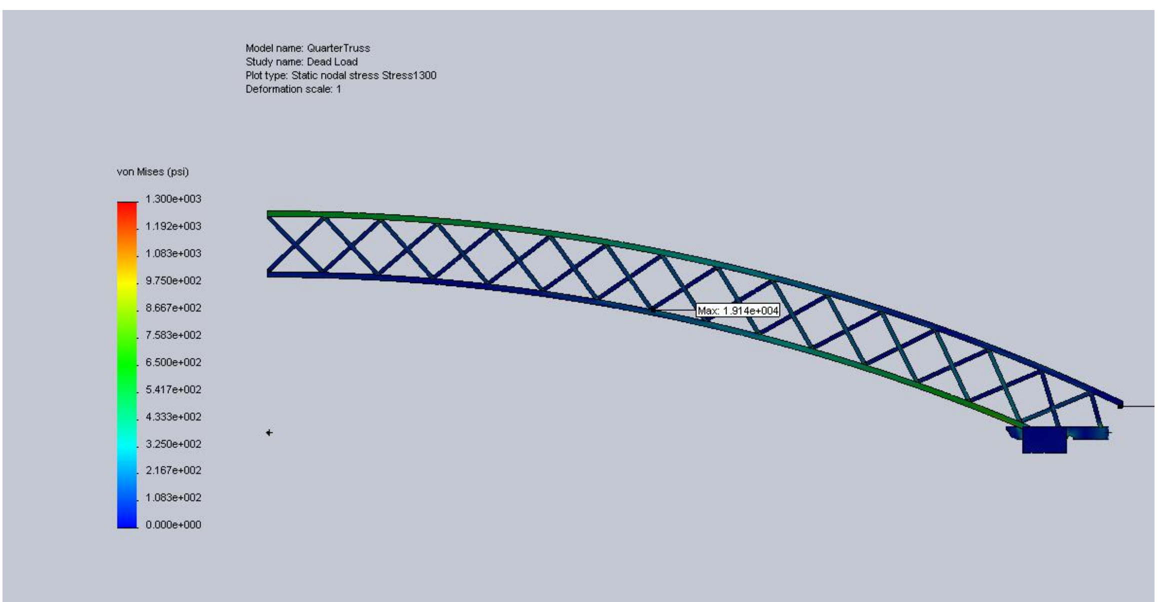

QuarterTruss-Dead Load-Stress-Stress1300

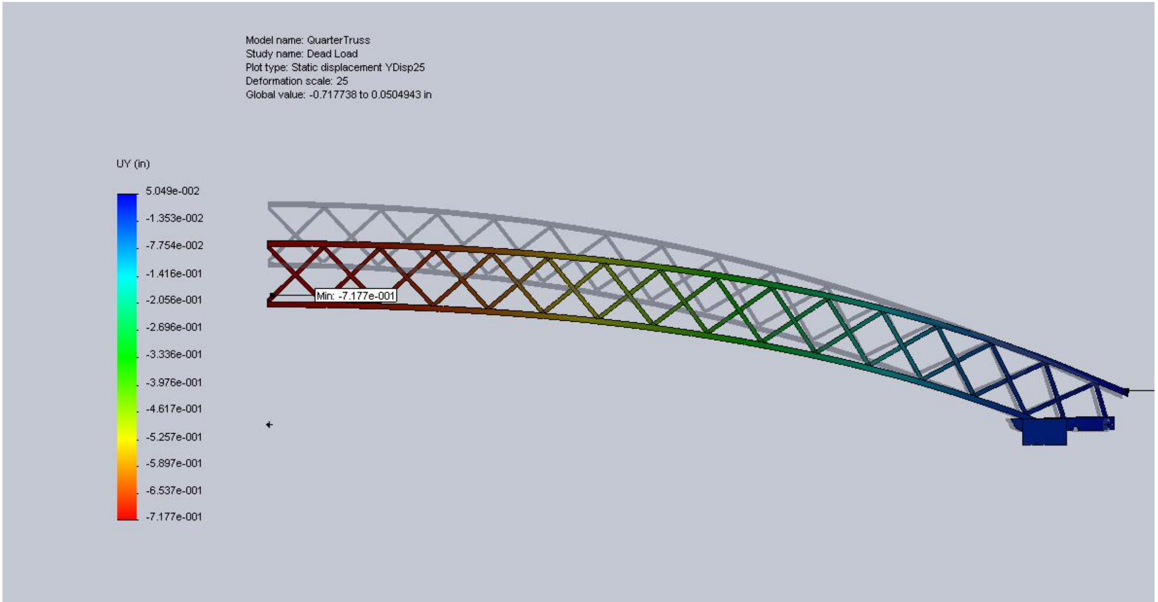

QuarterTruss-Dead Load-Displacement-YDisp25

QuarterTruss-Dead Load-Strain-Strain

Stress analysis of QuarterTruss
Dead and Prestress

Table of Contents

List of Figures

Description

Summarize the FEM analysis on QuarterTruss

Loads and Restraints

Load

Load name	Selection set	Loading type	Description
Pressure-1 <BothChordsQ2-1>	on with Pressure - 17.95 psi normal to reference plane Edge< 1 >	Sequential Loading	
Pressure-2 <WallBearingH-1>	on with Pressure - 17.95 psi normal to reference plane Edge< 1 >	Sequential Loading	
Pressure-3 <WallBearingH-1>	on with Pressure - 17.95 psi normal to reference plane Edge< 1 >	Sequential Loading	
Pressure-4 <WallBearingH-1>	on with Pressure - 17.95 psi normal to reference plane Edge< 1 >	Sequential Loading	
Pressure-5 <>	on with Pressure - 17.95 psi normal to reference plane Top Plane	Sequential Loading	
Pressure-6 <>	on with Pressure - 17.95 psi normal to reference plane Top Plane	Sequential Loading	
Pressure-7 <>	on with Pressure - 17.95 psi normal to reference plane Top Plane	Sequential Loading	
Pressure-8 <>	on with Pressure - 17.95 psi normal to reference plane Top Plane	Sequential Loading	
Pressure-9 <>	on with Pressure - 17.95 psi normal to reference plane Top Plane	Sequential Loading	
Pressure-10 <>	on with Pressure - 17.95 psi normal to reference plane Top Plane	Sequential Loading	
Pressure-11 <>	on with Pressure -	Sequential Loading	

	17.95 psi normal to reference plane Top Plane		
Pressure-12 <>	on with Pressure -17.95 psi normal to reference plane Top Plane	Sequential Loading	
Pressure-13 <>	on with Pressure -17.95 psi normal to reference plane Top Plane	Sequential Loading	
Pressure-14 <>	on with Pressure -17.95 psi normal to reference plane Top Plane	Sequential Loading	
Pressure-15 <>	on with Pressure -17.95 psi normal to reference plane Top Plane	Sequential Loading	
Pressure-16 <>	on with Pressure -17.95 psi normal to reference plane Top Plane	Sequential Loading	
Pressure-17 <>	on with Pressure -17.95 psi normal to reference plane Top Plane	Sequential Loading	
Pressure-18 <>	on with Pressure -17.95 psi normal to reference plane Top Plane	Sequential Loading	
Pressure-19 <>	on with Pressure -17.95 psi normal to reference plane Top Plane	Sequential Loading	
Pressure-20 <BothChordsQ2-1>	on 1 Face(s) with Pressure -36.93 psi normal to reference plane Top Plane	Sequential Loading	

Connector Definitions

Connector name	Selection set	Loading type	Description
Spring Connector-1 <IronBlockTopQ-1, IronBlockBottomQ-1>	Spring(Flat parallel faces) Connectors on 2 Face(s); with distributed normal stiffness of 1.12e+006 (lb/in)/in^2 and distributed shear stiffness of 0 (lb/in)/in^2; with pre-tension of 6520.00000	Sequential Loading	

	N		
Spring Connector-2 <IronBlockBottomH-1, IronBlockTopH-1>	Spring(Flat parallel faces) Connectors on 2 Face(s); with distributed normal stiffness of 1.12e+006 (lb/in)/in^2 and distributed shear stiffness of 0 (lb/in)/in^2; with pre-tension of 6520.00000 N	Sequential Loading	
Spring Connector-3 <IronBlockTopH-85, IronBlockBottomH-56>	Spring(Flat parallel faces) Connectors on 2 Face(s); with distributed normal stiffness of 1.12e+006 (lb/in)/in^2 and distributed shear stiffness of 0 (lb/in)/in^2; with pre-tension of 6520.00000 N	Sequential Loading	
Spring Connector-5 <IronBlockTopH-87, IronBlockBottomH-58>	Spring(Flat parallel faces) Connectors on 2 Face(s); with distributed normal stiffness of 1.12e+006 (lb/in)/in^2 and distributed shear stiffness of 0 (lb/in)/in^2; with pre-tension of 6520.00000 N	Sequential Loading	
Spring Connector-6 <IronBlockBottomH-59, IronBlockTopH-88>	Spring(Flat parallel faces) Connectors on 2 Face(s); with distributed normal stiffness of 1.12e+006 (lb/in)/in^2 and distributed shear stiffness of 0 (lb/in)/in^2; with pre-tension of 6520.00000 N	Sequential Loading	
Spring Connector-7 <IronBlockTopH-89, IronBlockBottomH-60>	Spring(Flat parallel faces) Connectors on 2 Face(s); with distributed normal stiffness of 1.12e+006 (lb/in)/in^2 and distributed shear stiffness of 0 (lb/in)/in^2; with pre-tension of 6520.00000	Sequential Loading	

	N		
Spring Connector-8 <IronBlockBottomH-61, IronBlockTopH-90>	Spring(Flat parallel faces) Connectors on 2 Face(s); with distributed normal stiffness of 1.12e+006 (lb/in)/in^2 and distributed shear stiffness of 0 (lb/in)/in^2; with pre-tension of 6520.00000 N	Sequential Loading	
Spring Connector-9 <IronBlockTopH-91, IronBlockBottomH-62>	Spring(Flat parallel faces) Connectors on 2 Face(s); with distributed normal stiffness of 1.12e+006 (lb/in)/in^2 and distributed shear stiffness of 0 (lb/in)/in^2; with pre-tension of 6520.00000 N	Sequential Loading	
Spring Connector-10 <IronBlockBottomH-63, IronBlockTopH-92>	Spring(Flat parallel faces) Connectors on 2 Face(s); with distributed normal stiffness of 1.12e+006 (lb/in)/in^2 and distributed shear stiffness of 0 (lb/in)/in^2; with pre-tension of 6520.00000 N	Sequential Loading	
Spring Connector-11 <IronBlockTopH-93, IronBlockBottomH-64>	Spring(Flat parallel faces) Connectors on 2 Face(s); with distributed normal stiffness of 1.12e+006 (lb/in)/in^2 and distributed shear stiffness of 0 (lb/in)/in^2; with pre-tension of 6520.00000 N	Sequential Loading	
Spring Connector-13 <IronBlockTopH-95, IronBlockBottomH-66>	Spring(Flat parallel faces) Connectors on 2 Face(s); with distributed normal stiffness of 1.12e+006 (lb/in)/in^2 and distributed shear stiffness of 0 (lb/in)/in^2; with pre-tension of 6520.00000	Sequential Loading	

	N		
Spring Connector-14 <IronBlockBottomH-67, IronBlockTopH-96>	Spring(Flat parallel faces) Connectors on 2 Face(s); with distributed normal stiffness of 1.12e+006 (lb/in)/in^2 and distributed shear stiffness of 0 (lb/in)/in^2; with pre-tension of 6520.00000 N	Sequential Loading	
Spring Connector-15 <IronBlockTopH-97, Bearing_Block3-1>	Spring(Flat parallel faces) Connectors on 2 Face(s); with distributed normal stiffness of 1.12e+006 (lb/in)/in^2 and distributed shear stiffness of 0 (lb/in)/in^2; with pre-tension of 6520.00000 N	Sequential Loading	
Spring Connector-16 <IronBlockTopH-44, Bearing_Block3-1>	Spring(Flat parallel faces) Connectors on 2 Face(s); with distributed normal stiffness of 1.12e+006 (lb/in)/in^2 and distributed shear stiffness of 0 (lb/in)/in^2; with pre-tension of 6520.00000 N	Sequential Loading	
Spring Connector-17 <IronBlockTopH-94, IronBlockBottomH-65>	Spring(Flat parallel faces) Connectors on 2 Face(s); with distributed normal stiffness of 1.12e+006 (lb/in)/in^2 and distributed shear stiffness of 0 (lb/in)/in^2; with pre-tension of 6520.00000 N	Sequential Loading	
Spring Connector-18 <IronBlockTopH-86, IronBlockBottomH-57>	Spring(Flat parallel faces) Connectors on 2 Face(s); with distributed normal stiffness of 1.12e+006 (lb/in)/in^2 and distributed shear stiffness of 0 (lb/in)/in^2; with pre-tension of 6520.00000	Sequential Loading	

	N		
Spring Connector-21 <tie2-1, Bearing_Block3-1>	Spring(Flat parallel faces) Connectors on 2 Face(s); with total normal stiffness of 42203 lb/in and total shear stiffness of 0 lb/in; with pre-tension of 6000.00000 N	Sequential Loading	

Mesh Control Information

Control-2 <IronBlockBottomQ-1, IronBlockBottomH-1, IronBlockBottomH-56, IronBlockBottomH-57, IronBlockBottomH-58, IronBlockBottomH-59, IronBlockBottomH-60, IronBlockBottomH-61, IronBlockBottomH-62, IronBlockBottomH-63, IronBlockBottomH-64, IronBloc...	Mesh control on 66 Face(s) with seed 0.3125 in, 3 layers and ration 1.5.
Control-4 <WallBearingH-1>	Mesh control on 1 Component(s) with seed 63.4987 mm, 3 layers and ration 1.5.
Control-6 <Bearing_Block3-1>	Mesh control on 2 Face(s) with seed 0.5 in, 3 layers and ration 1.5.

Reaction Forces

Selection set	Units	Sum X	Sum Y	Sum Z	Resultant
Entire Body	lb	-23.4454	2016.28	0.381709	2016.41

Study Results

Default Results

Name	Type	Min	Location	Max	Location
XDisp	UX: X Displacement	-0.0391381 in Node: 398	(2735.6 mm, 8891.74 mm, 6265.02 mm)	0.0187758 in Node: 156343	(5390.23 mm, 7444.5 mm, 6265.02 mm)
Stress1300	VON: von Mises Stress	0.00214668 psi Node: 5200	(8418.42 mm, 7008.45 mm, 6254.45 mm)	12047.9 psi Node: 78801	(6703.24 mm, 7046.87 mm, 6238.98 mm)
YDisp25	UY: Y Displacement	-0.396075 in Node: 1004	(-1389 mm, 9200.89 mm, 6265.02 mm)	0.00438964 in Node: 114685	(7101.63 mm, 6768.33 mm, 6166.59 mm)
Strain	ESTRN: Equivalent Strain	1.55115e-009 Node: 5200	(8418.42 mm, 7008.45 mm, 6254.45 mm)	0.00698877 Node: 115130	(8282.73 mm, 6692.13 mm, 6166.59 mm)

QuarterTruss-Dead Load+Prestress-Displacement-XDisp

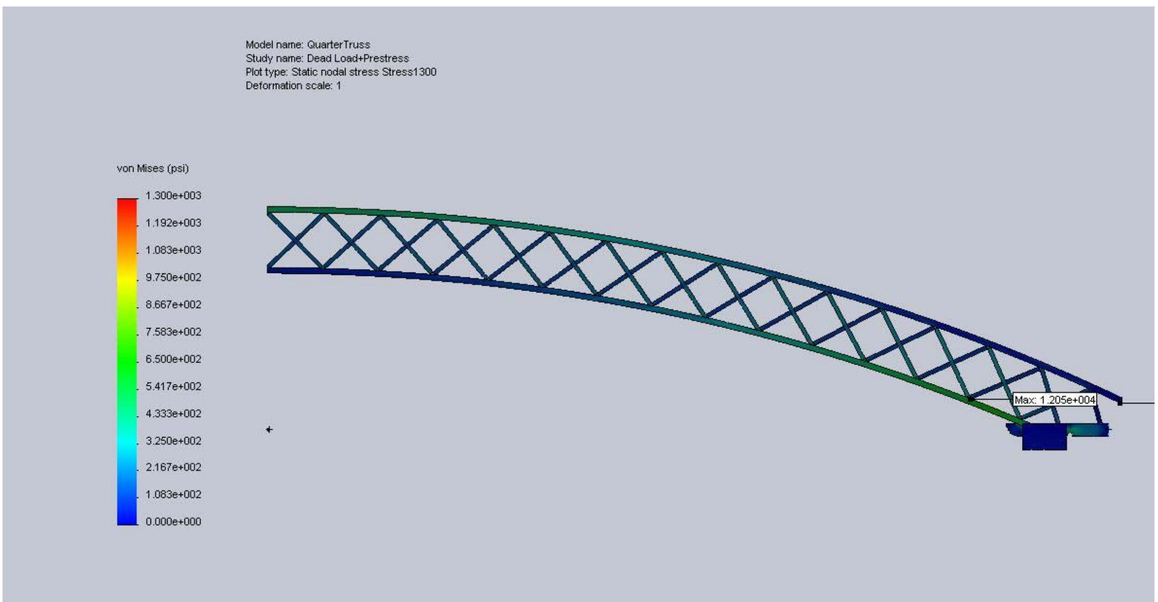

QuarterTruss-Dead Load+Prestress-Stress-Stress1300

QuarterTruss-Dead Load+Prestress-Displacement-YDisp25

QuarterTruss-Dead Load+Prestress-Strain-Strain

Stress analysis of QuarterTruss
Dead, Prestress & Snow

Table of Contents

List of Figures

Description

Summarize the FEM analysis on QuarterTruss

Load

Load name	Selection set	Loading type	Description
Pressure-1 <BothChordsQ2-1>	on with Pressure -47.86 psi normal to reference plane Edge< 1 >	Sequential Loading	
Pressure-2 <WallBearingH-1>	on with Pressure -47.86 psi normal to reference plane Edge< 1 >	Sequential Loading	
Pressure-3 <WallBearingH-1>	on with Pressure -47.86 psi normal to reference plane Edge< 1 >	Sequential Loading	
Pressure-4 <WallBearingH-1>	on with Pressure -47.86 psi normal to reference plane Edge< 1 >	Sequential Loading	
Pressure-5 <>	on with Pressure -47.86 psi normal to reference plane Top Plane	Sequential Loading	
Pressure-6 <>	on with Pressure -47.86 psi normal to reference plane Top Plane	Sequential Loading	
Pressure-7 <>	on with Pressure -47.86 psi normal to reference plane Top Plane	Sequential Loading	
Pressure-8 <>	on with Pressure -47.86 psi normal to reference plane Top Plane	Sequential Loading	
Pressure-9 <>	on with Pressure -47.86 psi normal to reference plane Top Plane	Sequential Loading	
Pressure-10 <>	on with Pressure -17.95 psi normal to reference plane Top Plane	Sequential Loading	
Pressure-11 <>	on with Pressure -47.86 psi normal to reference plane Top Plane	Sequential Loading	

Pressure-12 <>	on with Pressure -47.86 psi normal to reference plane Top Plane	Sequential Loading	
Pressure-13 <>	on with Pressure -47.86 psi normal to reference plane Top Plane	Sequential Loading	
Pressure-14 <>	on with Pressure -47.86 psi normal to reference plane Top Plane	Sequential Loading	
Pressure-15 <>	on with Pressure -47.86 psi normal to reference plane Top Plane	Sequential Loading	
Pressure-16 <>	on with Pressure -47.86 psi normal to reference plane Top Plane	Sequential Loading	
Pressure-17 <>	on with Pressure -47.86 psi normal to reference plane Top Plane	Sequential Loading	
Pressure-18 <>	on with Pressure -47.86 psi normal to reference plane Top Plane	Sequential Loading	
Pressure-19 <>	on with Pressure -47.86 psi normal to reference plane Top Plane	Sequential Loading	
Pressure-20 <BothChordsQ2-1>	on 1 Face(s) with Pressure -47.86 psi normal to reference plane Top Plane	Sequential Loading	

Reaction Forces

Selection set	Units	Sum X	Sum Y	Sum Z	Resultant
Entire Body	lb	-214.156	5173.21	-2.38204	5177.64

Study Results

Default Results

Name	Type	Min	Location	Max	Location
XDisp	UX: X Displacement	-0.103069 in Node: 7943	(2246.87 mm, 8975.35 mm, 6240.41 mm)	0.134697 in Node: 156560	(6906.19 mm, 6898.3 mm, 6265.02 mm)
Stress2	VON: von Mises Stress	0.00484067 psi	(8418.42 mm, 7008.45 mm,	37087.6 psi Node: 72176	(3044.34 mm, 8121.06 mm,

		Node: 5200	6254.45 mm)		6166.59 mm)
YDisp25	UY: Y Displacement	-1.33975 in Node: 41307	(-1280.23 mm, 8701.54 mm, 6242.79 mm)	0.0458651 in Node: 769	(8441.86 mm, 7058.84 mm, 6265.02 mm)
Strain1	ESTRN: Equivalent Strain	3.49778e-009 Node: 5200	(8418.42 mm, 7008.45 mm, 6254.45 mm)	0.0126245 Node: 115130	(8282.73 mm, 6692.13 mm, 6166.59 mm)

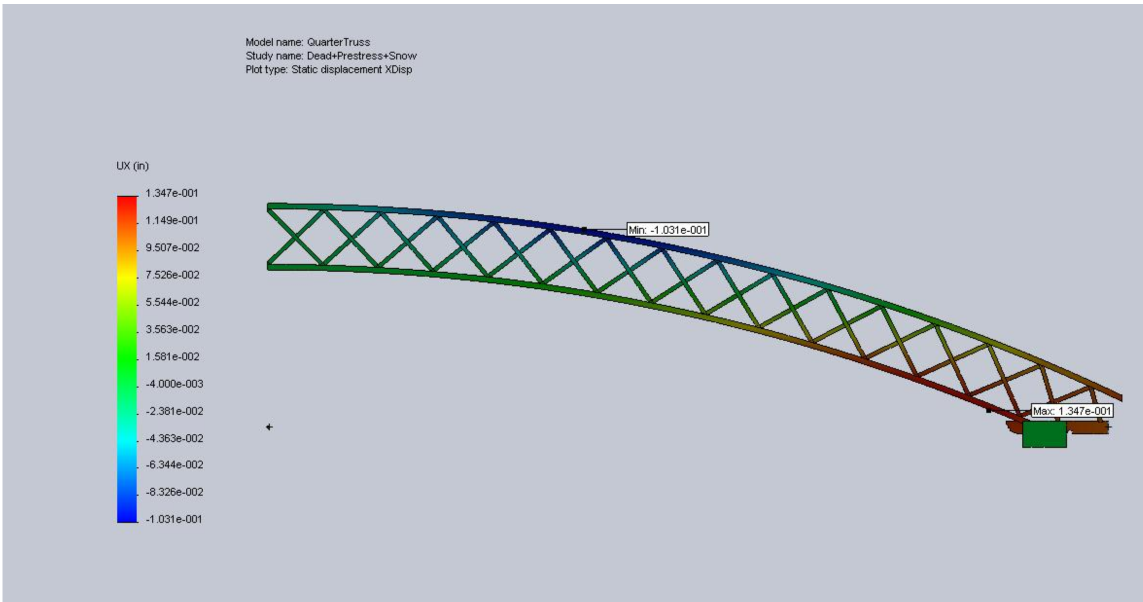

QuarterTruss-Dead+Prestress+Snow-Displacement-XDisp

QuarterTruss-Dead+Prestress+Snow-Stress-Stress2

QuarterTruss-Dead+Prestress+Snow-Displacement-YDisp25

QuarterTruss-Dead+Prestress+Snow-Strain-Strain1

Stress analysis of QuarterTruss
Dead, Prestress, Snow, Displacement

Table of Contents

List of Figures

Description

Summarize the FEM analysis on QuarterTruss

Load

Load name	Selection set	Loading type	Description
Pressure-1 <BothChordsQ2-1>	on with Pressure - 47.86 psi normal to reference plane Edge< 1 >	Sequential Loading	
Pressure-2 <WallBearingH-1>	on with Pressure - 47.86 psi normal to reference plane Edge< 1 >	Sequential Loading	
Pressure-3 <WallBearingH-1>	on with Pressure - 47.86 psi normal to reference plane Edge< 1 >	Sequential Loading	
Pressure-4 <WallBearingH-1>	on with Pressure - 47.86 psi normal to reference plane Edge< 1 >	Sequential Loading	
Pressure-5 <>	on with Pressure - 47.86 psi normal to reference plane Top Plane	Sequential Loading	
Pressure-6 <>	on with Pressure - 47.86 psi normal to reference plane Top Plane	Sequential Loading	
Pressure-7 <>	on with Pressure - 47.86 psi normal to reference plane Top Plane	Sequential Loading	
Pressure-8 <>	on with Pressure - 47.86 psi normal to reference plane Top Plane	Sequential Loading	
Pressure-9 <>	on with Pressure - 47.86 psi normal to reference plane Top Plane	Sequential Loading	
Pressure-10 <>	on with Pressure - 17.95 psi normal to reference plane Top Plane	Sequential Loading	
Pressure-11 <>	on with Pressure - 47.86 psi normal to reference plane Top Plane	Sequential Loading	
Pressure-12 <>	on with Pressure -	Sequential Loading	

	47.86 psi normal to reference plane Top Plane		
Pressure-13 <>	on with Pressure -47.86 psi normal to reference plane Top Plane	Sequential Loading	
Pressure-14 <>	on with Pressure -47.86 psi normal to reference plane Top Plane	Sequential Loading	
Pressure-15 <>	on with Pressure -47.86 psi normal to reference plane Top Plane	Sequential Loading	
Pressure-16 <>	on with Pressure -47.86 psi normal to reference plane Top Plane	Sequential Loading	
Pressure-17 <>	on with Pressure -47.86 psi normal to reference plane Top Plane	Sequential Loading	
Pressure-18 <>	on with Pressure -47.86 psi normal to reference plane Top Plane	Sequential Loading	
Pressure-19 <>	on with Pressure -47.86 psi normal to reference plane Top Plane	Sequential Loading	
Pressure-20 <BothChordsQ2-1>	on 1 Face(s) with Pressure -47.86 psi normal to reference plane Top Plane	Sequential Loading	

Reaction Forces

Selection set	Units	Sum X	Sum Y	Sum Z	Resultant
Entire Body	lb	625.938	8118.02	-0.409785	8142.12

Study Results

Default Results

Name	Type	Min	Location	Max	Location
XDisp	UX: X Displacement	-0.635331 in Node: 141058	(8003.55 mm, 6615.93 mm, 6217.39 mm)	5.48768e-005 in Node: 99594	(7800.46 mm, 6488.93 mm, 6166.59 mm)
Stress1300	VON: von Mises Stress	0.0221506 psi Node: 5205	(8441.85 mm, 6997.37 mm,	42065.7 psi Node: 114021	(-1368.36 mm,

			6254.45 mm)		6706.72 mm, 6181.18 mm)
YDsip25	UY: Y Displacement	-0.197133 in Node: 771	(8441.86 mm, 7058.84 mm, 6166.59 mm)	0.819569 in Node: 136	(-1256.74 mm, 9264.01 mm, 6265.02 mm)
Strain	ESTRN: Equivalent Strain	1.60056e-008 Node: 5205	(8441.85 mm, 6997.37 mm, 6254.45 mm)	0.00854454 Node: 142273	(7185.35 mm, 6643.08 mm, 6209.19 mm)

QuarterTruss-Dead+P+S+Disp-Displacement-XDisp

QuarterTruss-Dead+P+S+Disp-Stress-Stress1300

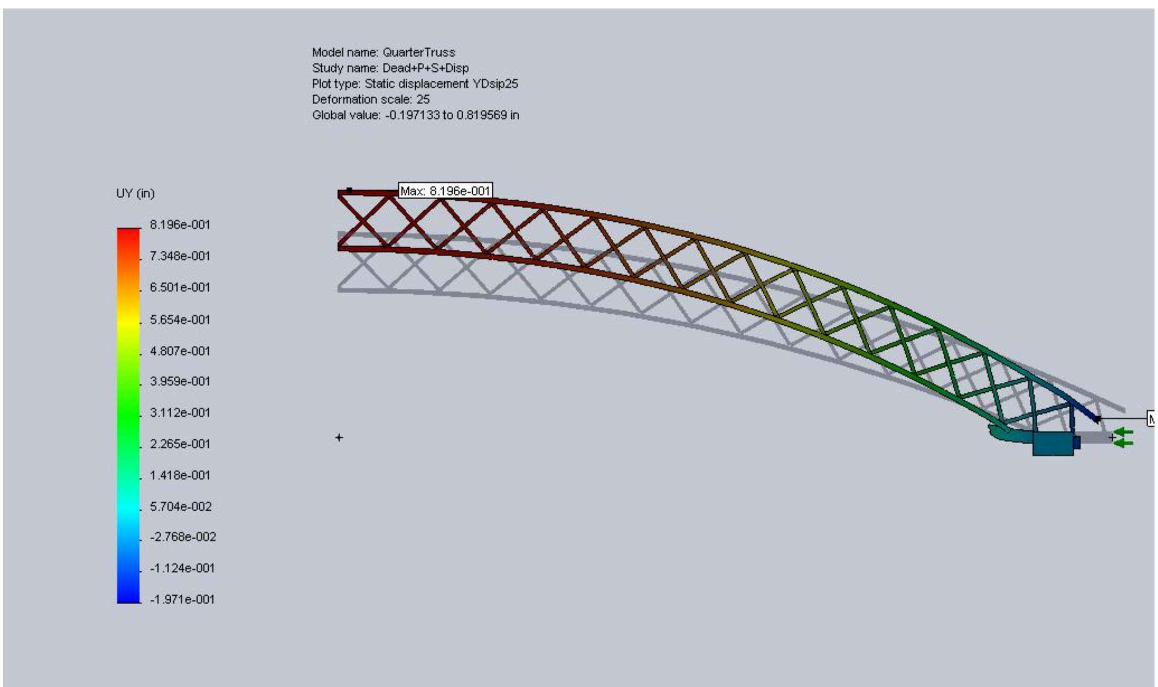

QuarterTruss-Dead+P+S+Disp-Displacement-YDsip25

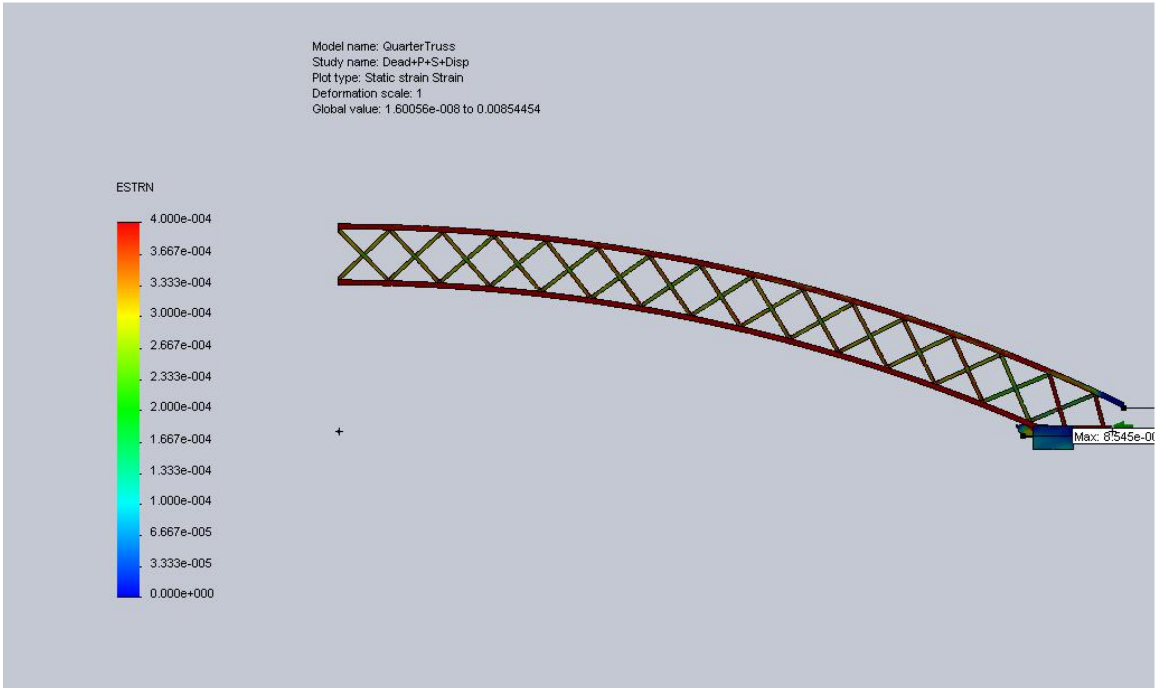

QuarterTruss-Dead+P+S+Disp-Strain-Strain

Stress analysis of RoofPurlinsDeckNailersPlaster3 Snow Load

Table of Contents

List of Figures

Description

Summarize the FEM analysis on RoofPurlinsDeckNailersPlaster3

Study Properties

Study name	Snow
Analysis type	Static
Mesh Type:	Mixed Mesh
Solver type	FFEPlus
Inplane Effect:	Off
Soft Spring:	Off
Inertial Relief:	Off
Thermal Effect:	Input Temperature
Zero strain temperature	50.000000
Units	Fahrenheit
Include fluid pressure effects from COSMOSFloWorks	Off
Friction:	Off
Ignore clearance for surface contact	Off
Use Adaptive Method:	Off

Units

Unit system:	English (IPS)
Length/Displacement	in
Temperature	Fahrenheit
Angular velocity	rad/s
Stress/Pressure	psi

Material Properties

Solid Bodies

No.	Body Name	Material	Mass	Volume
1	LathFQ-1	Eastern White Pine	67.8125 lb	5098.68 in^3
2	LathFQ-2	Eastern White Pine	67.8125 lb	5098.68 in^3
3	LathFQ-3	Eastern White Pine	67.8125 lb	5098.68 in^3
4	LathFQ-4	Eastern White Pine	67.8125 lb	5098.68 in^3
5	PurlinH-1	Eastern White Pine	29.7035 lb	2233.34 in^3
6	PurlinH-10	Eastern White Pine	29.7035 lb	2233.34 in^3

7	PurlinH-11	Eastern White Pine	29.7035 lb	2233.34 in^3
8	PurlinH-12	Eastern White Pine	29.7035 lb	2233.34 in^3
9	PurlinH-13	Eastern White Pine	29.7035 lb	2233.34 in^3
10	PurlinH-14	Eastern White Pine	29.7035 lb	2233.34 in^3
11	PurlinH-15	Eastern White Pine	29.7035 lb	2233.34 in^3
12	PurlinH-16	Eastern White Pine	29.7035 lb	2233.34 in^3
13	PurlinH-17	Eastern White Pine	29.7035 lb	2233.34 in^3
14	PurlinH-18	Eastern White Pine	29.7035 lb	2233.34 in^3
15	PurlinH-2	Eastern White Pine	29.7035 lb	2233.34 in^3
16	PurlinH-3	Eastern White Pine	29.7035 lb	2233.34 in^3
17	PurlinH-35	Eastern White Pine	29.7035 lb	2233.34 in^3
18	PurlinH-36	Eastern White Pine	29.7035 lb	2233.34 in^3
19	PurlinH-37	Eastern White Pine	29.7035 lb	2233.34 in^3
20	PurlinH-38	Eastern White Pine	29.7035 lb	2233.34 in^3
21	PurlinH-39	Eastern White Pine	29.7035 lb	2233.34 in^3
22	PurlinH-4	Eastern White Pine	29.7035 lb	2233.34 in^3
23	PurlinH-40	Eastern White Pine	29.7035 lb	2233.34 in^3
24	PurlinH-41	Eastern White Pine	29.7035 lb	2233.34 in^3
25	PurlinH-42	Eastern White Pine	29.7035 lb	2233.34 in^3
26	PurlinH-43	Eastern White Pine	29.7035 lb	2233.34 in^3
27	PurlinH-44	Eastern White Pine	29.7035 lb	2233.34 in^3
28	PurlinH-45	Eastern White Pine	29.7035 lb	2233.34 in^3
29	PurlinH-46	Eastern White Pine	29.7035 lb	2233.34 in^3
30	PurlinH-47	Eastern White Pine	29.7035 lb	2233.34 in^3
31	PurlinH-48	Eastern White Pine	29.7035 lb	2233.34 in^3
32	PurlinH-49	Eastern White Pine	29.7035 lb	2233.34 in^3
33	PurlinH-5	Eastern White Pine	29.7035 lb	2233.34 in^3

34	PurlinH-50	Eastern White Pine	29.7035 lb	2233.34 in^3
35	PurlinH-6	Eastern White Pine	29.7035 lb	2233.34 in^3
36	PurlinH-7	Eastern White Pine	29.7035 lb	2233.34 in^3
37	PurlinH-8	Eastern White Pine	29.7035 lb	2233.34 in^3
38	PurlinH-9	Eastern White Pine	29.7035 lb	2233.34 in^3
39	TieRodHalf-1	Ductile Iron (SN)	244.941 lb	858.22 in^3
40	TrussQ-1	Eastern White Pine	202.84 lb	15251.1 in^3
41	TrussQ-2	Eastern White Pine	202.84 lb	15251.1 in^3
42	plasternailer-1	Eastern White Pine	12.8683 lb	967.538 in^3
43	plasternailer-13	Eastern White Pine	12.8683 lb	967.538 in^3
44	plasternailer-14	Eastern White Pine	12.8683 lb	967.538 in^3
45	plasternailer-15	Eastern White Pine	12.8683 lb	967.538 in^3
46	plasternailer-16	Eastern White Pine	12.8683 lb	967.538 in^3
47	plasternailer-17	Eastern White Pine	12.8683 lb	967.538 in^3
48	plasternailer-18	Eastern White Pine	12.8683 lb	967.538 in^3
49	plasternailer-19	Eastern White Pine	12.8683 lb	967.538 in^3
50	plasternailer-2	Eastern White Pine	12.8683 lb	967.538 in^3
51	plasternailer-20	Eastern White Pine	12.8683 lb	967.538 in^3
52	plasternailer-3	Eastern White Pine	12.8683 lb	967.538 in^3
53	plasternailer-4	Eastern White Pine	12.8683 lb	967.538 in^3
54	plasternailer-5	Eastern White Pine	12.8683 lb	967.538 in^3
55	plasternailer-6	Eastern White Pine	12.8683 lb	967.538 in^3

Shells

No.	Shell Name	Material	Formulation	Thickness	Mass/Volume
1	Shell-1	Eastern White Pine	Thin	1 in	242.508 lb /0.658733 in^3
2	Shell-2	Eastern White Pine	Thin	1 in	242.508 lb /0.658733 in^3
3	Shell-6	Plaster	Thin	0.5625 in	7034.84 lb

					/0.318243 in^3
4	Shell-7	Plaster	Thin	0.5625 in	7034.84 lb /0.318243 in^3

Material name:	Eastern White Pine
Description:	
Material Source:	Library files
Material Library Name:	ewpine
Material Model Type:	Linear Elastic Isotropic

Property Name	Value	Units	Value Type
Elastic modulus	1.24e+006	psi	Constant
Poisson's ratio	0.344	NA	Constant
Shear modulus	7.346e+005	psi	Constant
Mass density	0.0133	lb/in^3	Constant
Tensile strength	10600	psi	Constant
Compressive strength	4800	psi	Constant
Yield strength	10600	psi	Constant
Thermal expansion coefficient	2.7778e-006	/Fahrenheit	Constant
Thermal conductivity	1.605e-006	BTU/(in.s.F)	Constant
Specific heat	0.59723	Btu/(lb.F)	Constant

Material name:	Ductile Iron (SN)
Description:	
Material Source:	Library files
Material Library Name:	cosmos materials
Material Model Type:	Linear Elastic Isotropic

Property Name	Value	Units	Value Type
Elastic modulus	1.7405e+007	psi	Constant
Poisson's ratio	0.31	NA	Constant
Shear modulus	1.1168e+007	psi	Constant
Mass density	0.28541	lb/in^3	Constant
Tensile strength	1.2498e+005	psi	Constant
Yield strength	79986	psi	Constant
Thermal expansion coefficient	6.1111e-006	/Fahrenheit	Constant
Thermal conductivity	0.0010031	BTU/(in.s.F)	Constant
Specific heat	0.1075	Btu/(lb.F)	Constant

Material name:	Plaster
Description:	Plaster
Material Source:	Library files
Material Library Name:	plaster
Material Model Type:	Linear Elastic Isotropic

Property Name	Value	Units	Value Type
Elastic modulus	2.5e+007	psi	Constant
Poisson's ratio	0.25	NA	Constant
Shear modulus	1e+007	psi	Constant

Mass density	0.7986	lb/in^3	Constant
Tensile strength	325	psi	Constant
Compressive strength	825	psi	Constant
Yield strength	325	psi	Constant
Thermal expansion coefficient	9.2e-006	/Fahrenheit	Constant
Thermal conductivity	6.6874e-007	BTU/(in.s.F)	Constant
Specific heat	0.23889	Btu/(lb.F)	Constant

Loads and Restraints

Restraint

Restraint name	Selection set	Description
Restraint-1 <TrussQ-1>	on 1 Face(s)Roller/Sliding	
Restraint-2 <TrussQ-1, PurlinH-17, PurlinH-16, PurlinH-15, PurlinH-14, PurlinH-13, PurlinH-12, PurlinH-11, PurlinH-10, PurlinH-9, PurlinH-8, PurlinH-7, PurlinH-6, PurlinH-5, PurlinH-4, PurlinH-3, PurlinH-2, PurlinH-1>	on 19 Face(s) symmetry	
Restraint-4 <PurlinH-1, PurlinH-2, PurlinH-3, PurlinH-4, PurlinH-5, PurlinH-6, PurlinH-7, PurlinH-8, PurlinH-9, PurlinH-10, PurlinH-11, PurlinH-12, PurlinH-13, PurlinH-14, PurlinH-15, PurlinH-16, PurlinH-17>	on 17 Face(s) symmetry	
Restraint-6 <DeckShell-1, TrussQ-1, DeckShell-2>	on 2 Edge(s) with respect to reference geometry Face< 1 > with rotation 0.000000 rad along plane Dir 1 rotation 0.000000 rad along plane Dir 2 displacement 0.000000 in normal to reference plane	
Restraint-7 <DeckShell-1, PurlinH-10, DeckShell-2, PlasterShellFH-1, PlasterShellFH-2>	on 4 Edge(s) with respect to reference geometry Face< 1 > with rotation 0.000000 rad along plane Dir 1 rotation 0.000000 rad along plane Dir 2 displacement 0.000000 in normal to reference plane	
Restraint-8 <TrussQ-2>	on 1 Face(s) with displacement 0.000000 in along face Dir 2.	
Restraint-9 <TrussQ-2, PurlinH-50, PurlinH-49, PurlinH-48, PurlinH-47,	on 18 Face(s) symmetry	

PurlinH-46, PurlinH-45, PurlinH-44, PurlinH-43, PurlinH-42, PurlinH-41, PurlinH-40, PurlinH-39, PurlinH-38, PurlinH-37, PurlinH-36, PurlinH-35, PurlinH-18>		
Restraint-10 <PurlinH-18, PurlinH-35, PurlinH-36, PurlinH-37, PurlinH-38, PurlinH-39, PurlinH-40, PurlinH-41, PurlinH-42, PurlinH-43, PurlinH-44, PurlinH-45, PurlinH-46, PurlinH-47, PurlinH-48, PurlinH-49, PurlinH-50>	on 17 Face(s) symmetry	

Load

Load name	Selection set	Loading type	Description
Pressure-3 <DeckShell-1, DeckShell-2, TrussQ-2>	on 2 Face(s) with Pressure 0.21 psi normal to reference plane Edge< 1 >	Sequential Loading	

Connector Definitions

Connector name	Selection set	Loading type	Description
Elastic Connector-3 <plasternailer-1, plasternailer-2, plasternailer-3, plasternailer-4, plasternailer-5, plasternailer-13, plasternailer-6>	Elastic support Connectors on 7 Face(s); with total normal stiffness of 197.5 lb/in and total shear stiffness of 0 lb/in	Sequential Loading	
Elastic Connector-4 <plasternailer-14, plasternailer-15, plasternailer-16, plasternailer-17, plasternailer-18, plasternailer-19, plasternailer-20>	Elastic support Connectors on 7 Face(s); with total normal stiffness of 197.5 lb/in and total shear stiffness of 0 lb/in	Sequential Loading	

Contact

Contact state: Touching faces - Bonded

Contact Set-1	Bonded contact pair: Between selected entities of PurlinH-1 and TrussQ-1
Description:	
Contact Set-3	Bonded contact pair: Between selected entities

	of DeckShell-1 and DeckShell-2
Description:	
Contact Set-4	Bonded contact pair: Between selected entities of PurlinH-18 and TrussQ-2
Description:	
Contact Set-5	Bonded contact pair: Between selected entities of TrussQ-2 and TrussQ-1
Description:	
Contact Set-6	Bonded contact pair: Between selected entities of DeckShell-2 and DeckShell-1
Description:	
Contact Set-7	Bonded contact pair: Between selected entities of plasternailer-1 and plasternailer-20
Description:	
Contact Set-29	Bonded contact pair: Between selected entities of LathFQ-4 and plasternailer-1
Description:	
Contact Set-31	Bonded contact pair: Between selected entities of PlasterShellFH-1 and LathFQ-2
Description:	

Mesh Information

Mesh Type:	Mixed Mesh
Mesher Used:	Standard
Automatic Transition:	On
Smooth Surface:	On
Jacobian Check:	4 Points
Element Size:	82.55 mm
Tolerance:	4.1275 mm
Quality:	High
Number of elements:	165622
Number of nodes:	341513
Time to complete mesh(hh;mm;ss):	00:03:41
Computer name:	PDH-KWOODMAN

Mesh Control Information:

Control-4 <plasternailer-17, plasternailer-19, plasternailer-18, plasternailer-20>	Mesh control on 4 Component(s) with seed 1.375 in, 3 layers and ration 1.5.

Reaction Forces

Selection set	Units	Sum X	Sum Y	Sum Z	Resultant
Entire Body	lb	-2.68394	16829.1	0.816091	16829.1

Reaction Moments

Selection set	Units	Sum X	Sum Y	Sum Z	Resultant
Entire Body	lb-in	2089.88	-784.901	-174.209	2239.2

Free-Body Forces

Selection set	Units	Sum X	Sum Y	Sum Z	Resultant
Entire Body	lb	-0.0621483	0.126291	-0.371909	0.397654

Free-body Moments

Selection set	Units	Sum X	Sum Y	Sum Z	Resultant
Entire Body	lb-in	2306.78	1037.22	8647.08	9009.38

Study Results

Default Results

Name	Type	Min	Location	Max	Location
Strain1	ESTRN: Equivalent Strain	1.60645e-008 Element: 85263	(5145.27 mm, -1358.96 mm, 200.438 mm)	0.00231216 Element: 83619	(3845.96 mm, -1687.05 mm, 140.865 mm)
Displacement3	UX: X Displacement	-0.181215 in Node: 212695	(-13098 mm, -1552.85 mm, 136.234 mm)	0.17664 in Node: 188139	(3747.1 mm, -1552.85 mm, 136.234 mm)
Displacement4	UY: Y Displacement	-0.684976 in Node: 20154	(-4662.74 mm, 810.09 mm, -2186.34 mm)	0.0403518 in Node: 195690	(-14506.3 mm, -1340.69 mm, 136.234 mm)
Stress2	VON: von Mises Stress	0.0192609 psi Node: 186176	(5085.11 mm, -1307.61 mm, 185.446 mm)	12956.1 psi Node: 166643	(3841.82 mm, -1688.58 mm, 139.862 mm)
Stress3	VON: von Mises Stress	0.0192609 psi Node: 186176	(5085.11 mm, -1307.61 mm, 185.446 mm)	12956.1 psi Node: 166643	(3841.82 mm, -1688.58 mm, 139.862 mm)

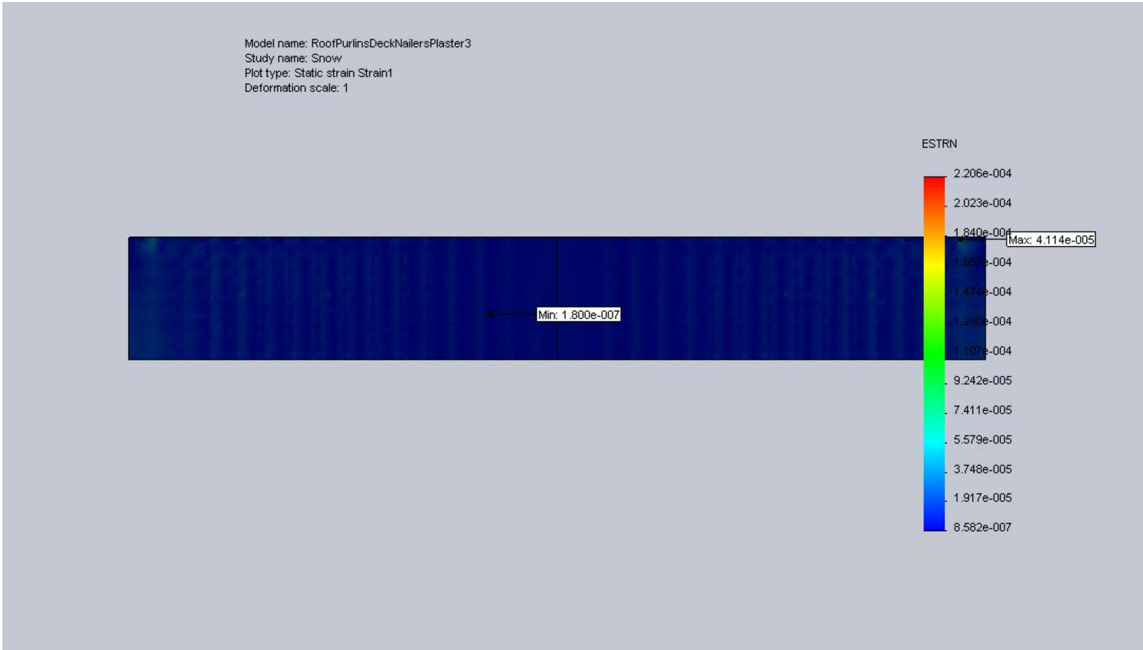

RoofPurlinsDeckNailersPlaster3-Snow-Strain-Strain1

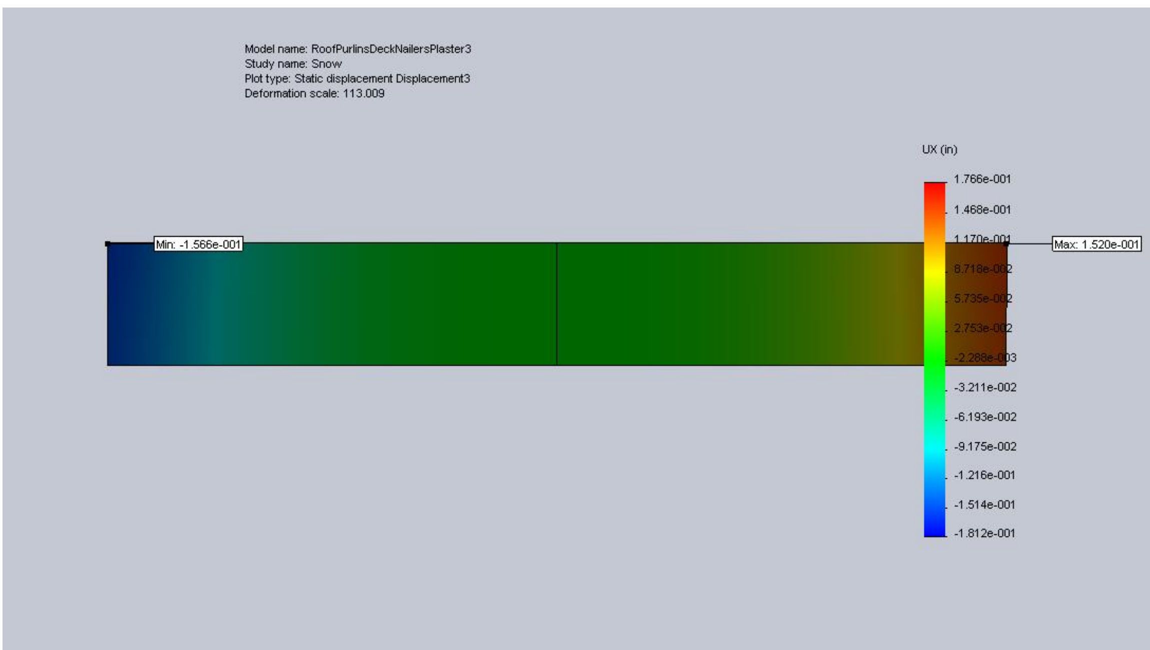

RoofPurlinsDeckNailersPlaster3-Snow-Displacement-Displacement3

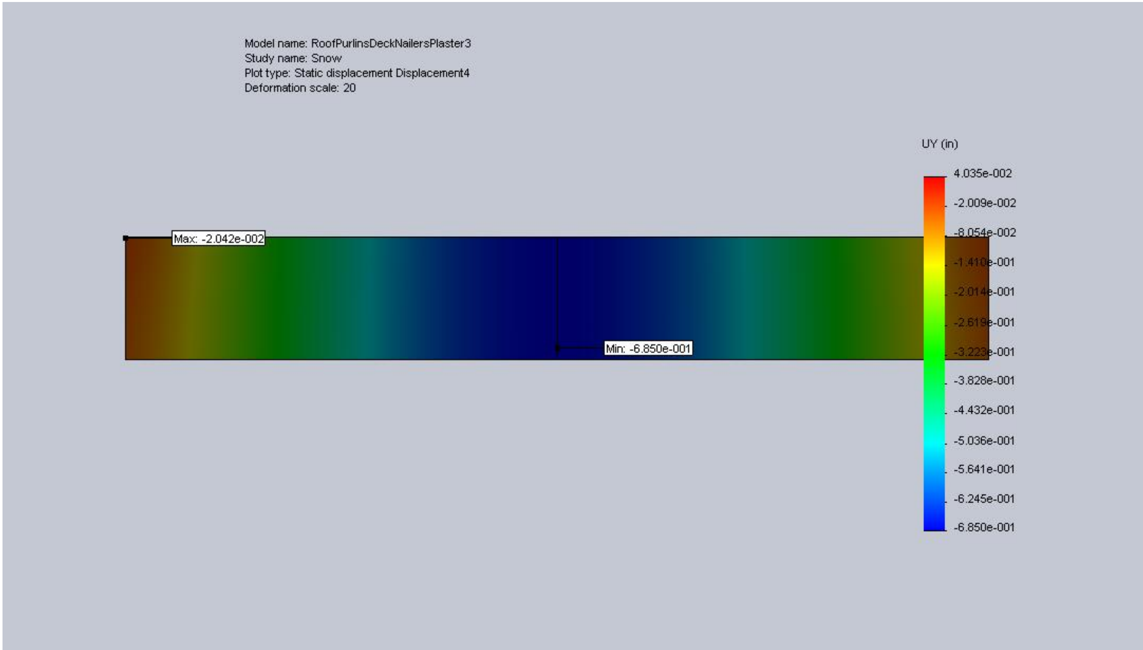

RoofPurlinsDeckNailersPlaster3-Snow-Displacement-Displacement4

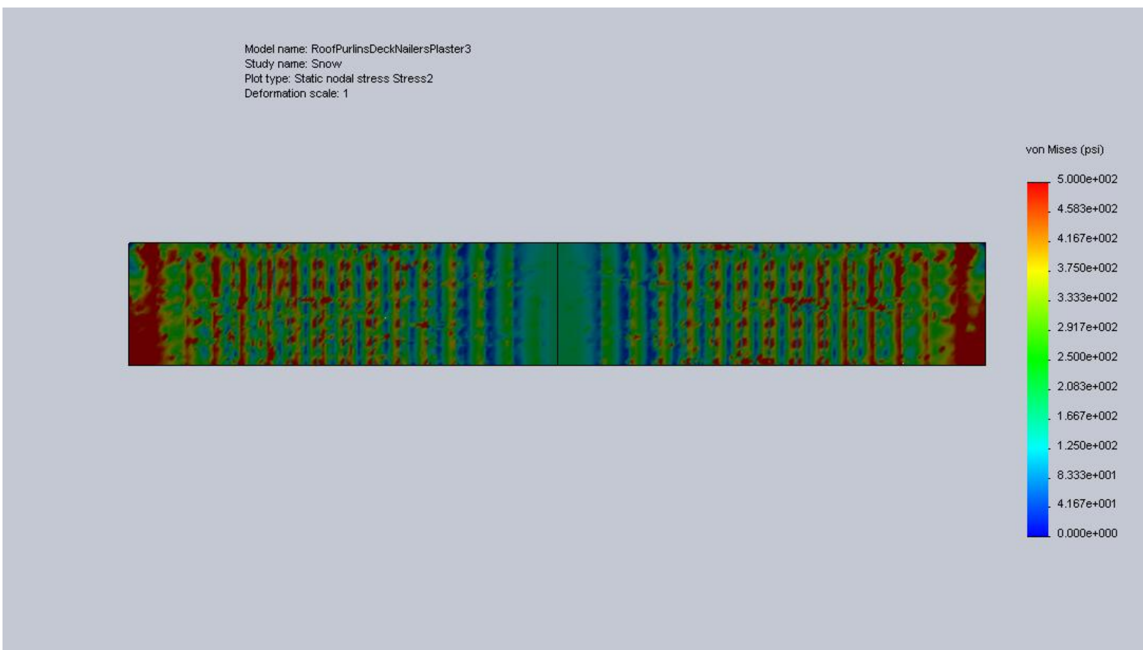

RoofPurlinsDeckNailersPlaster3-Snow-Stress-Stress2

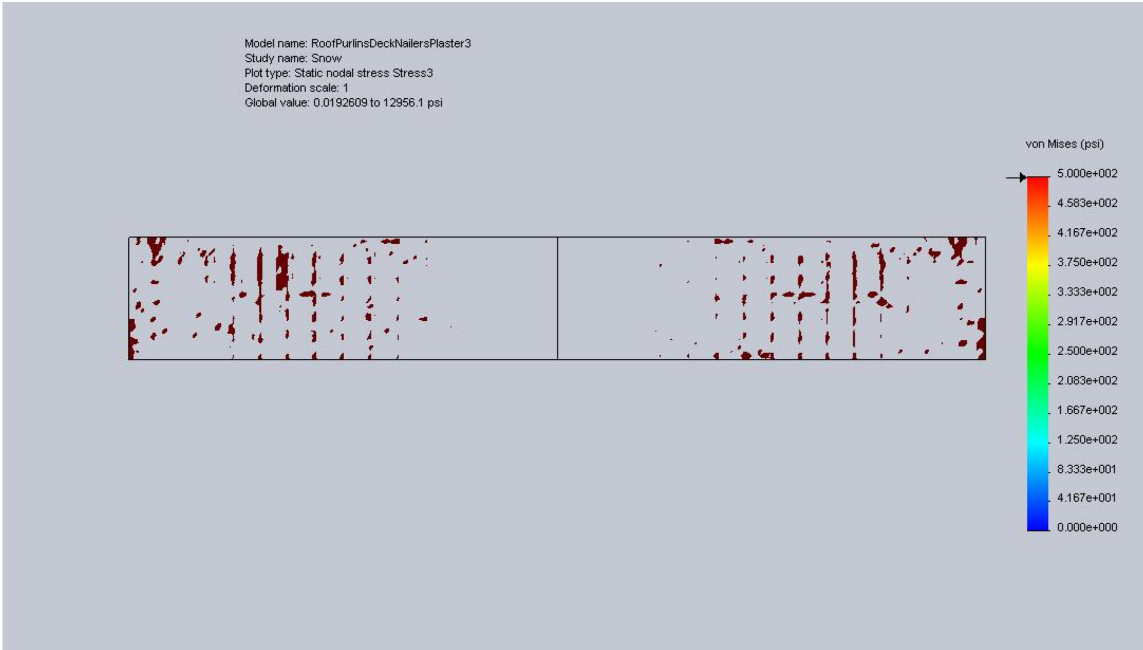

RoofPurlinsDeckNailersPlaster3-Snow-Stress-Stress3

Stress analysis of RoofPurlinsDeckNailersPlaster3 Thermal Increase

Table of Contents

List of Figures

Description

Summarize the FEM analysis on RoofPurlinsDeckNailersPlaster3

Load

Load name	Selection set	Loading type	Description
Temperature-1 <plasternailer-18, LathFQ-4, PlasterShellFH-1, LathFQ-3, plasternailer-5, plasternailer-19, plasternailer-13, plasternailer-20, LathFQ-1, plasternailer-6, plasternailer-4, LathFQ-2, plasternailer-16, plasternailer-17, plasternailer-14...	on 59 Component(s) with temperature 100 Fahrenheit	Sequential Loading	

Reaction Forces

Selection set	Units	Sum X	Sum Y	Sum Z	Resultant
Entire Body	lb	2.51323	-16.7393	-2.63316	17.1305

Reaction Moments

Selection set	Units	Sum X	Sum Y	Sum Z	Resultant
Entire Body	lb-in	42165.1	-7632.34	-33.7291	42850.3

Study Results

Default Results

Name	Type	Min	Location	Max	Location
Strain1	ESTRN: Equivalent Strain	6.41378e-010 Element: 88647	(5138.68 mm, -1367.91 mm, 160.84 mm)	0.00980836 Element: 13812	(3930.27 mm, -864.013 mm, 52.914 mm)
Stress3500	VON: von Mises Stress	0.00225719 psi Node: 183742	(5155.42 mm, -1375.81 mm, 234.659 mm)	20125.5 psi Node: 30581	(3927.91 mm, -865.2 mm, 54.97 mm)

XDisp	UX: X Displacement	-0.196145 in Node: 226045	(-13299 mm, -864.821 mm, 110.834 mm)	0.191177 in Node: 221085	(3948.16 mm, -864.821 mm, 110.834 mm)
YDisp	UY: Y Displacement	-0.139764 in Node: 104673	(2907.69 mm, -447.314 mm, -2356.14 mm)	0.153288 in Node: 165854	(-4624.18 mm, -1687.62 mm, 136.234 mm)

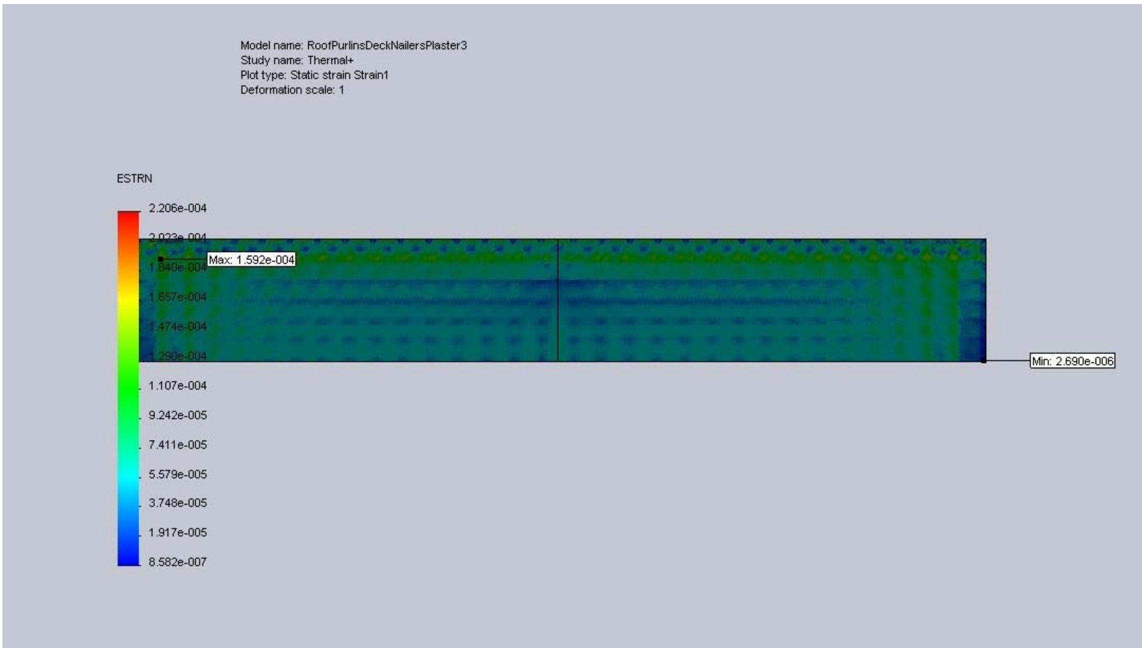

RoofPurlinsDeckNailersPlaster3-Thermal+-Strain-Strain1

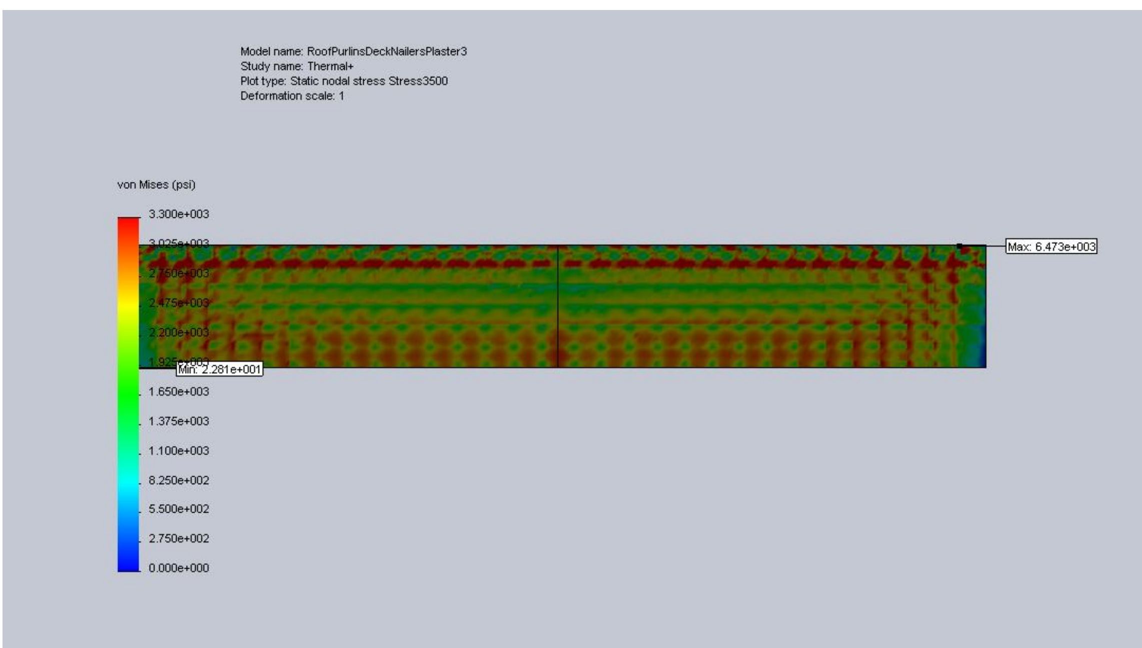

RoofPurlinsDeckNailersPlaster3-Thermal+-Stress-Stress3500

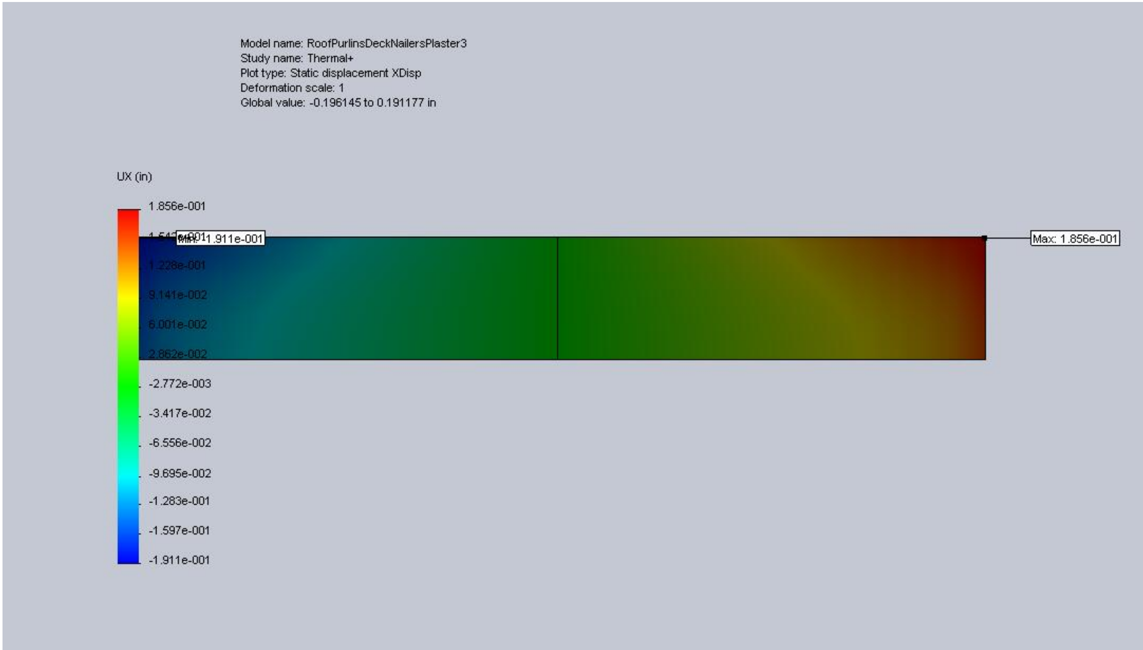

RoofPurlinsDeckNailersPlaster3-Thermal+-Displacement-XDisp

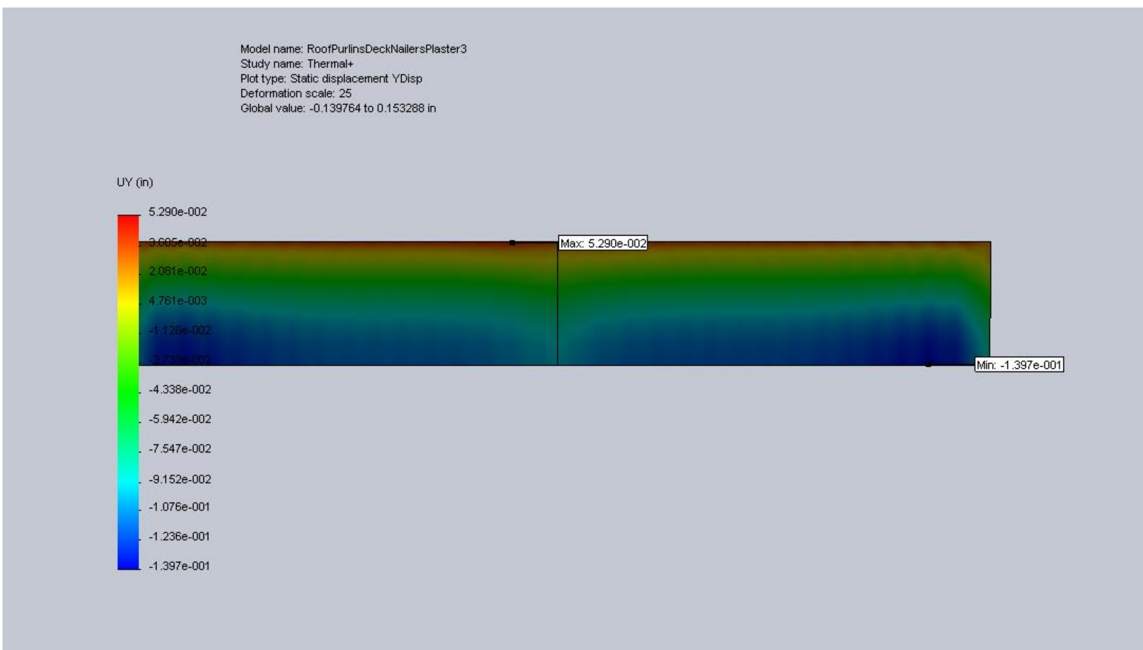

RoofPurlinsDeckNailersPlaster3-Thermal+-Displacement-YDisp

Stress analysis of RoofPurlinsDeckNailersPlaster3 Thermal Decrease

Table of Contents

List of Figures

Description

Summarize the FEM analysis on AutoRecover Of RoofPurlinsDeckNailersPlaster3

Load

Load name	Selection set	Loading type	Description
Temperature-1 <plasternailer-18, LathFQ-4, PlasterShellFH-1, LathFQ-3, plasternailer-5, plasternailer-19, plasternailer-13, plasternailer-20, LathFQ-1, plasternailer-6, plasternailer-4, LathFQ-2, plasternailer-16, plasternailer-17, plasternailer-14...	on 59 Component(s) with temperature 30 Fahrenheit	Sequential Loading	

Reaction Forces

Selection set	Units	Sum X	Sum Y	Sum Z	Resultant
Entire Body	lb	3.39985	16.5663	3.07993	17.1898

Reaction Moments

Selection set	Units	Sum X	Sum Y	Sum Z	Resultant
Entire Body	lb-in	-42250	7628.87	-86.9652	42933.3

Free-Body Forces

Selection set	Units	Sum X	Sum Y	Sum Z	Resultant
Entire Body	lb	4.95739	-49.3397	-20.1441	53.5235

Free-body Moments

Selection set	Units	Sum X	Sum Y	Sum Z	Resultant
Entire Body	lb-in	149291	6672.1	-24932.6	151505

Study Results

Default Results

Name	Type	Min	Location	Max	Location
XDisp	UX: X Displacement	-0.19118 in Node: 221085	(3948.16 mm, -864.821 mm, 110.834 mm)	0.196143 in Node: 226045	(-13299 mm, -864.821 mm, 110.834 mm)
Stress3500	VON: von Mises Stress	0.00123067 psi Node: 183742	(5155.42 mm, -1375.81 mm, 234.659 mm)	20125.5 psi Node: 30581	(3927.91 mm, -865.2 mm, 54.97 mm)
YDisp50	UY: Y Displacement	-0.153289 in Node: 165854	(-4624.18 mm, -1687.62 mm, 136.234 mm)	0.139764 in Node: 104673	(2907.69 mm, -447.314 mm, -2356.14 mm)
Iso2500	VON: von Mises Stress	0.00123067 psi Node: 183742	(5155.42 mm, -1375.81 mm, 234.659 mm)	20125.5 psi Node: 30581	(3927.91 mm, -865.2 mm, 54.97 mm)
Strain	ESTRN: Equivalent Strain	8.89259e-010 Node: 183742	(5155.42 mm, -1375.81 mm, 234.659 mm)	0.0145423 Node: 30581	(3927.91 mm, -865.2 mm, 54.97 mm)

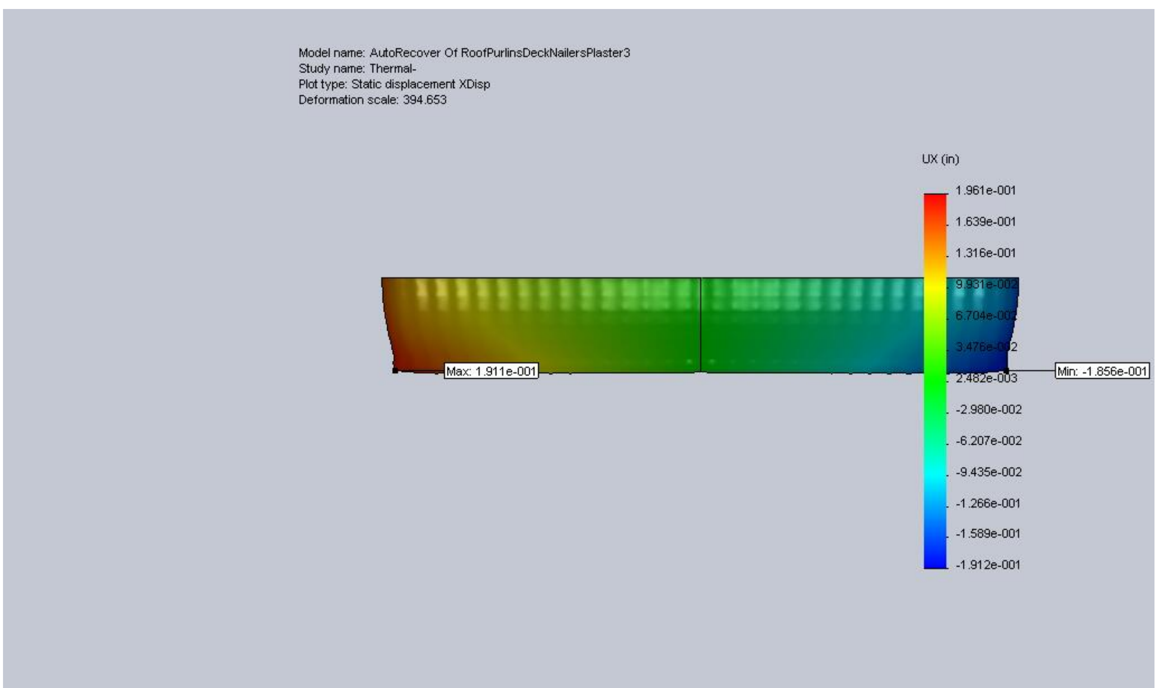

RoofPurlinsDeckNailersPlaster3-Thermal--Displacement-XDisp

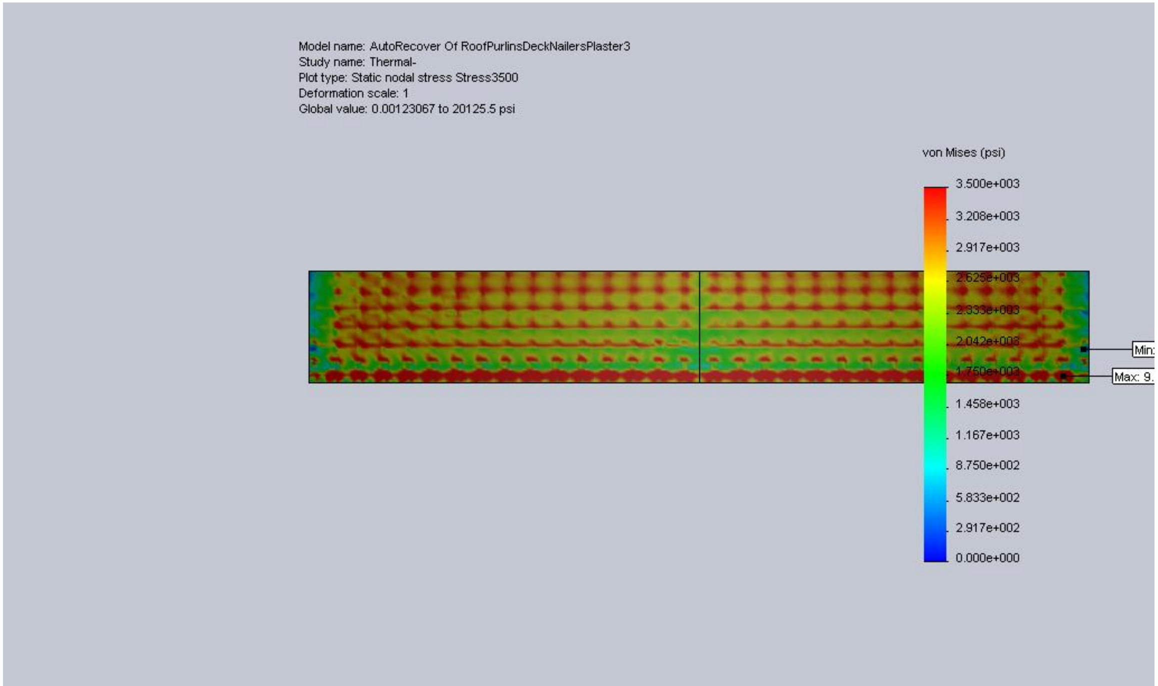

RoofPurlinsDeckNailersPlaster3-Thermal--Stress-Stress3500

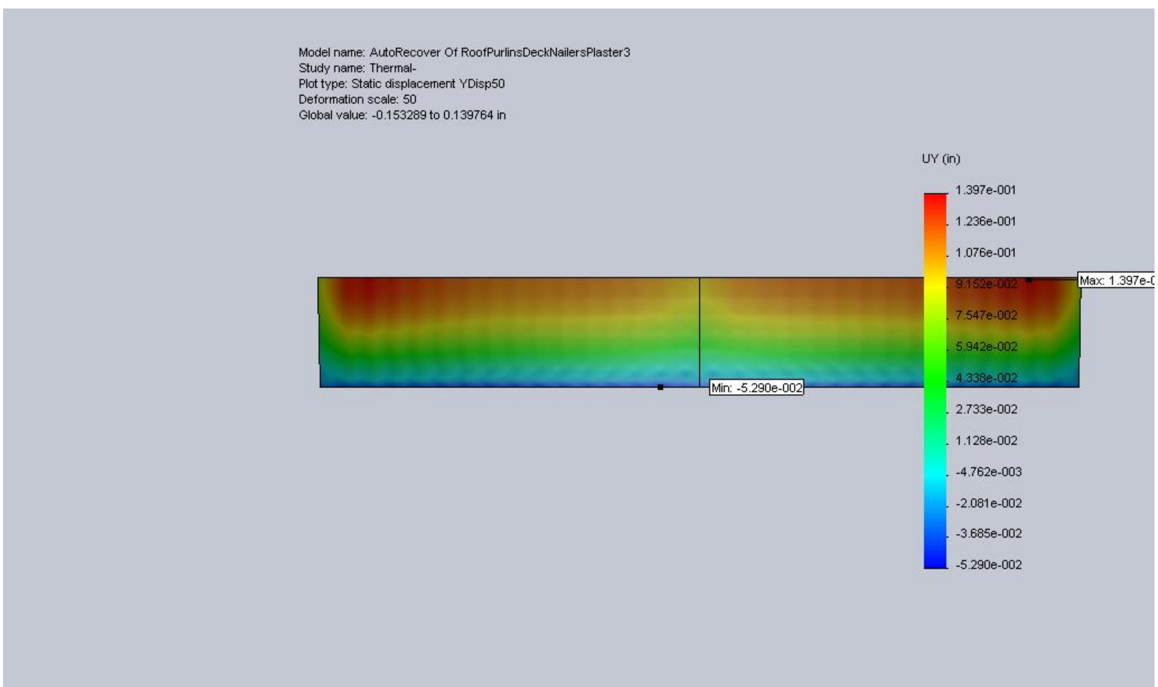

RoofPurlinsDeckNailersPlaster3-Thermal--Displacement-YDisp50

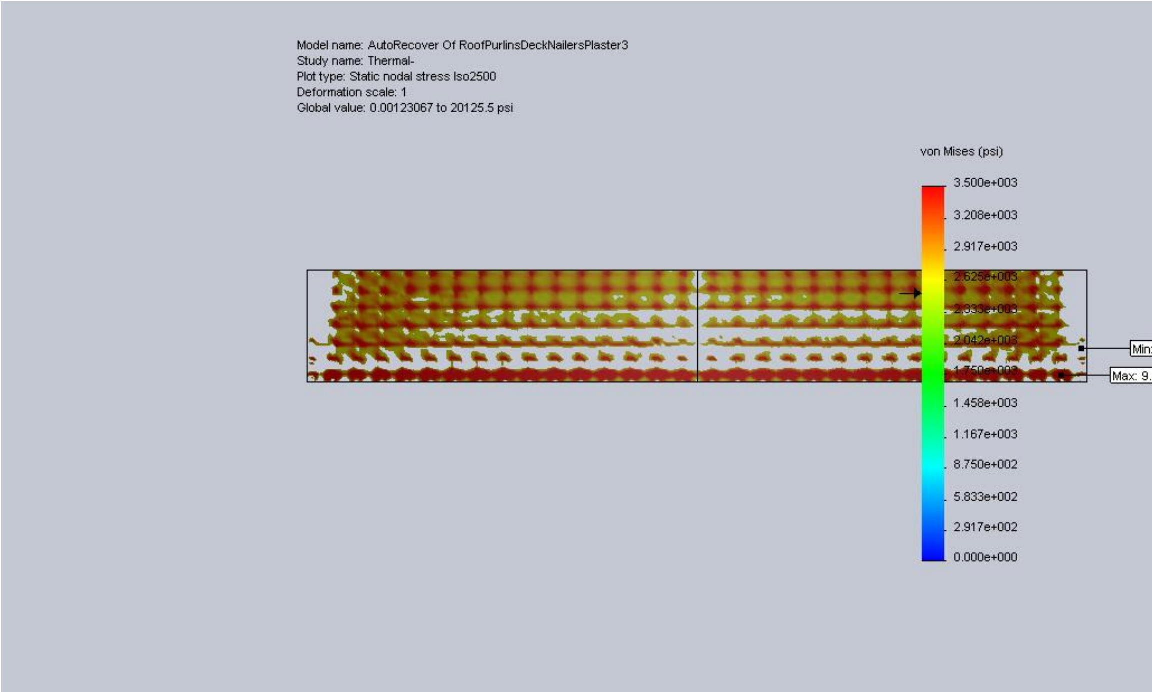

RoofPurlinsDeckNailersPlaster3-Thermal--Stress-Iso2500

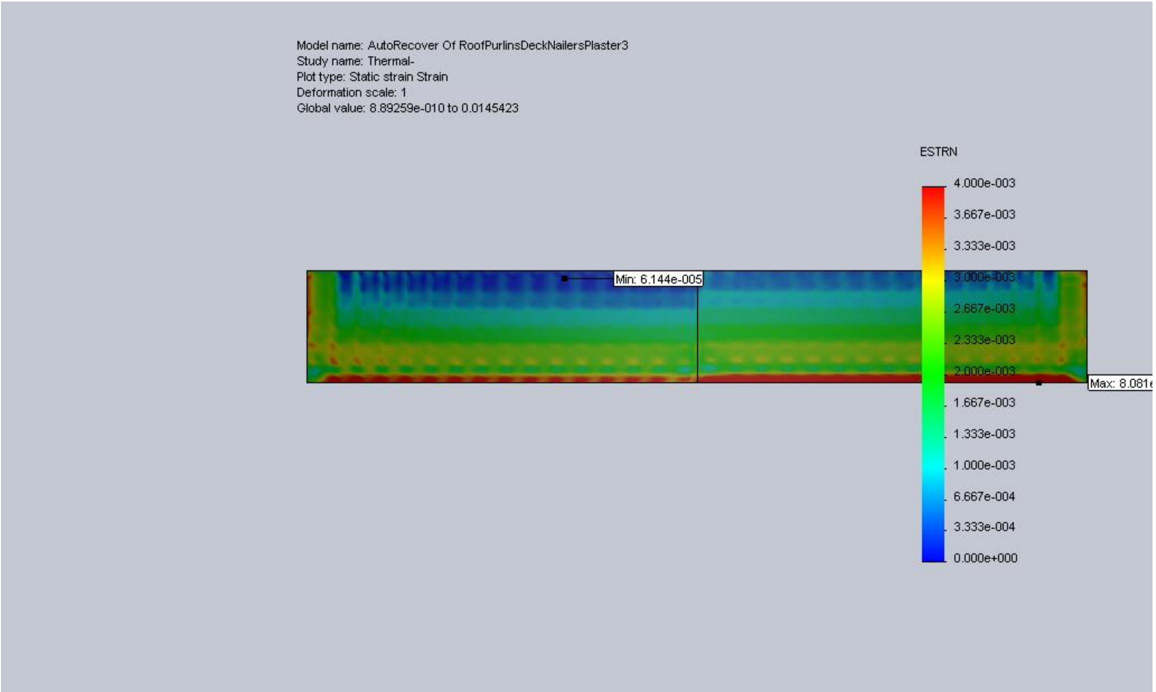

RoofPurlinsDeckNailersPlaster3-Thermal--Strain-Strain

Stress analysis of RoofPurlinsDeckNailersPlaster3

Table of Contents

List of Figures

Description

Summarize the FEM analysis on RoofPurlinsDeckNailersPlaster3

Load

Load name	Selection set	Loading type	Description
Pressure-3 <DeckShell-1, DeckShell-2, TrussQ-2>	on 2 Face(s) with Pressure 0.21 psi normal to reference plane Edge< 1 >	Sequential Loading	
Temperature-1 <PlasterShellFH-1, PlasterShellFH-2, TieRodHalf-1, PurlinH-48, PurlinH-49, PurlinH-50, PurlinH-44, PurlinH-45, PurlinH-46, PurlinH-47, PurlinH-41, PurlinH-42, PurlinH-43, PurlinH-37, PurlinH-38, PurlinH-39, PurlinH-40, DeckShell-2, Pu...	on 41 Component(s) with temperature 50 Fahrenheit	Sequential Loading	

Reaction Forces

Selection set	Units	Sum X	Sum Y	Sum Z	Resultant
Entire Body	lb	11.5081	16859.4	-0.0496709	16859.4

Reaction Moments

Selection set	Units	Sum X	Sum Y	Sum Z	Resultant
Entire Body	lb-in	-13953	2122.06	-36.1036	14113.5

Study Results

Default Results

Name	Type	Min	Location	Max	Location
Stress1500	VON: von Mises Stress	0.00585376 psi Node: 183742	(5155.42 mm, -1375.81 mm, 234.659 mm)	11562.4 psi Node: 166643	(3841.82 mm, -1688.58 mm, 139.862 mm)
Iso1500	VON: von Mises Stress	0.00585376 psi Node: 183742	(5155.42 mm, -1375.81 mm, 234.659 mm)	11562.4 psi Node: 166643	(3841.82 mm, -1688.58 mm, 139.862 mm)

Iso2500	VON: von Mises Stress	0.00585376 psi Node: 183742	(5155.42 mm, -1375.81 mm, 234.659 mm)	11562.4 psi Node: 166643	(3841.82 mm, -1688.58 mm, 139.862 mm)
Iso500	VON: von Mises Stress	0.00585376 psi Node: 183742	(5155.42 mm, -1375.81 mm, 234.659 mm)	11562.4 psi Node: 166643	(3841.82 mm, -1688.58 mm, 139.862 mm)
XDisp	UX: X Displacement	-0.12235 in Node: 196001	(-13135.8 mm, -1568.38 mm, 136.234 mm)	0.119642 in Node: 170215	(3784.98 mm, -1568.38 mm, 136.234 mm)
YDisp	UY: Y Displacement	-0.701509 in Node: 340786	(-4962.4 mm, 804.332 mm, 136.234 mm)	0.0535284 in Node: 195689	(-14506.3 mm, -1410.94 mm, 136.234 mm)
Strain	ESTRN: Equivalent Strain	4.22982e-009 Node: 183742	(5155.42 mm, -1375.81 mm, 234.659 mm)	0.00641794 Node: 299293	(-14377.6 mm, -1084.45 mm, -1627.48 mm)

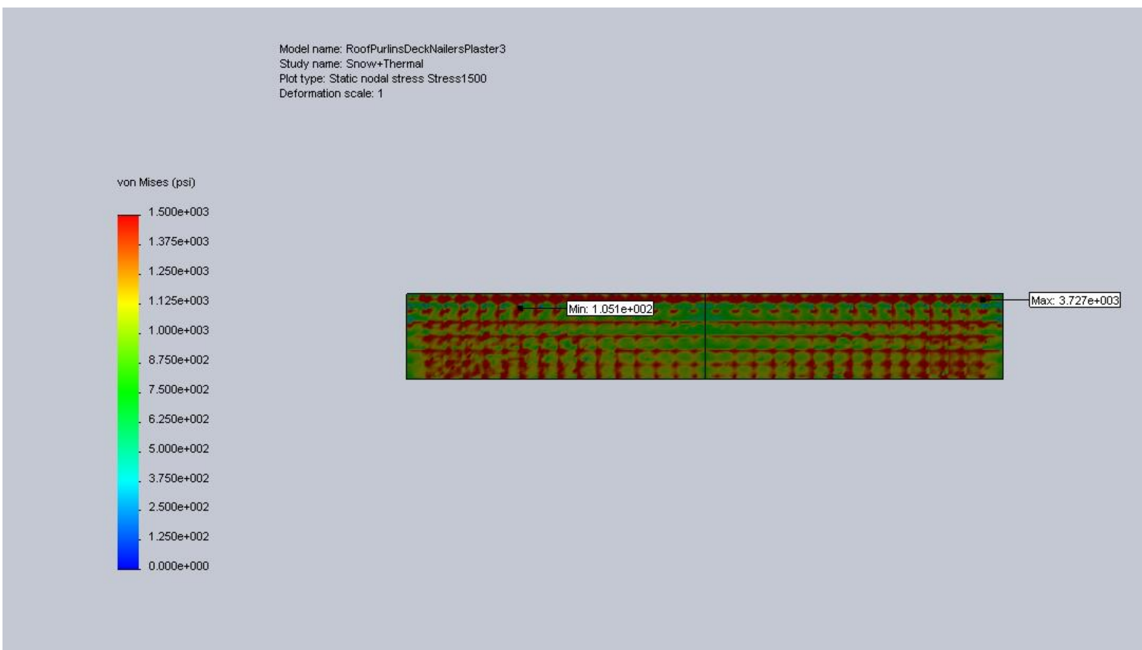

RoofPurlinsDeckNailersPlaster3-Snow+Thermal-Stress-Stress1500

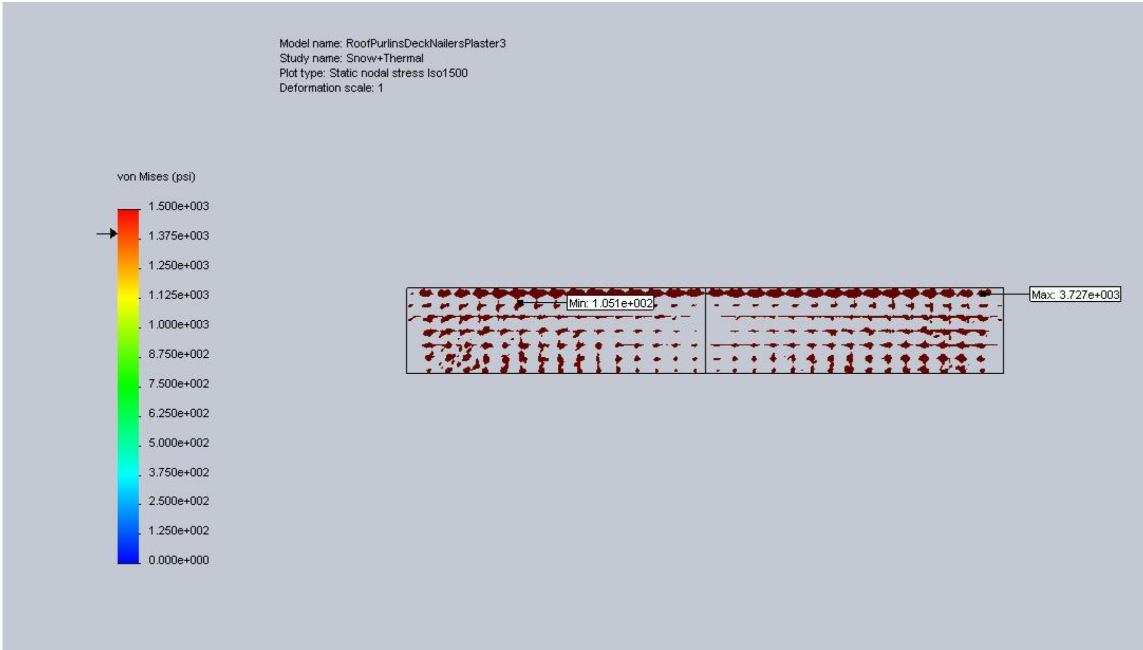

RoofPurlinsDeckNailersPlaster3-Snow+Thermal-Stress-Iso1500

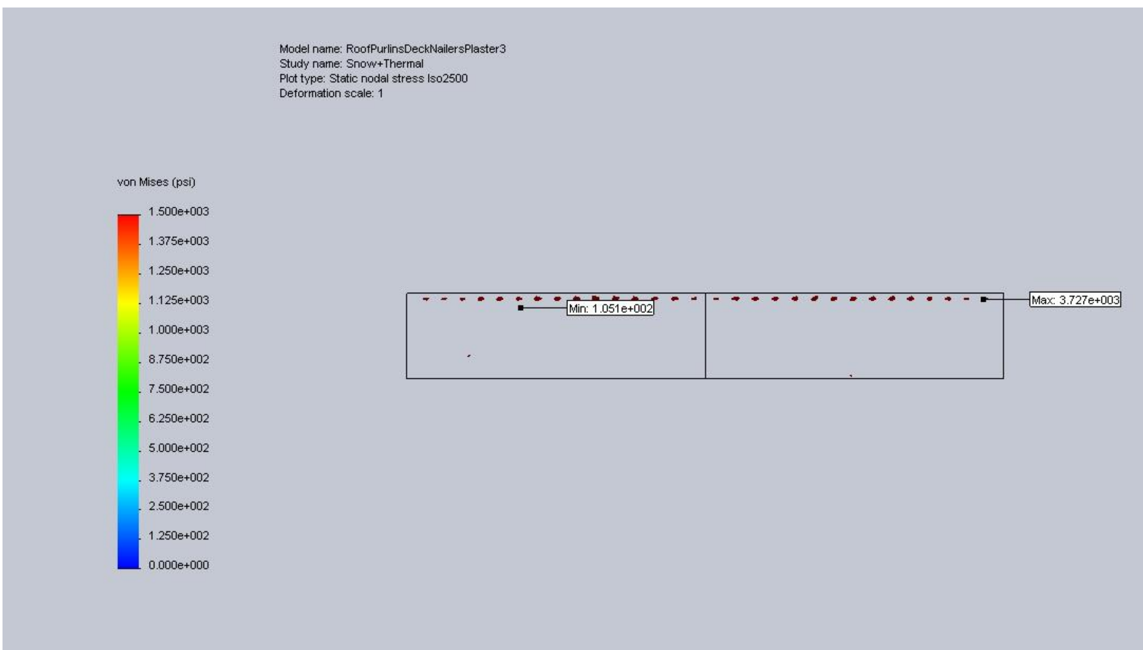

RoofPurlinsDeckNailersPlaster3-Snow+Thermal-Stress-Iso2500

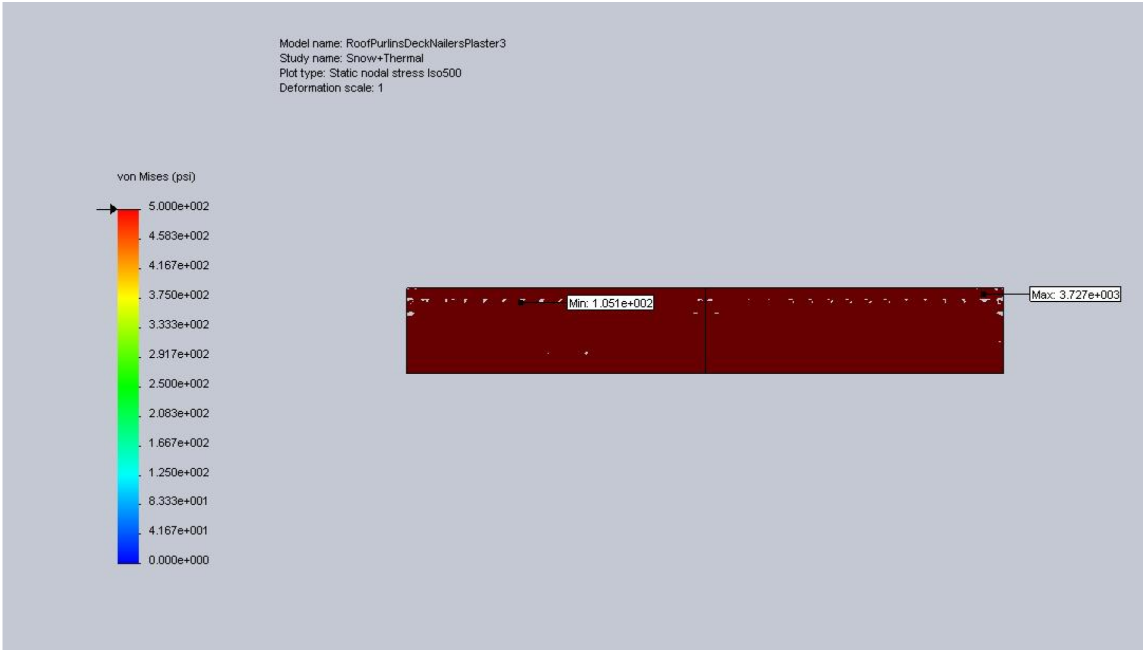

RoofPurlinsDeckNailersPlaster3-Snow+Thermal-Stress-Iso500

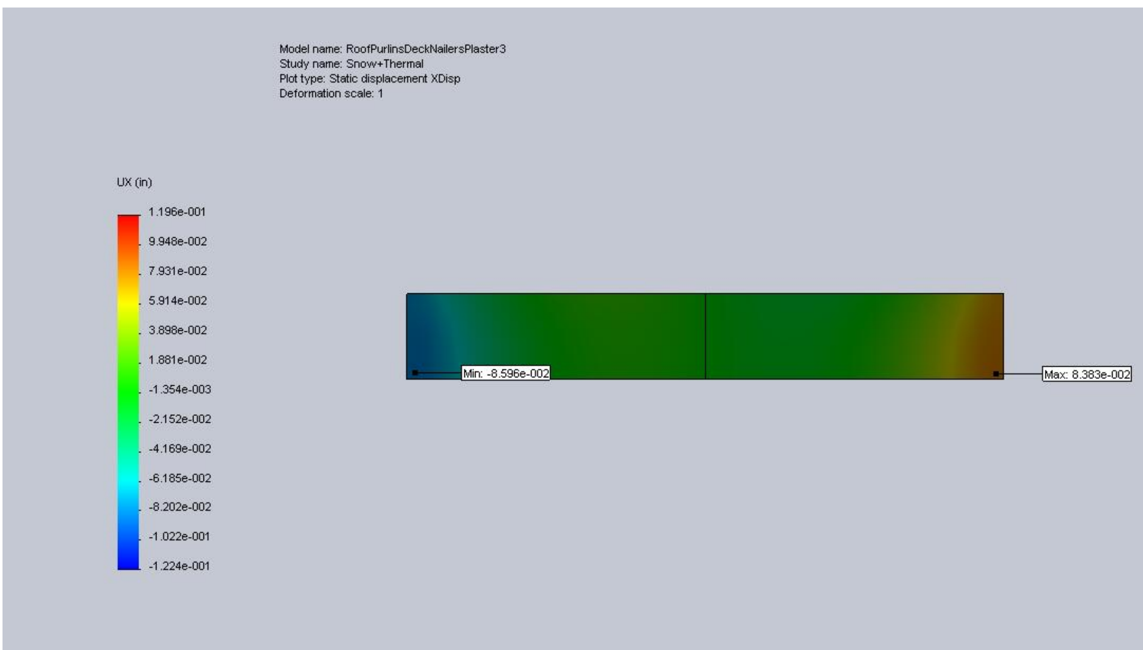

RoofPurlinsDeckNailersPlaster3-Snow+Thermal-Displacement-XDisp

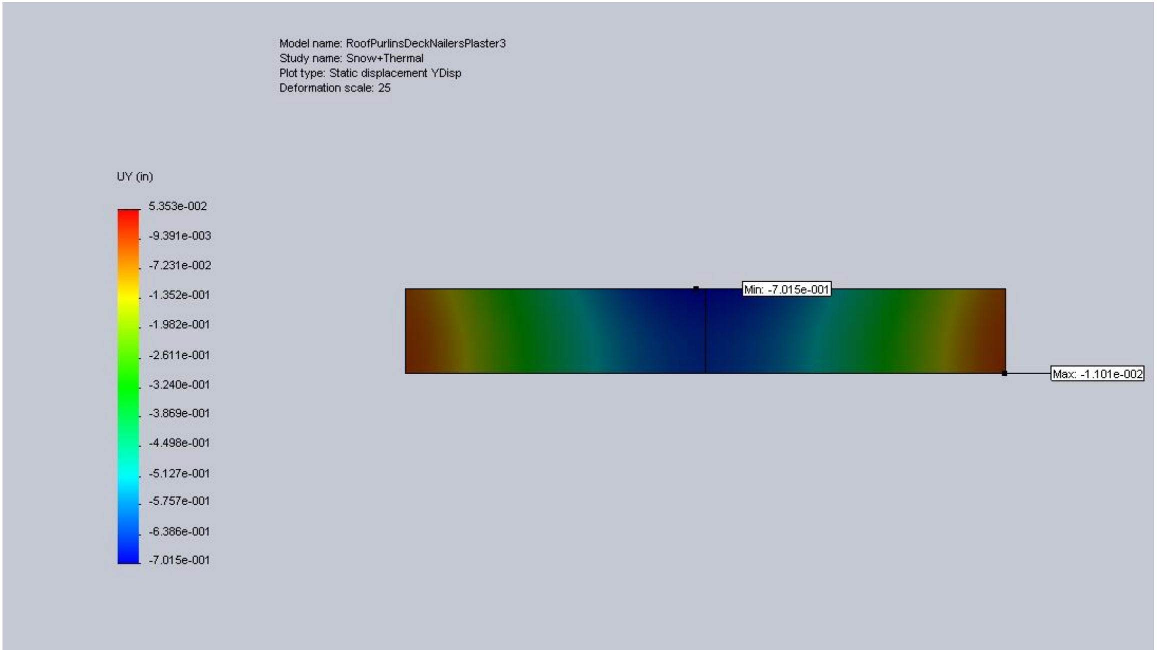

RoofPurlinsDeckNailersPlaster3-Snow+Thermal-Displacement-YDisp

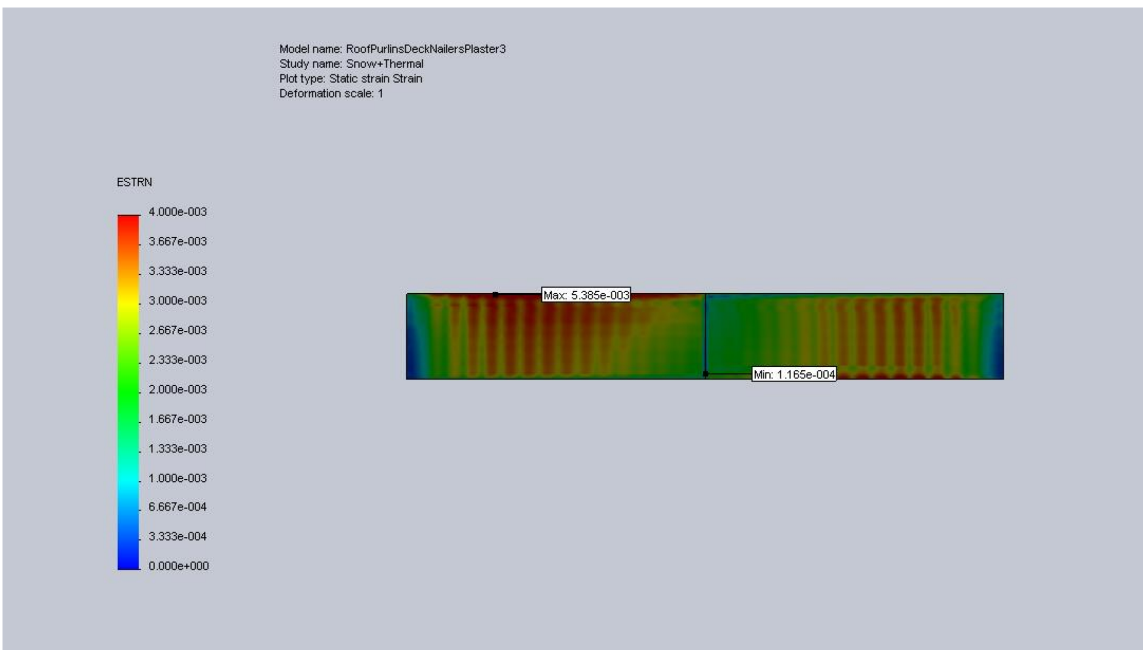

RoofPurlinsDeckNailersPlaster3-Snow+Thermal-Strain-Strain